NASA-CR-72892

ALLOYING OF CHROMIUM TO RESIST NITRIDATION

BY
R. A. PERKINS

LOCKHEED MISSILES & SPACE COMPANY

PREPARED FOR
NATIONAL AERONAUTICS AND SPACE ADMINISTRATION

NASA-LEWIS RESEARCH CENTER
CONTRACT NAS 3-13210
JOSEPH R. STEPHENS, PROJECT MANAGER

NOTICE

This report was prepared as an account of Government-sponsored work. Neither the United States, nor the National Aeronautics and Space Administration (NASA), nor any person acting on behalf of NASA:

A.) Makes any warranty or representation, expressed or implied, with respect to the accuracy, completeness, or usefulness of the information contained in this report, or that the use of any information, apparatus, method, or process disclosed in this report may not infringe privately-owned rights; or

B.) Assumes any liabilities with respect to the use of, or for damages resulting from the use of, any information, apparatus, method or process disclosed in this report.

As used above, "person acting on behalf of NASA" includes any employee or contractor of NASA, or employee of such contractor, to the extent that such employee or contractor of NASA or employee of such contractor prepares, disseminates, or provides access to any information pursuant to his employment or contract with NASA, or his employment with such contractor.

Requests for copies of this report should be referred to

National Aeronautics and Space Administration
Scientific and Technical Information Facility
P. O. Box 33
College Park, Md. 20740

NASA-CR-72892
LMSC-D008017

FINAL REPORT

ALLOYING OF CHROMIUM TO RESIST NITRIDATION

by

R. A. Perkins

LOCKHEED MISSILES & SPACE COMPANY
Sunnyvale, California 94088

prepared for

NATIONAL AERONAUTICS AND SPACE ADMINISTRATION

July 1971

CONTRACT NAS 3-13210

NASA Lewis Research Center
Cleveland, Ohio 44135
Joseph R. Stephens, Project Manager

FOREWORD

This report covers work performed under Contract NAS-3-13210 for the period 1 July 1969 to 28 February 1971. The work was administered by the NASA-Lewis Research Center, with Mr. Joseph R. Stephens as Project Manager.

This report was prepared by Mr. R. A. Perkins of the Metallurgy & Composites Laboratory, Materials Sciences Directorate, Lockheed Palo Alto Research Laboratory, Palo Alto, California. Research tasks were performed under the direction of Mr. Perkins as Principal Investigator and Project Manager. Program supervision was provided by Dr. T. E. Tietz, Manager of the Metallurgy & Composites Laboratory.

The following members of the Laboratory assisted in conducting the experimental work:

Alloy Preparation

J. F. Fitzpatrick, A. T. Davinroy, E. K. Montgomery

Environmental Exposure

E. K. Montgomery

Metallography

W. C. Coons, A. R. Hansen, L. Iosty

Transmission Electron Microscopy

E. H. Rennhack, P. F. Lindberg

X-Ray Diffraction

C. M. Packer, J. C. Robinson

Electron Probe Analysis

J. B. Saunders

ABSTRACT

This report presents the results of an investigation to determine the most effective alloy additions for controlling the nitrogen embrittlement of chromium and to identify the mechanism(s) by which embrittlement is reduced. Based on bend DBTT, additions of 1 to 2 at.% rare earths or thorium give the best resistance to embrittlement. Their effectiveness is increased by the addition of 2 to 3 at.% zirconium. These elements promote ductile behavior in nitrogen-contaminated chromium by providing a dispersion of secondary phases (oxides, nitrides, intermetallics, or excess metal) that is capable of activating dislocation sources.

CONTENTS

ILLUSTRATIONS

TABLES

Section 1

SUMMARY

A study has been made to determine the most effective alloy additions for controlling the nitrogen embrittlement of chromium and to identify the mechanism by which embrittlement is reduced. Eighteen different alloying elements comprising three different groups have been investigated: Group 1 (Nitride Formers)—Zr, Hf, Th, Ti, V, Cb, Ta; Group 2 (Solid Solution Strengtheners)—Mo, W, Re, Fe, Mn, Co, Ru; and Group 3 (Rare Earths)—Y, La, Pr, Mischmetal. Their effectiveness was measured by retention of bend ductility after 100 hr—in air, oxygen, and nitrogen at 2100°F (1422°K). All tests were made with 0.030-in.-thick sheet.

The addition of 1 to 2 at.% rare earths or thorium afforded the best resistance to oxidation, nitridation, and nitrogen embrittlement. Binary alloys in the recrystallized state had a bend DBTT of 300 to 400°F (422 to 478°K) before exposure and 400 to 700°F (478 to 644°K) after exposure to air for 100 hr at 2100°F. Yttrium was the most effective of all additions studied and limited the increase in bend DBTT on air exposure to less than 100°F (56°C or K). The effectiveness of the rare earths and thorium was increased by the addition of 1 to 2 at.% zirconium. A Cr-2Zr-1Th alloy had a bend DBTT of 400°F (478°K) before and after exposure to air for 100 hr at 2100°F (1422°K). Cr-2Zr-0.25La and Cr-3Zr-0.1Y alloys had only a 300°F (167°C or K) increase in bend DBTT on air exposure compared with an increase of over 600°F (383°C or K) for binary Cr-Y or Cr-La alloys with 0.1 to 0.25 rare earth content. Zirconium creates a random distribution of rare earth phases and minimizes the formation of banded structures in chromium-rare earth alloys.

These additions aid in the formation of thin adherent oxide scales that greatly restrict nitrogen pickup by the alloy. Surface oxides, however, are not absolute barriers to nitrogen. Rare earths, Th, and Zr are selectively oxidized internally, and internal oxidation prior to air exposure significantly increases their effectiveness for reducing nitrogen embrittlement. Although yttrium inclusions appear to scavenge nitrogen, none of these additions form nitrides internally. All nitrogen dissolved by the alloy precipitates as Cr_2N in platelet form on cooling from high temperature. The additions, however, do appear to reduce nitrogen solubility and limit the amount of chromium nitride formed.

Neither the large nitride precipitates nor the chromium nitride case on chromium appears to be a major source of brittleness. The increased DBTT is postulated to result from dislocation pinning by small nitride particles that precipitate on cooling. Ductility can be promoted by the formation of free dislocations. This requires the activation of dislocation sources. Small particles of secondary phases in the matrix can provide the needed sources. It is concluded that the mechanism by which rare earths, Th, and Zr decrease nitrogen embrittlement is through the generation and multiplication of free dislocations by the random dispersions of oxides, intermetallics, and other secondary phases that these elements introduce in the structure.

Section 2
INTRODUCTION

Chromium-base alloys are promising high-temperature materials for advanced air-breathing gas turbine engines. They have a weight advantage over nickel- and cobalt-base alloys and have good strength and oxidation resistance at temperatures above the normal operating range for the superalloys. Their resistance to oxidation above 2000°F (1366°K) is much better than that of columbium- or molybdenum-base alloys which have been developed for use in this temperature range. Chromium has a significant advantage over all other refractory metals with respect to scaling behavior above 2000°F (1366°K). Although the surface is stable in air, oxygen and nitrogen diffuse into the metal. Contamination with nitrogen is particularly harmful, causing severe embrittlement of the alloy. This behavior has placed undue restrictions on the use of chromium and has resulted in efforts to develop useful chromium alloys for gas turbine engines. A major advance in engine performance and design could be realized by solving the problem of nitrogen contamination.

Alloying of chromium to control nitridation is a feasible approach to solving the contamination problem. Strong nitride formers such as aluminum, titanium, zirconium, hafnium, thorium, and the rare earths show a scavenging effect for nitrogen and appear to retard nitridation. Dilute concentrations of the rare earths (Y, La, and Pr) have been used to improve resistance to oxidation and nitridation of many chromium alloys. The increase in nitridation resistance is limited, however, and further improvements are desired. Also, some of these additions have undesirable side effects. Several have an adverse effect on the ductile-to-brittle transition temperature at critical levels of concentration. Many of them, particularly the rare earths, produce low-melting phases that limit the temperature of use. Some additions also can have an adverse effect on the hot workability of chromium. A careful balance between composition and structure will be required to achieve the desired balance of nitridation resistance, high-temperature strength, and low-temperature ductility. Sufficient work has been done to demonstrate that alloying can be used to improve resistance to nitridation, but considerable work remains to be done before greatly improved chromium-base alloys can be developed.

The next step in this effort is to determine the most effective approach for the control of nitridation by alloying. The results of some studies indicate that alloying to control oxide films on the surface is required. Others suggest that alloying to reduce solid solubility and to precipitate nitride phases is the controlling factor. The mechanism by which nitridation is controlled must be delineated to determine the optimum approach. This is of particular importance when the undesirable side effects of alloying are taken into consideration. Simple screening studies that are not designed to develop such an understanding can easily miss the only effective approach to solving the problem. By developing an understanding of the compositional and microstructural factors that govern behavior, on the other hand, studies can be guided in a manner that has the best chance for technical success.

Section 3
TECHNICAL BACKGROUND

3.1 EMBRITTLEMENT OF CHROMIUM

The ductile-to-brittle transition in chromium has been studied extensively during the past 15 years. Comprehensive reviews of work on this important aspect of mechanical behavior have been prepared by Tietz and Wilson (Ref. 1) and Maykuth and Gilbert (Ref. 2). The mode of fracture in chromium undergoes a transition from a ductile fibrous fracture at high temperature to a brittle cleavage fracture at low temperature. In chromium, this transition is very sharp; that is, it occurs over a rather narrow temperature range. The temperature for this transition is variable over wide limits, however, depending on composition, structure, and loading conditions. Factors which are known to govern the transition temperature in chromium include purity, grain size and shape, alloy additions, surface conditions, deformation and annealing substructures, precipitates and dispersed phases, stress system, and the rate of loading. The complex interrelations of these variables and the fact that many variables have not been specified or controlled in prior studies make any evaluation of the available data extremely difficult.

Nonetheless, the behavior of chromium has been fairly well characterized and the critical factors that must be controlled to produce useful alloys have been identified. Basically, the behavior of chromium with respect to embrittlement is similar to that of molybdenum, and much of the technology developed for molybdenum is applicable to chromium (and vice versa). The better chromium alloys developed to date are close parallels to the better molybdenum alloys. The alloys are low in total alloy content; have only a mild solid solution strengthening, and utilize a combination of dispersed phases, purity, and microstructural control to achieve a desired balance of properties. One of the most significant developments in chromium alloys during recent years has been the use of carbide dispersions to control strength and ductility (Ref. 3). A similar approach is used to control the properties of molybdenum. Hot/cold work and control of grain structure also are used to reduce the ductile-to-brittle transition temperature and to control the high-temperature strength of both chromium and molybdenum alloys. Much of the extensive data and basic understanding of the interplay between structure, composition, and properties developed for molybdenum alloys in the past few years is directly applicable to the control of structure and properties in chromium.

Chromium and molybdenum, however, have two basic differences with respect to ductile-brittle behavior that have unduly complicated alloy development efforts and retarded the development of useful chromium-base alloys. Chromium, unlike molybdenum, has a solubility for nitrogen at elevated temperatures and is severely embrittled by small amounts of this impurity. Chromium containing in excess of 80 ppm nitrogen and/or carbon in the absence of reactive metal stabilizers will not exhibit bend ductility at room temperature under any conditions (Ref. 2). Low interstitial chromium, on the other hand, is ductile to -40°F (233°K) in the warm-worked condition.

Second, the ductile-to-brittle transition temperature of chromium is far more sensitive to recrystallization than that of molybdenum. In the recrystallized state, chromium has a much lower tolerance for interstitial impurities than molybdenum and much higher levels of purity are required to achieve ductility at low temperature. Grain boundaries act as sources for crack nucleation in polycrystalline chromium, and the rate of crack propagation is accelerated by nitrogen in solid solution (Ref. 4). The development of useful chromium-base alloys will depend to a large extent on the control of nitrogen content and on the control of metallurgical structure.

3.2 CONTROL OF NITROGEN

With the use of high-purity raw materials and carefully controlled processing, chromium can be prepared with a very low nitrogen content. However, on heating in air or other nitrogen-bearing atmospheres, nitrogen diffuses rapidly into chromium. Thus, not only must nitrogen be reduced to a low level in mill products but also the pickup of nitrogen from the atmosphere during service must be prevented.

Early studies on the control of nitrogen in chromium were concerned with the addition of nitrogen scavengers (Refs. 5,6). Elements having a strongly negative free energy of formation for the nitride were found to be capable of reducing Cr_2N and precipitating stable nitrides from solid solution. Significant reductions in the ductile-to-brittle transition temperature, particularly for recrystallized chromium, were achieved by dilute additions of Al, Ta, Cb, Y, Ce, Ti, and Zr (Ref. 6). A tantalum-modified alloy was ductile in bending at -148°F (173°K) compared with a DBTT of 419°F (488°K) for unalloyed chromium in the recrystallized condition.

The reduction in transition temperature has been attributed to the removal of nitrogen from solid solution by the precipitation of stable nitrides. The strong nitride formers (Ti, Zr) formed nitrides from the melt, whereas the weaker nitride formers (Cb, Ta) formed nitrides by a solid-state reaction (Refs. 5,6). A 1% Cb addition to high-nitrogen Cr resulted in the formation of a complex $(Cb, Cr)_2N$ precipitate, which replaced the Cr_2N precipitate formed on cooling from the melt. This nitride interchange process required heating for 20 hr at 2291°F (1523°K) to complete the reaction (Ref. 6). Ryan (Ref. 5) also reports that a carbide interchange reaction of $Cr_{23}C_6$ to CbC occurs in Cr.

It is interesting to note than an identical carbide interchange reaction occurs in molybdenum and is used to control the ductile-to-brittle behavior and strength of molybdenum alloys (Ref. 7). In Cb (or Ti) modified alloys, Mo_2C precipitated on cooling from the solution temperature is completely replaced by a fine dispersion of CbC(TiC) on aging for long times at 2372°C (1573°K) to 3092°F (1973°K). Completion of the conversion process restores ductility to molybdenum and provides the best combination of properties. Perkins (Ref. 8) studied the mechanisms of the carbide interchange reactions in molybdenum and provided a rational explanation for observed behavior. Critical factors in the process include the relative free energies of Mo_2C and CbC phases and the ratio of Cb to Mo in the alloy. At proper concentrations, a nonequilibrium Mo_2C phase precipitates on cooling due to the limited availability and slow diffusion rate of columbium atoms. On reheating, Cb diffusion occurs and the more stable CbC phase is precipitated. The Mo_2C phase is taken back into solution and eventually is completely

replaced by the CbC dispersion. The diffusion of columbium is the rate-controlling factor in the process. Over 1000 hr were required to complete the conversion at 2192°F (1473°K), while less than 15 min were required at 3092°F (1973°K) (Ref. 8). The knowledge obtained from the study of this reaction is directly applicable to nitride conversion reactions in Cr.

Statistically, the alloy must be designed to provide a reasonable probability for the formation of the reactive metal nitride as rapidly as nitrogen diffuses inward. Otherwise, the nitrogen concentration in solid solution will increase and Cr_2N will be precipitated. The important factor will be the ratio of reactive metal to chromium atoms and not the ratio of reactive metal to nitrogen atoms. The mobility of the reactive metal species in chromium will play an important part in determining the effectiveness of the additions. Atoms with a high diffusion rate in Cr should be most effective. This factor is deemed more important than the free-energy difference between the two nitrides. Only a moderate difference in free energy is needed to effect an interchange reaction. Unless the metal atoms possess sufficient mobility, a very large free-energy difference is useless. A rapidly diffusing species of only a moderate free-energy difference would be more effective.

Many other factors will govern the effectiveness of alloy additions to block nitridation. Distribution of the alloy additions in Cr can be of considerable importance. Grain boundaries provide an easy path for diffusion. In molybdenum, for example, carbon diffuses very rapidly along the grain boundaries compared with its diffusion in a grain (Ref. 8). This is most likely true of carbon and nitrogen in chromium. Elements that preferentially segregate to grain boundaries may be particularly effective in retarding nitridation. A high local concentration of a nitride former along major diffusion routes into the alloy should be most helpful; this may be the reason why the rare earths such as La and Y, with their low solid solubility in Cr, improve nitridation resistance. Also, these additions in themselves may be present as a liquid phase that will diffuse very rapidly along the boundaries. Incipient melting in the service temperature range is a problem in the use of rare earths for this purpose.

The diffusion rate of nitrogen in the alloy also is likely to be an important consideration in determining the effectiveness of nitride stabilizers. If the mobility of the nitride-forming element is not sufficiently high, stable nitride formation can be enhanced by reducing the rate of nitrogen diffusion. The critical factor will be the relative diffusion rates of nitrogen and the reactive alloy addition, and a favorable ratio can be achieved from either direction. This effect is clearly demonstrated by recent work of Bonesteel, Lytton, and Tietz on the internal oxidation of columbium (Ref. 9). If a Cb-1Zr alloy is heated in air at atmospheric pressure, oxygen diffuses rapidly into the alloy with resultant embrittlement. In 2 min at 2012°F (1373°K), sufficient diffusion occurs to completely embrittle 0.060-in. (0.152 cm)-thick sheet. By reducing the partial pressure of oxygen to a value of about 10^{-6} Torr (1.33×10^{-4} N/m^2) where the rate of arrival at the surface is less than the inward diffusion rate, a complete change in behavior occurs. With a slow pickup of oxygen, a fine dispersion of ZrO_2 is formed internally as fast as the oxygen reaches the surface and diffuses into the alloy. After 100 hr at 1472°F (1073°K), alloys have picked up as much as 1500 ppm of oxygen

without becoming embrittled. At 1550 ppm of oxygen, the alloy has over 10% uniform elongation at room temperature. If the temperature or gas pressure is increased so that oxygen enters more rapidly, the desired ZrO_2 precipitate does not form and embrittlement will occur.

Thus, in attempting to control the nitridation of chromium, the use of alloy additions to reduce the diffusion rate of nitrogen should be considered as an approach to increasing the effectiveness of nitride formers. The additions to control diffusion need not necessarily be nitride formers in themselves. They may be elements that slow the rate of bulk or grain boundary diffusion of nitrogen in chromium or they may be elements that modify oxide or nitride scales to form types that may govern the rate of nitrogen diffusion into the alloy. They can be used in conjunction with nitride formers to increase their effectiveness or they can be nitride formers that serve a dual purpose in the alloy.

These are but a few of many factors that must be considered in any systematic study of alloying of chromium to prevent nitridation. Some of these factors have not received adequate attention or even been considered in past work. A wide variety of alloys must be studied to determine the relative importance of these and other factors that will control nitrogen pickup and embrittlement. An identification of basic mechanisms governing behavior will be an important factor in the development of improved alloys.

3.3 CONTROL OF STRUCTURE

Limiting the inward diffusion of nitrogen or producing stable nitride precipitates will not necessarily prevent the embrittlement of chromium. In the final analysis the structure that is generated as a result of the alloy addition and its interaction with the thermal and gaseous environments will govern the ductile-to-brittle behavior. Most alloy additions have a detrimental effect on the bend transition temperature of chromium as the level of addition is increased. Abrahamson and Grant (Ref. 10) and Sully (Ref. 11) found an increase in transition temperature of several hundred degrees with less than 1 at. % of solute for most metals in Cr. Abrahamson and Grant also found that a peak in transition temperature occurred at about 5 at. %, and that further alloying tended to lower the DBTT. In this study, only Be and Ru were found to give an immediate decrease in transition temperature. Henderson et al. (Ref. 6), on the other hand, found that Al, Ti, Ta, Cb, Y, Ce, Tr, and Zr significantly decreased the DBTT in both the warm-worked and recrystallized conditions when added in stoichiometric proportions to the interstitials present in the alloy ($0.02\ O_2 + 0.002\ N_2$). Al, Ce, and Ti had the greatest effect at 0.5 to 3.0 times the stoichiometric level. A critical range for minimum DBTT with an increase in DBTT at higher levels of addition was found in all cases.

Alloying to control nitridation must be balanced carefully to prevent embrittlement by the alloy addition itself. Obviously, intergranular precipitates and certain types of aging reactions must be avoided for optimum results. Certain types of nitride precipitates that may be formed also can embrittle chromium. Solie and Carlson (Ref. 4) point out that Cr_2N precipitates will embrittle chromium on attaining a critical size and concentration. Perkins (Ref. 8) demonstrated that a recrystallized molybdenum alloy exhibited over 25% elongation at room temperature with a fine dispersion of spherical CbC particles and less than 1% elongation with a fine dispersion of CbC platelets. No intergranular precipitates were formed in either case. The DBTT in tension was increased from a value of -50°F (228°K) to a value of +300°F (422°K) by changing

the form of the carbide dispersion within the grains of the recrystallized alloy. Alloying to control the nature of precipitated nitride phases in chromium will be a very important aspect of a program to prevent nitrogen embrittlement.

It is likely that some nitride-forming alloying additions will tend to produce a nitrogen-rich case below the surface during nitridation. Aluminum and titanium are added to steel, for example, to accelerate nitrogen pickup and case formation in nitriding grades of steel. The formation of hard cases below the surface of chromium may not be desirable, since it is a notch-sensitive material. Control of alloying to minimize the formation of hard outer (surface) cases may be important. A nitride layer (Cr_2N) cannot form on the surface until the metal below the surface becomes saturated in N_2. In studying the carburization of Mo alloys, Perkins (Ref. 8) observed that the addition of Cb and/or Ti prevented the formation of a carbide case on the surface during heating in methane at low pressures. The factor that governed this behavior was the rate of arrival of carbon at the surface relative to the rate of inward diffusion. If carbon arrived faster than it diffused inward (high methane pressure or low temperature), a Mo_2C case could be formed. Ti and Cb acted to continually remove carbon from solid solution by the precipitation of carbides internally. In effect, this reduced the concentration of nitrogen in solid solution and prevented case formation at gas pressures and temperatures where unalloyed molybdenum developed a carbide case. It was also found that Cb and Ti significantly decreased the depth of diffusion of carbon in molybdenum for a given set of conditions.

The interplay between the environment and structure may be a key factor governing the effectiveness of alloy additions. Alloy elements and concentrations that retard nitridation and embrittlement for a given temperature and nitrogen pressure may not be effective at different temperatures or pressures, where a change in the nature of nitride precipitates, nitrogen gradients, or surface scales may occur. Data must be evaluated carefully and the basic mechanisms controlling the process defined in order to assess the overall utility of specific alloy additions.

Grain size and shape maybe another important factor governing nitridation behavior. Grain boundary diffusion is much more rapid than bulk diffusion. Grain structure also governs the ductile-brittle behavior of any given material. Much of the data on grain size indicates that coarse-grained chromium is more ductile than fine-grained material (Ref. 2). Solie and Carlson (Ref. 4) postulate that cracks initiate at grain boundaries and that the probability of crack nucleation governs the ductile-to-brittle transition temperature. Refining the grain size increases this probability and hence should raise the transition temperature. Coarse-grained material also should be more resistant to nitridation. A decrease in grain boundary area is a decrease in the number of rapid diffusion paths. Grain shape also may be important. Plate-shaped grains with long boundaries parallel to the surface may be more resistant to nitridation than equiaxed structures. It is important to recognize that grain size and shape may govern both the nitrogen diffusion process and the DBTT of a given alloy. In comparing the effectiveness of various alloy additions, every effort should be made to standardize grain structure.

Deformation substructures also have an important effect on the DBTT and must be controlled. Cold or warm working is normally used to lower the DBTT of chromium. A light prestrain of recrystallized chromium can produce a similar effect (Ref. 2) and

heavy cold working is not essential. Chromium that has been strained through the Lüders strain at high temperature will continue to deform in a ductile manner at low temperature (Ref. 2). Tietz and Lytton (Ref. 12) observed a similar behavior in molybdenum. Merely passing one Lüders band through recrystallized Mo sheet (3 to 5% strain) shifted the DBTT from 86°F (303°K) to 14°F (263°K). It is clear that deformation substructures and thermal mechanical history of test samples must be controlled to evaluate the effect of alloy additions on nitridation embrittlement. Particular attention must be given to side effects that can provide a misleading interpretation of observed behavior.

Section 4

TECHNICAL APPROACH

4.1 PROGRAM PLAN

This research program was designed to identify the most effective alloy additions for reducing the embrittlement of chromium by nitrogen and to identify the mechanism(s) by which embrittlement is reduced. The goal of the program was to provide guidelines for the development of chromium alloys resistant to embrittlement by nitridation during air exposure for thousands of hours at 2000°F (1366°K) and above. The effectiveness of alloy additions in this study was measured by the retention of bend ductility in chromium alloy sheet after a 100-hr exposure to air, nitrogen, and oxygen at 2100°F (1422°K). The mechanisms were delineated by correlating bend ductility with composition, microstructure, and environmental exposure for a wide range of alloy additions and concentrations.

The research program was conducted in three sequential tasks. In Task I, unalloyed chromium and 48 binary alloys were screened for nitridation and oxidation behavior. Eighteen different alloying elements comprising three different groups were studied: Group 1 – Ti, Zr, Hf, Th, V, Cb, and Ta; Group 2 – Mo, W, Mn, Re, Fe, Ru, and Co; Group 3 – Y, La, Pr, and Mischmetal. Group 1 represents strong nitride formers; group 2 represents solid solution additions; and group 3 represents sparingly soluble rare earths. This selection of alloys provides a good cross section of the various types of additions that can control nitridation behavior in chromium alloys. Sheet samples were heated for 100 hr at 2100°F (1422°K) in high-purity nitrogen and in air. Kinetics of nitridation were determined by volumetric measurements of nitrogen consumption. A 90°-4t bend test at a cross-head rate of 1 in./min (2.54 cm/min) was used to establish the approximate ductile-to-brittle transition temperature, and microhardness surveys were taken to evaluate the depth of contamination. The materials also were characterized with respect to microstructure.

Based on the results of the Task I study, 10 of the most promising compositions were selected for a more detailed study in Task II. Kinetics of oxidation on air exposure were studied at 2100 and 2400°F (1422 and 1589°K) by continuous weighing. In addition, samples were exposed to pure oxygen and air for 100 hr at 2100°F (1422°K) for bend ductility tests. Preoxidation studies were conducted to determine the effect of oxide scales and internal oxidation on resistance to nitridation. Detailed microstructural studies were made to delineate the basic factors controlling the nitridation and oxidation processes. Particular attention was given to the correlation of properties, composition, structure, and treatment to provide an understanding of the mechanisms involved. Transmission electron microscopy, electro-microprobe analyses, and x-ray diffraction measurements were employed to identify important structural features.

Five ternary alloy compositions were selected for evaluation in Task III. The most effective combinations of elements as determined from the Task I and Task II studies were used to design these alloys. The materials were studied as in Task II except that the continuous weighing tests in air were not conducted. The effect of preoxidation treatments on resistance to nitridation was evaluated as in Task II. The results of all studies were analyzed and correlated to develop a basic understanding of the mechanisms by which alloying controls the resistance of chromium to nitridation and nitrogen embrittlement.

Based on the results of this study, the best approach to alloying chromium for resistance to nitridation was identified. Critical factors in the application of this approach to the development of alloys were defined and recommendations for factoring the results into existing or subsequent alloy development programs were formulated.

4.2 ALLOY PREPARATION

Materials

The chromium used to prepare all alloys was purchased from the Materials Research Corporation, Orangeburg, N. Y. MARZ-grade Iochrome crystals produced by vapor decomposition of chromium iodide with a nominal purity of 99.996% were procured. The metal was identified as Lot 689 and was reported to contain 10 ppm carbon, 20 ppm oxygen, 1 ppm nitrogen, and 0.2 ppm hydrogen. All alloying additions with the exception of thorium, manganese, and Mischmetal also were obtained from Materials Research Corporation. The highest grade of purity available was used in each case. Crystal bar thorium prepared by the iodide process was purchased from Alpha Organics, Inc., Beverly, Mass. High-purity manganese and Mischmetal were obtained from Atomergic Chemetals Co., Long Island, N. Y.

Melting and Casting

All alloys were prepared by arc melting and drop casting by the nonconsumable electrode process under helium at a pressure of 1-1/2 atm (1515×10^2 N/m^2). The alloys were prepared by the Lockheed Palo Alto Research Laboratory using a specially constructed button melting furnace. The molds designed for arc melting and drop casting the chromium alloys are shown in Figure 1. They are interchangeable water-cooled copper mold inserts that are sealed to a hole in the center of a water-cooled copper-base plate. The mating surfaces have a 6° taper to facilitate insertion or removal, and an O-ring is used to provide a vacuum seal. A jack was used to hold the mold inserts firmly in place. The inserts are 3 in. (7.62 cm) in diameter by 3 in. (7.62 cm) high. The ingot cavity in the drop cast mold is 1 in. (2.54 cm) in diameter by 1-1/4 in. (3.18 cm) deep with a 3° taper to facilitate ingot removal. The sloping sidewalls of both molds initially were designed with a 100° included angle.

As work on melting and casting proceeded, several minor changes were made in the original design of the drop-cast mold and miscellaneous furnace parts. Water channels were enlarged in the upper portion of the drop-casting mold to provide better cooling and to allow the use of greater power at the end of the pour. Localized melting with the copper mold tended to occur due to inadequate cooling. A further change was made following the melting of the first 10 alloy ingots. It was found that a portion

of alloy tended to remain on the slope of the conical entrance to the mold cavity and that even with adequate cooling it was often difficult to free this material with the arc and make it flow onto the mold. Extreme care was mandatory in this final sequence of melting to avoid arcing into the copper mold and thus contaminating the melt. The conical entrance of the casting mold design was altered to an included angle of 80° instead of the 100° angle on the initial design to alleviate this problem.

The technique for alloy preparation was as follows:

(1) A 120-g charge of the bulk components was placed in the consolidation mold insert (Figure 1a). The furnace was pumped to 10^{-5} Torr (1.33×10^3 N/m^2) and back filled with reactor grade helium to 1-atm (1010×10^2 N/m^2) pressure. (Note: the pressure during melt rises to about 1-1/2 atm (1515×10^2 N/m^2) as a result of gas expansion.) The titanium getter button was melted for 1 min and the arc was then transferred to the chromium alloy charge. The hearth plate contains two cavities for melting titanium getter buttons and two tungsten striker pins for arc ignition. The alloy charge was melted with an arc current of 300–500 A until the complete charge appeared to be molten. The button ingot was turned over and remelted from the backside to assure complete consolidation. Following each melt, the furnace walls, hearth, cover plate, and electrode were thoroughly cleaned to remove all vapor deposits. A disposable titanium sheet-metal liner was installed in the furnace to facilitate cleaning of deposits from the interior surface. This is an essential step in maintaining high purity, since the vapor deposits oxidize on exposure to air and any carryover into the next melt would result in contamination of the alloy.

(2) The drop-cast mold (Figure 1b) was then placed in the hearth plate and the alloy was arc melted and drop cast in three successive melts. Again, the furnace was cleaned after each melt. The evacuation, backfill, and gettering procedures which were described under item (1), above, were used for each melt. As shown in Figure 2, each drop-cast ingot had a button-shaped top somewhat larger in diameter than the 1-in.-long cylindrical portion. After each drop-cast melt, the ingot was inverted and suspended above the mold cavity by its enlarged top. On melting, the first metal to melt was the bottom of the previously melted ingot. This metal flowed down and solidified on the wall of the entrance cone, forming a seal and a support for the remaining molten metal which formed a pool that temporarily bridged the mold cavity. By applying the arc over the center of this pool and supplying sufficient power, the supporting solid metal skin was melted and metal flowed into the 1-in. (2.54 cm)-diameter mold cavity. The remaining metal on the mold entrance cone was then caused to flow down and join that which filled the cavity. The latter operation required a smooth sweeping motion of the arc over the residual metal. On the last drop-cast melt, the ingot was hot topped by gradually decreasing the power input while holding the arc over the top of the casting.

The as-cast ingots had a smooth side wall and a minimum pipe. Typical ingots are shown in Figure 2.

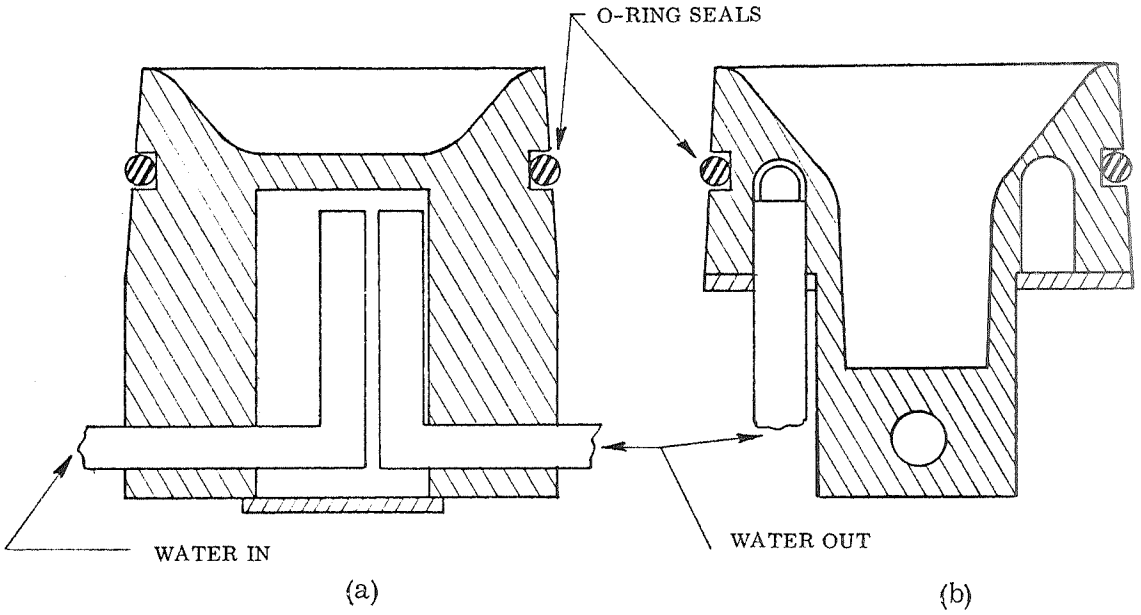

Figure 1 Consolidation Mold (a) and Drop-Casting Mold (b).

(a) (b)

Figure 2 Appearance of Drop-Cast Chromium Alloys (×1). (a) Cr-1 at.% Ru, Typical of All But the Rare Earth Alloys; (b) Cr-1 at.% Mischmetal, Typical of Alloys Containing Rare Earths.

Chromium alloys with the rare earths (Y, Pr, La, and Mischmetal) were observed to have an unusual behavior in melting. As shown in Figure 2b, the upper section of the drop-cast ingots tends to creep up the sloping side walls of the copper mold. This behavior requires extensive conditioning between melts and results in a low yield. The effect may be due to lowered surface tension and change in contact angle with copper. In all other alloys, a smooth button head (Figure 2a) forms on the ingot.

Spectrographic and wet chemical analyses plus hardness measurements were made on unalloyed chromium and selected alloys to qualify the melting practices and to provide a continuing check on quality. The results presented in Table 1 show that alloys meet the basic program requirements of 125 ppm maximum total interstitial content. Recovery of alloy additions in all cases was above 95%. No significant variations in chemistry or structure within a given ingot or lot of material were found, indicating that the melting process used resulted in alloys of very high quality.

4.3 PRIMARY WORKING

Extrusion

All alloys were extruded to a sheet bar in order to break up the cast structure and to produce a material suitable for direct rolling to sheet.

Extrusion procedures were developed to satisfactorily work all alloys, including those containing the highest percentages of the refractory metals. The upper (pipe section) of each ingot was cropped off and the side wall was lathe turned to remove local defects. The surface-conditioned billet was wrapped in one turn of 0.005-in. (0.0127 cm)-thick molybdenum foil and canned in mild steel, as illustrated in Figure 3. The canned billets were preheated at 2200°F (422°K) in a flowing atmosphere for 30 min. Just prior to the extrusion of a billet, an unheated copper cup (shown with the billet in Figure 3) was placed in the extrusion container, which was preheated to 300°F (422°K). A graphite-base lubricant was applied to the hot container walls and the heated billet was dropped into the cup and extruded at a ram speed of 24 in./min (61 cm/min). The billets were extruded to a 1.0 in. (2.54 cm) wide by 0.290 in. (0.737 cm) thick sheet bar with a total reduction ratio of 6:1. Ram travel versus time and extrusion load versus ram travel were recorded autographically for each extrusion. All work was done at the Lockheed Palo Alto Research Laboratory using a 350-ton (317,513 kg) vertical shell nosing press modified for extrusion. Data on extrusion conditions, loads, and behavior are given in Appendix A.

The hot extrusions were packed immediately in alumina insulation (Fiberfrax or bubble grain) for slow cooling to room temperature. Two extrusions of Cr-Cb alloys cracked on cooling in early tests as a result of too rapid a cooling rate. Differential contraction of canning materials and the chromium alloys on cooling was found to be a critical factor in the production of sound, high-quality extrusions.

Initially, the alloy billets were canned directly in mild steel. The resultant sheet bars, however, had a very rough surface that required extensive conditioning. It was found that surface condition could be improved significantly by canning in molybdenum. This effect is shown in Figure 4. The alloys extruded in molybdenum cans or sheaths had a smooth surface and were uniform in thickness. Those canned or sheathed with

Table 1

CHEMICAL ANALYSIS OF ALLOYS

Alloy	Added			Obtained				
	Form[a]	at.%	wt%	Alloy (wt%)	C (ppm)	O (ppm)	H (ppm)	N (ppm)
Cr-973	I	Unalloyed		–	<10	70	5	30
Cr-95-1	I	Unalloyed		–	20	90	7	40
Cr-96-1	I	Unalloyed		–	10	30	7	50
Cr-98-1	SB	Unalloyed		–	10	60	3	70
Cr-917	I		1.7Hf	1.55Hf	80	16	15	40
Cr-912	I	0.5Cb	0.89Cb	0.77Cb	18	70	11	40
Cr-938	I	0.5V		0.61V 0.003Cu <0.02W	<10	50	22	40
Cr-943[b]		2.0Ta		6.53Ta 0.189Cu <0.02W	<10	140	54	60
Cr-95010	S	0.5Y	0.85Y	0.82Y				
Cr-9151-2	S	1.0Y	1.70Y	1.55Y				
Cr-9125	S	0.5Y	0.85Y	0.87Y				
Cr-NASA[c]				0.002Fe	<10	32	0.8	52

(a) I – Ingot
SB – Sheet Bar
S – Sheet

(b) Alloy contaminated, heat remelted.

(c) Analysis provided by NASA.

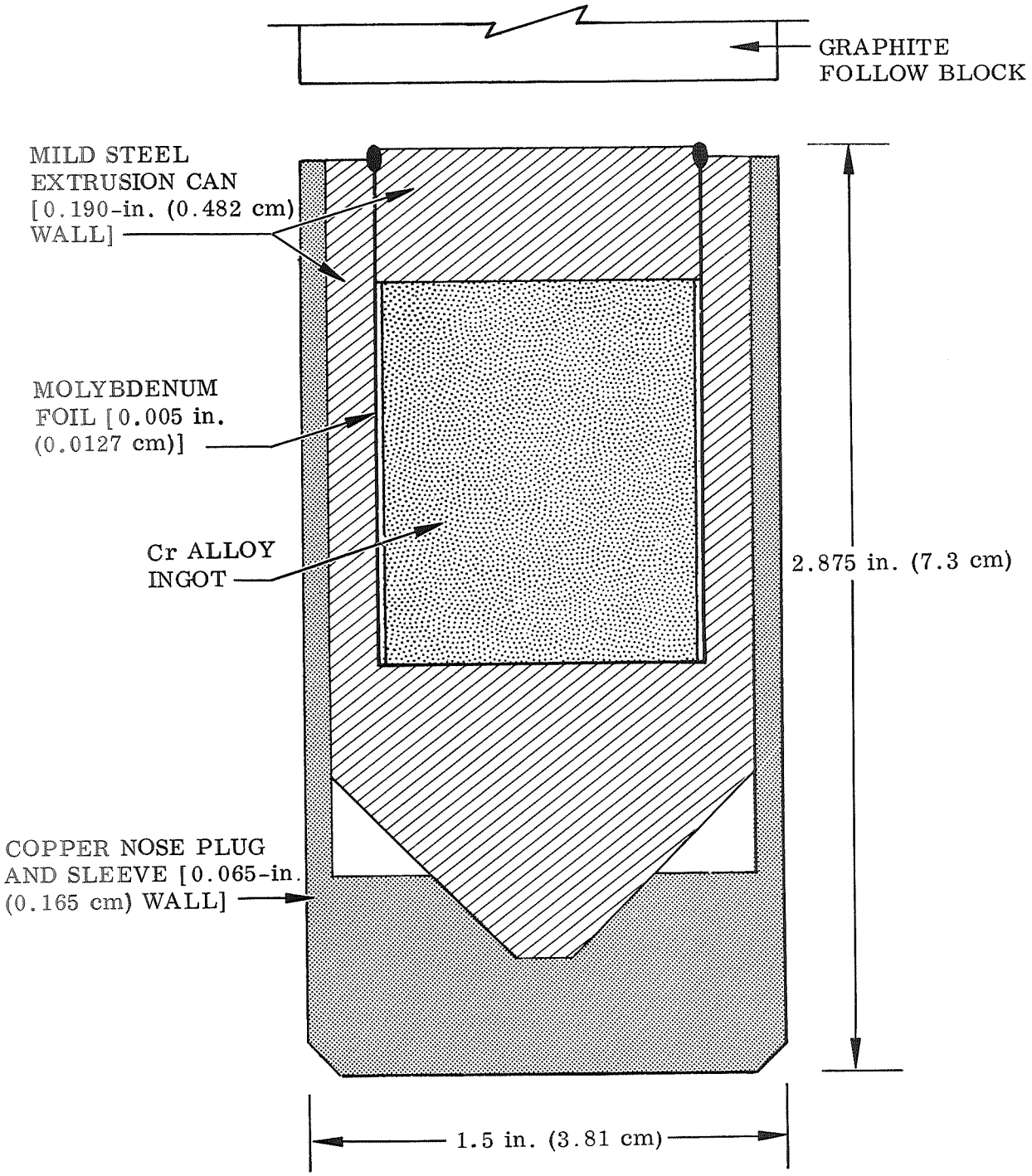

Figure 3 Extrusion Billet Configuration – Longitudinal Section Through Center (×2).

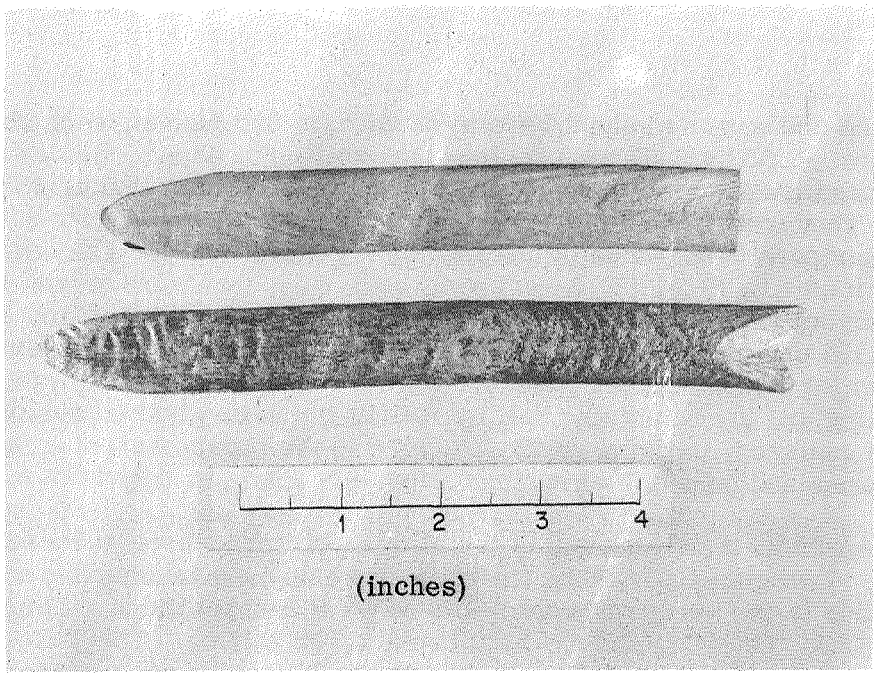

Figure 4 Surface Conditions of Extruded Sheet Bars After Removal of Sheath and Canning Materials. Top: Cr-2 at.% Hf sheet bar, sheathed in molybdenum and extruded in mild steel can. Forward end of extrusion is cropped. Bottom: Cr-2 at.% Ti sheet bar sheathed in mild steel and extruded in molybdenum can.

iron, on the other hand, had a rough surface and large variations in thickness. Molybdenum, however, has a thermal expansion coefficient of 1/3 to 1/2 that of chromium. Alloys canned in molybdenum were restrained from contracting on cooling and invariably cracked if the molybdenum component was a significant portion of the total section thickness. It was found that cracking occurred when molybdenum sleeves 0.030 to 0.060 in. (0.0762 to 0.152 cm) thick were used to sheath a 1-in. (2.54 cm)-diameter billet. By using a 0.005-in. (0.0127 cm) molybdenum sleeve, crack-free extrusions with an excellent surface condition were produced consistently. As shown in Appendix A, all the alloys produced in this program extruded without difficulty once the problems of canning materials and cooling rates were resolved.

Extrusions were decanned by pickling with nitric acid. The cleaned extrusions were approximately 6 in. (15.23 cm) long by 7/8 in. (2.22 cm) wide by 3/16 in. (0.476 cm) thick. Local surface defects were removed by grinding on a 120-grit water-cooled abrasive belt. Each sheet bar was then recrystallized by annealing in helium at 1 atm (1010×10^2 N/m^2) for 1 hr at 2400°F (1589°K). The billets were placed in a molybdenum crucible which was heated by induction in a vacuum furnace backfilled with helium. A Pt-10 Rh thermocouple was used to measure and control the annealing temperature.

Rolling

The conditioned and annealed sheet bars were cut into two pieces, each about 2.5 by 0.8 by 0.150 in. (6.35 by 2.03 by 0.38 cm), for rolling to sheet. Before rolling the bars were heated for 30 min at 1800 to 2200°F (1255 to 1478°K) in a tube furnace purged with helium. They were rolled to 0.040-in. (0.102-cm) thick sheet with 10% reduction in thickness per pass on a 2-high Stanat laboratory rolling mill. The mill was 5-in. (12.7-cm) diameter by 8-in. (20.3-cm) wide work rolls that were heated to 800°F (700°K) by internal electrical heaters. All rolling was done at a surface speed of 100 in./min (254 cm/min). The samples were reheated to the rolling temperature in flowing helium for 5 min between passes. Half of the total reduction was accomplished by cross-rolling and the remaining half by rolling in the original extrusion direction, to produce an equiaxed, uniform grain structure in the finished sheet. Data on the rolling conditions and behavior of various alloys are given in Appendix A.

As shown in Appendix A, all but six of the alloys were processed successfully to high-quality sheet. Two alloys (Cr-2Cb, Cr-2Ta) broke up on extrusion and were not reprocessed due to the marginal workability of these compositions. Four other alloys (Cr-2Mo, Cr-2Co, Cr-4Co, and Cr-2Pr) broke up on rolling. The 2-Co and 2-Mo alloys were rolled bare and cracking was probably due to excessive contamination. Alloys with 4% Co and Mo were rolled to good-quality sheet when canned in iron, indicating good workability for these alloy systems. The Cr-2Pr also broke up on rolling bare; in this case, however, failure was deemed to be due to hot shortness. This alloy contained excessive amounts of Pr in the grain boundaries. It was rolled from 2000°F (1366°K), which is above the melting point of Pr (1686°F; 1192°K).

The rare-earth-containing alloys formed liquid phases at the processing temperature used for the other alloys. It was found that rolling from 1900°F (1311°K) and annealing at 1800°F (1255°K) provided the best results in processing alloys with Y, La, and Th. At higher temperatures, samples tended to bond to each other during final annealing.

The most fabricable alloys in this study were those containing Y, La, Pr, Mischmetal, Th, Mn, Zr, and Hf. These alloys at all levels of additions were rolled bare to high-quality sheet with excellent yields. The least workable alloys were those containing Cb and Ta at all levels of additions. Extrusions of these alloys were badly cracked, and the yields on rolling were very low. The solid solution strengthtned alloys containing W, Mo, Re, and Co were very difficult to roll bare but presented no problems in working when clad in mild steel. Cladding also increased the recovery in sample preparation. The rolled sheet was cut into samples before the cladding was removed. This added reinforcement greatly reduced the tendency for specimens to crack during the cutting operation.

4.4 SAMPLE PREPARATION

Rolled sheet was cut into test specimens (0.3 by 0.9 in.; 0.76 by 2.28 cm) with an abrasive cutoff wheel using flood cooling. A specialized fixture was used to position the blanks to ensure accurate cutting of the specimens. Rolled sheet generally was 0.040 to 0.050 in. (0.103 to 0.127 cm) thick as-rolled and was conditioned to a 0.030-in. (0.076 cm) thickness by surface grinding equal amounts from both sides. This process removed any contamination from rolling in air. Double-backed tape was

used to hold the blanks on the surface grinding table, and flood cooling with clear water was used to prevent burning. It was found that the soluble cutting oils commonly used as coolants destroyed the tape adhesive and samples could not be retained on the grinding bed for more than a few passes.

All alloys except the 4Co alloy were successfully ground to finished sheet. The Co alloy was very brittle, and all samples cracked during grinding. No material useful for testing was recovered from this alloy. Some difficulty with cracking was also encountered in processing the 4Zr and the Cr-2Zr-0.25La alloys. High-quality samples free of cracks were readily prepared from all other materials.

After grinding, all specimens were recrystallized for 1 hr at 1800 to 2400°F (1255 to 1589°K) in high-purity helium at 1-atm (1010×10^2 N/m^2) pressure (Appendix A). Samples of each alloy were placed on end in a small molybdenum cup, and several cups were placed in a large molybdenum pipe (susceptor). Top and bottom cover plates were used to provide uniform temperatures for heating by induction. Temperature was measured and controlled with a Pt-Pt/Rh thermocouple inserted in a specimen cup. The chamber was evacuated to $< 10^{-5}$ Torr ($< 1.33 \times 10^{-3}$ N/m^2) and back-filled with high-purity (reactor grade) helium to 760 Torr (1010×10^2 N/m^2). In this program, it was desired to evaluate the effect of selected alloy additions on nitridation behavior. The bend DBTT was used as a measure of alloy effectiveness. It was essential, therefore, that uncontrolled variables such as edge or surface condition not be allowed to alter the results or mask the true effects of alloying. Consequently, the surface and edge of all specimens were electropolished prior to exposure to air, nitrogen, or helium.

Recommended polishing solutions for chromium based on phosphoric, sulfuric, and nitric acids were tried without success. Good surface finishes could not be obtained by straight chemical dissolution or by electropolishing in these solutions. The standard electropolish solution used for molybdenum alloys was found to produce an excellent polish on chromium and its alloys. This solution consists of 25 ml of H_2SO_4 in 175 ml of methyl alcohol. The sample was made the anode and was polished for 3 to 4 min with a current density of 20 to 30 A/in.^{2} (129 to 193 A/m^2) with the solution at room temperature. The polished sample had a mirror finish, and all sharp edges were smoothly rounded. The polish also revealed the microstructure of the alloy and clearly delineated any edge or surface cracks. It permitted screening of samples prior to exposure to reject those that were defective.

A special polishing cell was constructed for electropolishing the test specimens. The specimen was supported at the ends by Pt-Pd-Au alloy strips and dipped into the solution. A Pd-Au alloy sheet cathode surrounded the sample on all sides with a spacing of about 1/4 in. (0.635 cm) in all directions. Each sample was polished 4 min at 20 to 30 A/in.^{2} (129 to 193 A/m^2). Only the center section and edges were polished; the ends at the anode contact points were relatively unaffected. The polished samples were examined for cracks or defects at 10× and 100× magnification on all surfaces prior to test. Cracked specimens were rejected if sufficient samples existed or were used for nitrogen exposures, since these samples were not bend tested after exposure. Crack-free samples were selected wherever possible for air, oxygen, and helium exposures. Each sample were measured and weighed prior to test.

4.5 ENVIRONMENTAL EXPOSURE

Two types of experiments were conducted in this program. In the first type, the effects of different environments on structure and bend ductility were determined. Test specimens were exposed to high-purity nitrogen or oxygen (99.997 + pure) and to air for 100 hr at 2100°F (1422°K). In addition, samples were exposed to high-purity helium for 100 hr at 2100°F (1423°K) to provide a material with the same thermal treatment for comparison. It is not possible to determine conclusively the effects of nitridation and air exposure on the ductile-brittle transition and microstructure unless the thermal exposure factor is taken into consideration.

Exposures to pure oxygen and nitrogen were conducted in a modified Sieverts apparatus in which the volume of gas consumed by the samples could be measured. These measurements, in turn, were converted to weight-gain data to provide basic information on reaction mechanisms and kinetics. Gas-metal reactions are commonly studied by pressure or volumetric techniques, particularly to obtain free-energy data (Ref. 13). In the second type of test, continuous weight change measurements were made at 2100°F (1422°K) and 2400°F (1589°K) to provide data on reaction kinetics in air. These data were compared with results from tests in nitrogen and oxygen by the volumetric procedure.

Baseline and Volumetric Studies

The nitrogen, oxygen, air, and thermal helium exposure for pure gas kinetic and air baseline data were made in a test setup similar to that shown in Figure 5. A Kanthal-wound creep furnace with a 3-in. (7.62 cm)-i.d. by 15-in. (38.1 cm)-long hot zone was used to expose nine samples from one alloy simultaneously. Each sample weighed about 1 g and had a total surface area of about 4 cm^2. The three thermal exposure samples were sealed in a quartz tube filled with high-purity helium. The three air exposure samples were centered vertically in open-ended quartz tubes using a local depression from two sides to keep the sample from falling through. Temperature was measured by a Pt-Pt-10 Rh thermocouple attached to one of the three nitrogen exposure tubes in the center of the furnace. Furnace temperature was controlled to 2100°F ± 5 (1422°K ± 3°) by a second couple adjacent to the windings. The three nitrogen or oxygen exposure samples were placed in closed-end quartz tubes, as shown in Figure 5. These tubes were fastened to a glass manifold by O-ring seals. The manifold in turn was connected to a ballast flask and gas burette for measurement of gas consumption and to a vacuum and nitrogen or oxygen distribution manifold for atmosphere control. The apparatus initially was designed for reaction kinetic studies in pure nitrogen; in later tests, it was used with pure oxygen in place of nitrogen with no modification other than the use of an ice-water cold trap in place of a liquid nitrogen trap.

In operation, the entire system was evacuated to less than 10^{-5} Torr (1.33×10^{-3} N/m^2) and outgassed by warming the glass surfaces. It was then back-filled with high-purity nitrogen or oxygen to a pressure of 1 atm (1010×10^2 N/m^2) and sealed by a stopcock from the gas manifold. The furnace, preheated to 2100°F (1422°K), was then raised into position as shown. The pressure in the system was balanced by 1 atm (1010×10^2 N/m^2) by adjusting the leveling bottle as the gas expanded. Mercury was

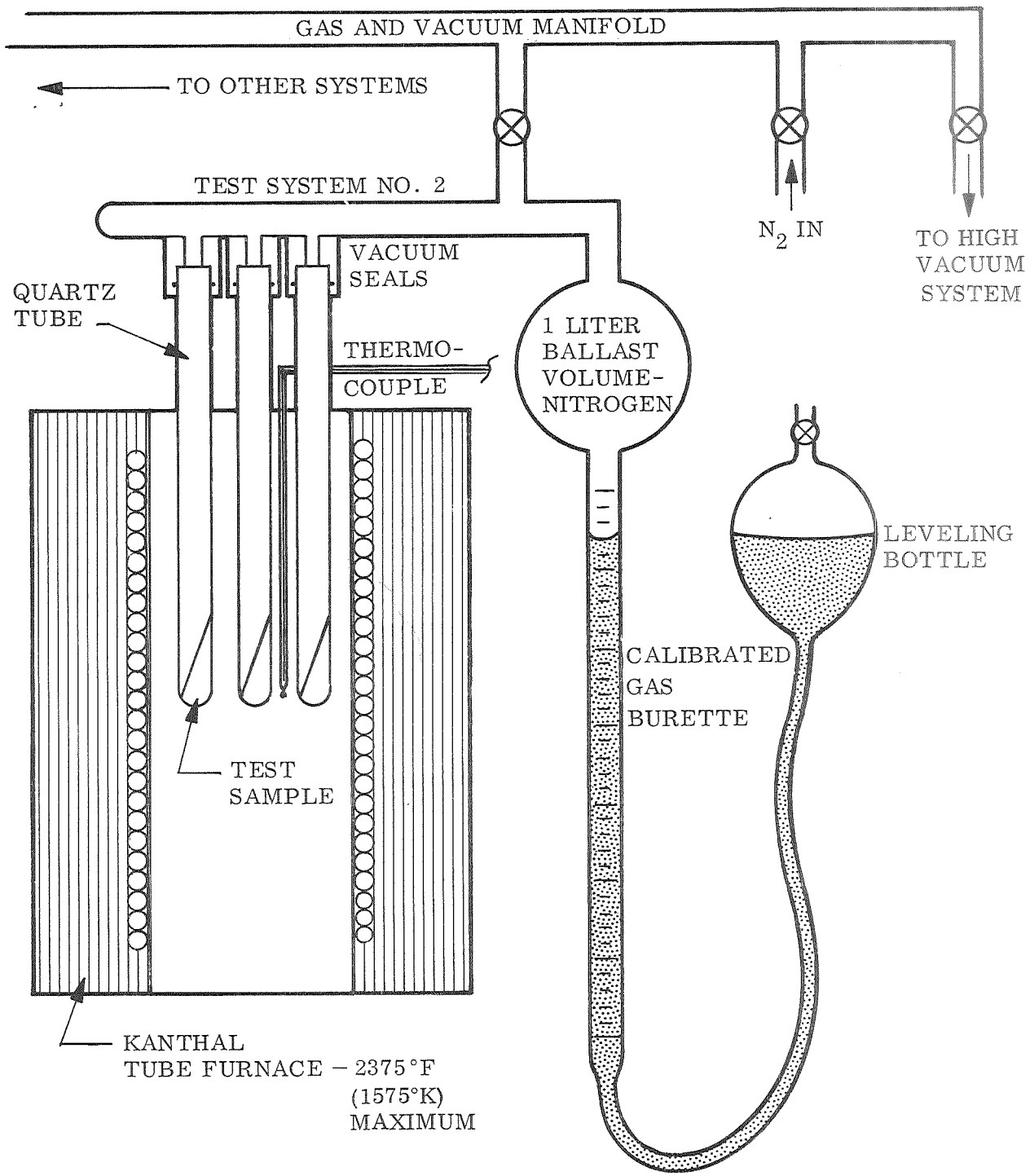

Figure 5 Schematic Diagram of Nitridation Apparatus.

used as the pressure leveling medium. After the initial expansion, periodic readings of gas volume were taken by adjusting the leveling bottle to balance pressure on both sides. The gas was maintained at 1-atm (1010×10^2 N/m^2) pressure by periodic adjustment of the leveling bottle. As gas was consumed by reaction with the samples, mercury rose in the gas burette as a result of the pressure imbalance. Periodically, the leveling bulb was reset to balance the pressure to 1 atm (1010×10^2 N/m^2) in the system, and the total volume of gas consumed was obtained from the difference in mce mercury levels between the initial and final balance points. The system was balanced every 4 to 8 hr during the first 50 hr of test. The burettes were refilled with nitrogen from the manifold as needed to keep the mercury level within a range where readings could be obtained. All measurements of gas consumption were made to the nearest cubic centimeter. The entire system was calibrated initially with inert samples to establish basic hot and cold volumes for reference. All gas volumes were corrected for variations in ambient temperature using a measured expansion factor of 3 cc/°C.

This system has several unique advantages with respect to conducting the program. First, all nine samples were exposed to the same thermal environment, providing a common base for comparison. Second, the air and nitrogen or oxygen samples were handled so that accurate before-and-after weights of specimens and all solid reaction products were obtained. Third, the three nitrogen or oxygen test samples were exposed to identical gaseous environments with respect to pressure and composition. Fourth, a static nitrogen or oxygen atmosphere was used to minimize contaminants; the use of an all-glass system also minimized contaminants. Fifth, a record of nitrogen or oxygen consumption versus time was obtained for all three samples added together. This record was reduced to a per unit-area basis for calculation purposes. A photograph of the four test stands used in these experiments is shown in Figure 6.

Continuous Weight Change Studies

Continuous weight air oxidation studies were performed with an automatic recording thermobalance. A schematic of the apparatus is shown in Figure 7. For these tests, a free-flowing air environment was used in which air was allowed to enter the furnace at the base and flow upward past the test sample. The chimney effect in a heated tube furnace was used to establish the vertical flow in the test section.

The test samples for these tests were 1 by 1 by 0.020 in. (2.54 by 2.54 by 0.076 cm). Each sample was suspended on a platinum wire from a quartz hook located just above the hot zone. Some difficulty was encountered with the continuous weight tests due to air currents in the furnace. A small draft is required to provide an atmosphere of constant composition. Although this was cut to minimum value, the sample tended to move about with a random pendulum motion. Occasionally, the sample wire touched the balance heat shield. At the balance sensitivity required to measure and record the weight gain, some instability and erratic behavior resulted. In most cases, this effect was factored out and a smooth weight-gain curve obtained. Tests were run for 100 hr at 2100°F (1422°K) and 25 hr at 2400°F (1584°K).

Initial tests indicated that some material was evaporating from the samples. A quartz tube was inverted over specimens in two tests to collect and weigh any evaporating species. A thin film of green oxide was collected in each case. The quartz shattered on cooling, however, and it was not possible to obtain a direct measure of the weight of

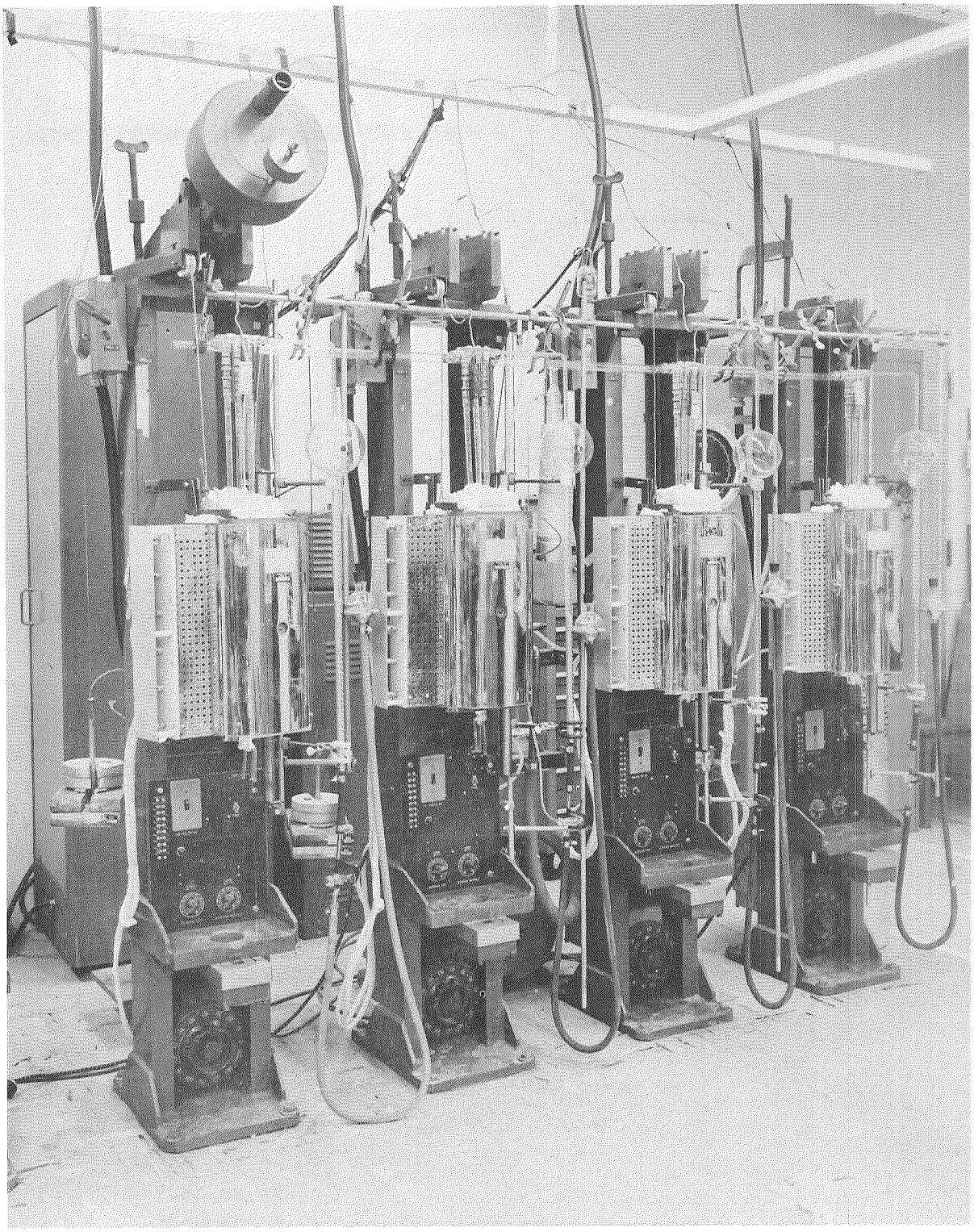

Figure 6 Nitridation/Oxidation Volumetric Test Stands.

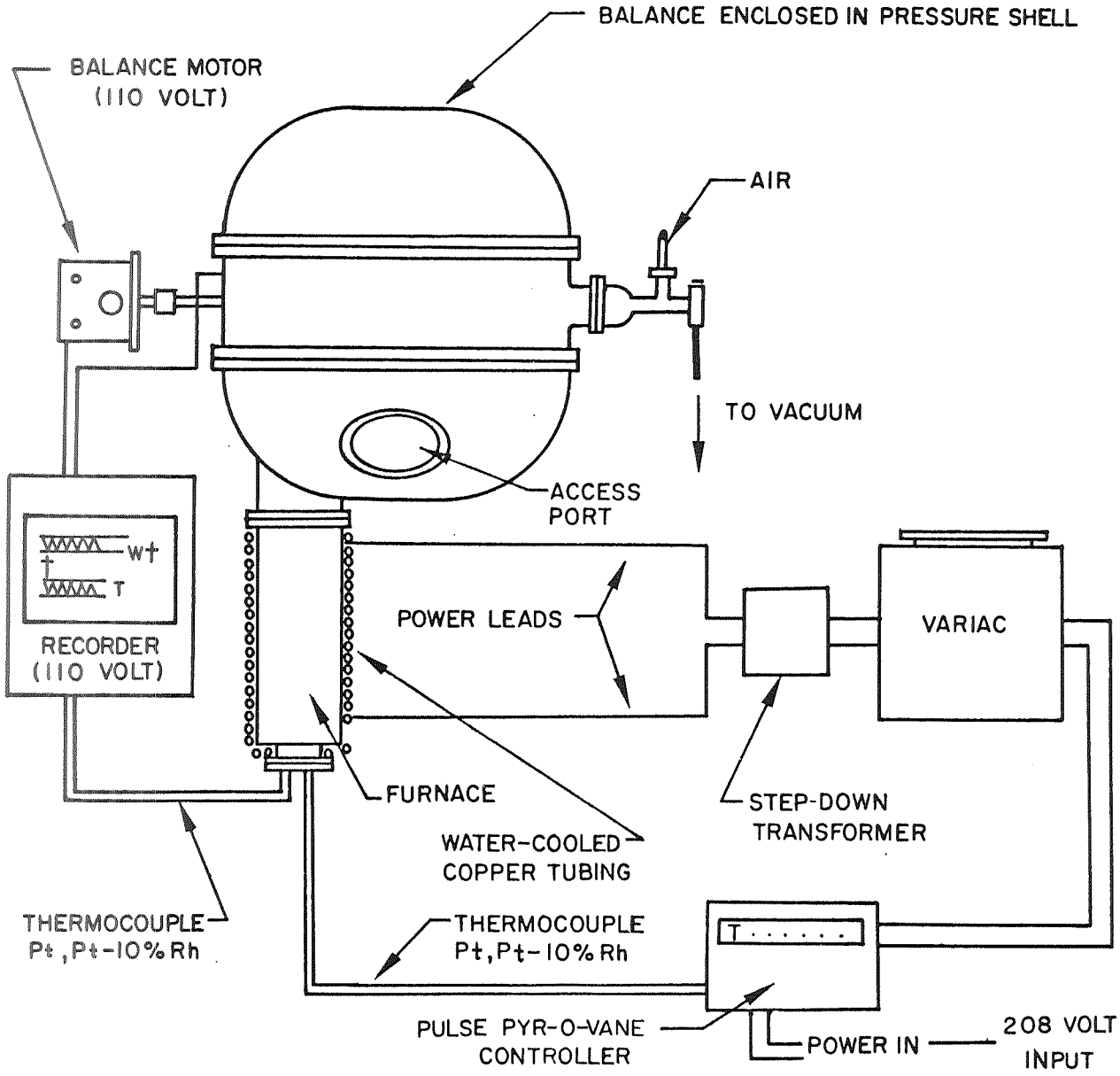

Figure 7 Schematic of Recording Thermobalance System.

condensed material. It appeared that less than a milligram of material was condensed. The measured sample weight gain after test (sample plus oxide scale) and the recorded weight gains were in reasonably good agreement for most tests. In some cases the measured gain was slightly higher than the recorded gain while in other cases it was lower. There was no consistent pattern of behavior, nor was there any indication that evaporation or collection of evaporated species was an important factor in these tests. No attempt was made to collect evaporation products in remaining tests, since the weight loss did not appear to be a significant factor and the experimental technique is unduly complicated.

4.6 TESTS AND EVALUATION

Bend Ductile-To-Brittle Transition Temperature

The ductile-to-brittle transition temperature (DBTT) in bending was determined for the helium-oxygen-, and air-exposed samples. Fixtures and procedures were designed in compliance with the Materials Advisory Board Specification for Testing Refractory Metals (Report MAB 192-M).

The bend test appratus consisted of a three-point loading fixture adapted to a tensile test machine. The sample was supported on stainless steel blocks with a span of 0.5 in. (1.27 cm). Each block had a 0.050-in. (0.127 cm) radius at the support points. A stainless punch with a radius of 0.125 in. (0.318 cm) was used to make the bend by forcing it down between the specimen supports at a fixed cross-head speed of 1.0 in./min (2.54 cm/min). The bend radius with 0.030 to 0.032 in. (0.076 to 0.08 cm) sheet was 4.17 to 3.90t, depending on exact sheet thickness. The bend fixture was enclosed within a hinged-door tube furnace that could be heated to 1800°F (1255°K). The specimen temperature was measured by a chromel-alumel thermocouple contacting the specimen surface next to the punch. The temperature was controlled by a second couple located at the furnace windings. The apparatus was installed in a 200-lb (90.8 kg) tensile test machine. The load versus ram travel was recorded on a chart, allowing calculation of bend angle at fracture in partially ductile fractures and control of the process to bend to a 90° angle in the case of ductile tests.

The samples to be tested were placed on the bend anvil with no load applied and were held for 5 min or until temperature became steady at the desired test level. A load of less than 1 lb (0.45 kg) was then applied by hand and the cross-head motion of 1 in./min (2.54 cm/min) was started to produce the bend. Cross-head motion was reversed when a 90-deg bend had been achieved or when fracture occurred as indicated by a drop in load. In general, the first bends for each alloy were made with the thermal control (helium) samples to establish the baseline behavior. A starting temperature of 400°F (478°K) was selected for each material. Subsequent bends were made at temperatures 200°F (93°K) higher or lower, depending on whether the failure was brittle or ductile. As experience was gained with each alloy and condition of exposure, the actual transition temperature could be approximated in 2 or 3 tests to within ±100°F (±38°K). In all cases, careful evaluation of behavior in preceding tests with similar materials was needed to bracket the DBTT with the three test samples available for evaluation.

Hardness

Knoop (KHN) or Vickers diamond pyramid hardness (DPH) readings were taken on all metallographic samples with a microhardness tester. A 100-g load was applied to form the indentation. An average of the diagonal measurements of the square impression was used to calculate the DPH number. A minimum of three readings was taken across the sheet thickness on each sample to obtain an average hardness value. If the readings were widely scattered, additional readings were taken to establish reliable values. Multiple traverses were made on all Task I binary samples. Nitride case thickness and hardness were measured in the samples where distinct nitride cases had formed on the surface during air exposure.

Metallography

Special metallographic procedures developed by W. C. Coons (Ref. 14) were applied to preparation of the chromium alloys for microscopic studies and magnifications to 3000×. Details of the equipment and procedures are given in Reference 14. One-half of a fractured bend test specimen was sandwiched between linen-phenolic tabs and mounted in red bakelite. The mount was ground on 600-grit silicon carbide paper to form a flat surface and was given an initial polish with 1-μ diamond paste. Final polishing was done on an automatic polisher, using a special blend of polishing oxides. Two cubic centimeters of a stock solution of 2 g NaOH and 35 g $K_3Fe(CN)_6$ in 200 cc H_2O were added to the polishing well of the automatic polisher to facilitate preparation of a smooth, scratch-free surface. The samples were etched electrolytically in a solution of 20 parts HF, 10 parts HNO_3, and 100 parts water for 1/2 sec at about 10 V.

Transmission Electron Microscopy

The crack sensitivity of chromium and chromium-base alloys at room temperature precluded the use of conventional die punching as a means of obtaining suitable specimens. Limited attempts to obtain such specimens by electrochemical machining and spark discharge met with little success, primarily because most common electrode materials erode at a rate that significantly exceeds that of chromium or its alloys. Consequently, a new thin-foil preparation technique was developed for chromium-base materials.

All the foils examined in this program were prepared by the disc method. For this purpose, several 2.3-mm-diameter discs were removed from the flat sections of bend specimens. Specimens were thinned to 0.015 in. (0.038 cm) by abrasive belt polishing. Disc removal was accomplished with an ultrasonic impact grinder, using a 0.23-cm-i.d., type 304 stainless steel, energy transfer tube coupled to a carborundum-water slurry. Basically, the operation consisted of transmitting the sonic energy to the stainless steel tube, which set up vibrations in the slurry. These vibrations caused the carborundum particles adjacent to the tube end to move about, causing a grinding action that paralleled the contour of the tube. The grinding action produced a microscopic groove whose depth progressively increased with time until complete penetration of the wrought section was achieved. All discs were subsequently lightly ground on 120-grit energy and ultrasonically cleaned in methyl alcohol. Thinning of the discs was accomplished in a twin-jet electropolisher using a bath consisting of 20 parts $HClO_4$ plus 80 parts ethyl alcohol

(by volume) refrigerated to 32°F (273°K). Optimum results were achieved with an applied voltage of 10 V and a current density of 3.5 A/cm^2. After polishing, the foils were washed in ethyl alcohol cooled with liquid nitrogen and ultrasonically cleaned in methyl alcohol. The foils were examined at magnifications of 15,000 to 60,000 diameters with a Siemans Elmiskop 1A-125 electron microscope. Gun tilt was used to develop maximum contrast in the field. Specimens were examined with both bright and dark field techniques. Electron diffraction patterns were taken on selected precipitates for possible identification. All prints were enlarged to 2× to provide a final magnification of 30,000 to 120,000× for evaluation of structure.

X-Ray Diffraction Analysis

Selected samples of oxide scales were characterized by x-ray diffraction using Debye-Scherrer techniques with powder samples and Ni-filtered Cu-K alpha radiation. Calculated d-values were compared with those of known materials using standard ASTM cards for identification.

Electron Microprobe Analysis

Selected samples were examined for distribution of O, N, Cr, and alloy additions with an Applied Research Laboratories EMK electron-beam probe microanalyzer. The nitrogen peak was standardized on a sample of Cr_2N, and the oxygen peak was standardized on ZrO_2 for scanning of those elements. Element distributions were studied both by counting scans and by x-ray image techniques. Specimen current and backscattered electron images also were made to define structural features. Samples were studied at magnifications of 250 to 8000×. Standard metallographic specimens were used and corresponding light micrographs were provided as guides to general structure.

Chemical Analysis

All chemical analyses were made by the Oregon Metallurgical Corporation, Albany, Oregon. Vacuum extraction and inert gas fusion were used for hydrogen and oxygen analyses. Nitrogen was measured by the micro Kjedahl process, and carbon was determined by the conductrimetric method. Standard wet chemical procedures were used for metallic alloy additions.

Section 5
EXPERIMENTAL RESULTS

5.1 REACTION WITH NITROGEN

Unalloyed chromium and 42 binary alloys from Task I were exposed to high-purity nitrogen for 100 hr at 2100°F (1422°K). The volume of nitrogen consumed was measured for three samples of each alloy as a function of time. Readings were converted to weight gain per unit area using the density of nitrogen at ambient conditions. The data are tabulated in Appendix B. Plots of the data were made to establish reaction kinetics, and the results along with actual measured weight gains after exposure are summarized in Table 2.

All the samples (0.3 by 0.9 by 0.030 in.; 0.76 by 2.28 by 0.076 cm) for each alloy were converted completely to chromium nitride (Cr_2N) in 30 to 80 hr at 2100°F (1422°K). As shown in Table 2, the nitrogen contents based on both measured and calculated (from gas volume) weight gains range from 9.3 to 11.9 wt%. The stoichiometric composition of Cr_2N is 11.86 wt% nitrogen. The value obtained for pure chromium exposed to nitrogen was 11.38 wt% nitrogen based on the total weight gain after 100 hr at 2100°F (1422°K). The effect of alloying on the nitrogen content after 100-hr exposure to pure nitrogen is summarized in Figures 8 and 9. The solid solution additions that do not form nitrides (W, Mo, Re, and Ru) all reduce the total nitrogen content. This is the result of a reduced amount of material to form nitrides in the sample and does not necessarily indicate increased resistance to nitridation. All the other alloy additions form nitrides, and the total nitrogen content after exposure is essentially the same as that found for unalloyed chromium (Figure 9).

Reaction Rates

As shown in Table 2, the measured weight gains in most cases are in excellent agreement with the total weight gains calculated from nitrogen consumption (volume) data. These data clearly indicate that the volumetric measurements provide accurate data on reactions that occur and can be used with confidence to calculate reaction rates. All the alloys exhibited parabolic kinetics in their reaction with nitrogen. Typical data for a Cr-1Y alloy are plotted in Figure 10. A straight line of slope 1.97 is obtained from a log/log plot of the data. The slope n for parabolic kinetics is 2 from the relation

$$w^n = kt \qquad (1)$$

where

w = weight gain/unit area
t = time
k = rate constant

Table 2

RESULTS OF NITRIDATION STUDY

Alloy	Nitridation Behavior[a]					
	Measured		Calculated		Parabolic Rate Constant $[(mg/cm^2)^2/hr]$	Conversion Time (hr)
	Weight Gain (mg/cm^2)	Nitrogen Content (wt %)	Weight Gain (mg/cm^2)	Nitrogen Content (wt %)		
Cr	33.20	11.38	31.50	10.85	18.20	40
Cr – 1W	31.65	11.06	29.95	10.53	12.50	70
2W	32.18	10.67	29.98	10.04	12.85	50
4W	30.99	9.81	28.79	9.18	10.50	70
1Mo	34.39	10.25	32.40	10.00	14.30	50
4Mo	32.43	11.84	29.98	10.15	13.60	50
1Re	31.89	10.88	32.29	10.99	14.55	50
2Re	30.52	10.31	30.38	10.27	16.95	50
4Re	30.06	9.89	27.93	9.23	10.00	75
1Ru	31.25	10.99	29,08	10.30	15.30	40
2Ru	30.3	10.87	27.7	10.00	14.4	50
4Ru	30.2	10.32	29.3	10.05	18.2	45
1Mn	32.46	11.24	30.60	10.68	13.70	60
2Mn	32.01	11.31	28.92	10.45	12.00	65
4Mn	32.27	11.26	31.68	11.07	14.75	48
1Fe	33.1	11.32	33.6	11.50	18.9	45
2Fe	32.7	11.20	32.2	11.03	25.6	37
4Fe	29.5	10.70	28.5	10.4	36.7	23
1Co	31.4	11.27	31.1	11.2	18.0	50
0.5Ti	34.8	11.46	35.8	11.78	22.10	37
2Ti	30.74	12.00	33.18	12.83	21.40	35
0.5Zr	31.59	11.32	30.19	10.87	13.65	40
2Zr	32.31	11.37	33.18	11.64	13.30	60
0.5Hf	33.4	11.34	33.2	11.27	15.1	39
2Hf	34.6	11.42	34.7	11.43	19.6	39
0.5V	32.75	11.24	31.75	10.96	13.40	60
2V	32.31	11.27	30.85	10.82	13.25	50
0.5Cb	32.4	11.27	34.2	11.79	16.5	42
0.5Ta	31.83	11.21	31.80	11.20	15.10	50
0.5Y	31.8	11.33	30.60	10.93	15.2	50
1Y	32.3	11.36	30.65	10.86	12.7	64
2Y	30.3	10.88	28.95	10.42	9.9	60
0.5La	31.69	11.27	30.94	11.03	12.25	70
1La	31.43	11.26	31.14	11.16	12.90	65
2La	32.05	11.25	31.02	10.92	10.75	80
0.5Pr	32.1	11.35	30.18	10.80	14.7	50
1Pr	31.5	11.35	28.85	10.44	15.2	42
0.5MM	31.70	11.25	28.71	10.30	12.85	40
1MM	32.05	11.24	26.92	9.61	12.80	30
2MM	31.69	11.23	29.99	10.00	12.75	50
0.5Th	31.68	11.22	31.76	11.24	11.90	60
1Th	32.52	11.04	35.00	11.78	16.60	30
2Th	31.80	10.80	31.94	10.80	11.65	65

(a) 100 hr – 2100°F (1422°K) – Nitrogen

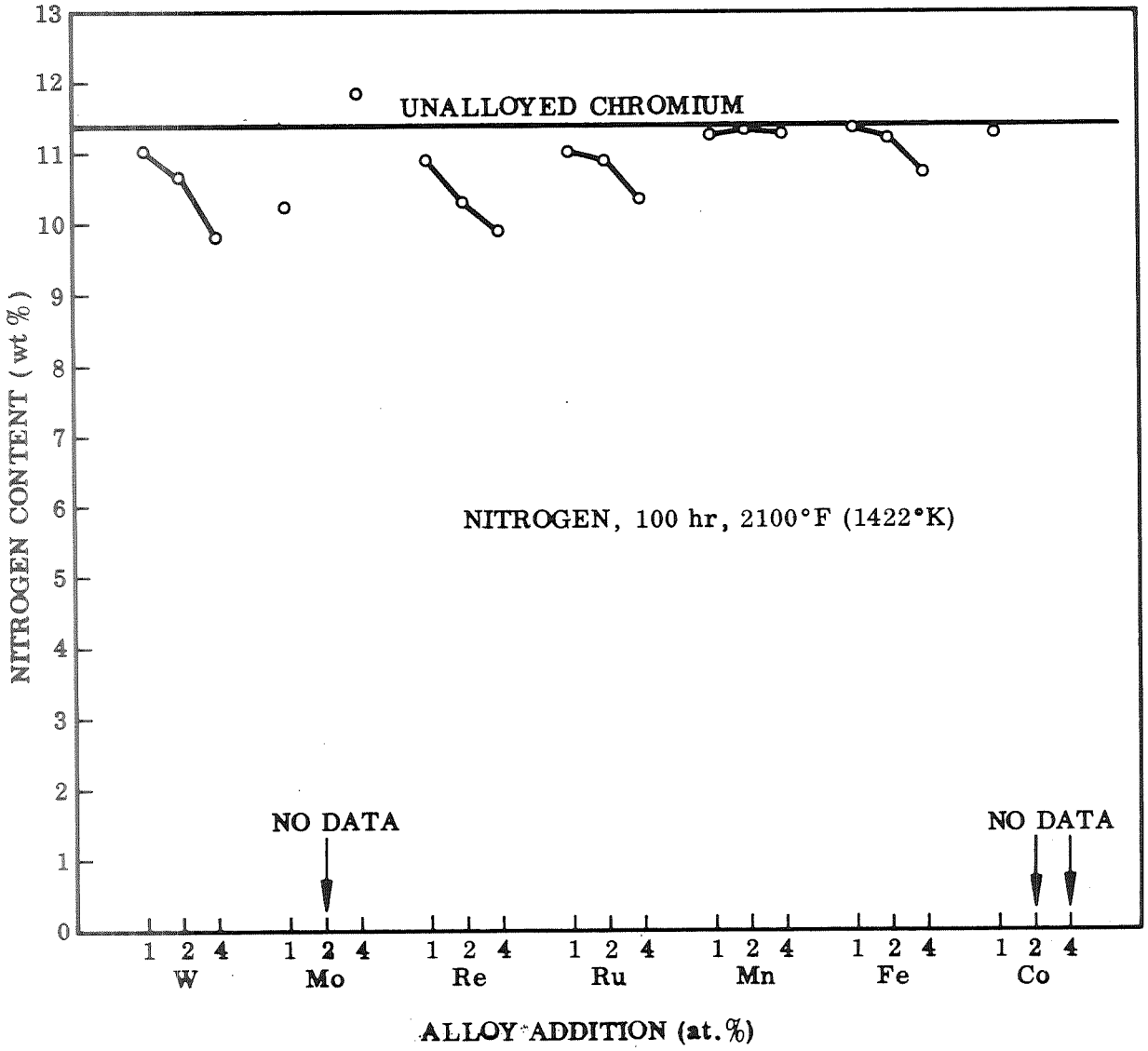

Figure 8 Effect of Solid-Solution Strengtheners on Nitrogen Content.

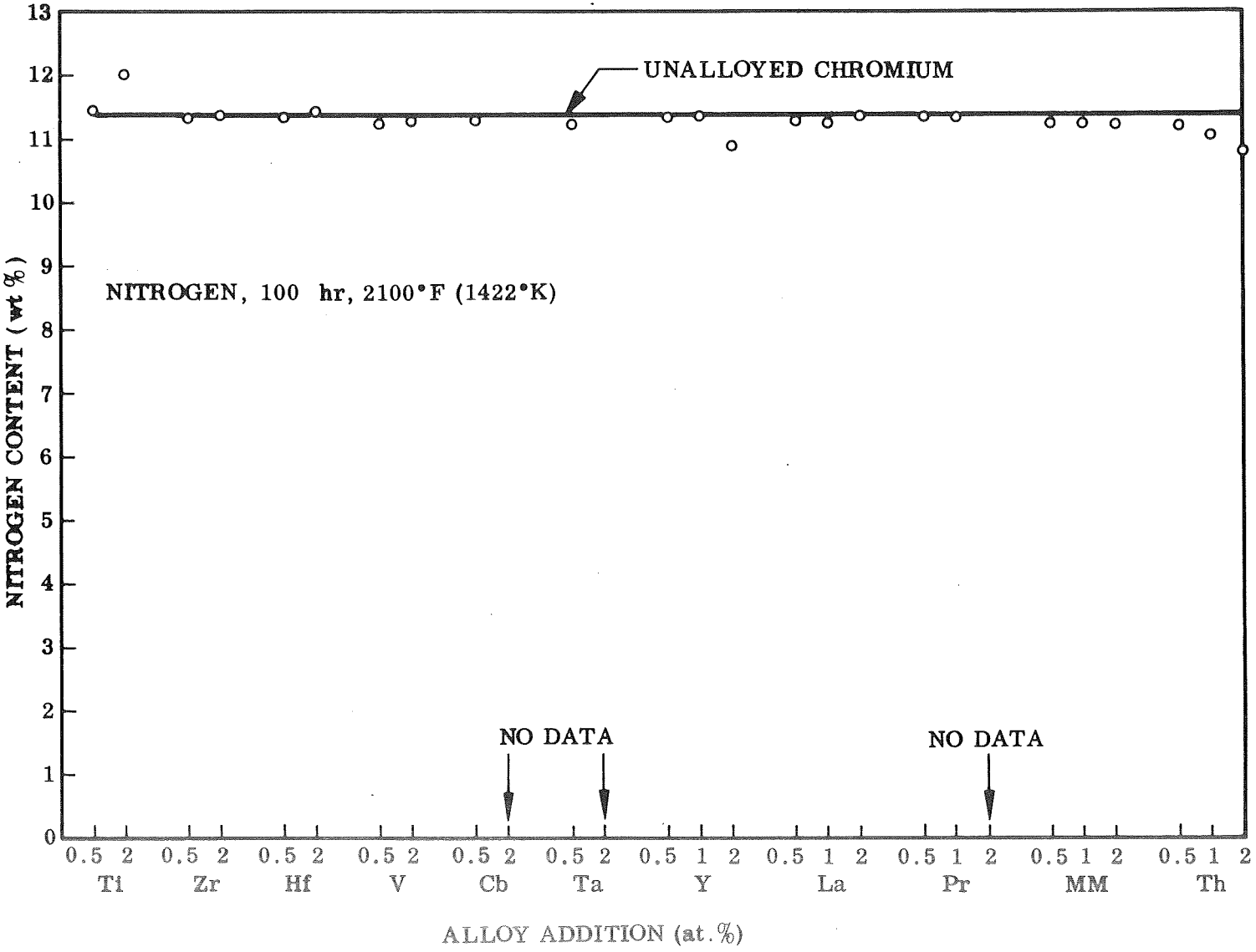

Figure 9 Effect of Nitride Formers and Rare Earths on Nitrogen Content.

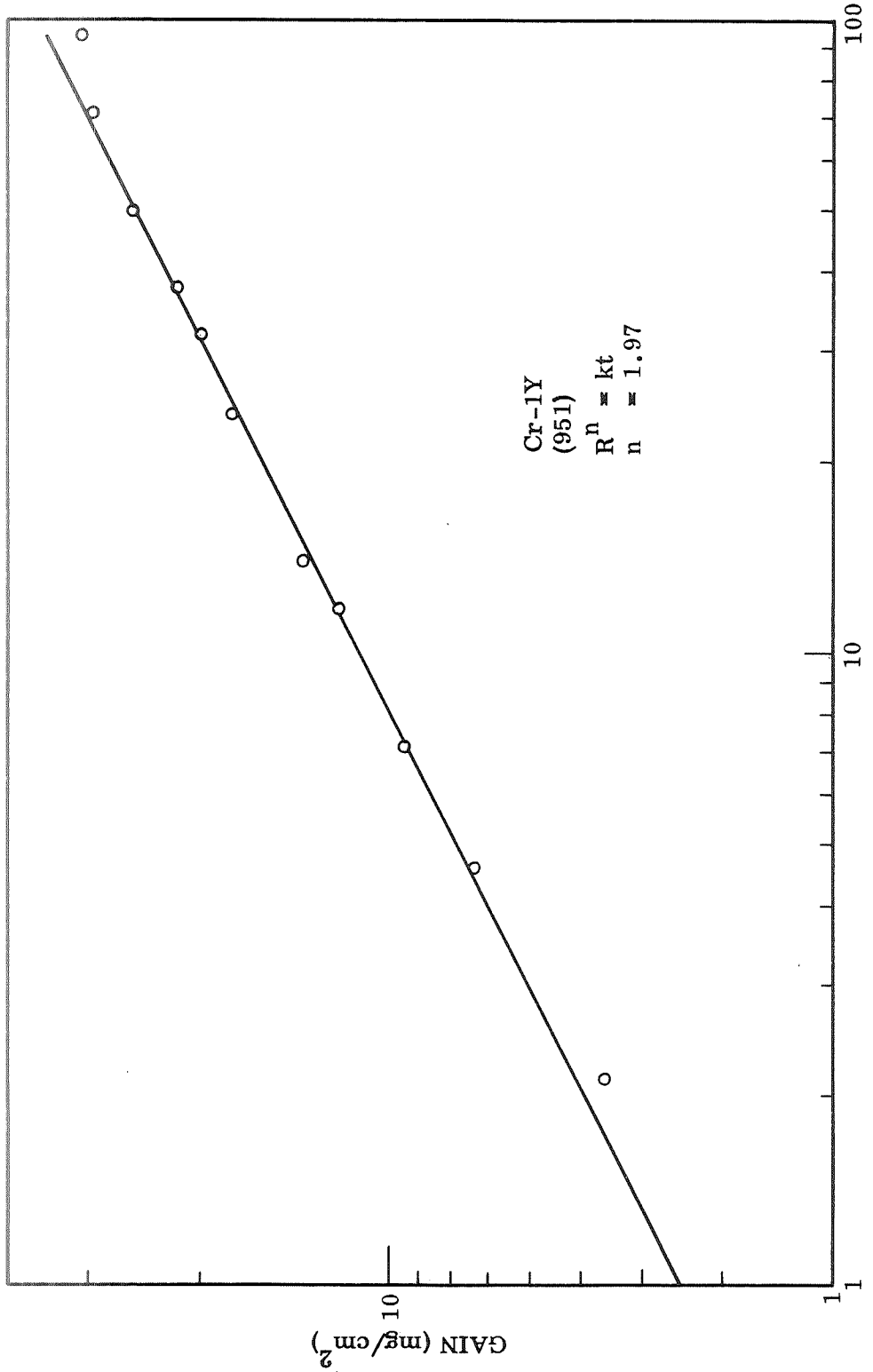

Figure 10 Log/Log Plot of Typical Nitridation Data, 2100°F (1422°K) – Nitrogen.

The rate exponent n for all alloys tested ranged from 1.75 to 2.22, with the majority of values lying between 2 and 2.2. No significant effect of alloying on the rate exponent was found.

Alloying did affect the rate of reaction, however, as shown in Figure 11. The parabolic rate constant is the slope of the straight line obtained from a plot of the square of the unit weight gain $(mg/cm^2)^2$ versus time. As shown in Figure 11, the slope is low for the Cr-Y alloys and high for the Cr-Ti alloys. Unalloyed chromium has a rate constant of 18.2 $(mg/cm^2)^2$ hr. The effect of alloying on the rate constant is summarized in Figures 12 and 13. The values range from a low of 9.9 for Cr-2Y to a high of 36.7 for Cr-4Fe. Actual values are presented in Table 2. The data as plotted in Figures 12 and 13 show no consistent effect of alloying; that is, all alloy additions except Fe and Ti reduce the reaction rate constant by about the same amount. No significant trends are indicated. Titanium and iron accelerate reaction rates and are the only additions found to have a detrimental effort.

As shown in Figure 11, the weight gain curves departed from a parabolic rate law after 40 to 80 hr and began to level off. This behavior results from the fact that the sheet is fully converted to a nitrogen-deficient Cr_2N at this point. This compound has a varying composition with a homogeneity range of 9.3 to 11.9 wt%. The lower limit in equilibrium with Cr is reached in less than half the time of exposure (100 hr), and the balance of exposure consists of final adjustment in composition to approach the nitrogen-rich (11.9%) phase boundary that would be in equilibrium with the gas phase. The kinetics at this point will depart from the initial parabolic kinetics since all the Cr has been converted to nitride.

As shown in Table 2, the time for conversion varied from a low of 23 to a high of 80 hr. No systematic influence of alloying on conversion time is indicated. The variations most likely result from variations in thickness and surface area to volume relations of the different test samples.

Structure and Properties

All the alloys with the exception of those containing Zr, Hf, and the rare earths appeared to be single-phase nitrides after exposure. Typical sections of the alloys that had distinct two-phase structures are shown in Figure 14, along with the structure of nitrided unalloyed chromium. The nitride first forms as a case on the surface. Gradually it grows inward from each side until the two advancing fronts meet at the centerline of the sample. At this point, conversion is complete and further adsorption of nitrogen adjusts composition to approach an equilibrium level. In all cases the structure is columnar with a growth interface at the centerline. Grain size varies, depending on the alloy; Zr and Hf additions give the finest structures. The large amount of second phase in these alloys nucleates a fine-grained structure. In none of these alloys (Zr, Hf, Y) could the second phase be identified as a nitride of these elements. In Zr and Hf alloys, the second phase was rapidly attacked by etchants used to delineate structure. The behavior was similar to that of the $Cr_2Zr(Hf)$ phase existing in the alloys prior to exposure. The second phase in Cr-Y alloys could not be retained on metallographic polishing. Only voids existed where particles or stringers of Y were located in the alloy prior to exposure.

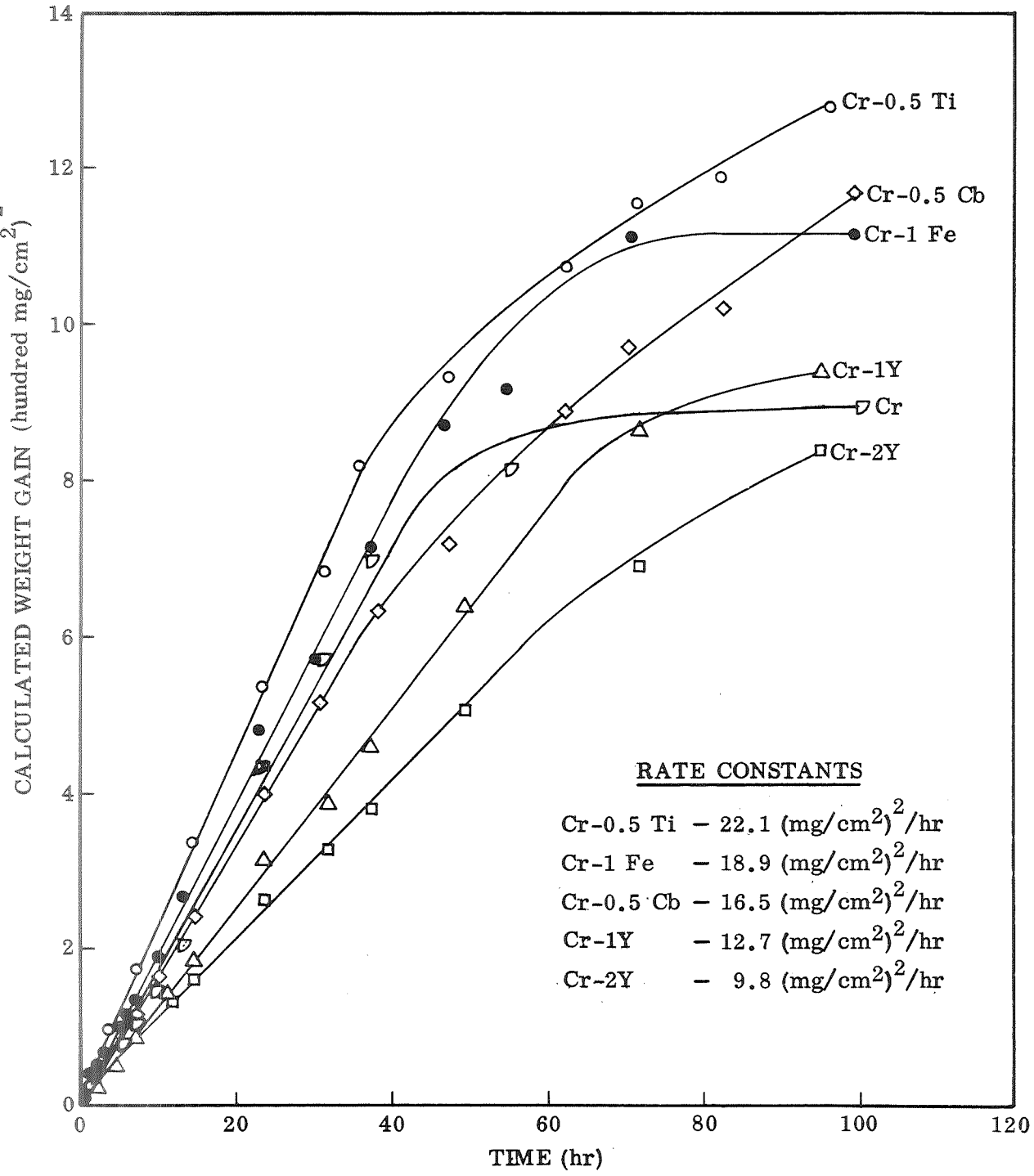

Figure 11 Typical Nitridation Parabolic Rate Curves for Chromium Alloys, 2100°F (1422°K) – Pure Nitrogen.

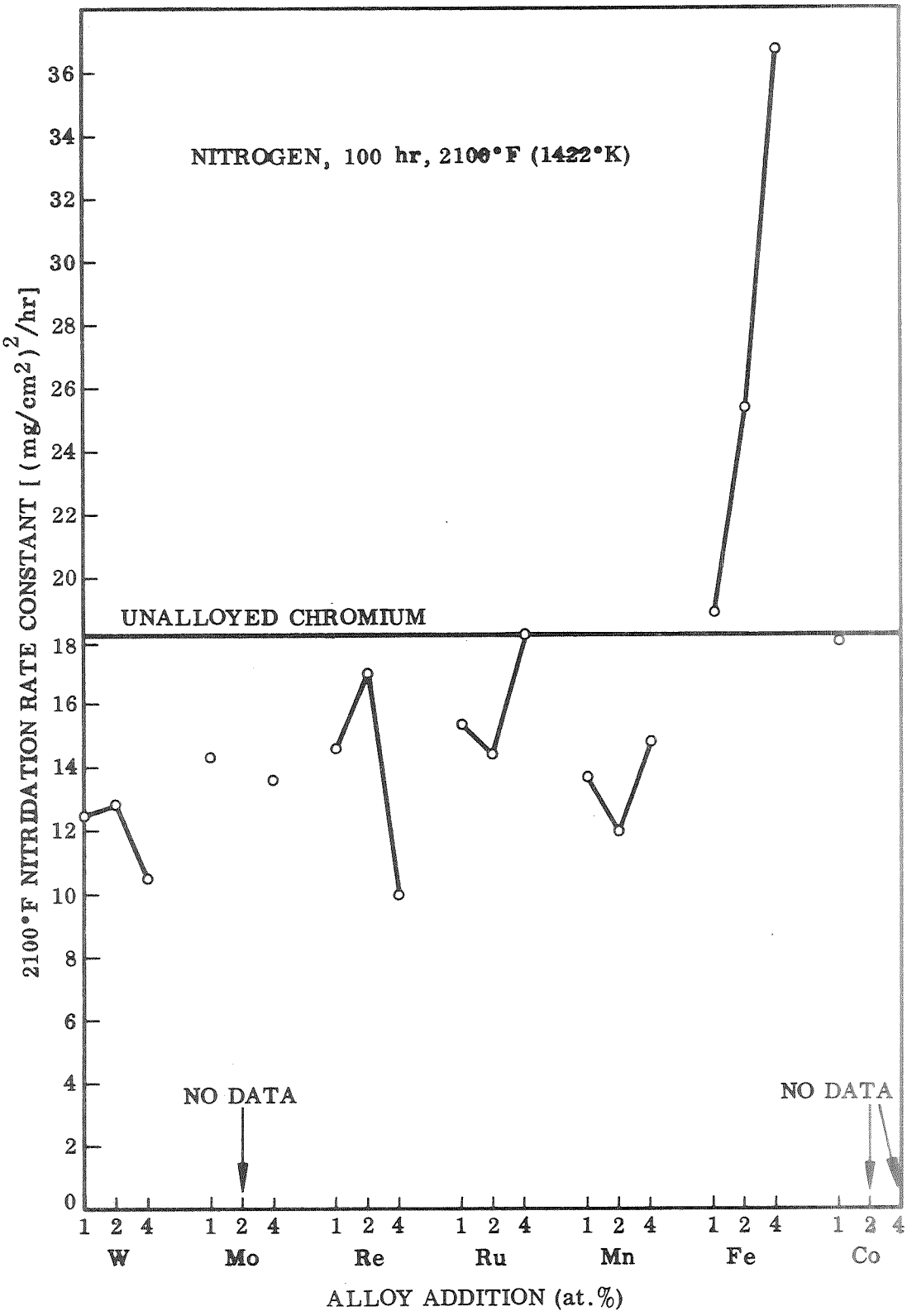

Figure 12 Effect of Solid-Solution Strengtheners on Nitridation Rate Constant.

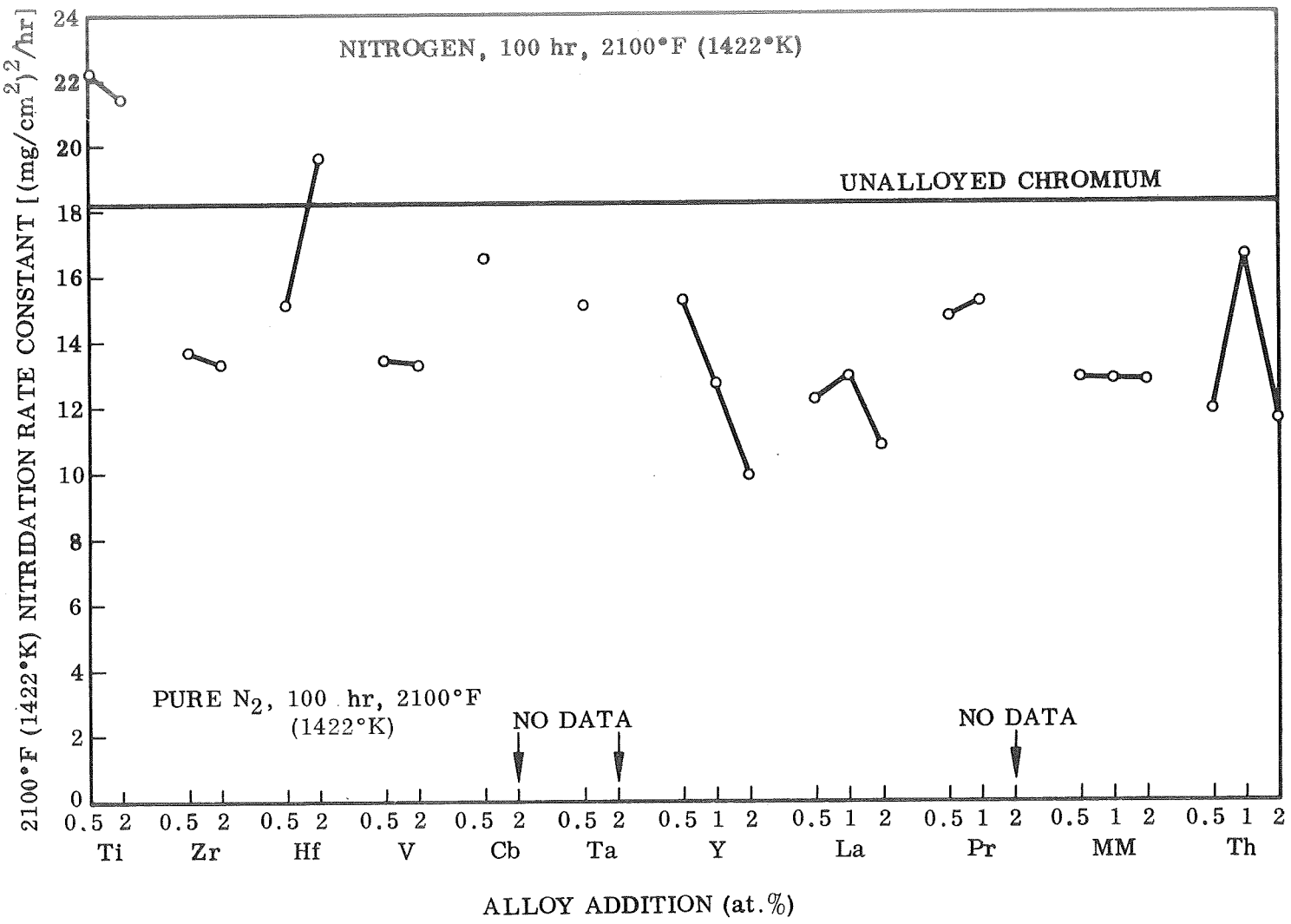

Figure 13 Effect of Nitride Formers and Rare Earths on Nitridation Rate Constant.

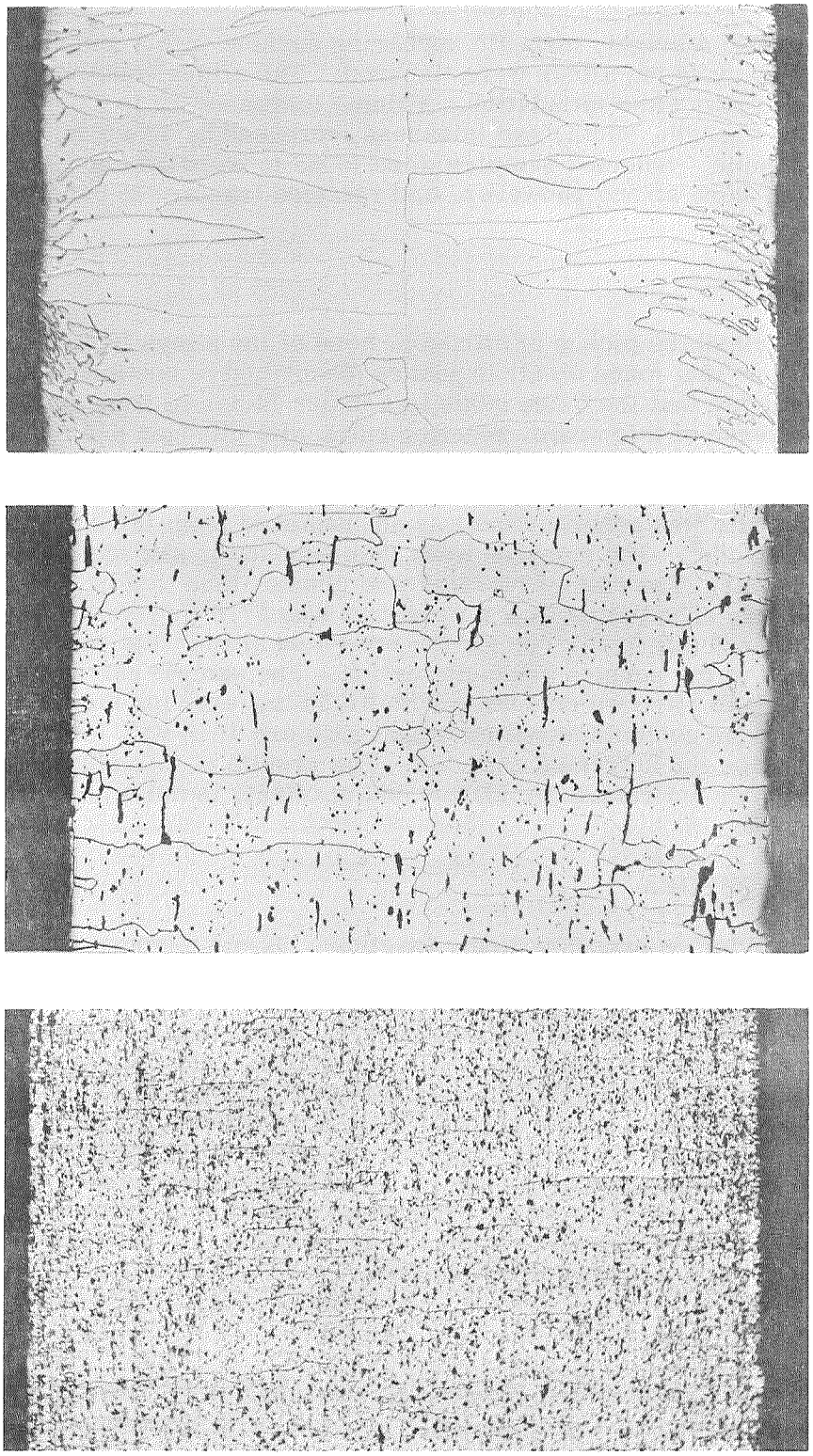

Figure 14 Cross Section of Nitrided Cr and Cr Alloys, 100 hr-2100°F (1422°K)-N_2, ×100.

All the nitrided alloys had a bright, metallic appearing surface with a smooth satin finish. The edges of many of the alloys were fissured. The alloys containing Y and Pr, however, had no cracks after nitridation. Volume increased 20 to 25% on conversion to the nitride. Length, width, and thickness increased by 7 to 8 mils (0.018 to 0.020 cm) for each sample. Selected samples were found to be brittle at 1800°F (982°K). The samples were strong, however, and resisted fracture in handling, cutting, and mounting.

Effect of Oxide Scales

Although alloying did retard the pickup of nitrogen, none of the alloys had resistance to nitridation comparable to that found on air exposure (described in section 5.3). Tests in nitrogen clearly indicate that the oxide scale is a major factor in resistance to nitridation. In the absence of this scale, reaction rates with nitrogen are extremely rapid. The effect of an oxide scale was checked by preoxidizing a sample prior to nitridation. Three samples of Cr-1La were exposed to oxygen for 50 hr at 2100°F (1422°K). The oxide scale was adherent and was not removed from the surface. The weight gain was 1.1 mg/cm^2. The samples were then exposed to nitrogen for 100 hr at 2100°F (1422°K). The rate of reaction was greater than that of samples that had not been preoxidized. The parabolic rate constant was 17.0 (mg/cm^2)^2/hr for the preoxidized sheet and 12.9 (mg/cm^2)^2/hr for the untreated alloy. The oxide scale was intact and still adhered to the surface after nitridation. The sample gained 30.4 mg/cm^2 total weight on exposure to nitrogen compared with 31.14 mg/cm^2 for the untreated alloy. Calculated nitrogen contents based on weight gain are 10.8 wt% for the preoxidized and 11.2 wt% for the untreated samples. The results of this study show that an oxide scale per se does not retard nitridation and,in effect, is not a protective coating.

5.2 REACTION WITH OXYGEN

The differences in behavior on exposure to air (section 5.3) and nitrogen (section 5.1) indicates that oxygen has an important role in the mechanism by which alloying retards nitridation. The development of a clear understanding of this mechanism, therefore, will require an understanding of the effect of alloying on the reaction with oxygen. These reactions were studied for unalloyed chromium and 10 binary alloys of chromium with Y, La, Cb, Zr, and Mn. These alloys were selected to represent the three different classes of binary alloys on the basis of their demonstrated potential for improving resistance to nitridation on air exposure (section 5.3). The samples were exposed to oxygen in the volumetric apparatus by the same procedures as used for nitrogen exposure. Gas consumption was measured as a function of time to obtain data on reaction kinetics. The exposed samples were evaluated for structure, ductility, and hardness. The data are tabulated in Appendix C.

Reaction Rates

The results of studies of reactions with oxygen are summarized in Table 3 and Figs. 15 through 24. The data are given on log-log plots for evaluation of rate law behavior. As shown in Table 3, the agreement of measured weight gains in oxygen with the gains calculated from the volume of oxygen consumed is excellent. as with the nitridation tests, the volumetric measurements provide a valid measure

Table 3

RESULTS OF OXIDATION STUDIES

Alloy	Oxygen – 2100°F				Air – 2100°F Weight Gain				Air – 2400°F		
	Weight Gain		Rate Exponent(a)	Parabolic Rate Constant	Static Test	Continuous Test		Rate Exponent(a)	Weight Gain Continuous Test		Rate Exponent(a)
	Meas. (mg/cm^2)	Calc. (mg/cm^2)		[$(mg/cm^2)^2/hr$]	(mg/cm^2)	Meas. (mg/cm^2)	Recorded (mg/cm^2)		Meas.	Recorded	
Cr	7.68	8.90	4.2 (< 11 hr) 1.7 (> 11 hr)	0.78	10.68	–	–	–	–	–	–
Cr-0.1Y	2.37	2.55	5.3	–	2.44	4.69	(b)	(b)	9.83	9.08	3.9 (< 6 hr) ∞ (> 6 hr) SS @ 11 hr
Cr-0.25Y	1.93	2.05	5.3	–	2.95	4.09	3.54	1.6 (< 6 hr) 5.3 (6 – 23 hr) 2.2 (< 23 hr)	22.0	22.6	2.8 (< 9 hr) SS @ 21.5 hr
Cr-0.5Y	1.70	1.62	∞	–	2.44	0.12	0.66	1.6 (< 10 hr) 4.4 (> 10 hr)	9.10	8.99	1.6 Initial 5.3 Final SS @ 9 hr
Cr-0.1La	1.63	1.43	5.3	–	1.84	1.92	3.30	1.4	13.89	14.46	1.1 Initial ∞ Final SS @ 5 hr
Cr-0.25La	2.14	2.07	5.3	–	3.20	0.29	0.31	1.0 (< 7 hr) 4.8 (> 7 hr)	8.82	8.62	1.9 Initial 3.8 Final
Cr-0.25Cb	8.21	9.68	1.5	~ 1.0	6.06	6.35	5.90	1.5 (< 9 hr) 2.2 (> 9 hr)	(b)	51.12	2.3
Cr-1.0Cb	25.36	25.63	1.5 (< 33 hr) 0.92 (> 33 hr)	~ 1.5	22.13	8.56	8.29	1.6 (< 18 hr) 6.0 (> 50 hr) SS @ 18 hr	36.98	26.86	4.4 Initial 1.6 Final
Cr-1.0Zr	3.58	2.82	2.2	0.22 (< 25 hr) 0.044 (> 30 hr)	4.61	1.82	1.26	1.0 (< 6 hr) 2.7 (10 – 30 hr) ∞ (> 30 hr)	(c)	39.02	1.8 (< 15 hr) Sat. @ 20 hr
Cr-3.0Zr	15.77	14.94	1.9	2.28	11.33	11.99	12.53	2.7 (< 30 hr) 5.1 (> 30 hr) SS @ 30 hr	12.00	10.64	6.5
Cr-3.0Mn	16.00	16.34	1.7 (< 13 hr) 2.3 (> 13 hr)	3.24 3.24	20.57	14.18	15.29	2.6	28.55	26.08	2.0

(a) Exponent n in $W^n = kt$ (general rate equation). SS = scale separation. Sat. = sample saturated; no further gain.
(b) Erratic data.
(c) Scale exploded on removal from furnace; no weight measurement.

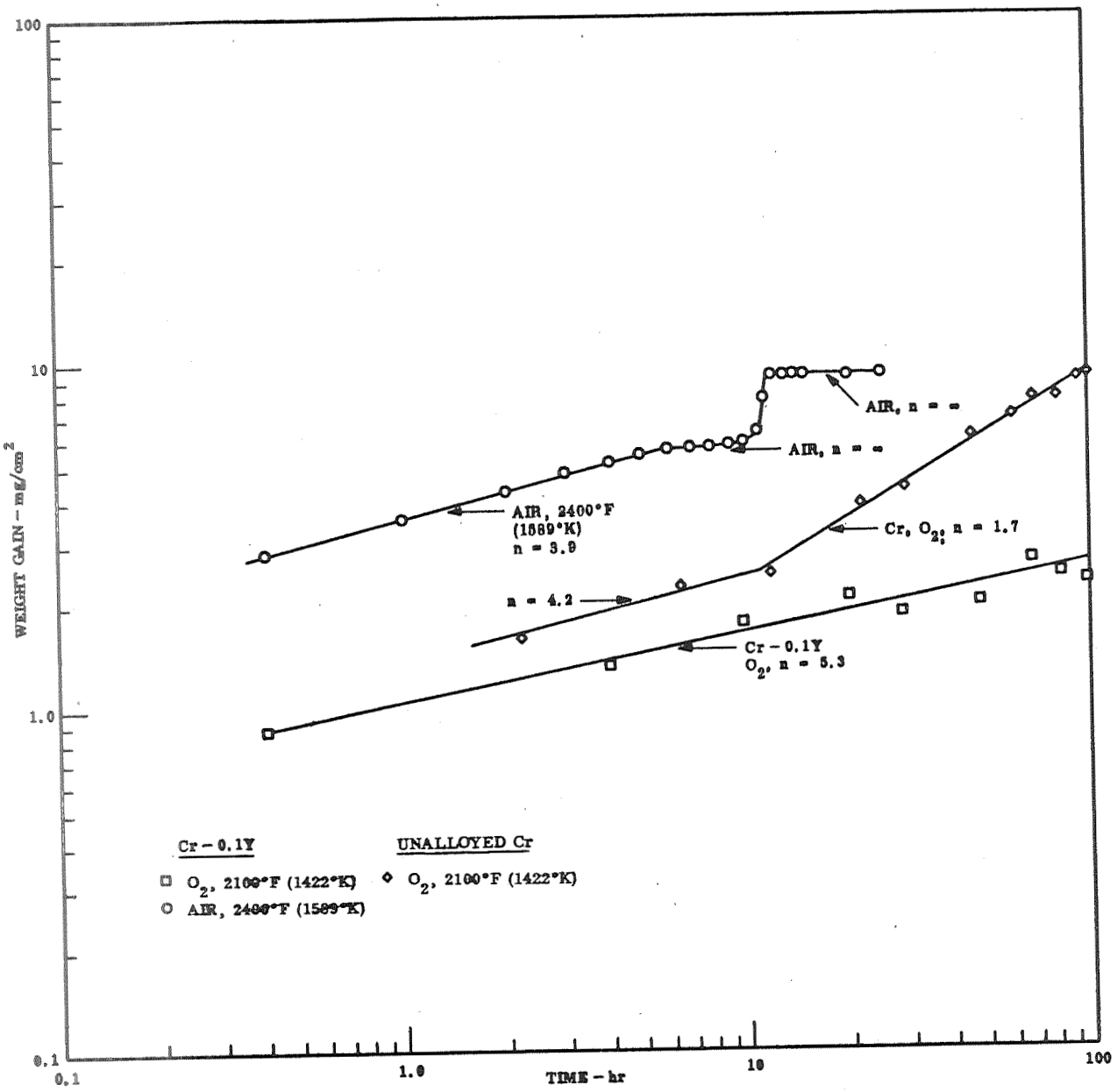

Figure 15 Oxidation Kinetics, Cr – 0.1Y .

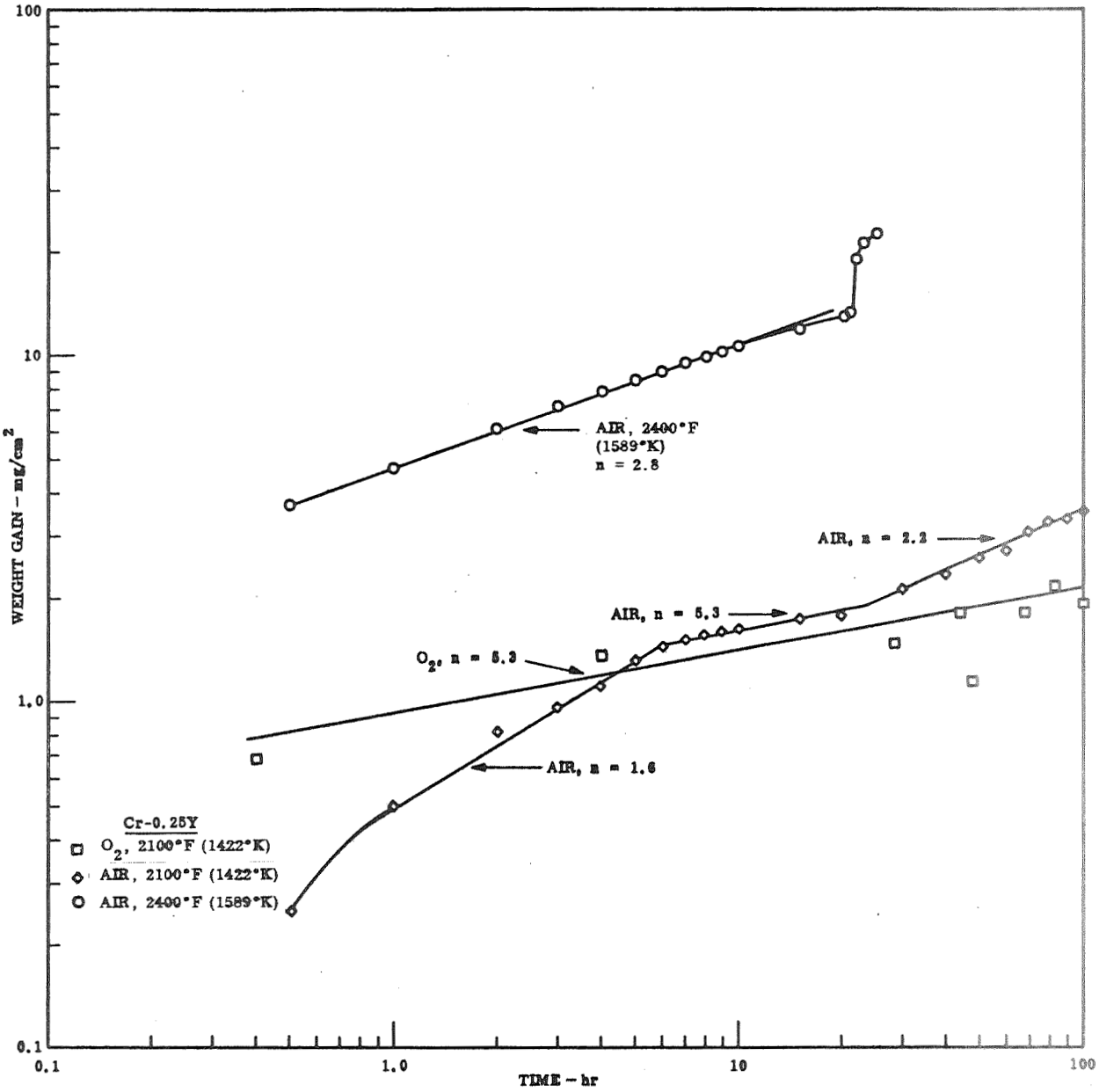

Figure 16 Oxidation Kinetics, Cr-0.25Y.

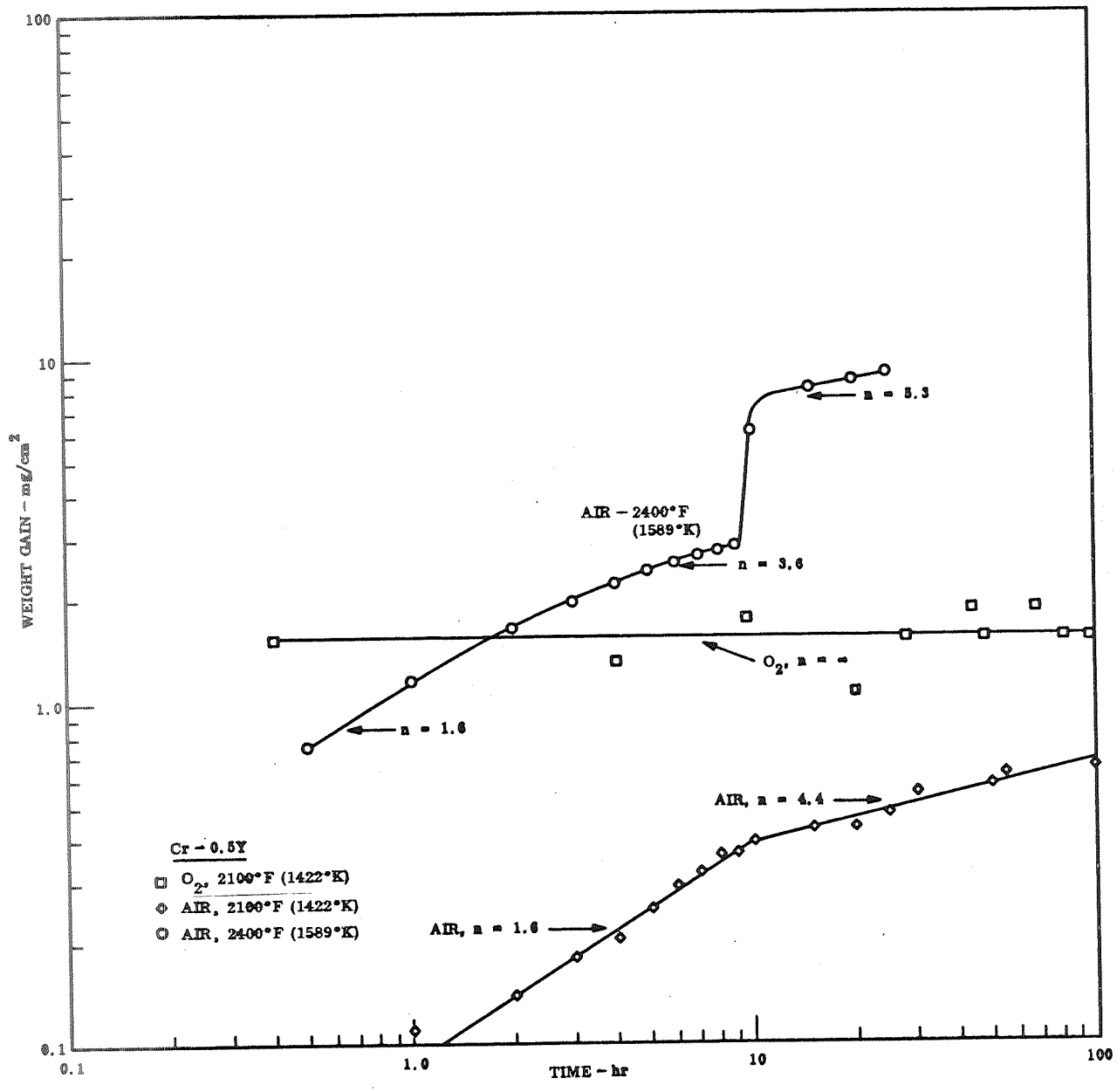

Figure 17 Oxidation Kinetics, Cr – 0.5Y.

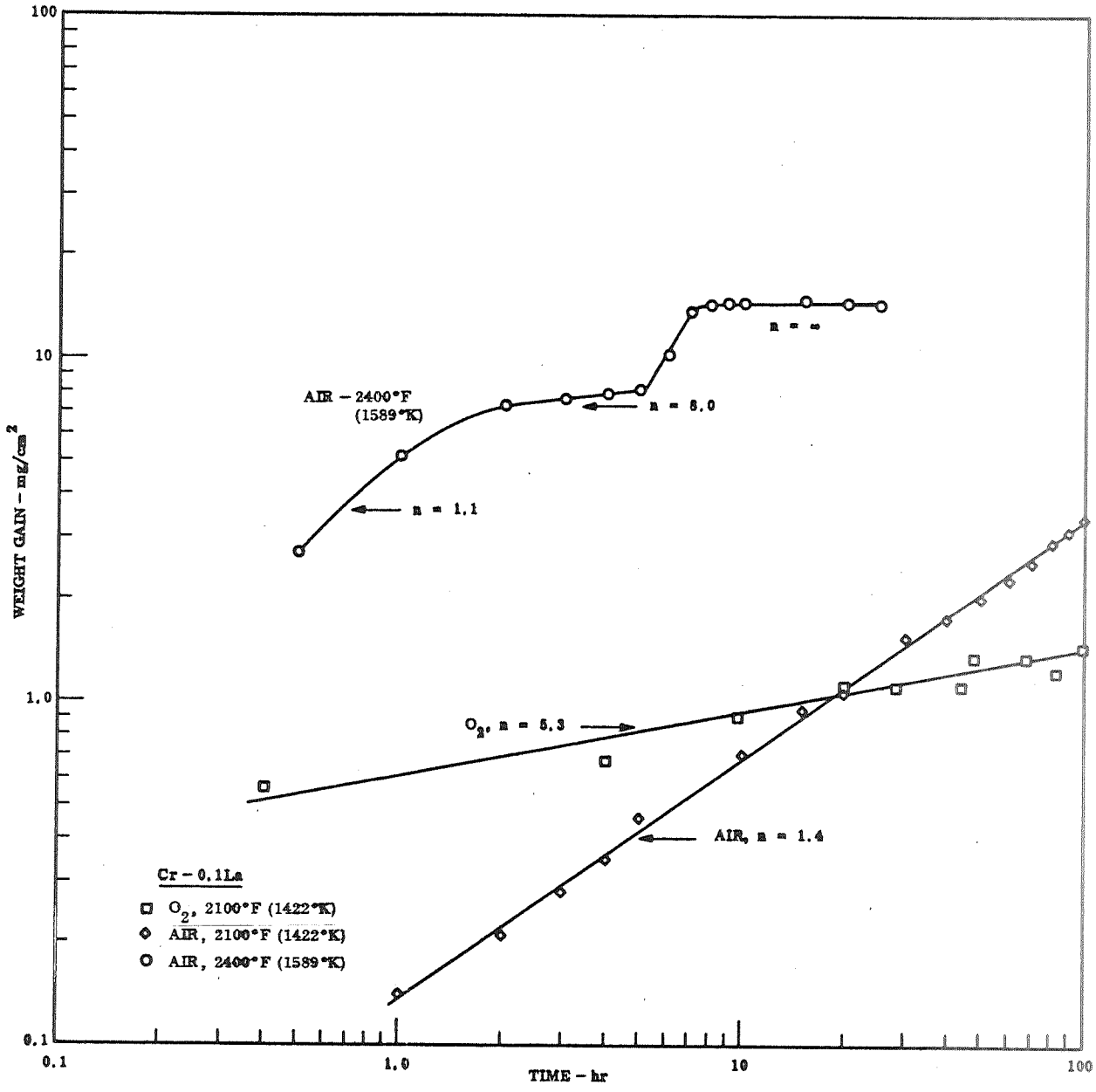

Figure 18 Oxidation Kinetics, Cr – 0.1La.

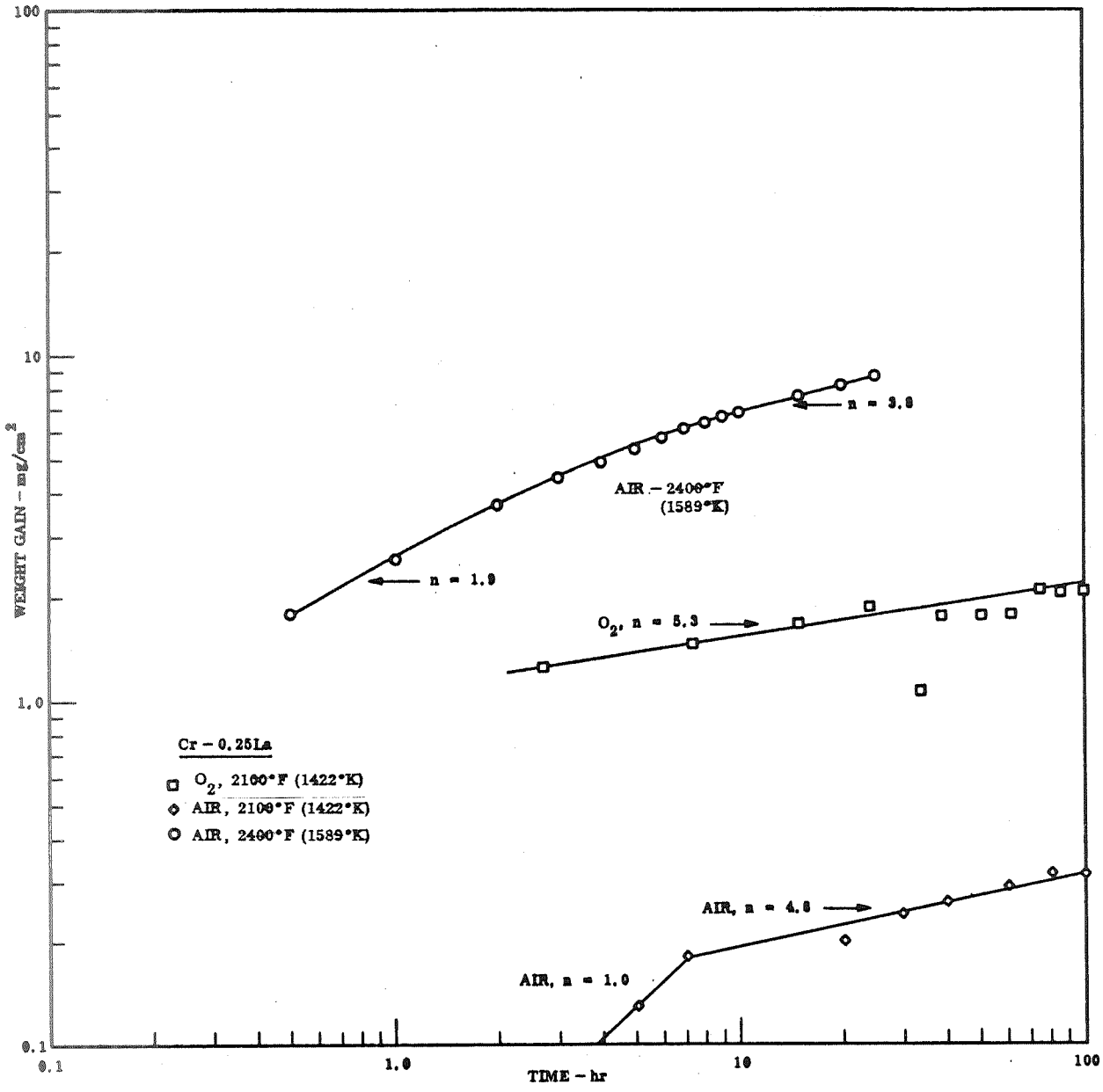

Figure 19 Oxidation Kinetics, Cr – 0.25La.

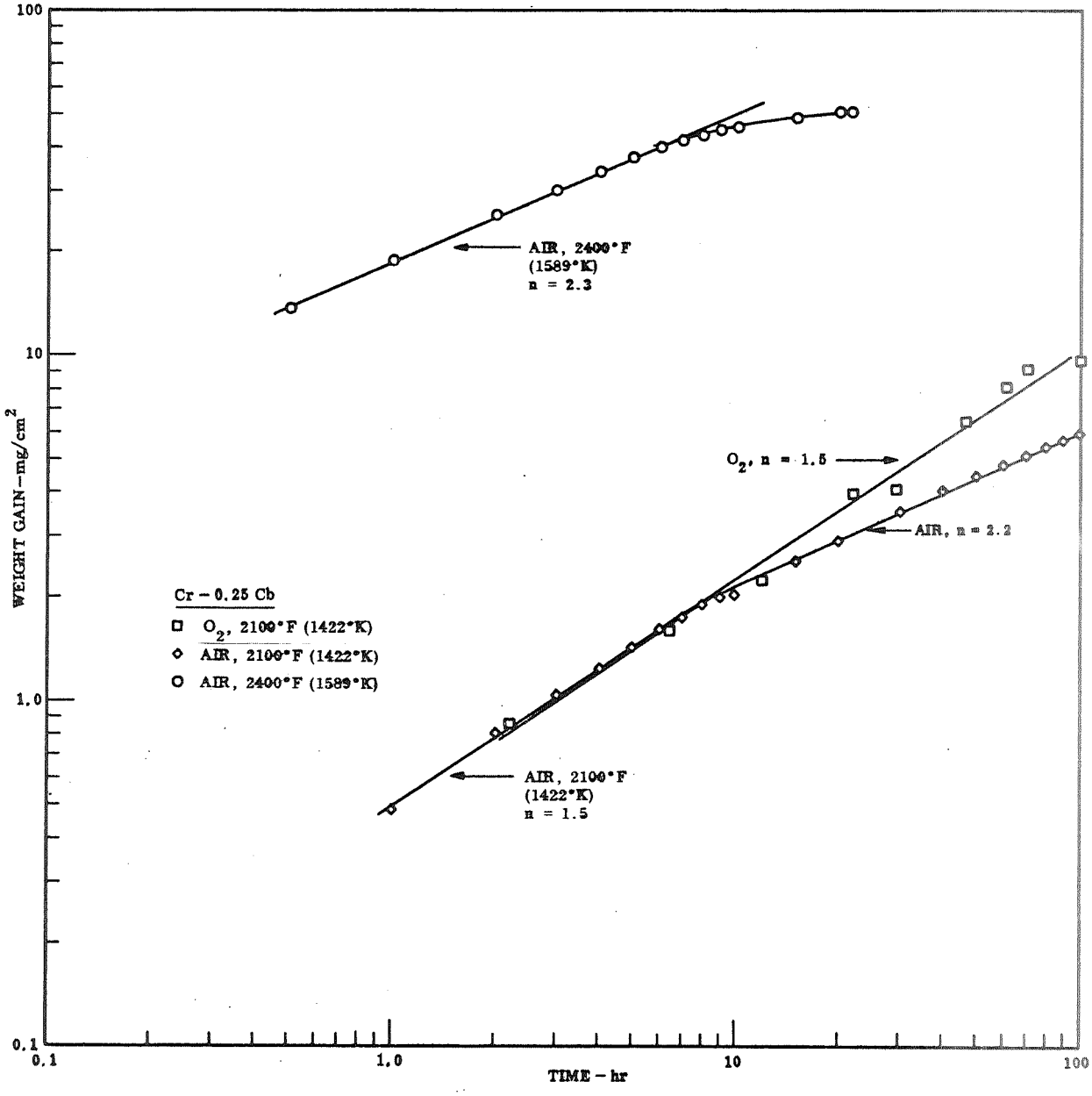

Figure 20 Oxidation Kinetics, Cr – 0.25Cb

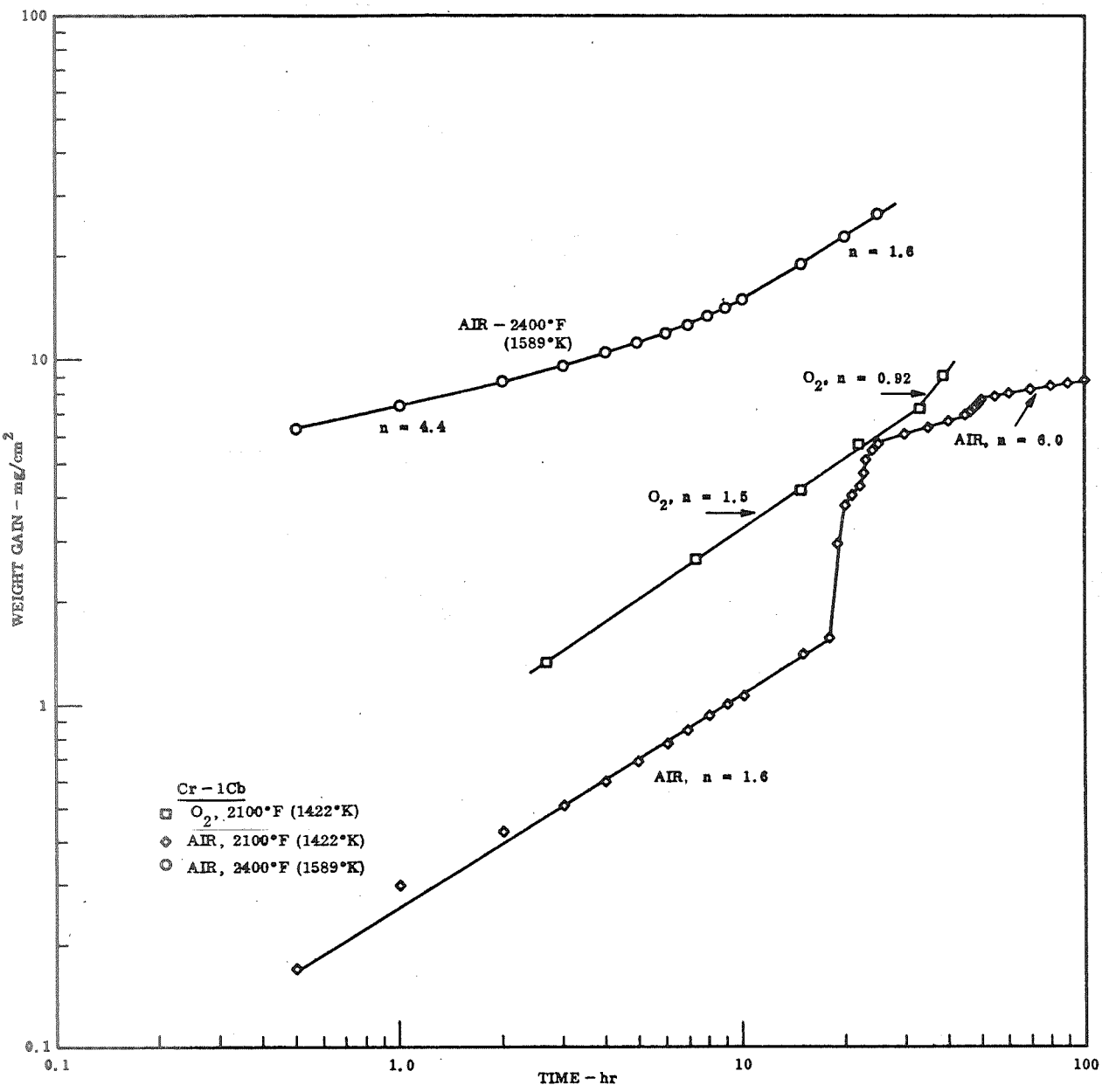

Figure 21 Oxidation Kinetics, Cr – 1.0Cb.

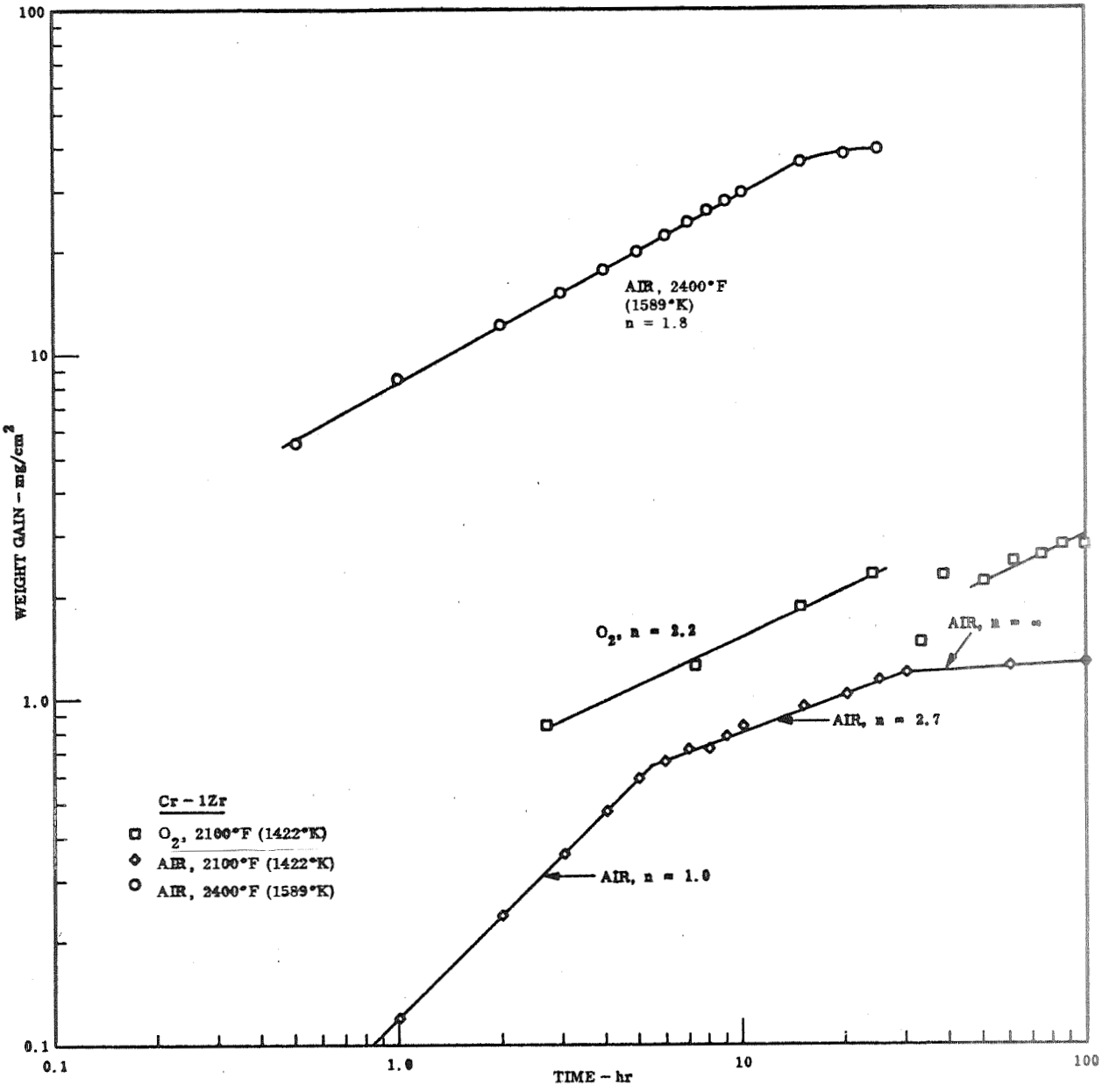

Figure 22 Oxidation Kinetics, Cr – 1.0Zr

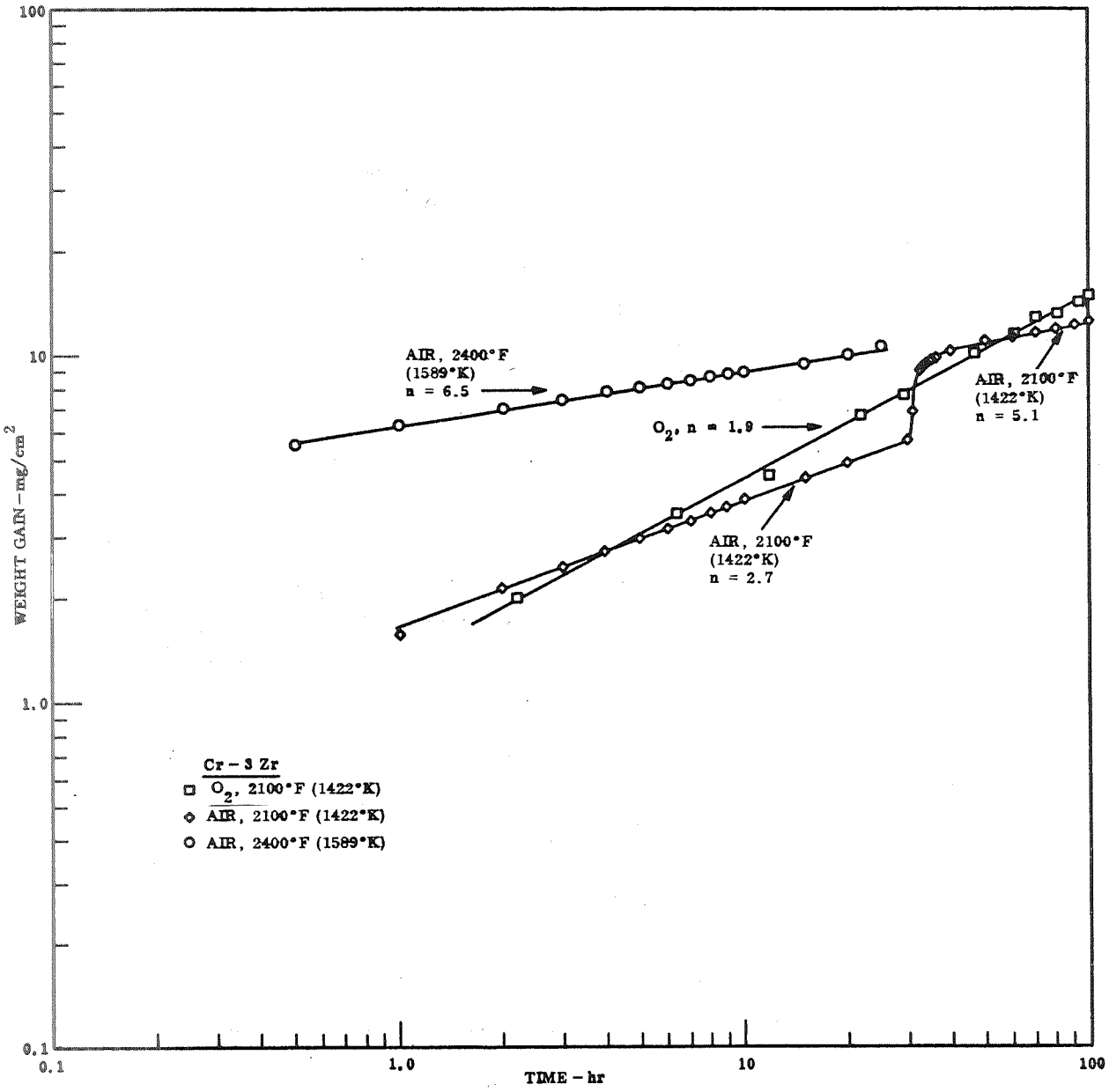

Figure 23 Oxidation Kinetics, Cr – 3.0Zr.

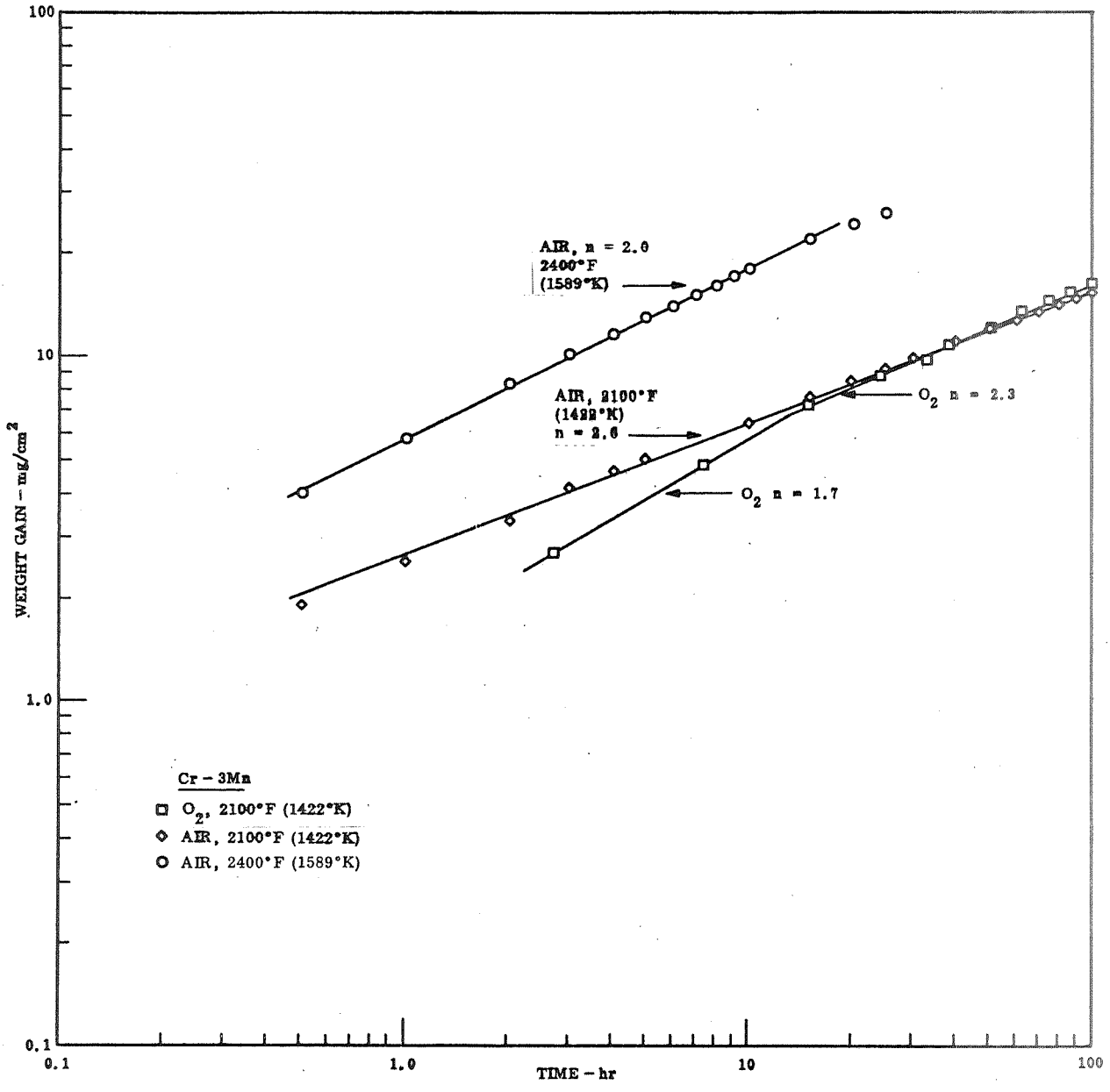

Figure 24 Oxidation Kinetics, Cr – 3.0Mn.

of the reaction that occurs. The scatter in data, however, is greater than that observed in nitridation tests due to the comparatively small volume consumption. In the nitridation tests, samples consumed over 300 cc of N_2 in 100 hr; in the oxidation tests, however, the Cr-rare earth alloys consumed only 15 to 20 cc of O_2 in 100 hr. A volume fluctuation of several cubic centimeters is negligible in the first case but is a significant shift in the second case. The system volume changes by 3 cc for each 1°C change in ambient temperature. Although room temperature is measured and corrections were made for each volume reading, small fluctuations still exist and show up as scatter in the rate data. The scatter is not too great, however, and the rate curves provide a good indication of behavior. The oxidation kinetics of unalloyed Cr (Figure 15) and alloys with Cb, Zr, and Mn (Figures 20 – 24) approach a parabolic rate law. The data on a log-log plot have a slope n of 1.5 to 2.3, where n is the rate exponent in the general rate equation

$$W^n = kt$$

The rate exponent is 1 for linear, 2 for parabolic, and 3 for cubic rate laws. The observed behavior agrees with data from other investigations on the oxidation of unalloyed Cr where a parabolic rate law is indicated.

Two interesting deviations from normal behavior were observed. A Cr-1Cb alloy shifted from a parabolic to a linear rate law after 33 hr at 2100°F (1422°K). The initial rate law, however, was not truly parabolic (n = 1.5). A dual oxidation process is suggested for this alloy, with concurrent linear and parabolic rate processes. The behavior is characteristic of alloys that form multilayer scales during oxidation. It is likely that a protective inner scale forms on the metal by a parabolic process and that a nonprotective outer scale forms from the inner scale by a linear process. In the early stages, most of the weight gain is in the formation of the inner scale and parabolic kinetics prevail. When the instantaneous rate of formation of the inner scale decreases to the same value as the linear rate at which the outer scale forms, the inner scale will reach a stable thickness and the oxidation process will appear to follow a linear rate law. This is illustrated schematically in Figure 25. If these reactions occur simultaneously, the gains are additive and the initial rate will not be truly parabolic. Rate exponents of less than n = 2 (e.g., n = 1.5) are characteristic of such systems. A similar behavior is indicated for the Cr-0.25 Cb alloy although no shift to linear behavior was noted out to 100 hr. The rate exponent for this alloy (n = 1.5), however, indicates a dual scale formation of the type described. All other alloys (Zr and Mn bearing) are indicated to have a single oxidation process of essentially parabolic kinetics. If multilayer scales are formed in these materials, all layers are protective with diffusion-controlled reaction kinetics.

A second deviation from parabolic behavior was observed for unalloyed Cr exposed to oxygen. As shown in Figure 15, the rate exponent for the first 11 hr of exposure was 4.2. The sample gained considerable weight within the first hour of test (~1.5 mg/cm^2) and had very little gain for the next 10 hr (~ 1 mg/cm^2). This behavior suggests a logarithmic rate law in which the weight gain is proportional to the logarithm of time (W = k log t). Such rate laws are characteristic of thin film formation on metals at low temperature but generally are not found in the thick film range characteristic of high-temperature oxidation.

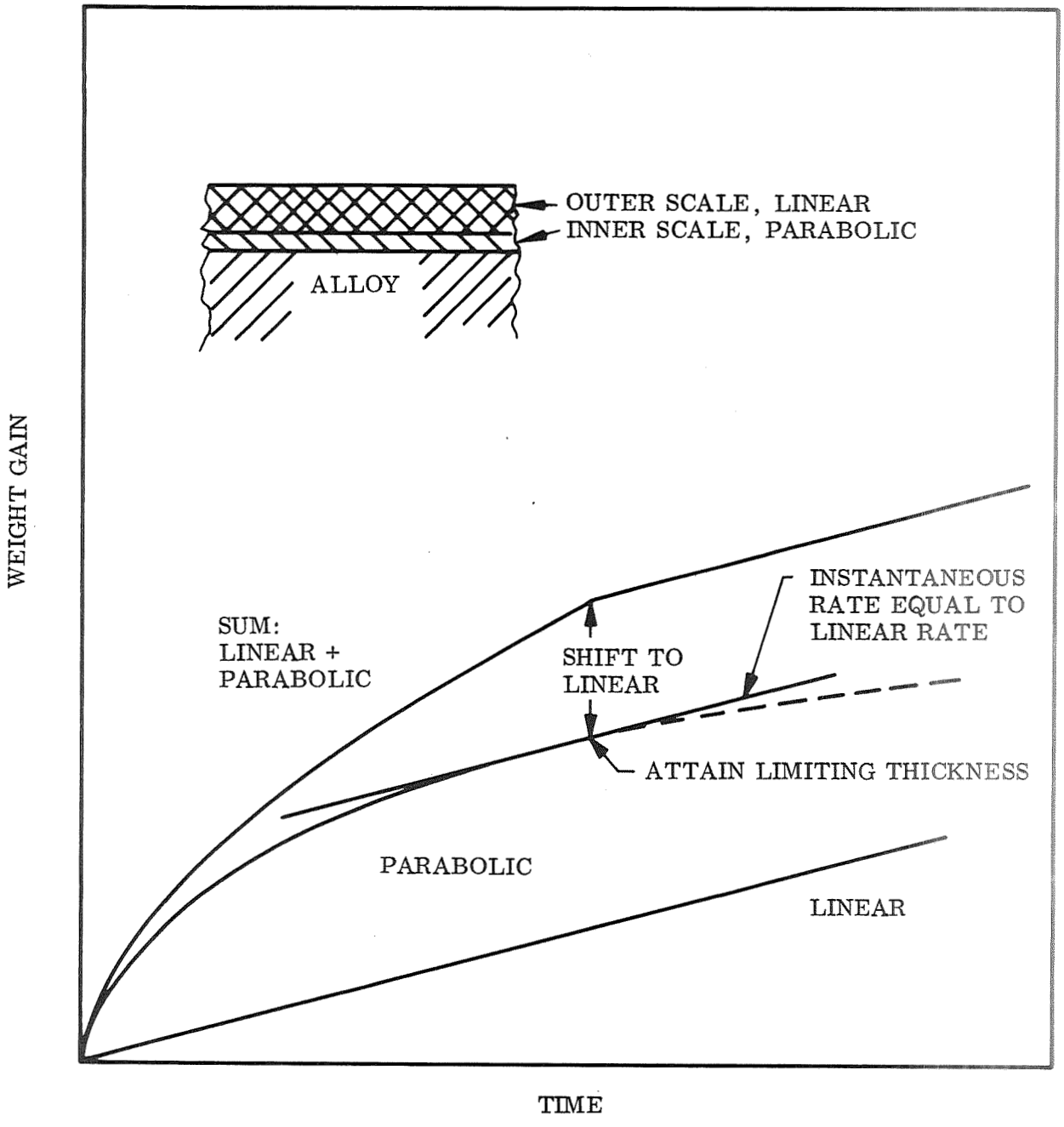

Figure 25 Change in Oxidation Rate Law in a Two-Layer Oxide System.

A logarithmic rate law behavior also is indicated for chromium alloys with 0.1 – 0.5 Y or La. As shown in Figures 15 through 19, these alloys have rate exponents of 5.3 to infinity on exposure to oxygen at 2100°F (1422°K). Unlike unalloyed Cr, however, the rate law does not shift to parabolic in times out to 100 hr. Almost half of the weight gain for these alloys occurs within the first hour of exposure. The data indicate a very rapid buildup of a thin oxide scale that is exceedingly protective. After the first hour, diffusion of metal or oxygen atoms through the oxide scale by the classic Wagner mechanism for parabolic behavior does not seem to be rate controlling for these materials.

Semilog plots of the data for Cr and Cr-rare earth alloys suggest that a logarithmic rate equation of the general type $W = k \log t$ may best describe the oxidation kinetics (Figure 26). As previously mentioned, logarithmic rate laws generally are characteristic of thin film oxide growth at very low temperature. Much of the theory devised to describe logarithmic oxidation behavior is based on electron transport phenomena. Mott and Cabrera's model for oxide film growth, for example, is valid only to 20 Å thickness, which is the largest thickness for which sufficient electrons can tunnel through an oxide. In other treatments, models involving ion transport, space charge effects, chemisorption, blocked diffusion paths (self- and mutual blockage), and nonisothermal conditions, to mention a few, have been proposed to describe logarithmic rate process. Due to the experimental difficulties involved in thin film oxidation, this is probably one of the least understood areas of oxidation behavior.

Of all the models proposed, only one would appear to be applicable to the behavior observed in the high-temperature oxidation of chromium alloys where thick films are formed. Evans (Ref. 15) proposed a model in which cavities or obstructions form within the film as the oxide grows. If metal vacancies control transport of ions through the film, these may collect at the metal-oxide interface to form cavities that ultimately block diffusion. The cavities reduce the effective surface area across which diffusion can occur. Although the actual process continues to be parabolic in regions where contact is maintained between scale and metal, the reduction in total area where this condition exists can result in an apparent logarithmic behavior. The cavity theory of Evans is based on a continuous reduction in the effective area for solid state diffusion across the scale/metal interface.

Cavities at the oxide-metal interface can form in several ways. One manner proposed by Evans to describe the behavior of zinc involves compressional stress in the oxide that causes blisters to form. The film rises as a series of small blisters with a cavity under each blister. If the walls of the blister are cracked and oxygen leaks through, fresh oxide will form and a linear rate law may be found. However, if the walls of the blister are air tight, the cavity acts as a barrier to both anion and cation diffusion and further film growth is impossible in this area. As oxidation continues, more cavities form and the total area which remains free from such diffusion barriers decreases with time. This will lead to a logarithmic type of rate expression. It should be noted, however, that in cavity-free areas the oxidation process continues to be diffusion controlled with parabolic rate law behavior. The apparent logarithmic behavior is due solely to the continuous decrease in surface area, where oxidation can proceed unhindered by interfacial cavities.

Metallographic examination of Cr, Cr-Y, and Cr-La test samples exposed to pure oxygen indicates that the cavity model, as proposed by Evans, will explain the apparent

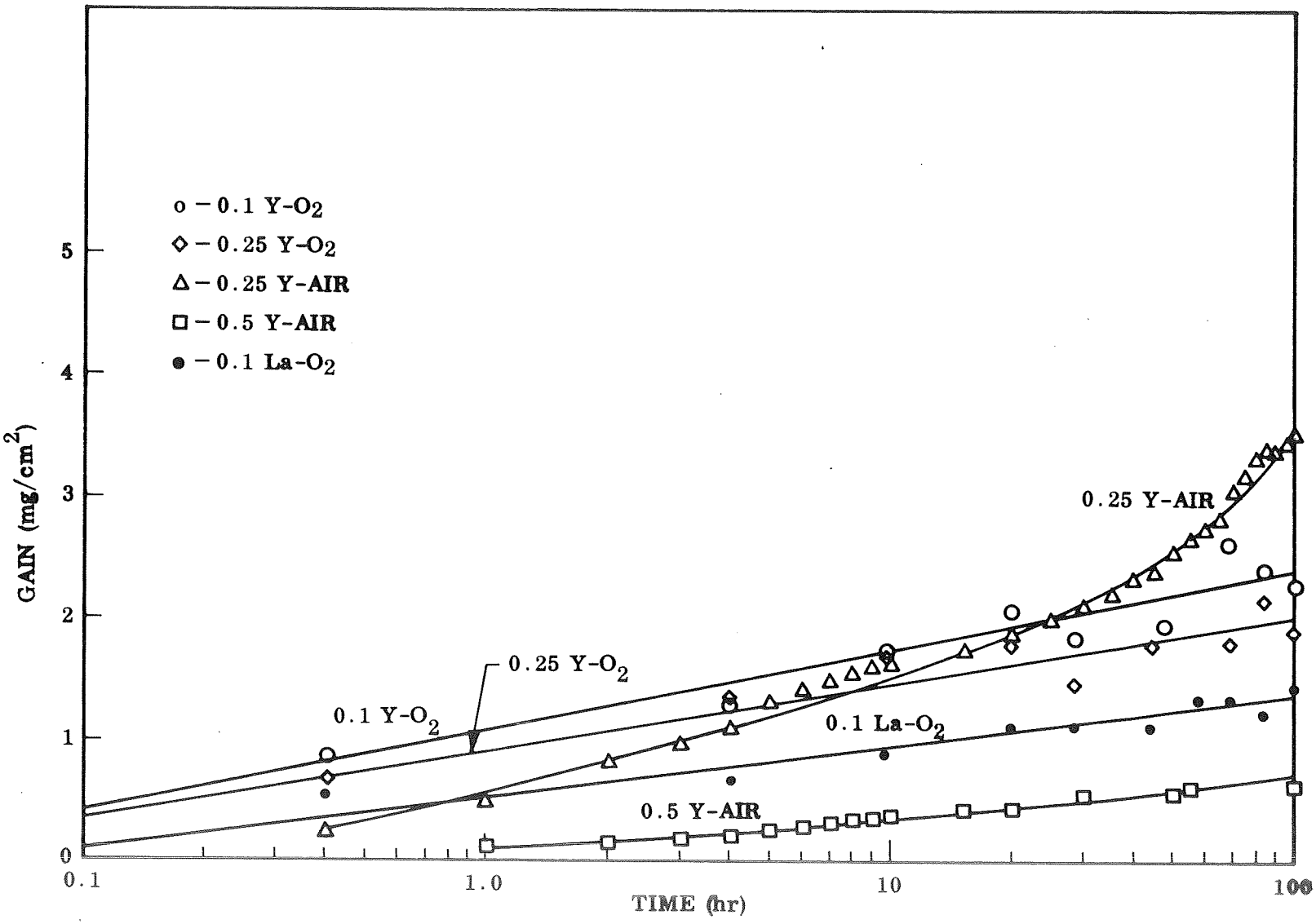

Figure 26 Logarithmic Plot of Weight Gains in Pure Oxygen and Air.

logarithmic behavior exhibited by these alloys at 2100°F (1422°K). The thin oxide scale in all cases is blistered, with large cavities formed at the oxide scale/metal interface (Figures 27 and 28). Cavities are 0.1 to 1 mil long by about 0.1 to 0.5 mil high. The oxide scale above the cavities appears to be intact. The contact across which diffusion can occur is minimal. The blisters are distributed in a wavelike pattern over the surface with about 1 to 5 mils of separation between wave crests or troughs. Metal contact exists only in the trough areas. The metal/scale interface is very uneven (pitted) as a result. The source of cavity formation is not clear. There is some indication that cavities may be formed over particles or stringers of Y or La that exist in the surface. As shown in Figure 29, however, the scale/metal interface has many small cavities comparable in size to the rare earth inclusions, although the number of cavities greatly exceeds that of the rare earth particles. On the other hand, the number of cavities and degree of scale separation increase with increased rare earth content.

The oxide scales on the rare earth containing alloys appear to be buckled, and compressional stresses in the scale as proposed by Evans (Ref. 15) in his model for zinc may be the major cause of blister formation. This behavior suggests that modification of the oxide scales with oxides of the rare earths increases the specific volume. The net effect is an increase in compressive stress, since the scale occupies a much larger volume than the metal it replaces. Another possible cause might be a reduction in oxide strength or increased plasticity that allows the oxide to deform and buckle under a given stress. Rare earth oxides may lower the softening point of chromium oxide. A check of phase diagrams for oxides did not yield any information on systems of Cr_2O_3 with rare earth oxides.

No oxide blisters or large interfacial cavities were found in oxidized samples of the other chromium alloys (containing Cb, Zr, Mn). As previously mentioned, these materials all have parabolic rate behavior and high rates of oxidation. The only exception is a Cr-1Zr alloy which had an oxidation rate approaching that of the rare earth modified alloys (Table 3). Although kinetics were parabolic, this alloy had a sharp drop in oxidation rate at about 80 hr. The rate decreased by a factor of almost 5. As shown in Figure 22, a flat logarithm-like portion of the oxygen rate data is indicated from 25 to 50 hr. Examination of the samples indicated the presence of porous bands in the oxide and a very uneven oxide/metal interface (pitted) (Figure 28). It is likely that scale separation and cavity formation occurred but that the effect was not as pronounced as that produced by the rare earths. The cavity walls may not have been impervious, and leakage of oxygen may have caused continuous slow growth of oxide scale in these areas after cavity formation. This addition (Zr), like the rare earths, forms a discrete second phase that could lead to discontinuities in the oxide and contribute to scale separation. Distinct second-phase particles are evident in the oxide on Zr-bearing alloys (Figures 28 and 29), whereas no second phases were detected in microscopic study of scales on binary alloys containing rare earths.

The oxide scale formed on Cr-Zr alloys was very adherent and had the greatest resistance to spalling on cooling of all alloys studied in this program. The excellent bond at the oxide/metal interface is shown in Figures 28 and 29. The oxide formed on Cr-Mn alloys, on the other hand, had the greatest tendency to spall, probably as a result of excessive oxide thickness. The scale on these alloys was very rough and had a distinctly fused appearance. Scales on columbium-bearing alloys also spalled on

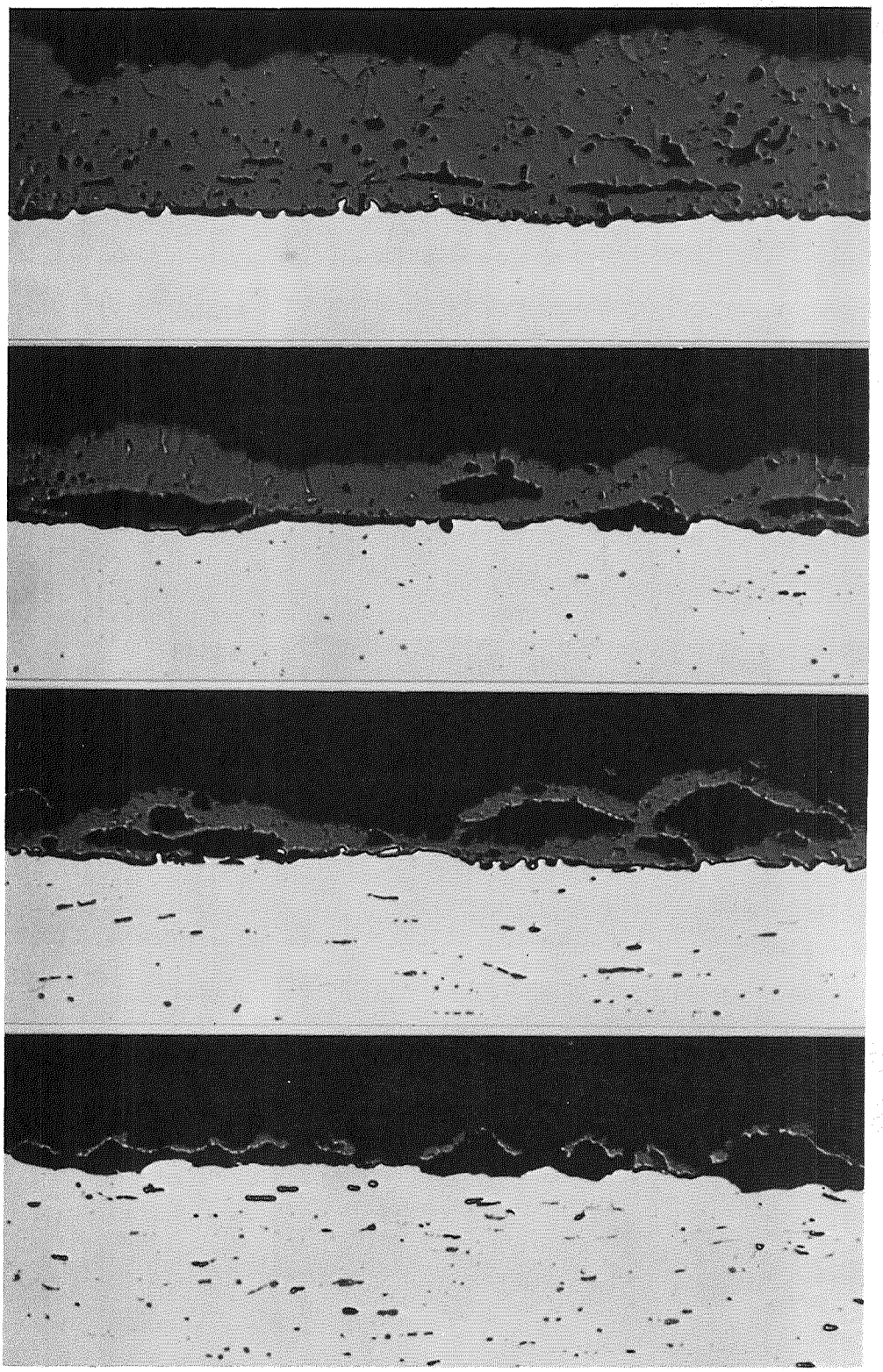

Figure 27 Effect of Y on Oxide Scales Formed on Cr, 100 hr-2100°F (1422°K)-O_2, ×500.

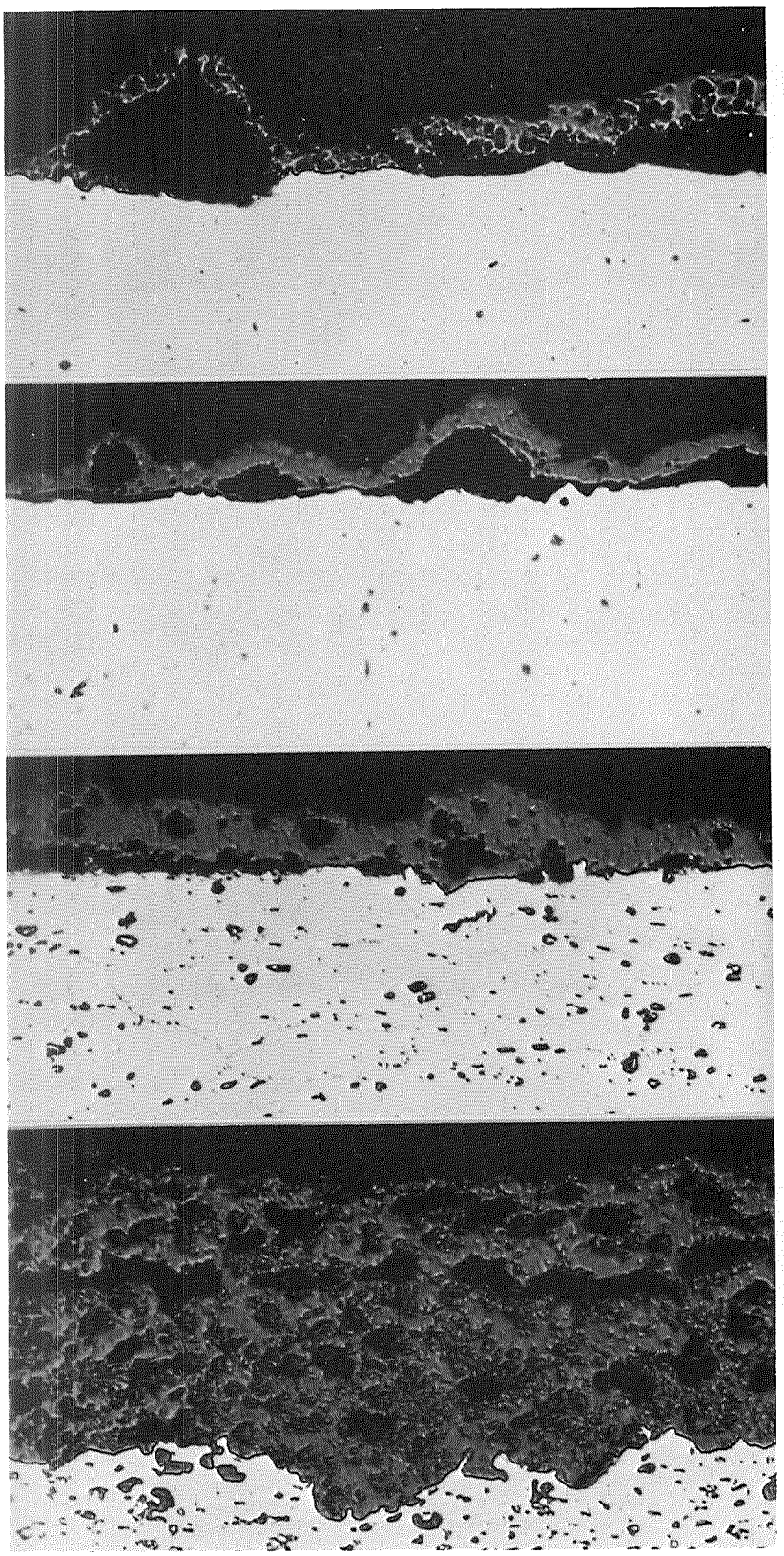

Figure 28 Oxide Scales Formed on Cr-La and Cr-Zr Alloys, 100 hr-2100°F (1422°K)-O_2, ×500.

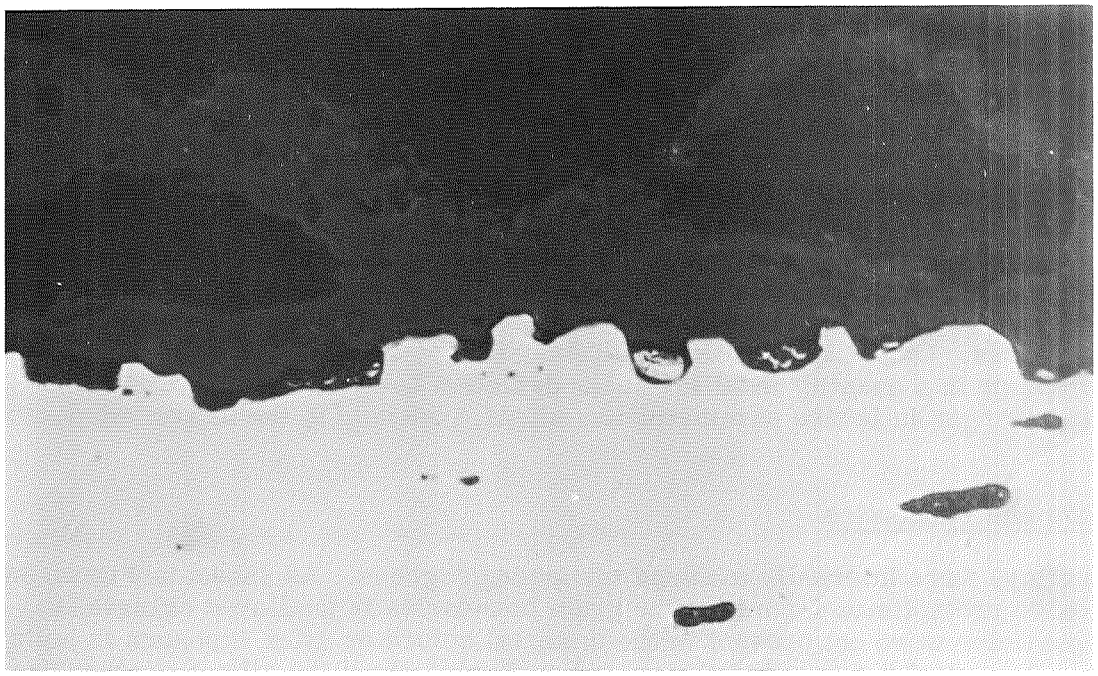

A3559 Cr-0.25La

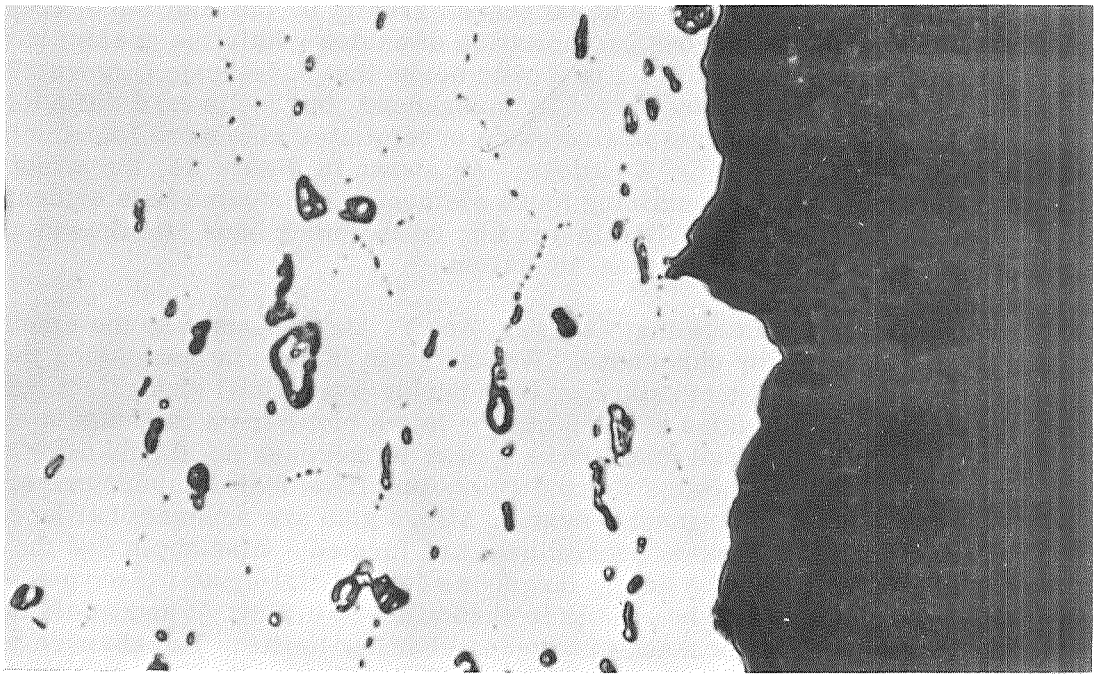

A3558 Cr-1Zr

Figure 29 Oxide/Metal Interfaces in Cr-La and Cr-Zr, 100 hr-2100°F (1422°K)-O_2, ×2000.

cooling; however, a thin inner scale adhered to the surface. The oxide had a distinct two-layer structure, and only the thick outer-layer spalled.

Oxide scales were removed from several alloys, ground to a powder, and analyzed for structure by x-ray diffraction using Debye-Scherrer techniques. The results, shown in Table 4, indicate that the oxide scales on Cr, Cr-Y, Cr-La, and Cr-Zr alloys were Cr_2O_3. The diffraction patterns all indexed as Cr_2O_3, with good agreement between d-values and intensity for the diffraction rings. No major change in lattice parameters was indicated and no extraneous lines characteristic in any second phase were evident in the patterns. Oxides of the alloy additions, if any, appeared to be in solid solution with Cr_2O_3 or in a quantity insufficient for detection by this method (< 1 wt%). If in solution, changes in lattice parameter are slight, probably in the 3rd or 4th decimal place.

Structure and Properties

All the alloys were internally oxidized to varying degrees. As shown in Figure 30, small oxide precipitates formed at the grain boundaries in unalloyed chromium. These particles were not present in the material before or after exposure to helium. Small oxide particles formed in the grain boundaries of all the alloys on exposure to oxygen. This effect is shown for Cr-1Zr in Figure 29, for Cr-1Cb and Cr-3Mn in Figure 30, and for Cr-0.1Y and Cr-0.5Y in Figure 31. The Cr-Cb alloys contained large oxide precipitates within the grain throughout the entire cross section. The solid solubility for oxygen appeared to be increased greatly by the addition of columbium. The manganese alloys also had gross precipitation of oxides within the grains; however, the effect was restricted to a depth of 1 to 2 mils below the oxide scale (Figure 30). Oxygen solubility appeared to be increased by manganese, but the inward diffusion of oxygen was limited. Small amounts of fine oxide precipitates also were found within the grains of Cr-Y, Cr-La, and Cr-Zr alloys. As shown in Figure 31, the effect was most pronounced in lean alloys containing these elements and became less evident as the alloy content was increased. With Mn and Cb, on the other hand, increased alloy content increased the severity of internal oxidation.

Analysis of all structures indicate that Cb, Mn, Zr, Y, and La increase the amount of oxygen that can be absorbed by chromium. Whether this is done by increasing the solid solubility for oxygen at high temperature or by a purely interstitial sink effect with formation of reactive metal oxides at temperature is not clear from the studies conducted on this program. Columbium and manganese appear to increase solid solubility in that oxide platelets typical of precipitates formed on cooling from high temperature are observed within the grains. Manganese-bearing alloys also are severely hardened in the case area where extensive oxide precipitates are formed. Zirconium and the rare earths, on the other hand, may be acting largely as interstitial sinks for oxygen. These elements are very sparingly soluble in chromium (< 0.5 at. %) and would not be expected to cause a major increase in oxygen solubility limits. The absence of large amounts of coarse precipitates within the grains of these alloys tends to support this hypothesis. In addition, the second-phase Cr_2Zr particles in Cr-Zr alloys appear to be altered by the inward diffusion of oxygen. As shown in Figure 29, the second-phase particles near the surface are darkened and similar in appearance to the oxide scale. Compound particles in the center of the sheet, however, have a light color and metallic appearance, as shown in Figure 32. This phase is darkened on exposure to

Table 4

X-RAY DIFFRACTION PATTERNS FOR OXIDE SCALES

Sample Pattern[a]		ASTM Pattern for Cr_2O_3	
d (Å)	Relative Intensity	d (Å)	I/I_1
3.60	S	3.633	74
2.66	VS	2.666	100
2.47	VS	2.480	96
		2.264	12
2.17	W	2.176	38
2.02	VW	2.048	9
1.81	M	1.8156	39
1.67	VS	1.672	90
		1.579	13
1.46	W	1.465	25
1.43	W	1.4314	40
1.29	VW	1.2961	20
1.24	VVW	1.2398	17
1.21	VVW	1.2101	7
		1.1731	14
1.15	VW	1.1488	10
1.12	VW	1.1239	10
1.09	VW	1.0874	17
1.04	W	1.0422	16
0.945	VW	0.9462	17
0.940	VW	0.9370	12
0.895	VW	0.8957	14
		0.8883	7
0.865	W	0.8658	23
0.841	VW	0.8425	8
0.833	VW	0.8331	11
		0.8263	9
0.799	VW	0.7977	15

(a) This pattern was obtained from scales on unalloyed Cr exposed to pure oxygen and air and on Cr-0.25 La, Cr-0.25Y, and Cr-1Zr exposed to pure oxygen.

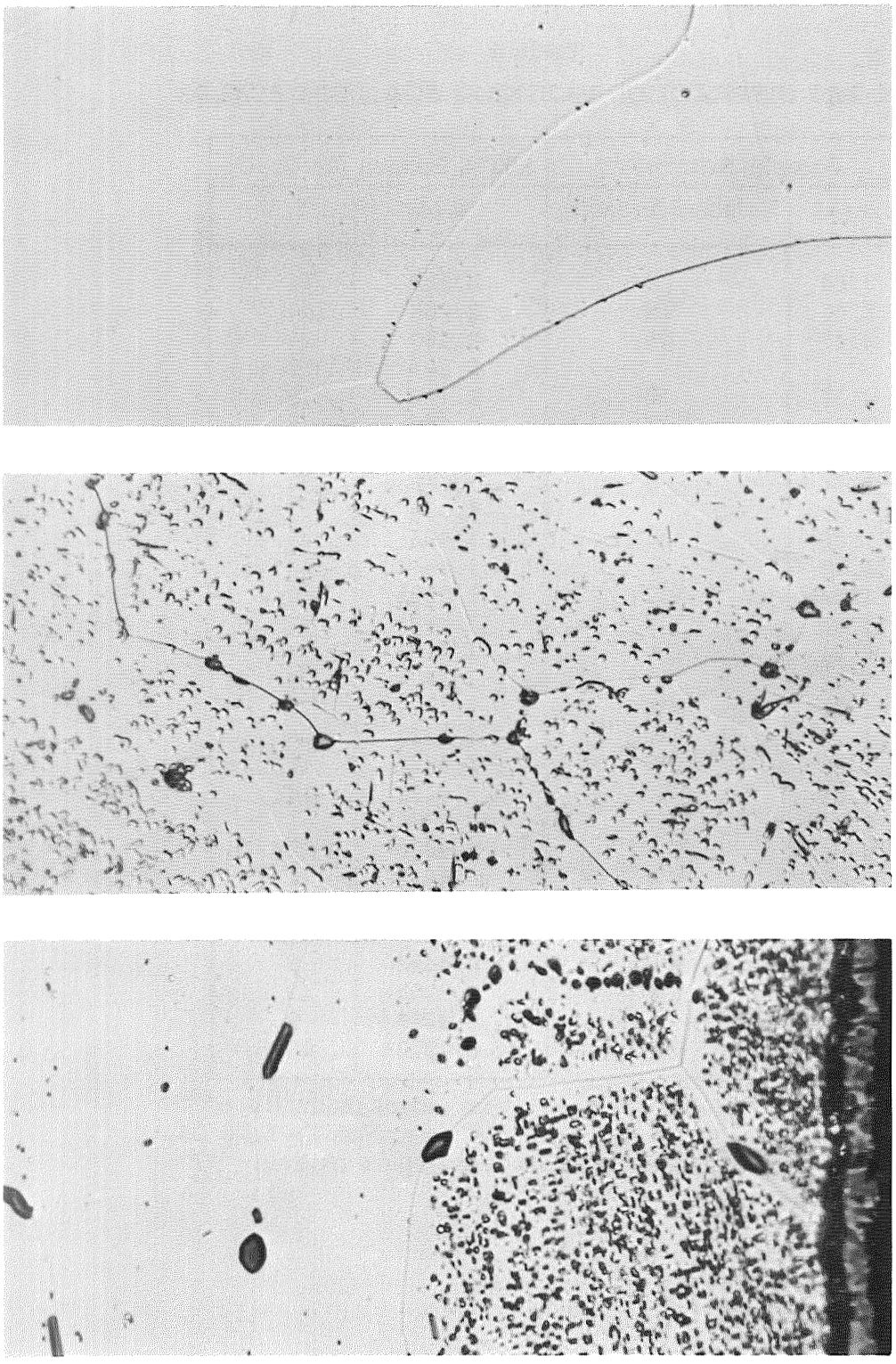

Figure 30 Internal Oxidation of Cr, Cr-Cb, and Cr-Mn Alloys, 100 hr-2100°F (1422°K)-O_2, ×1000.

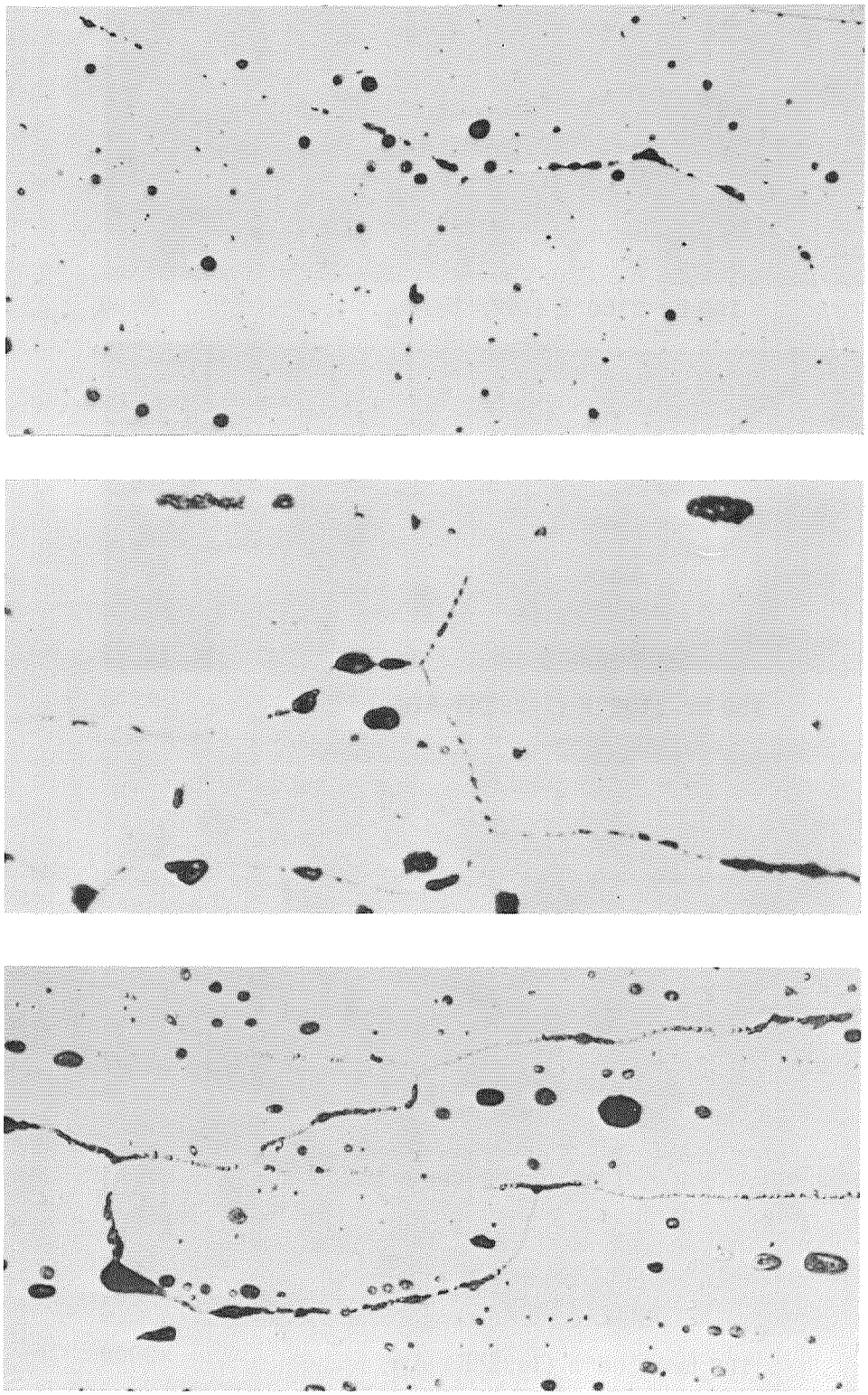

Figure 31 Internal Oxidation of Cr-Y Alloys, 100 hr-2100°F (1422°K)-O_2, ×1000.

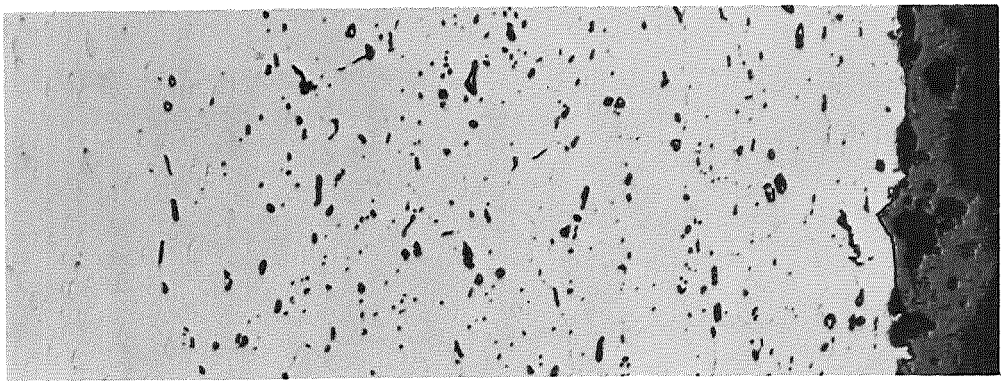

A3543 100 hr-2100°F (1422°K)-O_2 ×500

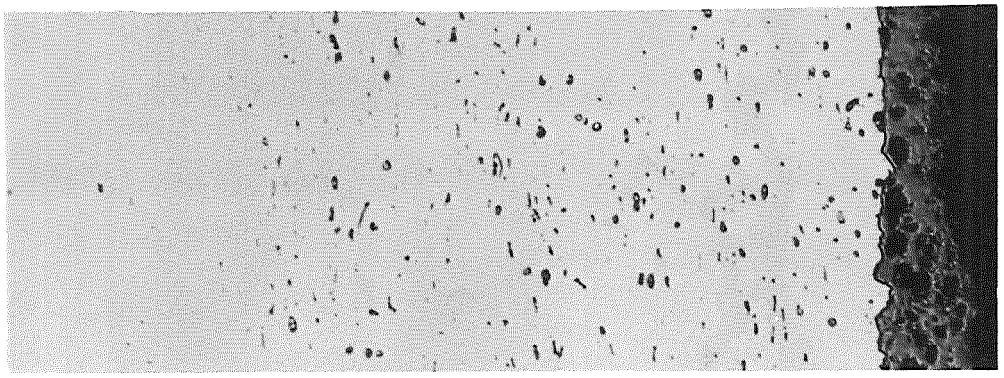

A3535 100 hr-2100°F (1422°K)-Air ×500

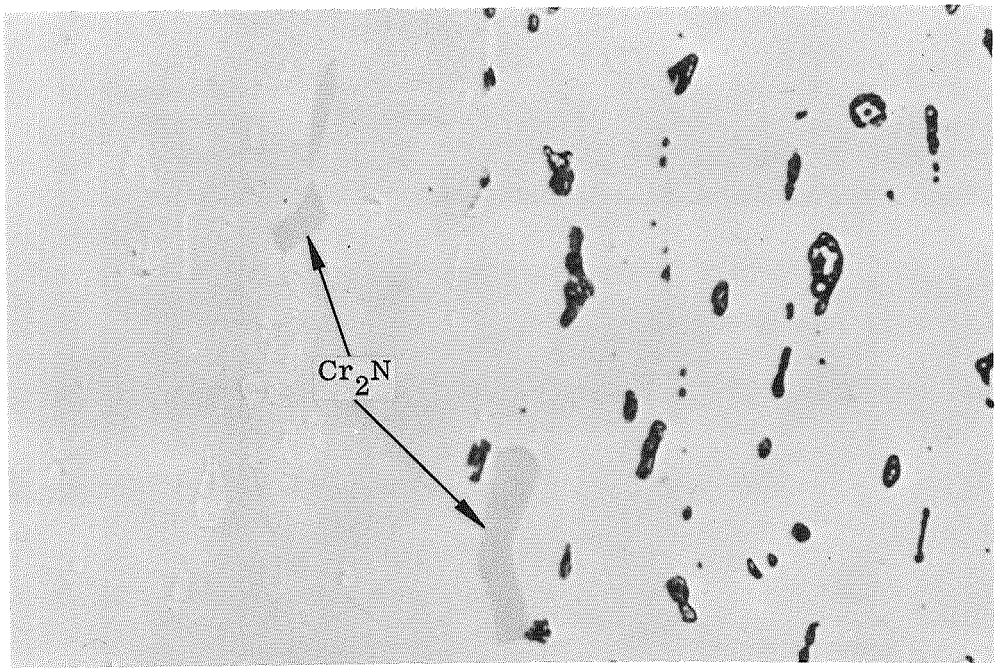

A3555 100 hr-2100°F (1422°K)-Air ×2000

Figure 32 Internal Oxidation/Nitridation of Cr-Zr Alloys.

both oxygen and air, indicating that reaction with oxygen causes the alteration. The depth of alteration is inversely proportional to zirconium content and directly proportional to time of exposure. As will be discussed in Section 6, electron microprobe studies could not confirm that this phase was converted to the oxide and no increase in oxygen content was detected. Detailed studies beyond the scope of this investigation are needed to delineate clearly the mechanisms of internal oxidation in chromium-base alloys.

The effect of internal oxidation on hardness and ductility is summarized in Table 5. With the exception of Cr-3Zr and Cr-3Mn, none of the alloys was hardened by exposure to oxygen for 100 hr at 2100°F. Even the Cr-Cb alloys, which were severely oxidized internally throughout the cross section, had the same hardness as samples annealed for 100 hr in helium. The Cr-3Mn alloy was severely hardened in the case region where gross precipitates occurred (Figure 30). Hardness in this region was 220 DPH, whereas the precipitate-free core had a hardness of 145 DPH. The Cr-3Zr was internally oxidized throughout the cross section and had a uniform hardness of 186 DPH. This is a significant increase in the base hardness of 152 DPH for the unoxidized alloy.

Table 5

EFFECT OF OXYGEN EXPOSURE ON HARDNESS AND DUCTILITY

Alloy	Hardness (DPH)		Bend DBTT [°F(°K)]			
			Helium		Oxygen	
	Helium	Oxygen	Brittle	Ductile	Brittle	Ductile
Cr	149	143	150(339)	200(366)	–	–
Cr-0.1Y	148	144	200(366)	300(422)	200(366)	300(422)
Cr-0.25Y	149	149	300(422)(a)	400(478)	<200(366)	200(366)
Cr-0.5Y	158	138	300(422)(a)	400(478)	200(366)(a)	300(422)
Cr-0.1La	150	148	300(422)	400(478)	300(422)	400(478)
Cr-0.25La	158	147	400(478)	500(533)	400(478)	500(533)
Cr-0.25Cb	158	137	300(422)(a)	400(478)	500(533)(a)	800(700)
Cr-1.0Cb	203	203	600(589)	<600(589)	700(644)	800(700)
Cr-1.0Zr	191	141	300(422)	400(478)	<300(422)	300(422)
Cr-3.0Zr	152	186	200(366)	300(422)	400(478)(a)	500(533)
Cr-3.0Mn	154	145(b)	300(422)	400(478)	<200(366)	200(366)

(a) Partially ductile.
(b) Internally oxidized case hardness: 220.

With the exception of Cr-Cb, the alloys were not embrittled by exposure to oxygen for 100 hr at 2100°F (1422°K). In fact, as shown in Table 5, many of the alloys had a lower DBTT after exposure to oxygen than they did on exposure to helium. The DBTT for Cr-0.25Y, 0.5Y, 1Zr, and 3Mn was 100–200°F (56–111°K) lower for samples exposed to oxygen. The Cr-3Mn and Cr-0.25Y alloys were most ductile, with a transition temperature of less than 200°F (366°K) for oxygen exposure compared to 400°F (478°K) for helium exposure. The two Cr-Cb alloys had significantly higher DBTT after exposure to oxygen, indicating that some embrittlement did occur. The Cr-1Cb alloy also

appeared to be less ductile in the annealed condition and had the highest DBTT on exposure to helium for 100 hr.

5.3 REACTIONS WITH AIR

Three samples of each binary alloy (Tasks I and II) were exposed to air for 100 hr at 2100°F (1422°K) in the same furnace with the helium control samples and the nitrogen- or oxygen-exposed samples. The samples were removed hot from the furnace and placed in Pyrex vials to collect the oxide scale that spalled on cooling. Scale and metal were weighed to obtain the total weight gain due to reaction with oxygen and nitrogen. These samples were used to determine the bend ductile-to-brittle transition temperature, hardness profiles, and general structure of the alloys. In addition to these tests, continuous weight experiments were conducted in air at 2100°F (1422°K) and 2400°F (1589°K) to determine reaction kinetics. The data from weight change, hardness, and DBTT measurements are presented in Appendixes D, E, and F, respectively.

Reaction Rates

The air oxidation behavior is much more complex than the behavior in pure oxygen. The weight gain in air is the result of concurrent reactions with oxygen and nitrogen. In addition to an oxide scale and internal oxidation, a nitride case and internal nitridation occur. The weight change is the additive gain for each of these four processes, and the observed rate behavior appears to change with time if one process or the other tends to predominate. This type of behavior makes any analysis of the data exceedingly difficult and precludes the use of weight gain data per se to evaluate reaction kinetics. Detailed structural studies are needed to understand behavior.

The weight change data for binary alloys are presented in Tables 3 (section 5.2) and 6. In general, the solid solution types of alloys (W, Mo, Re, Ru, Mn, Fe, Co) tended to form thick oxide scales and thick nitride cases, whereas alloys with Zr, Hf, and the rare earths formed thin oxide scales and thin nitride cases. This pattern is reflected in plots of weight change data for the different alloys, as shown in Figures 33 and 34. The total weight gain for the rare earth-, Zr-, and Hf-bearing alloys after 100 hr at 2100°F (1422°K) was 1 to 8 mg/cm^2, whereas the gain for all other alloys was in the range of 8 to 18 mg/cm^2.

The analysis of behavior in air is complicated because of the tendency for oxide scales to spall on cooling. This precludes metallographic study of the nature and thickness of oxide scales. In general, where sufficient scale was retained on the surface for study, the appearance was very similar to that of scales formed on the alloy in oxygen. The main difference in all cases between tests in air and in oxygen was the formation of a chromium nitride case beneath the oxide scale. As shown in Figure 35, even the most oxidation- and nitridation-resistant alloys (Cr-Y and Cr-La) formed a continuous case of Cr_2N beneath the oxide scale. The oxide is formed by oxidation of the Cr_2N case in air instead of oxidation of the alloy as in tests in oxygen. Nitrogen, in turn, must diffuse through the oxide and the nitride case to react with the alloy to form the nitride case.

Table 6

RESULTS OF AIR OXIDATION EXPOSURE

Alloy	Weight Gain (mg/cm^2)	Nitride Case Depth (mils)	Knoop Hardness			
			Base Alloy[a]	Nitride Case	Alloy Below Case	Alloy Center-Line
Cr	(b)	–	149	–	–	–
-1W	8.57	4.0	219	1400	217	217
2W	15.84	3.5	244	2042	286	286
4W	16.50	7.0	263	1886	340	340
1Mo	14.57	5.0	174	1660	240	204
4Mo	9.62	3.0	279	1750	307	307
1Re	13.11	5.0	179	1160	207	207
2Re	16.41	8.0	184	1340	219	219
4Re	16.58	6.0	235	1149	262	262
1Ru	8.86	2.0	179	1711	220	220
2Ru	7.62	2.0(c)	263	1334	260	260
4Ru	9.38	3.0(c)	268	503	294	294
1Mn	13.23	4.0	143	1900	177	177
2Mn	8.22	5.0	161	1740	182	182
4Mn	17.93	7.0	161	1930	197	197
1Fe	(b)	8.0(c)	173	1375	184	184
2Fe	(b)	3.5(c)	223	1884	224	224
4Fe	(b)	1.5	279	1470	266	266
1Co	11.40	2.0(c)	223	1678	235	235
0.5Ti	15.60	8.0	174	1725	272	272
2Ti	11.25	N/L	227	–		
0.5Zr	4.34	2.0	163	1501	247	204
2Zr	7.59	1.0	185	–	219	219
0.5Hf	7.23	0.5(c)	198	–	241	241
2Hf	7.55	0.5(c)	194	–	198	198
0.5V	13.86	3.5	179	1725	323	238
2V	11.12	Nil	179	–	310	310
0.5Cb	7.50	Nil	203	–	237	237
0.5Ta	18.60	7.0	179	1810	234	234
0.5Y	4.46	1.5	161	1613	180	180
1Y	5.81	1.5(c)	182	–	185	185
2Y	4.19	0.5(c)	179	–	201	201
0.5La	2.15	~1.0	137	1562	196	196
1La	2.19	~1.5(c)	163	–	200	200
2La	1.47	~0.5(c)	141	1624	190	190
0.5Pr	5.45	2.0	204	2078	215	215
1Pr	4.57	2.0	182	–	172	172
0.5MM	3.35	1.5(c)	168	1809	210	186
1MM	2.71	1.0(c)	174	1618	200	200
2MM	2.73	1.0(c)	168	1794	203	203
0.5Th	6.59	3.0(c)	174	1850	210	178
1Th	3.47	1.0(c)	145	1484	211	211
2Th	3.83	0.5(c)	158	–	270	208

(a) This reference is the hardness of the alloy after exposure to helium at 2100°F (1422°K) for 100 hr.
(b) Not determined.
(c) Discontinuous case.

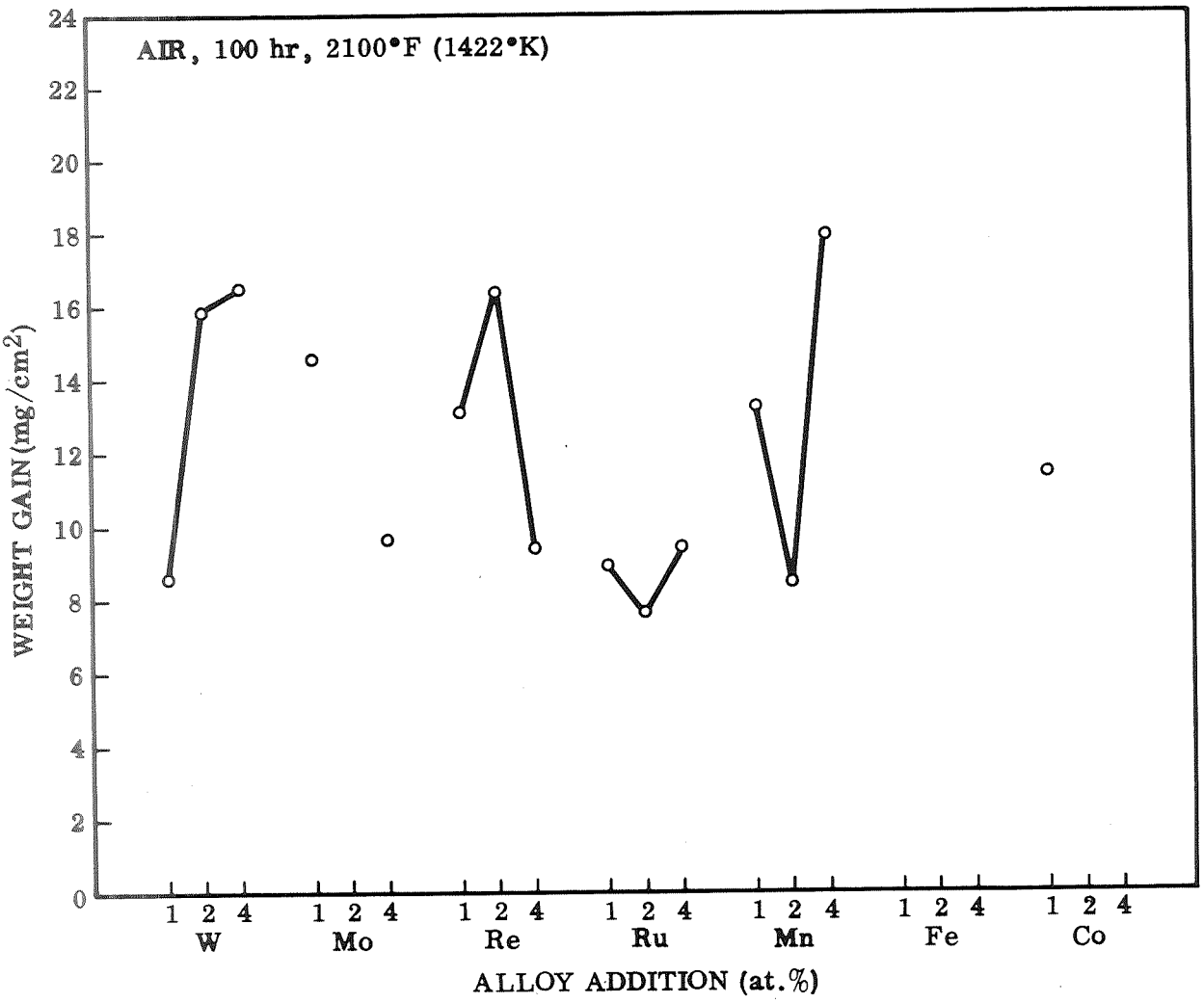

Figure 33 Effect of Solid Solution Additions on Air Oxidation Resistance.

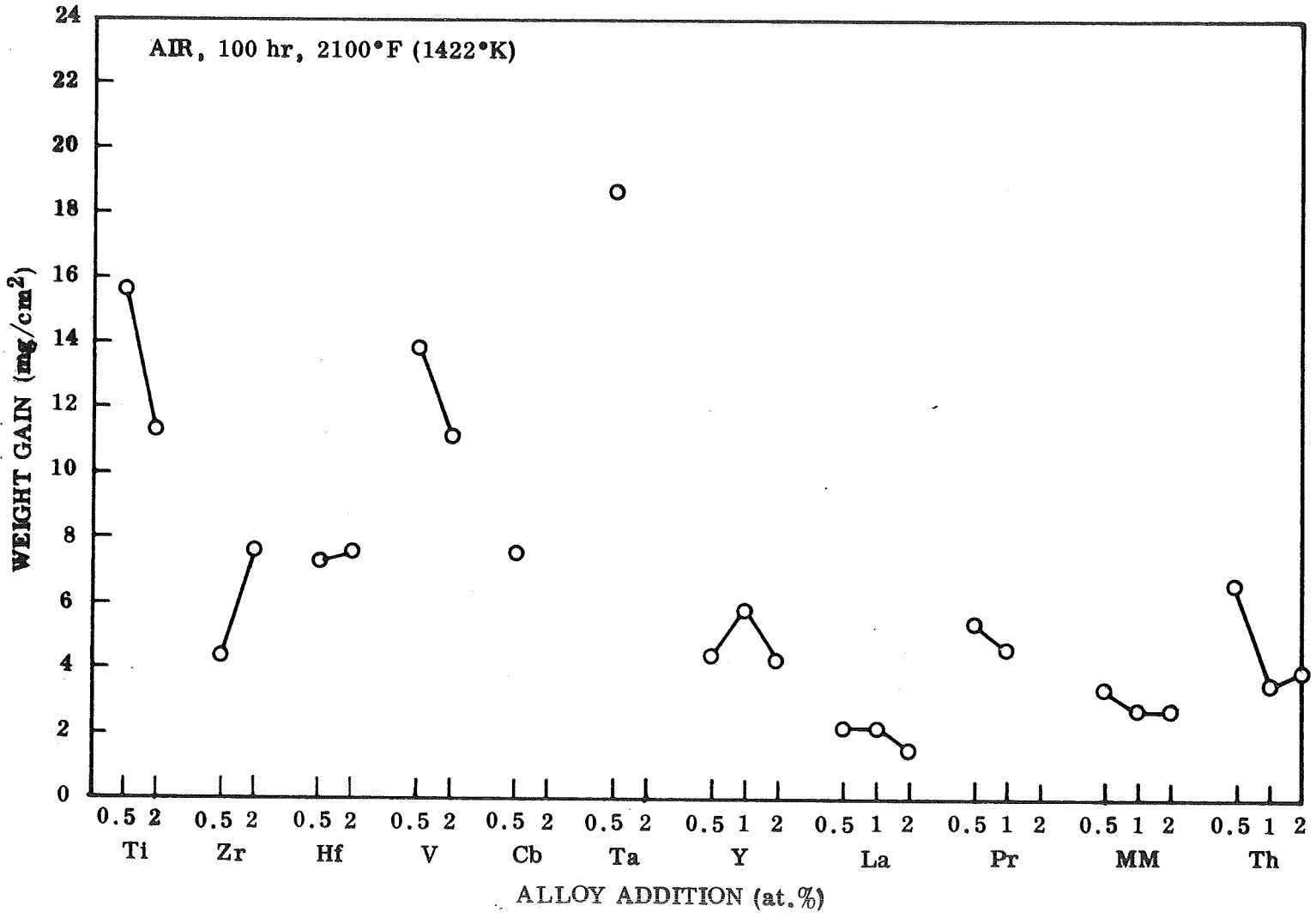

Figure 34 Effect of Nitride Formers and Rare Earths on Air Oxidation Resistance.

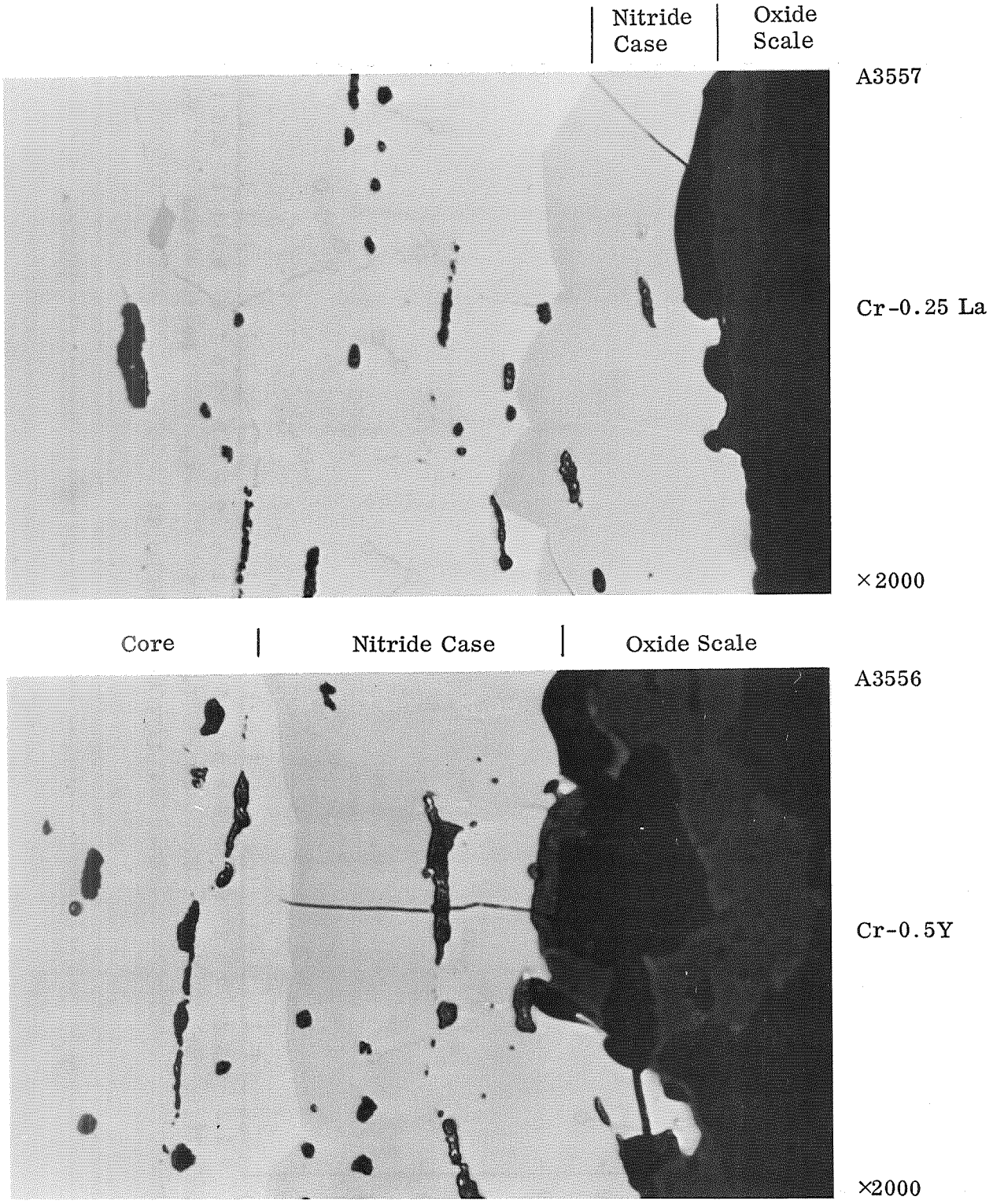

Figure 35 Oxide/Nitride/Core Interfaces in Cr-Y and Cr-La Alloys, 100 hr-2100°F (1422°K)-Air, Unetched.

The total amount of nitrogen reacting with the alloys appears to be considerably greater than the amount of oxygen reacting. Based on the relative thickness of nitride and oxide scales and the relative amounts of internal oxide and nitrides formed, most of the weight gain in air appears to come from the reaction with nitrogen. Since the total weight gains in air are comparable in many cases to those in oxygen (Table 3, section 5.2), it would appear that there is less reaction with oxygen in an air atmosphere than in pure oxygen. This may be the result of the reduced availability of oxygen in air (lower partial pressure) compared with the pure gas. Reaction rates normally would be expected to be proportional to the square root of the oxygen partial pressure where dissociation of oxygen molecules occurs for reaction. It is possible, however, that nitrogen in some way affects the reaction with oxygen by alteration of diffusion processes, adsorption sites, or interfacial reactions. Far more detailed studies are needed to clearly identify causes and effects.

The tendency for oxide scales formed in air to spall on cooling is probably due to a greater thermal expansion mismatch between the oxide and nitride than between the oxide and metal. Scales formed on chromium and its alloys in pure oxygen tend to be adherent and resist spalling on cooling. Similarly, the nitride case formed on the alloy is adherent and also resists spalling on cooling. As shown in Figure 35, there is no interfacial cracking between the nitride case and the metal. The effect of alloy composition on oxide spallation is summarized in Table 7.

Table 7

OXIDE SPALL CHARACTERISTICS OF ALLOYS

Total Spall at Red Heat	Total Spall at Black Heat	Partial Spall Near Ambient	Adherent Outer Scale	Adherent Subscale
Ti	Co	Y (high)	Zr	Cb
Mn	Ru	La	Hf	
Re	Mo	Mischmetal		
	W			
	V			
	Ta			
	Fe			
	Th			
	Y (low)			
	Pr			

Oxides on most of the alloys spalled while the samples were still hot, in a "black heat" range. Alloys with La, Mischmetal, and high levels of Y had very thin oxide scales that tended to spall from the edges near room temperature. The difference in behavior in these cases is believed to be the result of the relative thickness of the scales rather than the result of scale compositional effect. Thicker scales appear to result in high interfacial stresses and strong spallation tendencies. Zirconium and hafnium additions formed oxides with high resistance to spalling, even as fairly thick scales. Columbium

was the only addition that resulted in the formation of an adherent oxide subscale. The outer oxide layer spalled on cooling, while a thin inner oxide remained intact on the surface. In all other alloys, the Cr_2N case was exposed when the oxide scale spalled on cooling.

Structure

Cross sections of all samples were examined metallographically to determine the structural changes produced by air exposure (Figures 36 through 46). All alloys were fully recrystallized and had a single-phase solid (solid solution) structure prior to exposure except for those containing Hf, Zr, Th, Y, La, Pr, and Mischmetal (Ce-La alloy). These materials had two-phase microstructures at all levels of addition. The solid solubility of these elements in chromium is very low. Maximum limits of solubility are estimated to be in the range of 0.1 to 0.6 at.%. The published literature on these systems indicates considerable disagreement, with reported limits ranging from < 0.005 to 0.71% for Y in Cr, and from 0.05 to 0.6% for La in Cr. The solubility of Ce and Pr is reported to be < 0.14 at.% at 2300°F (1533°K), which is the same range as that for Y and La (Refs. 16,17,18). No data have been published for Th, but solubility is stated to be low. Zr and Hf are reported to have solubility limits of < 0.6 and < 0.3 at.%, respectively. Alloys containing 0.1 at.% La and Y and 0.5 at.% Ce (Mischmetal), Pr, Th, Zr, and Hf produced for this program were found to contain a second phase, indicating that the limit of solid solubility at 2100°F (1422°K) is considerably below these values. Typical structures are shown in Figures 43 through 46.

The excess Pr, Ce (Mischmetal), and La are liquid at 2100°F (1422°K). As shown in Figures 44 and 45, chromium alloys with these elements have a coarse equiaxed grain structure with the excess rare earth segregated at grain boundaries and grain triple points. Yttrium and thorium, on the other hand, are solid at 2100°F (1422°K) and alloys containing these metals have a banded structure with the excess Y or Th rolled out as long stringers (Figure 44). The grains in recrystallized sheet have an elongated (flattened) shape. The excess of Y or Th is not segregated at the boundaries in these alloys. A third type of structure is developed in alloys containing Zr or Hf. These additions form an intermetallic compound with Cr (Cr_2Zr, Cr_2Hf), which occurs as a random dispersion of rosettes or small islands (Figure 43). The individual particles average about 0.0001 in. (0.00025 cm) in diameter. These particles form during solidification of the alloy and are broken up and redistributed by extrusion and rolling. They nucleate a fine grain structure in chromium and prevent grain growth at high temperatures. Average grain diameter in Cr-Zr alloys is about 0.0005 in. (0.0013 cm) compared with 0.0025 in. (0.0063 cm) for unalloyed Cr or Cr-rare earth alloys.

Three major alterations of the structure were found: (1) formation of a nitride case, (2) formation of intergranular nitrides, and (3) formation of small nitride precipitates within the grains. In addition, some alloys contained intergranular oxides and fine oxide precipitates within the grains that were similar to those developed in samples exposed to pure oxygen. The general structural features with respect to nitride cases, intergranular nitrides, and nitride precipitates is illustrated by the photomicrographs of unalloyed chromium and a Cr-0.5Y alloy in Figure 36.

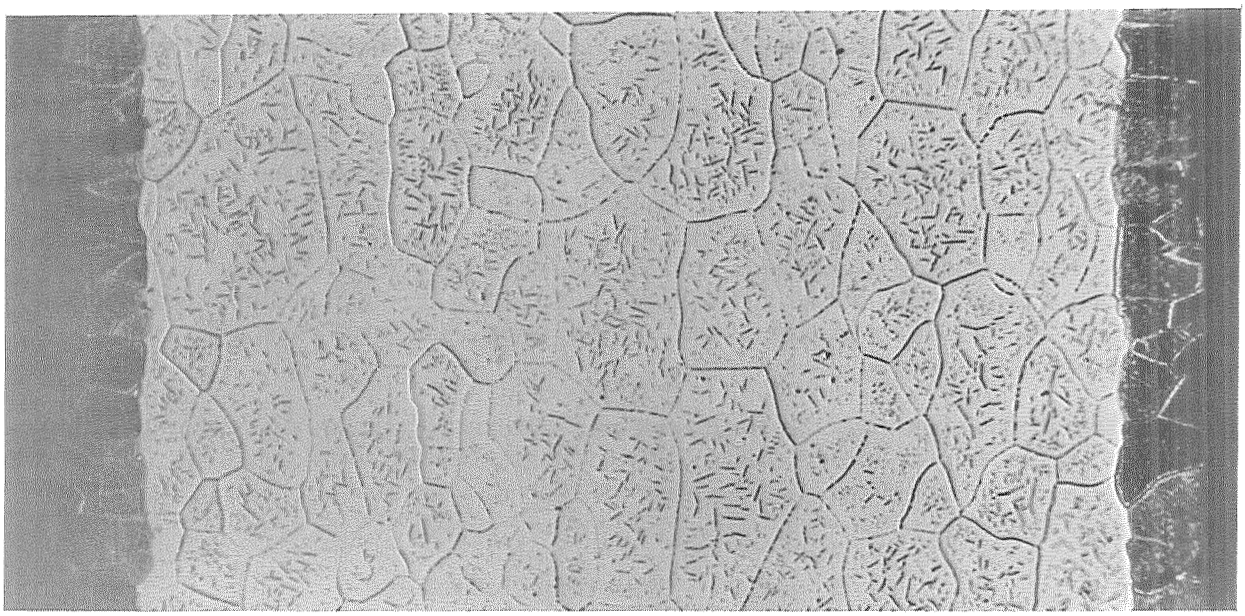

A5879 ×200

Unalloyed Chromium

A5886 ×200

Cr-0.5Y
9125-5

Figure 36 Distribution of Nitrides in Cr and Cr-Y Alloys, 100 hr-2100°F(1422°K)-Air, Etched.

Thermodynamically, in a gas-metal reaction the metal will absorb the gas (oxygen and/or nitrogen) until the gas content in solid solution at the surface stands in equilibrium with the gas phase or with an oxide or nitride scale on the surface. If the inward diffusion of the gas atoms (N or O) into the metal is very rapid compared with the rates at which the gas arrives at the surface, then the equilibrium condition will be approached slowly and a finite thickness of oxide or nitride scale will not form until the bulk of the metal becomes saturated with oxygen or nitrogen. Tests in pure nitrogen indicate that diffusion of nitrogen into the metal is very rapid and that in thin sections such as these [0.030 in. (0.076 cm)] saturation throughout the cross section occurs within the first hour of exposure. At this point, a nitride case will begin to form and grow in thickness.

Nitrogen may or may not continue to diffuse into the metal, depending on composition. In unalloyed chromium or in chromium alloys with negligible solid solubility for the alloy element, little if any additional nitrogen can diffuse into the metal. The basic phase rule for alloy systems,

$$P + F = C + 2 \quad \text{(with temperature and pressure as degrees of freedom}$$

or

$$P + F = C + 0 \quad \text{(with temperature and pressure fixed)}$$

dictates what structures can exist at equilibrium. With a two-component alloy ($C = 2$) in a single-phase field ($P = 1$), there can be 1 degree of freedom ($F = 1$). Thus, for Cr-N in the single phase (solid solution) region, the composition can be a degree of freedom at constant temperature and pressure. The nitrogen content can increase on exposure to the gas phase. However, when the solid solution becomes saturated in nitrogen, a second phase must form if nitrogen continues to be absorbed. The composition can no longer be a degree of freedom in this case, since when $P = 2$, $F = 0$. Thus, nitrogen will increase to the limit of solubility and no further nitrogen can dissolve in the alloy unless temperature or pressure is changed. From this point on, only a nitride case will form on the surface and the metal core will hold a constant composition of nitrogen dissolved in solid solution. Although nitrides cannot form within the alloy at constant temperature, the solubility of nitrogen decreases with temperature and nitrides will precipitate from solution within the grains and at the grain boundaries on cooling. The typical structure for unalloyed chromium heated in nitrogen is shown in Figure 36. A uniform distribution of Cr_2N platelets is precipitated within the grains through the entire cross section and a thick case of Cr_2N is formed on the surface. No massive particles of nitride are formed in the boundaries or in the grains. A similar behavior is found for Cr-Y and other Cr-rare earth, Cr-Zr, and Cr-Hf alloys in which very little of the Y or rare earth, Zr, or Hf enters into solid solution. With little if any of the alloy in solution, these alloys tend to behave as two-component systems. The structure for a typical Cr-Y alloy is shown in Figure 36 to illustrate this behavior. Under some conditions, the amount of these elements in solution apparently increases and the alloys will behave as true three-component systems. Figure 37 shows the presence of a moderate amount of massive Cr_2N in grain boundaries and at grain intersections that formed isothermally in a

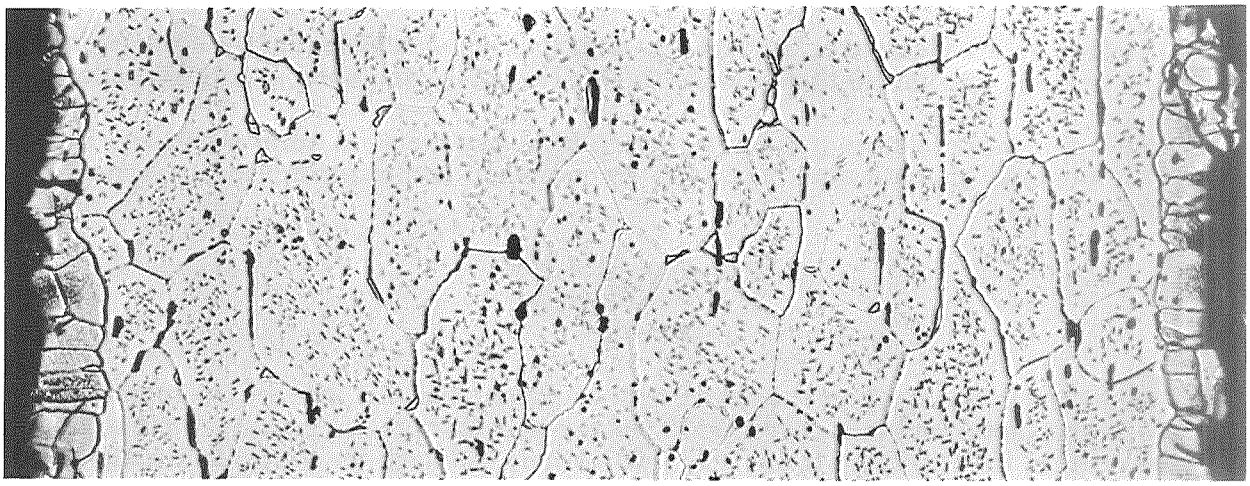

A5878 Cr-0.5Y (950-5) Etched ×200

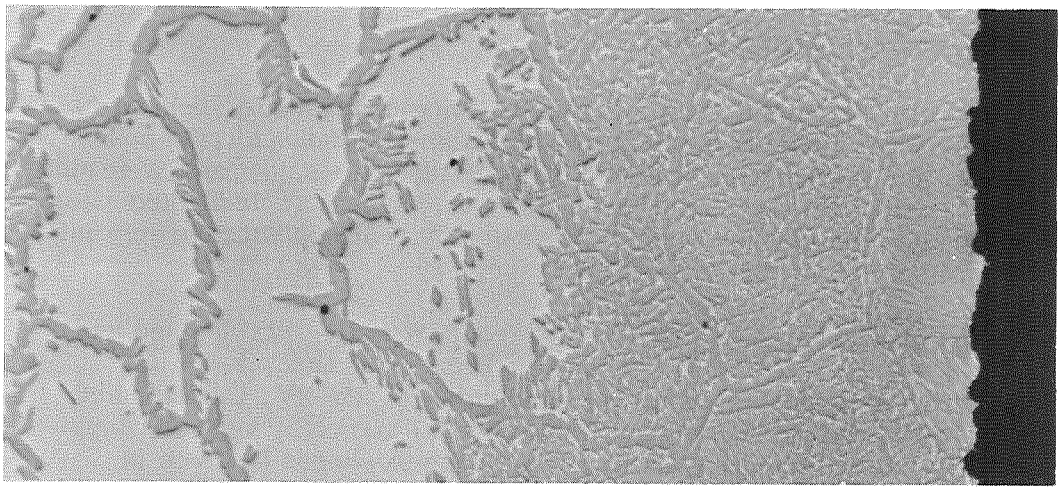

A1688

Cr-1Re
Unetched

×1000

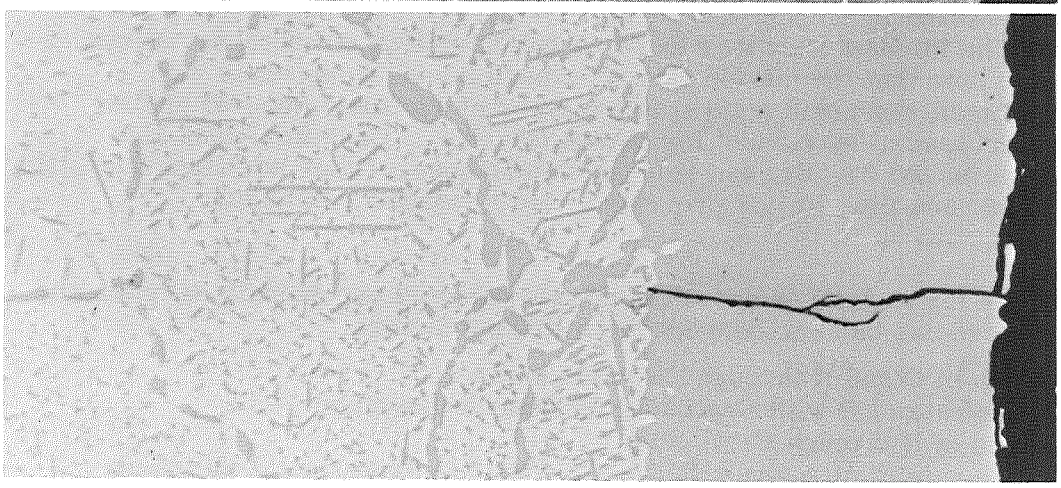

A1684

Cr-0.5V
Unetched

×1000

Figure 37 Variations in Nitride Case and Internal Nitrides in Cr Alloys, 100 hr-2100°F(1422°K)-Air.

Cr-0.5Y alloy on air exposure. A uniform distribution of nitride platelets precipitated within the grains, similar to that in pure Cr-N alloys, is also seen in this structure.

In a three-component system (Cr-M-N, where M is any metal in solid solution), the phase rule permits an additional degree of freedom and composition can be varied in a two-phase field:

$$P + F = C + 0$$
$$2 + F = 3 + 0$$
$$F = 1$$

Thus, even though the alloy is saturated with nitrogen, the nitrogen will continue to dissolve in the metal and massive nitride phases will form isothermally. The total nitrogen content will continue to increase with time, although the amount in solid solution will remain constant once the saturation level has been reached. This type of behavior is illustrated for Cr-V and Cr-Re alloys in Figure 37. Massive nitrides are formed in the grain boundaries and in the grains of both alloys. These structures have not been etched to reveal the fine nitride platelets that precipitate from solid solution on cooling.

The Cr-V and Cr-Re alloys illustrate one other interesting difference in behavior. In the alloys in which the alloy addition forms a nitride, a single-phase nitride case generally is formed. In the alloys in which the alloy addition does not form a nitride, however, the nitride case generally has a two-phase structure, with unreacted alloy material retained between the platelets of Cr_2N formed by reaction with chromium. The Cr-Re alloys typically show this type of behavior.

The general structure of representative alloys with respect to the nitride case and massive intergranular nitride formation is shown in Figures 38 through 45. A nitride case was formed during air exposure on all but three alloys: Cr-2V, Cr-2Ti, and Cr-0.5Cb. The structure and thickness of the case varied markedly with composition. A summary of behavior with respect to nitride case thickness is given in Table 8. The least amount of case was formed on alloys containing Hf, Zr, and the rare earths, and the thickest case was found on solid solution strengthened alloys. It is significant to note that the nitride case thickness tended to increase with increased alloy content for some solid solution types of additions (Mn, W) and to decrease with increased alloy content for others (Fe, Mo). Case thickness also decreased with increased Zr, Hf, and rare earth additions. Other additions had little effect on case thickness (Ru, Re) or prevented case formation completely (Cb, V, Ti).

The analysis of the formation and growth of nitride cases is exceedingly complex and depends upon the precise balance between the following factors:

(1) Diffusion of O and N through the oxide scale
(2) Reaction rate of O with Cr_2N at oxide/nitride interface
(3) Diffusion of N through Cr_2N case
(4) Reaction rate of nitrogen with the alloy at the nitride/metal interface
(5) Diffusion of nitrogen into the metal and solid solubility of nitrogen in the alloy.

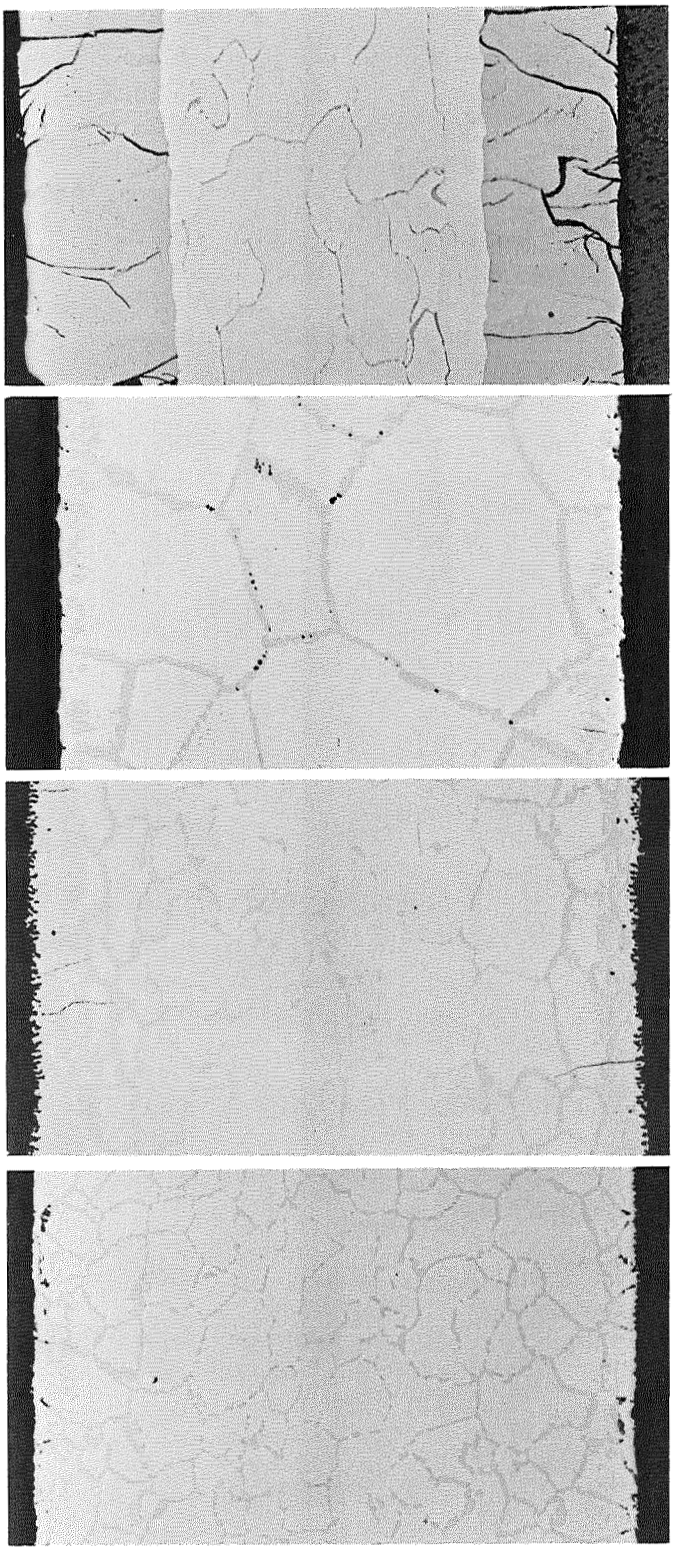

Figure 38 Cross Section of Cr-Fe and Cr-Ru Alloys, 100 hr-2100°F (1422°K)-Air, ×100, Unetched.

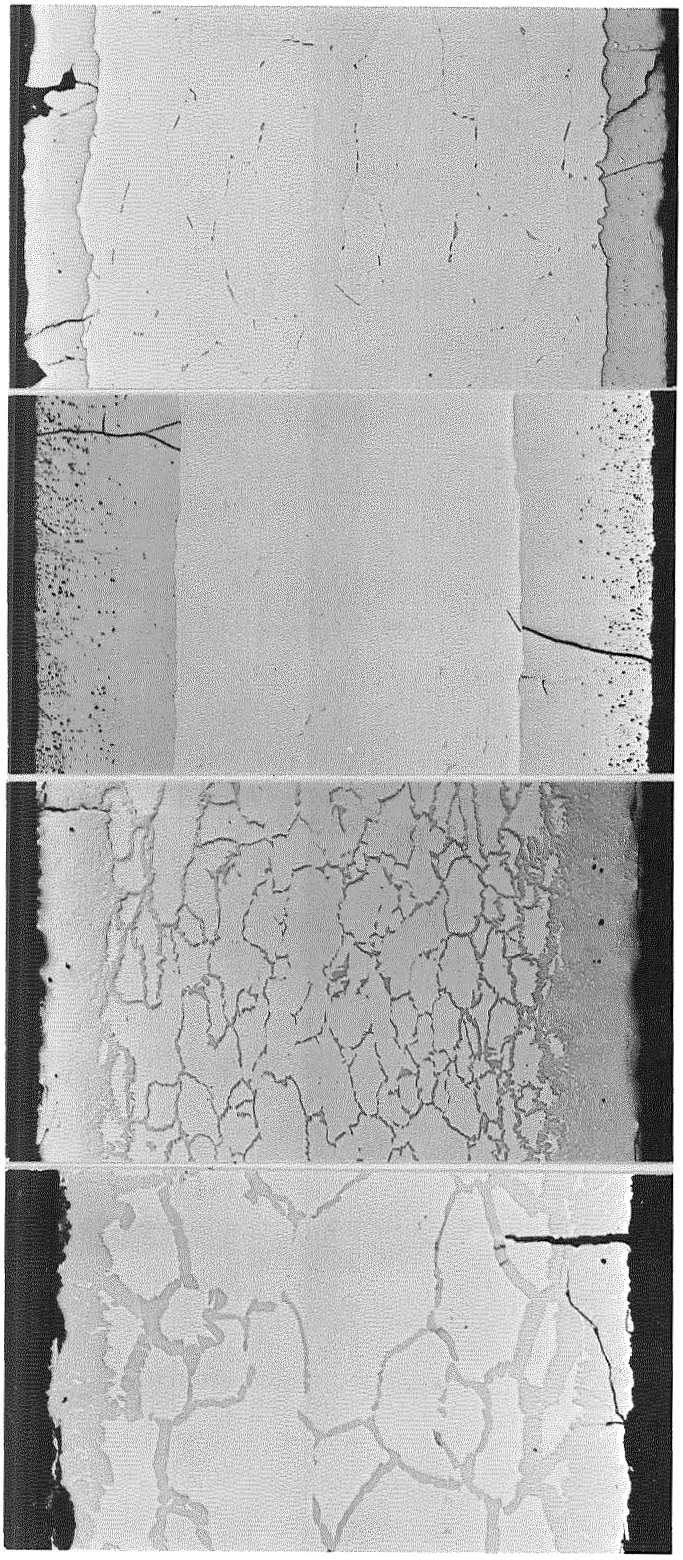

Figure 39 Cross Section of Cr-Mn, Cr-Re, and Cr-Co Alloys, 100 hr-2100°F(1422°K)-Air, ×100, Unetched.

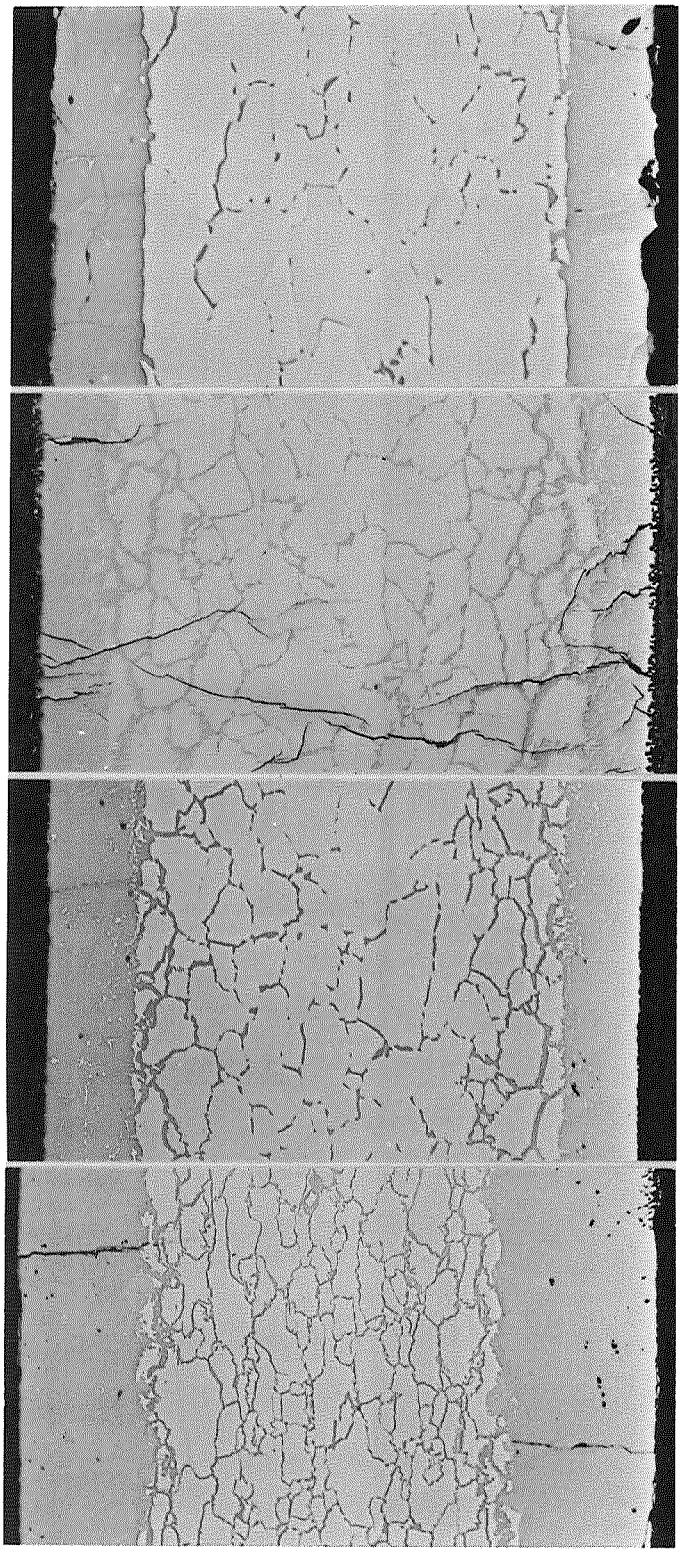

Figure 40 Cross Section of Cr-Mo and Cr-W Alloys, 100 hr-2100°F (1422°K)-Air, ×100, Unetched.

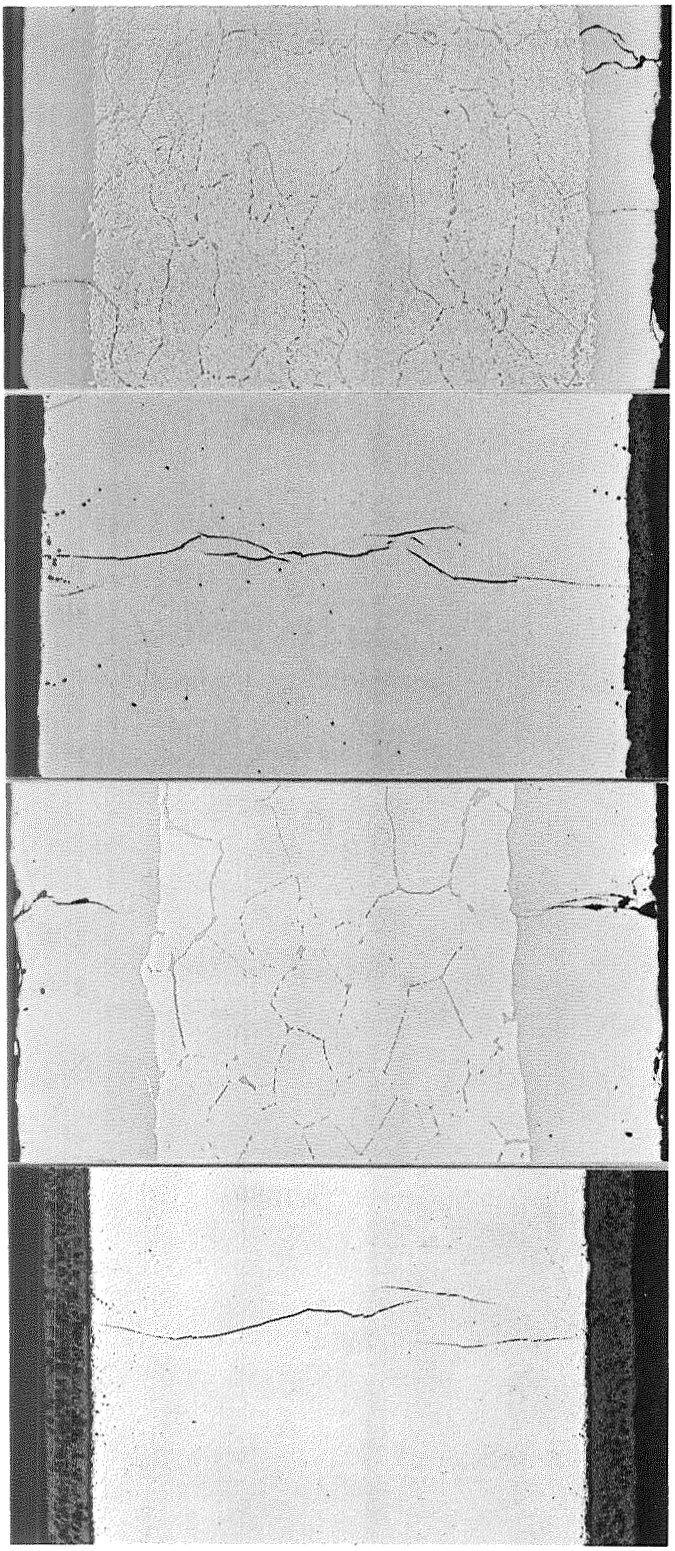

Figure 41 Cross Section of Cr-V and Cr-Ti Alloys, 100 hr-2100°F (1422°K)-Air, ×100, Unetched.

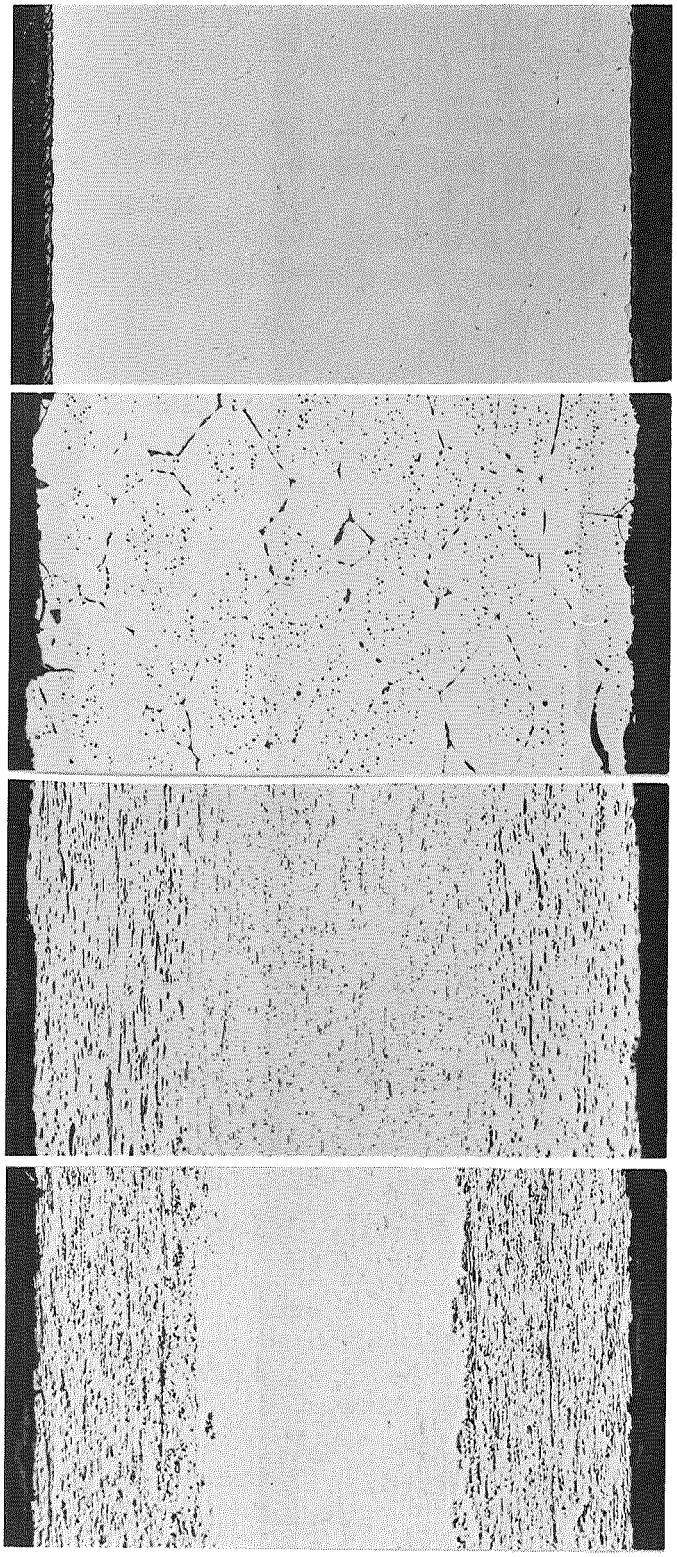

Figure 42 Cross Section of Cr-Cb, Cr-Ta, and Cr-Th Alloys, 100 hr-2100°F(1422°K)-Air, ×100, Unetched.

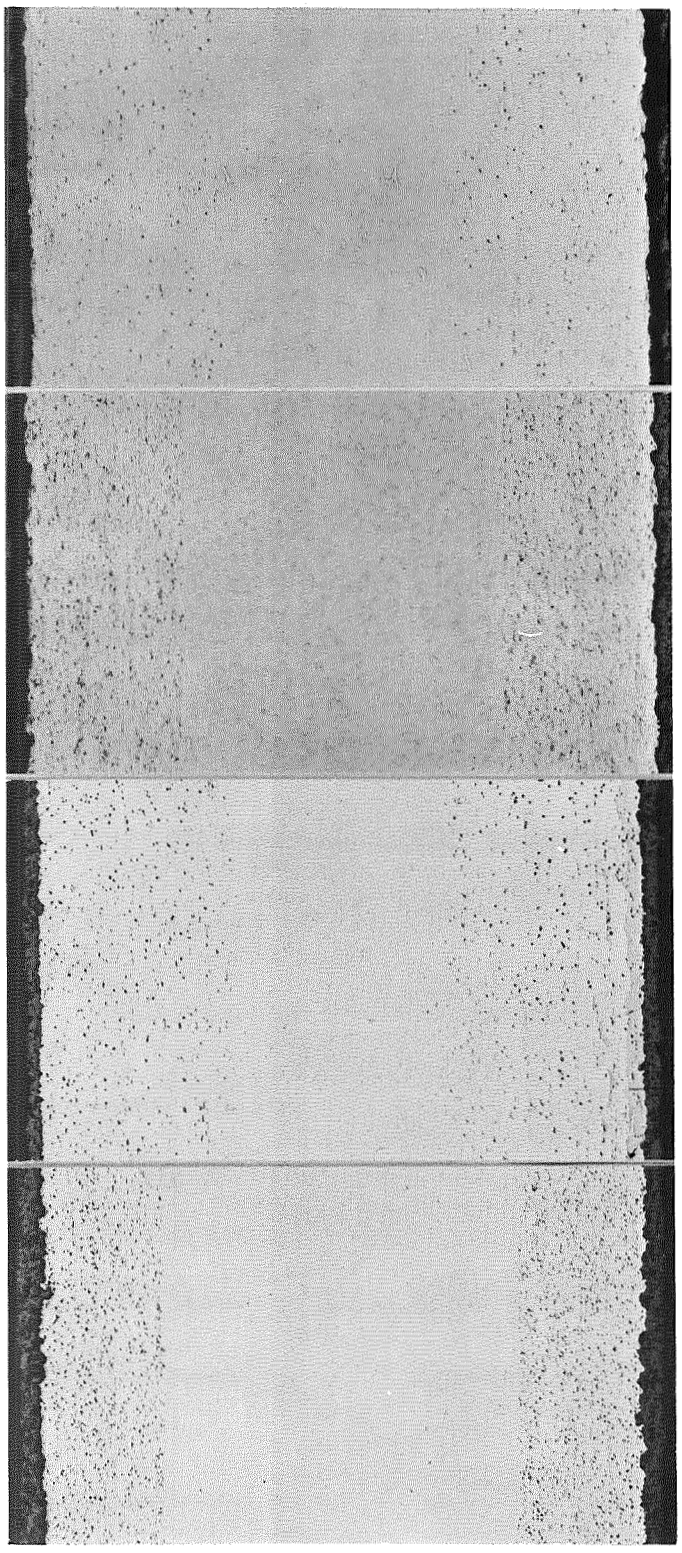

Figure 43 Cross Section of Cr-Zr and Cr-Hf Alloys, 100 hr-2100°F(1422°K)-Air, ×100, Unetched.

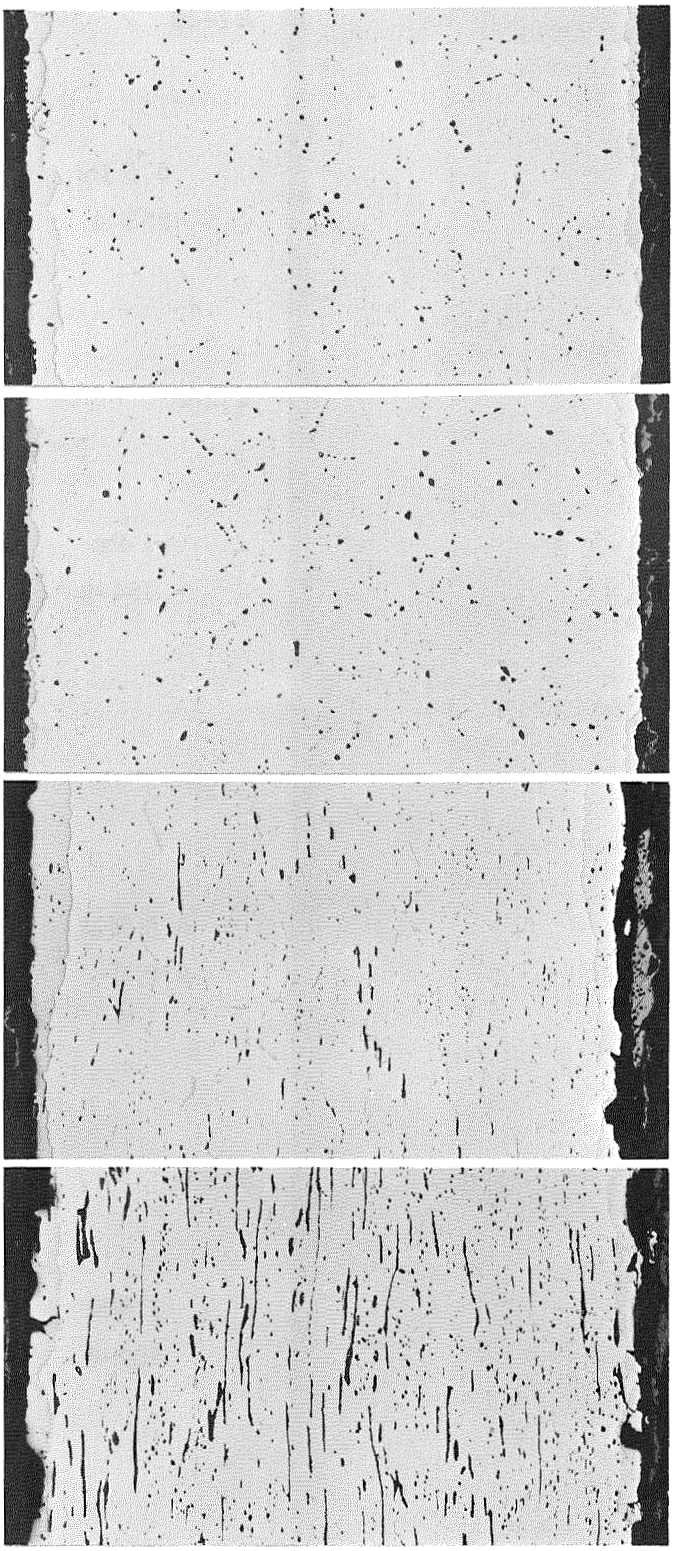

Figure 44 Cross Section of Cr-La and Cr-Y Alloys, 100 hr-2100°F (1422°K)-Air, ×100, Unetched.

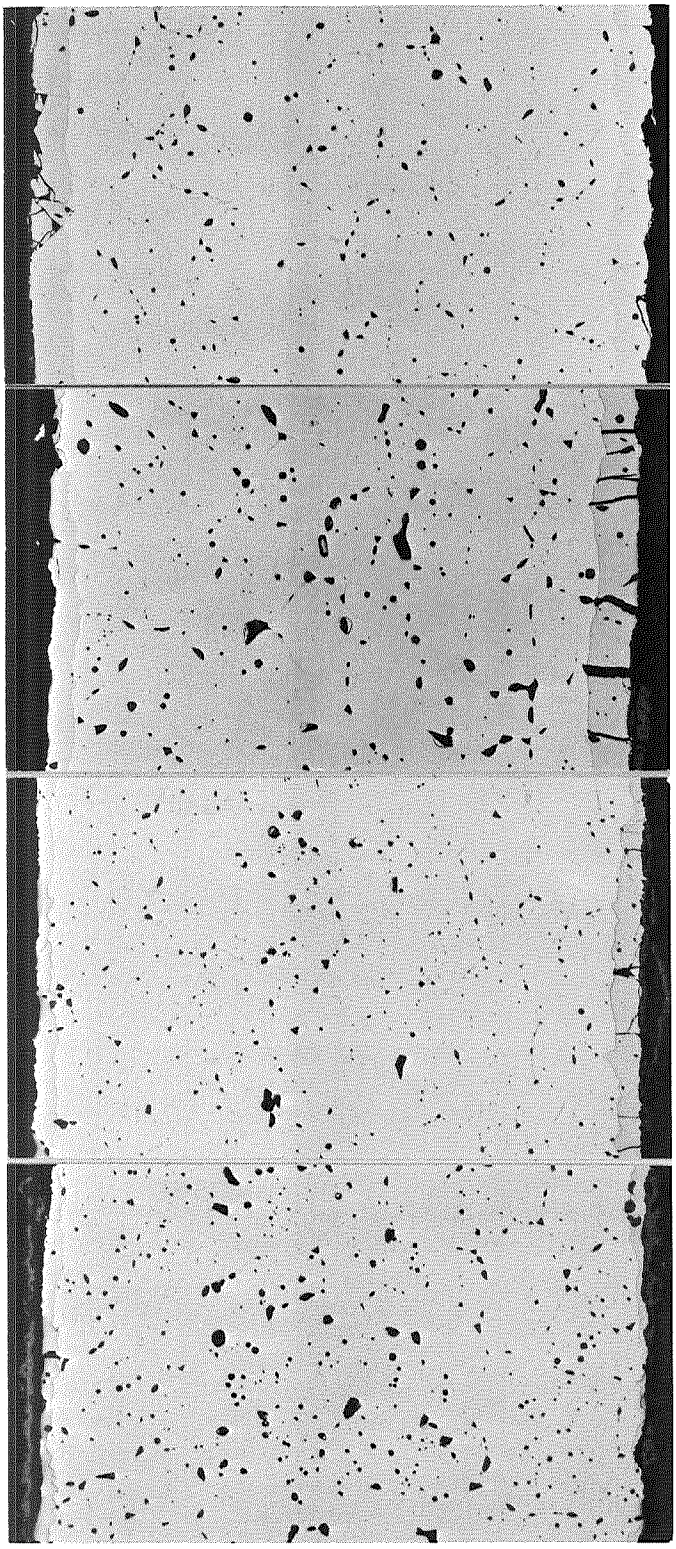

Figure 45 Cross Section of Cr-Pr and Cr-Mischmetal Alloys, 100 hr-2100°F(1422°K)-Air, ×100, Unetched.

Table 8

NITRIDE CASE THICKNESS IN AIR-EXPOSED ALLOYS
(The level of alloy addition is indicated in parentheses. Refer to Table 6.)

5 – 8 Mils per Side	3 – 4 Mils per Side	1 – 2 Mils per Side	0.1 – 0.5 Mils per Side	Nil
Ti (Low)	Fe (All)	Ru (Low)	Hf (All)	V (High)
Ta (All)	Mo (High)	Co (All)	Y (High)	Cb (Low)
Mo (Low)	W (Low)	Zr (All)	Th (High)	Ti (High)
W (High)	Ru (High)	Y (Low)	La (High)	
Re (All)	V (Low)	La (Low)		
Mn (All)		Pr (All)		
Ta (Low)		Mischmetal (All)		
		Th (Low)		

The diffusion of gaseous ions through oxide scales is most likely to be the slowest step of all these processes and is believed to govern the formation and growth of nitride cases. Interface or surface reactions in general tend to be very rapid, and it has been shown by tests in pure nitrogen that diffusion of nitrogen through the nitride and into the core also is very rapid. It is unlikely that these factors would goven case formation on exposure to air. The fact that the alloys that form the most protective oxides (Zr, Hf, and rare earths) in pure oxygen also have the least thick nitride case lends further support to the conclusion that oxide scales govern this process.

The only exception to this pattern appears to be the behavior of alloys containing V, Cb, and Ti. At least one composition in each of these systems did not develop a distinct nitride case on air exposure at 2100°F (1422°K) (Figures 41 and 42). With Ti and V, this occurred at high alloy additions (2 at.%) and appears to be the result of greatly increased solid solubility of nitrogen or internal nitridation. V and Ti are known to have a strong sink effect, for nitrogen in other metals, and most likely increase solid solubility or accelerate the inward diffusion of nitrogen to the point where a stable nitride case cannot be formed in 100 hr at 2100°F (1422°K). The V-containing alloys are heavily nitrided internally, as shown in Figure 37.

The behavior of columbium appears to be somewhat different. Lack of nitride case formation in alloys of this system most likely results from an oxide scale effect. Although columbium does not significantly improve resistance to oxidation and scaling in air or oxygen, it does promote formation of a very adherent thin inner subscale. The subscale does not retard oxidation since it, in turn, is oxidized to a nonprotective outer scale. However, the subscale can provide a major barrier to nitrogen diffusion and as such can restrict nitride case formation. In effect, the oxide subscale slows down the rate of arrival of nitrogen at the oxide/nitride interface to the point where it is less than the inward diffusion rate into the substrate at the nitride/metal interface. If the metal does not become fully saturated with nitrogen during exposure, a nitride case will not be formed. At sharp corners where fissures or breaks in this scale occur, a nitride did form on this alloy, as shown in Figure 46a.

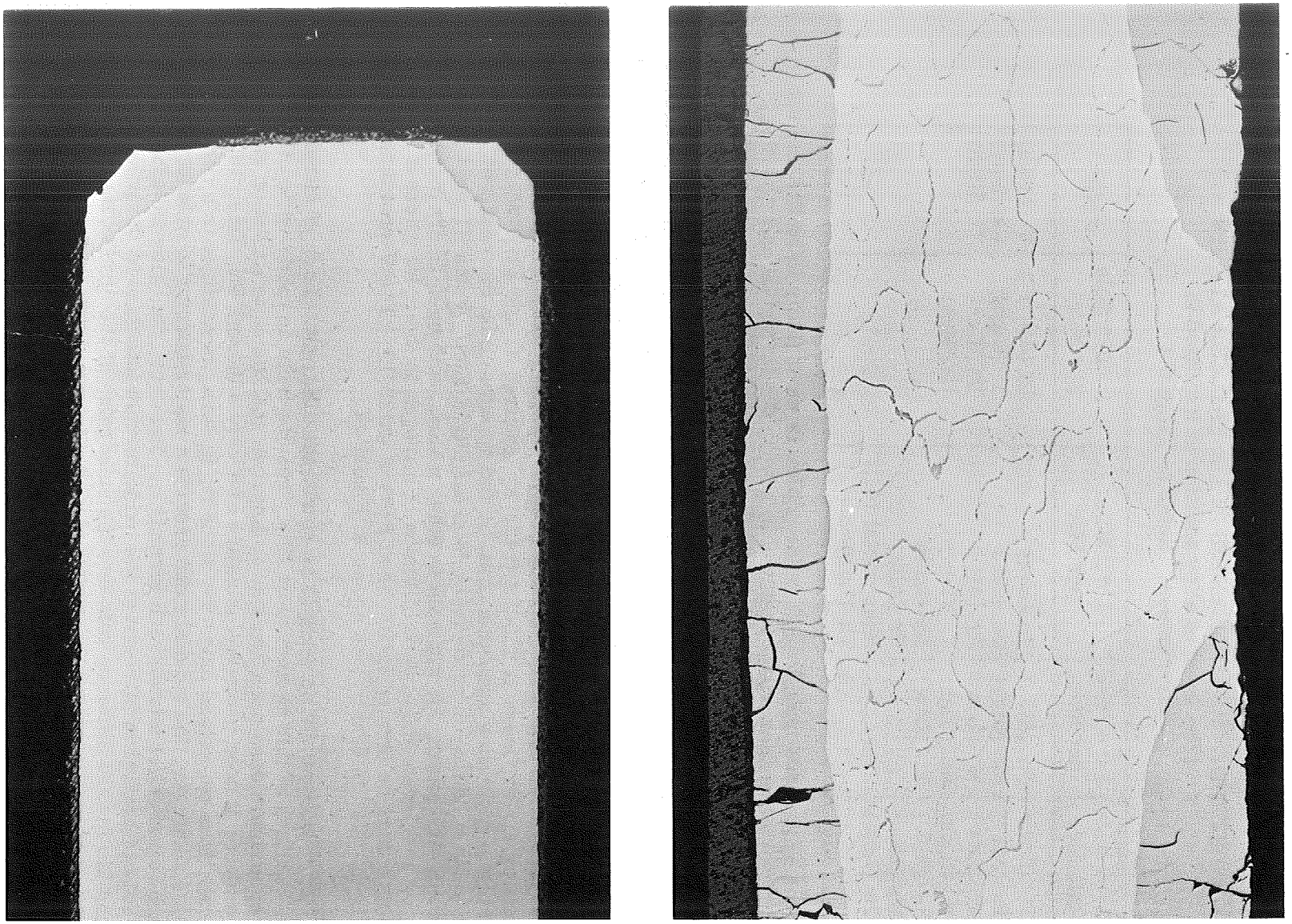

A-1406 ×100

a. Cr-0.5 Cb

A-1120 ×100

b. Cr-1 Fe

Figure 46 Influence of Oxide Scale on Nitride Case Formation.

Further evidence that the nature of oxide films governs nitride case formation is given by the observation that in some alloys a nitride case did not form or was thinner beneath the oxide scale on the areas of the surface that were shielded from electropolishing by support clips during the sample preparation step. This effect is shown for a Cr-Fe alloy in Figure 46b. The oxide scale formed over these regions was a much more effective barrier to nitrogen than that formed on the remainder of the sample. The scales spalled on cooling and could not be analyzed for composition or structure. Samples were studied prior to air exposure to detect surface changes that could account for this behavior. The surface of an electropolished Cr-2Mn alloy sample in the region of the support clips is shown in Figure 47. The metal under the contact strip is very fine grained compared with metal in the polished area, where 1 to 2 mils of the surface has been removed. In addition, it is worked and abraded from mechanical polishing. Electron probe scans revealed a slight decrease in alloy content at the surface in the polished area. The change, however, was not sufficient to account for the great difference in behavior. Upon exposure to air, the thickness of nitride case formed under the oxide scale in the contact region was about one-half to three-fourths of that formed in other (polished) regions. It is concluded that a change in surface condition – roughness, purity, strain, or grain size – nucleates an oxide film that is more resistant to nitrogen penetration in the unpolished region. The exact cause and nature of the change could not be established.

Still further evidence that oxide scales govern nitride case formation is found in the behavior of Cr-La, Y, Pr, and Mischmetal alloys. The nitride cases on alloys with other elements are irregular in thickness and are not formed in some regions or are thick in other regions beneath the oxide scale (Figures 44 and 45). This behavior reflects the irregular nature of the oxides on these metals, including the tendency for blister formation and interface separation. In addition, the nitride case is thinnest on the La and Mischmetal (La-Ce mix) alloys which have the best oxidation resistance in oxygen of all the alloys.

In addition to a nitride case, most of the binary alloys have a continuous network of massive nitride phase in the grain boundaries. This structure forms at temperature and is the result of continued nitrogen pickup in excess of the solid solubility limit. In essence, it can be considered the formation of a nitride case around each individual grain of the alloy. The additions most subject to development of this structure include Fe, Co, W, Mo, Re, and Ru at all levels to 4 at.% and Ti and V at low levels (less than 1 at.%) (Figures 38–41). In general, these are the alloys that form thick nitride cases on the surface. The oxides are poorly protective and allow excessive amounts of nitrogen to enter the alloy.

Continuous networks of nitride did not form at the boundaries of any of the other binary alloys. Occasional islands of nitride were found in the boundaries or at grain intersections of chromium alloys with Y, La, Pr, Th, Mischmetal, Zr, and Hf (Figures 42 through 45). Discontinuous networks of small nitride crystals were observed in Cr-Mn and Cr-Cb alloys (Figures 39 and 42). Alloys of Cr with large additions of Ti and V (Figure 41) had a very fine two-phase structure of nitride and matrix throughout and were much more heavily contaminated with nitrogen than any of the other alloys.

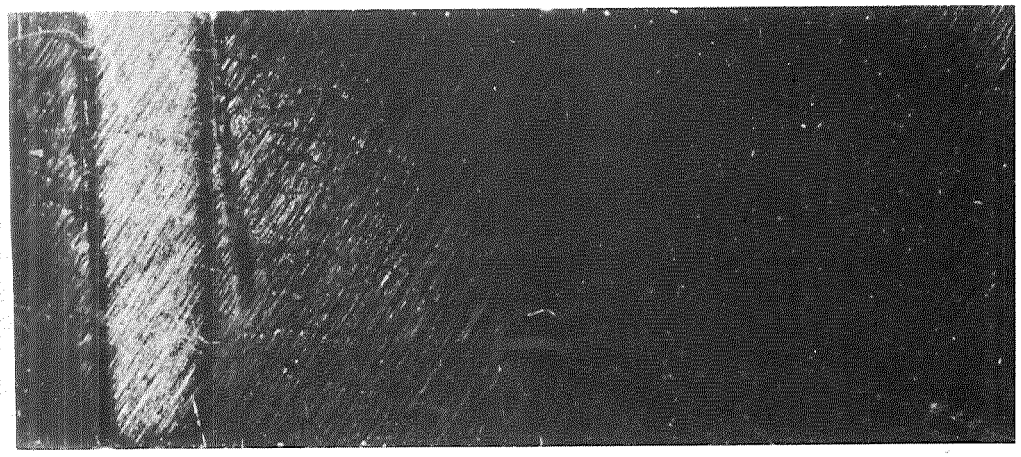

A2168 ×8

Contact Strip

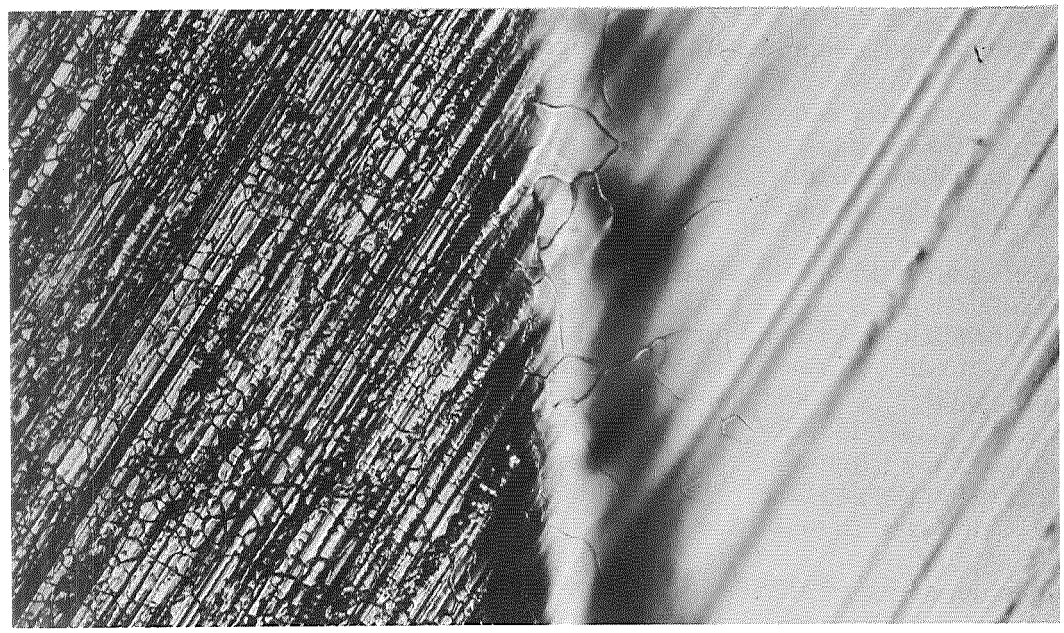

A2019 Surface Under Contact Strip | Electropolished Surface ×100

Figure 47 Surface Condition of Electropolished Specimens.

The formation of intergranular nitrides is not necessarily related to the oxide scales on the surface, since in all cases the metal is in equilibrium with a nitride case. This establishes the concentration gradient for inward diffusion and the driving force for continued pickup of nitrogen beyond the limit of solubility. Variations in the intergranular network, therefore, are more likely due to variations in solid solubility and diffusivity for nitrogen in the alloy. Low solubility and high diffusivity would favor network formation. Restricted diffusivity may be a key factor in this instance, since in all samples the metal is saturated with nitrogen as evidenced by case formation on the surface and a uniform dispersion of fine nitride precipitates within the grain throughout the cross section (Figure 37). The intergranular nitrides form in these alloys by selective nitriding of specific grains having favorable orientations. The nitrides formed in Cr-Y (Figure 48) and Cr-Mn (Figure 49) grow preferentially into one grain at a triple point or along one side of the boundary. This type of behavior is typical of conditions where the supply of the reacting element (N) is limited. In alloys where continuous networks form, all grains are uniformly nitrided irrespective of orientation.

Examination of etched structures indicates that elements such as Y, Mn, and Zr also lower the solid solubility for nitrogen at 2100°F (1422°K). These alloys have a smaller amount of large nitride platelets precipitated in the grains than unalloyed Cr does (Figure 36). The amount of nitride precipitate also decreases with increased alloy content for Y (Figure 48) and Zr (Figure 50). The effect of Zr is most striking and a Cr-3Zr alloy is almost free of nitride platelets precipitated in the grains. A high concentration of platelets is found in the Cr-1Zr alloys.

The fine structure of Cr-Y and Cr-Zr alloys was studied by transmission electron microscopy. Both alloys contain very small platelets of chromium nitride similar to those seen in optical examination at magnifications of 200 to 1000. Electron diffraction patterns obtained from the platelets could not be positively indexed as Cr_2N. The patterns were distorted due to strain or faulting and a positive identification was not possible. Platelets less than 100 Å wide by 1000 Å long were observed by transmission at magnifications of 30,000 to 120,000. Typical structures are shown in Figures 51 and 52. Small irregular islands of Y and Cr_2Zr secondary phases in the alloys also are evident in these structures. In addition, a very small particle precipitate (10 to 100 Å) was detected in several of the Cr-Y and Cr-Zr alloys (Figures 51 and 52). The precipitate appeared to form on preferred crystallographic planes aligned at right angles to each other. It is not known if this is a nitride, oxide, metal, or compound phase.

As discussed in section 5.2 on reactions with oxygen, alloys containing Zr, Hf, Th, Cb, Ta, Mn, and the rare earths were internally oxidized at 2100°F (1422°K). The same behavior was observed on exposure to air at this temperature. Oxide precipitates were formed in Cr-Mn and Cr-Cb alloys (Figure 49). The second phase in Cr-Zr, Hf, and Th alloys was darkened in a band on either side of the alloy (Figures 42 and 43) just as in the oxygen-exposed samples. The effect is shown at higher magnification in Figure 53. Darkening of the second phase in a contaminated zone is clearly evident. The phase appears to have been oxidized just as in the oxygen-exposed samples. Small islands of Cr_2N can be seen in both the contaminated and uncontaminated zones along grain boundaries of both alloys. These can be seen in Figure 53 on close inspection. Both oxygen and nitrogen have penetrated deeply into the alloy; however, the penetration of nitrogen is much greater than that of oxygen and extends into the core region where the second-phase particles are not darkened.

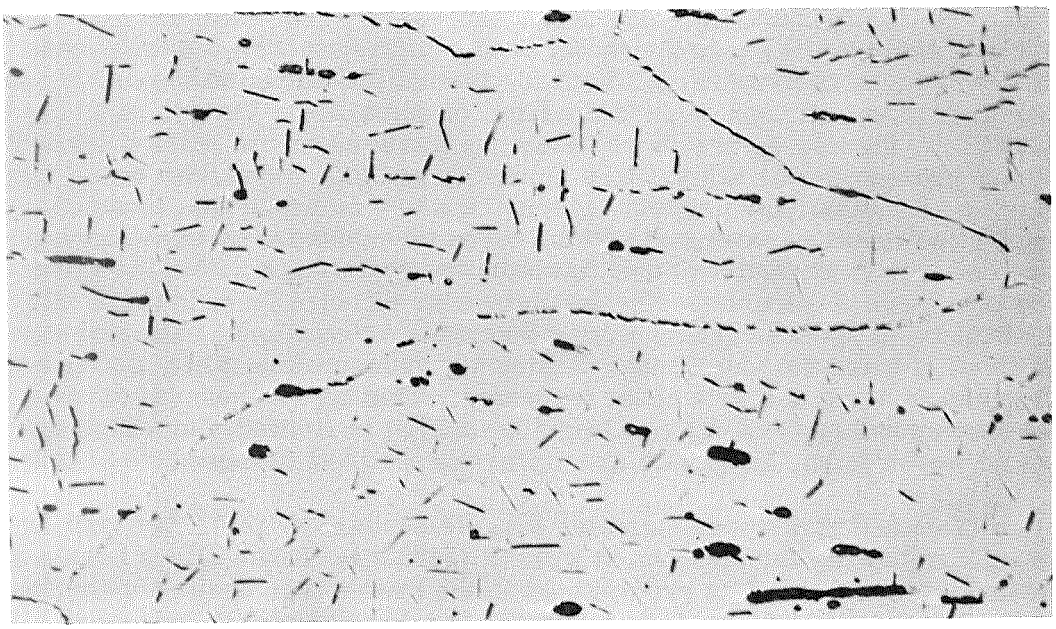

A3568 Cr-0.25Y ×1000

175 DPH DBTT >1000° F(811°K)

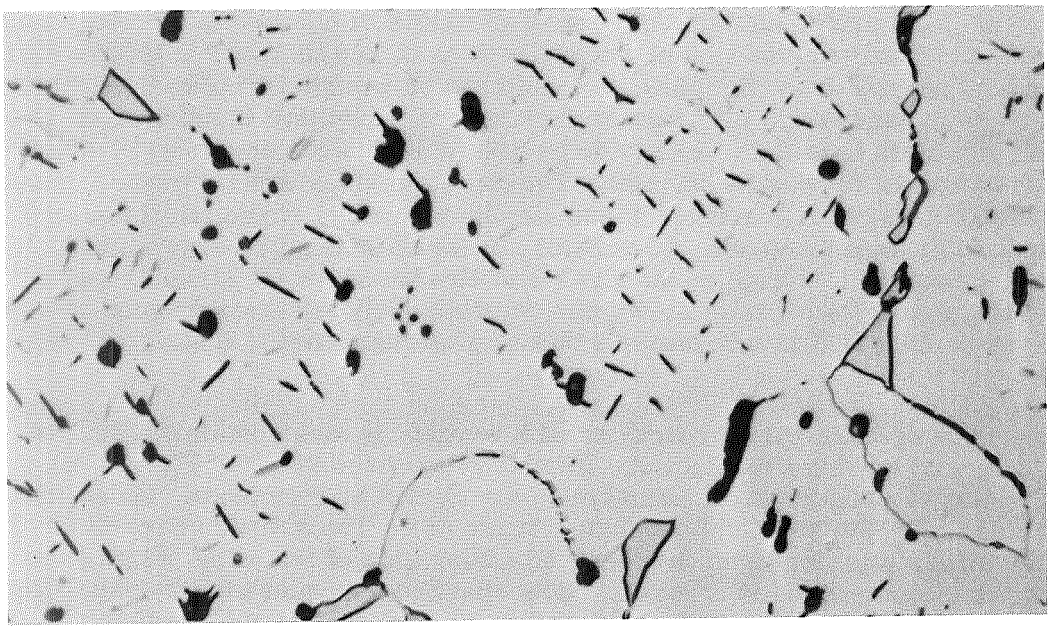

A5883 Cr-0.5Y ×1000

180 KHN DBTT < 400°F(478°K)

Figure 48 Structure of Cr-Y Alloys After Air Exposure, 100 hr-2100°F (1422°K)

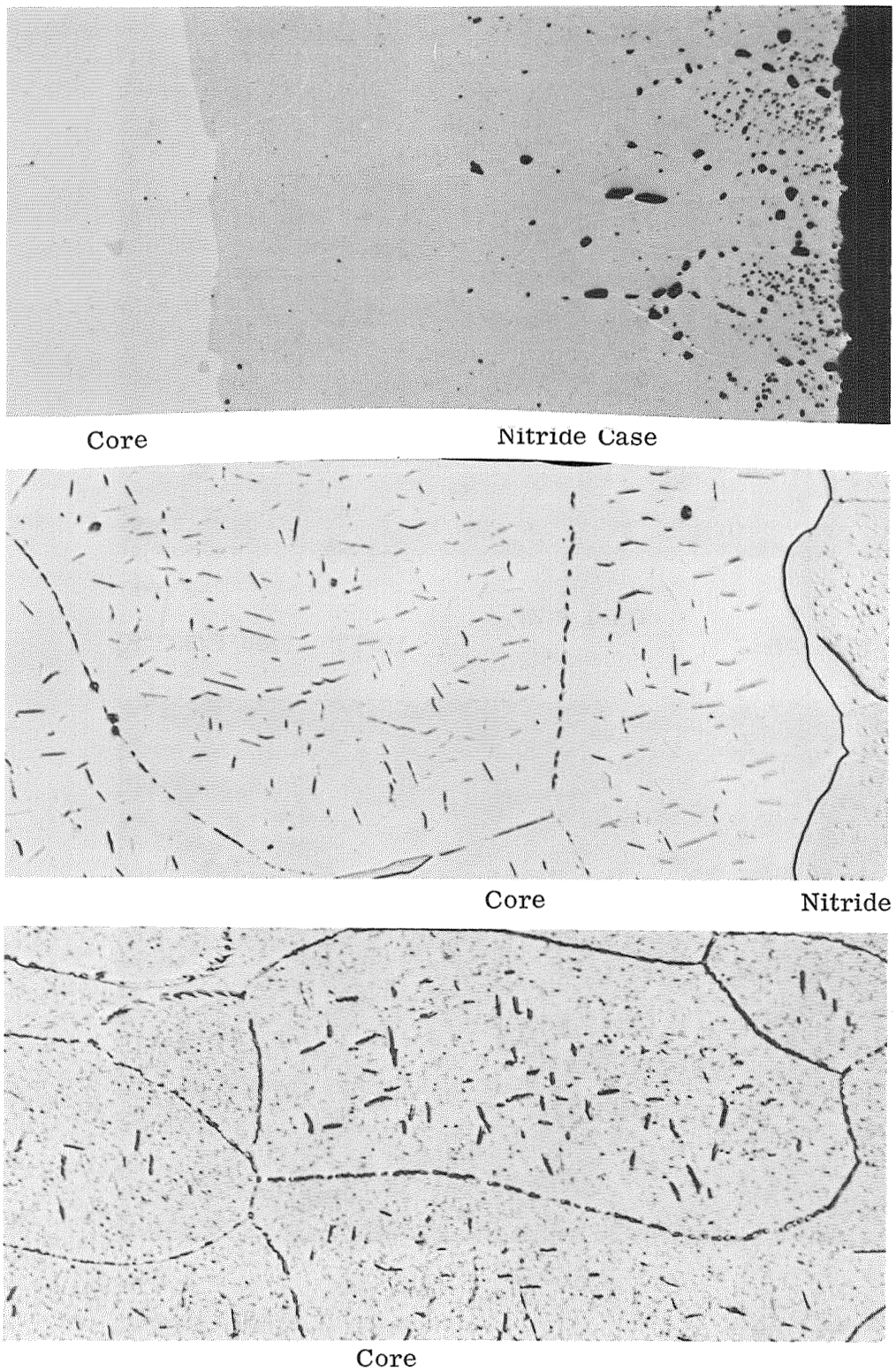

Figure 49 Structure of Internally Oxidizable Alloys After Air Exposure, 100 hr-2100°F (1422°K)-Air, ×1000.

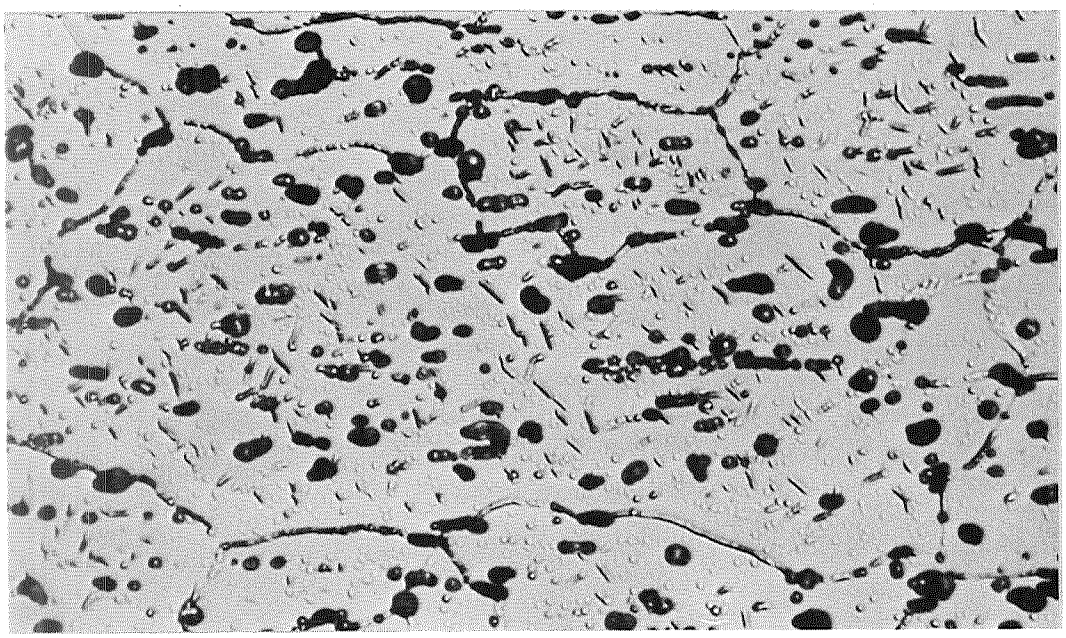

A3564 ×1000

Cr-1.0 Zr

175 DPH DBTT - 1200°F (922°K)

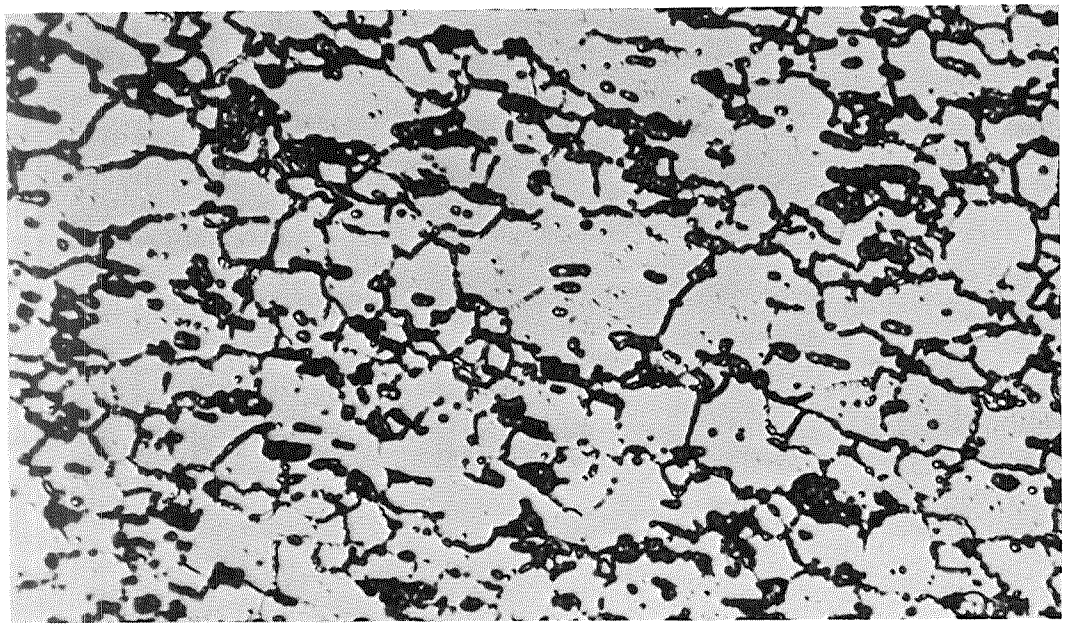

A3565 Cr-3.0 Zr ×1000

206 DPH DBTT < 1100°F (866°K)

Figure 50 Structure of Cr-Zr Alloys After Air Exposure, 100 hr-2100°F (1422°K).

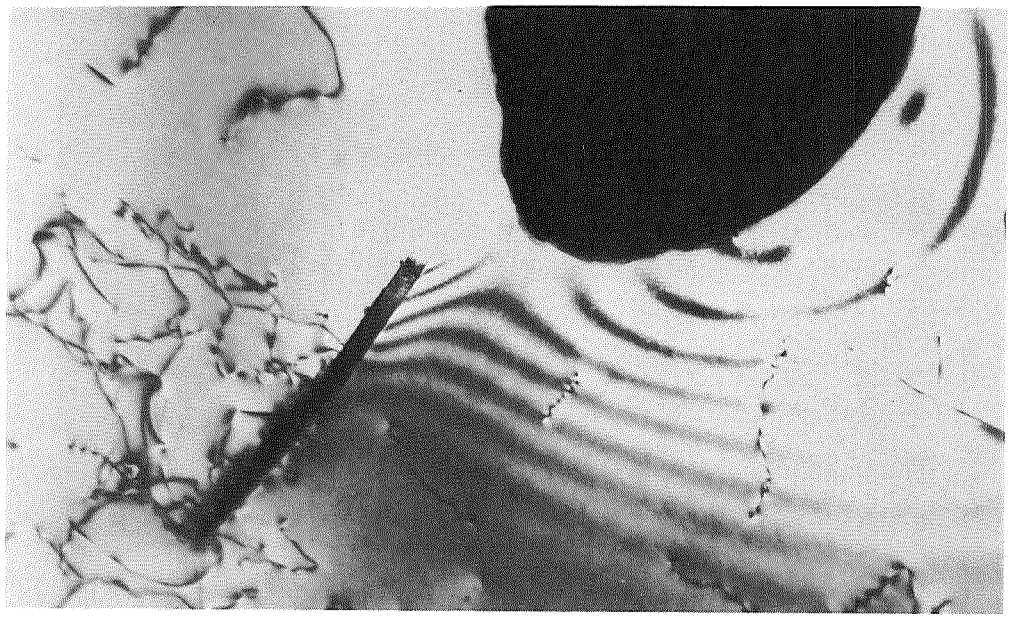

D242 ⟷ 1000 Å ×60,000

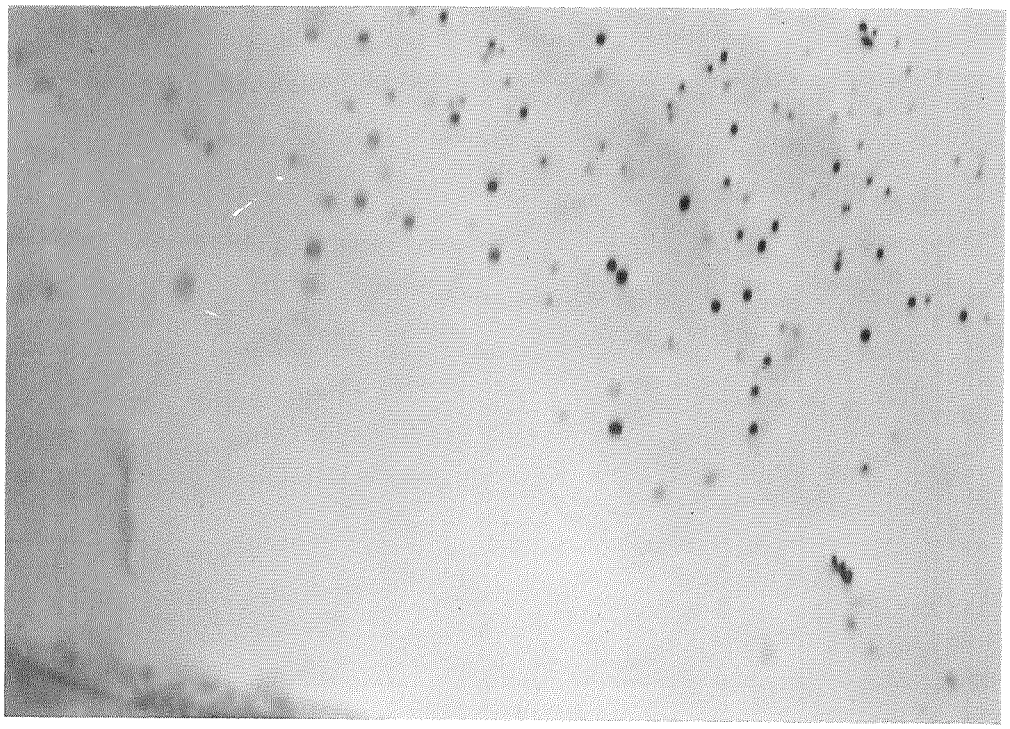

D231 ⟷ 500 Å ×120,000

Figure 51 Fine Precipitate in Cr-0.5Y(9125-5) Exposed 100 hr -2100°F(1422°K)-Air.

D86 2000 Å ×30,000

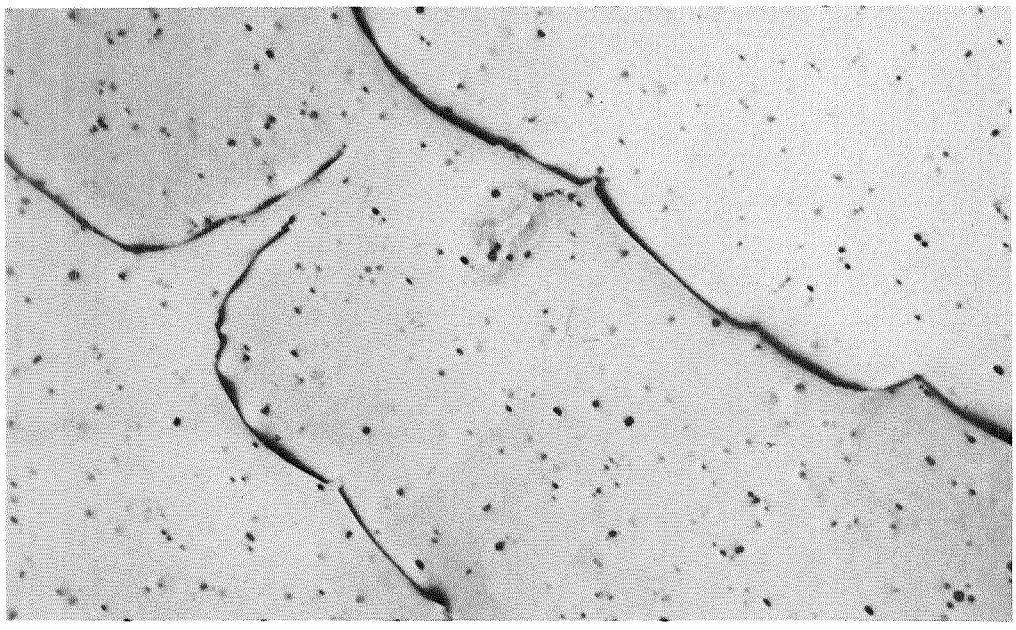

D157 500 Å ×120,000

Figure 52 Fine Precipitate in Cr-3.0 Zr(999-4) Exposed 100 hr-2100°F(1422°K)-Air.

Contaminated

Unaffected
Core

A2169 ×500

Cr-2Zr (9100-4)

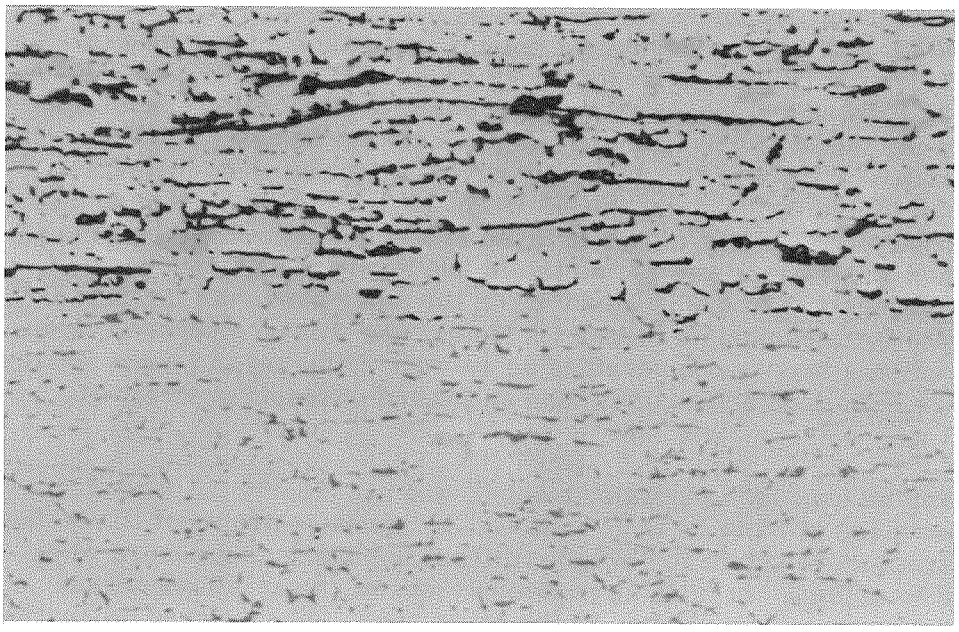

Contaminated

Unaffected
Core

A2171 ×500

Cr-2 Th(982-4)

Figure 53 Transition From Contaminated to Uncontaminated Cores in Cr-Zr and Cr-Th Alloys, 100 hr-2100°F (1422°K)-Air, Unetched.

Hardness

Hardness traverses were made on cross sections of helium- and air-exposed alloys to determine the effect of interstitital contamination on hardness and to measure the depth of contamination after air exposure. Hardness data for the initial series of binary alloys are tabulated in Appendix E and are summarized in Tables 5 and 6 and Figures 54 and 55. Data for supplemental binary alloys are presented in Table 9. With few exceptions, the substrate hardness was not increased greatly on exposure to air for 100 hr at 2100°F (1422°K). Hardness of the solid solution types of alloys was within 25 to 50 units of that for samples exposed to helium (Figure 54). Most of the interstitial contaminants (O and N) precipitate on cooling, and the precipitates formed on air cooling did not materially harden these alloys. The residual O or N in solution is likely to be very small and also did not harden the structure to any great extent. As shown in the previous discussion, the distribution of nitride precipitates is uniform across the section. Hardness also was uniform across the section, and no significant gradients were found in most of the alloys (Table 6).

Alloys containing Ti, Zr, Hf, V, Cb, Ta, Y, La, Mischmetal, and Th exhibited slightly more hardening after air exposure than the solid solution class of alloys. Base hardness increased by 25 to 100 units for these materials. The effects were not large and in many cases were not consistent. Again the nitride precipitate and residual nitrogen in solution did not materially harden the alloys.

With a few notable exceptions, hardness distribution again was uniform across the section. One Cr-V alloy had a large hardness gradient across the section due to extensive internal nitridation (Figure 37). Hardness ranged from 323 KHN just below the nitride case to 238 KHN at the sheet centerline for the Cr-0.5V alloy. A Cr-2V alloy, on the other hand, was uniform from surface to center at 310 KHN. Alloys with 0.5Zr, 0.5 Mischmetal, 0.5Th, and 2Th tended to have a slight hardness gradient from surface to center (Table 6). Values ranged from 210 to 270 KHN at the surface to 178 to 208 at the centerline. Other alloys in these systems did not have hardness gradients and the effect was largely restricted to the low levels of alloy addition. Tests with alloys containing 0.1 to 0.25 La and Y, on the other hand, did not reveal any hardness gradients from surface to center (Table 9). As will be discussed later (Section 6), these gradients may be the result of an outward diffusion and concentration of the alloy addition near the surface, rather than an inward diffusion gradient of oxygen or nitrogen.

Hardness data on samples exposed to helium, oxygen, and air clearly indicate that uniform hardness increases of 25 to 50 DPH units on air exposure are most likely due to nitrogen contamination. As shown in Table 9, little if any hardening occurs when samples are exposed to oxygen. In fact, as previously shown, many alloys soften slightly on heating in oxygen. Most alloys, on the other hand, are hardened on heating in air. The hardness increase is small and may be due to a somewhat higher residual nitrogen content in solid solution or a precipitation effect.

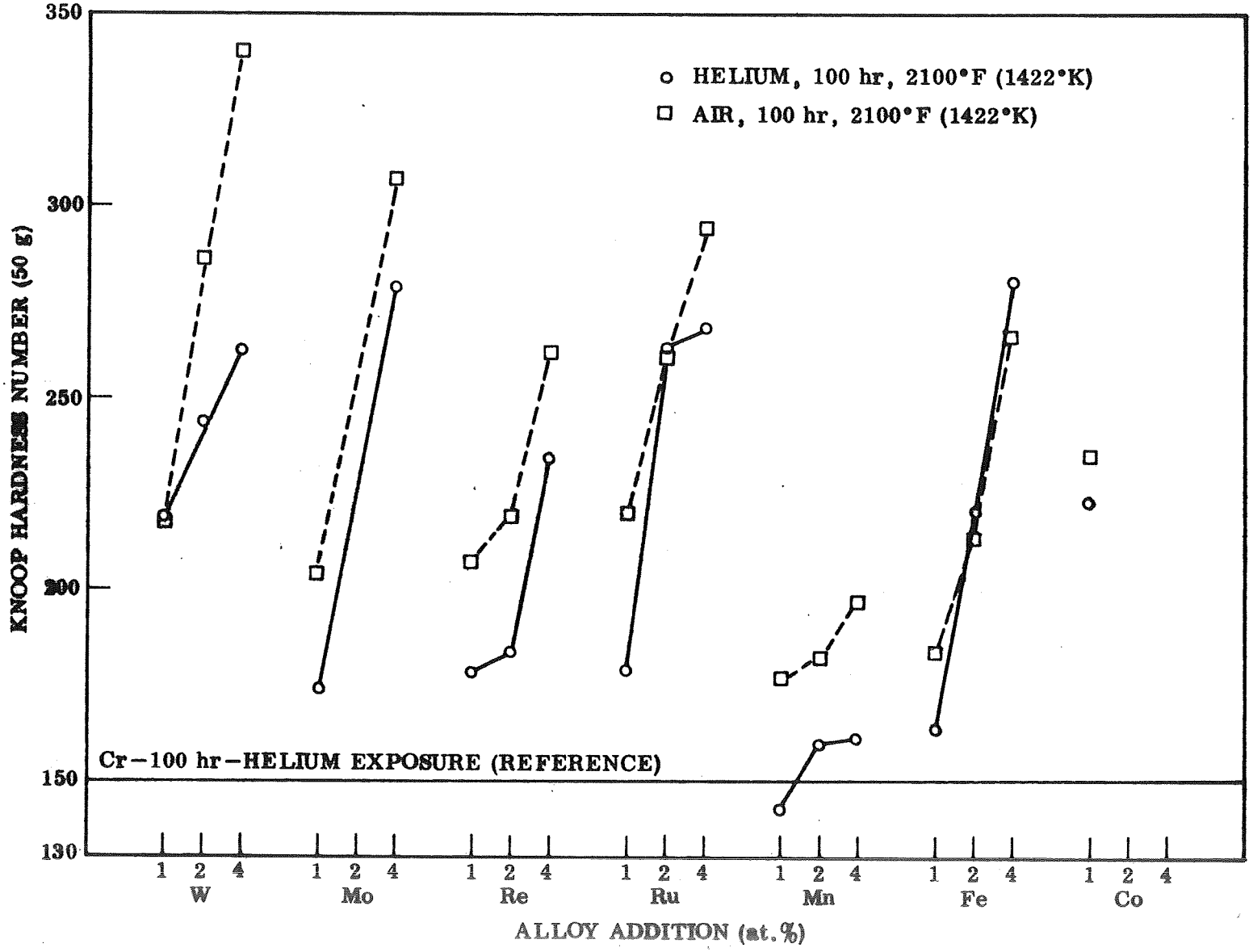

Figure 54 Effect of Solid-Solution Strengtheners on Hardness After Exposure to Air and Helium.

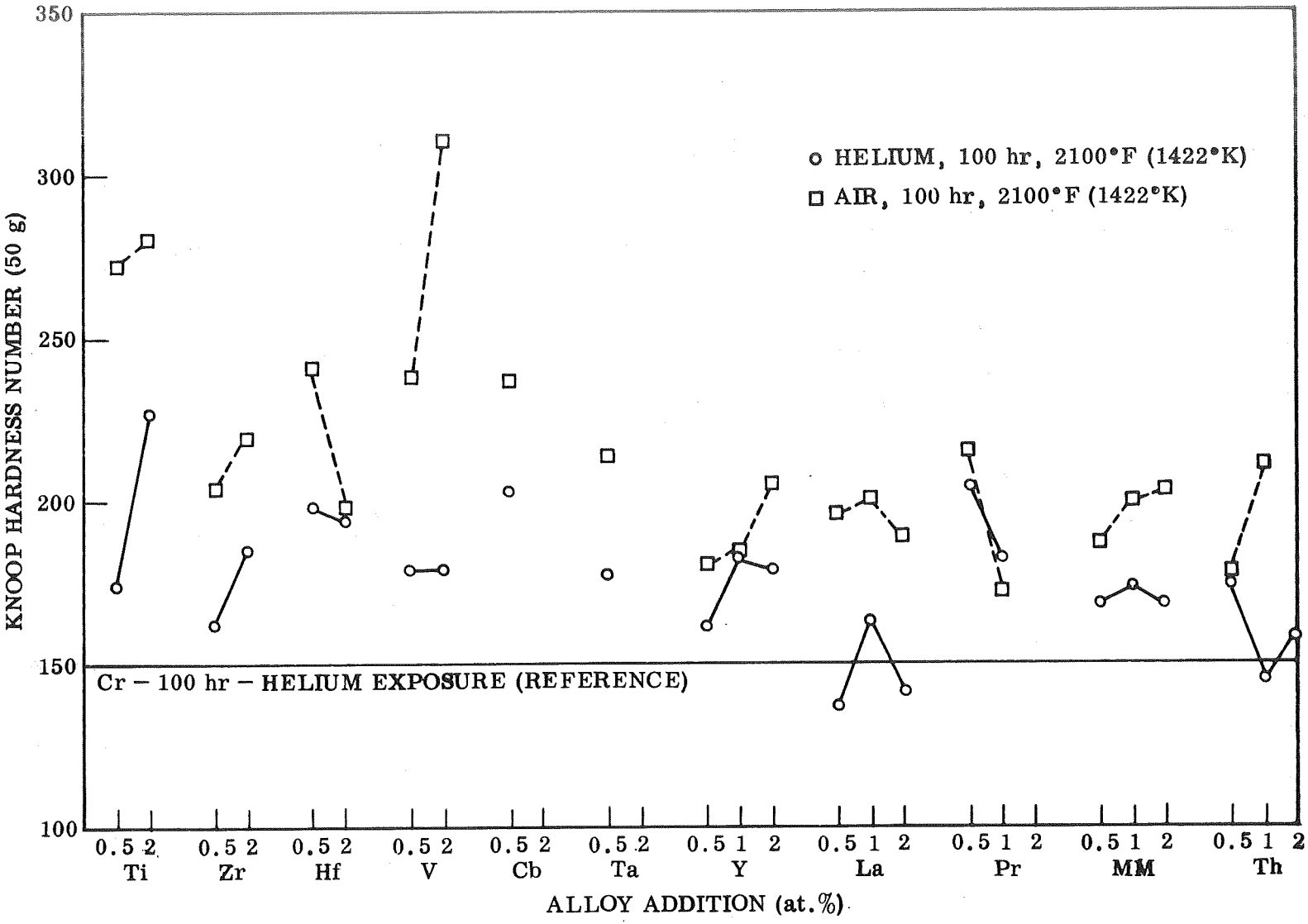

Figure 55 Effect of Nitride Formers and Rare Earths on Hardness After Exposure to Air and Helium.

Table 9

EFFECT OF ATMOSPHERE ON HARDNESS OF CHROMIUM ALLOYS
[Test conditions: 100 hr-2100°F (1422°K). All values in DPH.]

Alloy	Element		Air	
	Helium	Oxygen	Below Case	Sheet Center
1.00Cr	149	143	150	150
0.25Cb	158	137	194	194
1.0 Cb	203	203	195	195
1.0 Zr	191	141	175	175
3.0 Zr	152	186	203	203
4.0 Zr				
3.0 Mn	154	145	163	163
0.1 La	150	148	175	175
0.25La	158	147	170	170
0.1 Y	148	144		
0.25Y	149	149	175	175
0.5 Y	158	138	159	159

Nitrogen Embrittlement

The ductile-to-brittle transition temperature (DBTT) in bending was used to measure the extent of nitrogen embrittlement caused by heating in air for 100 hr at 2100°F (1422°K). Samples were bent 90° over a 4t radius at a punch travel rate of 1.0 in. (2.54 cm/min.) This is a very fast strain rate compared with that used by earlier investigators in this field and results in higher DBTT values. The data for the initial series of binary alloys are tabulated in Appendix F and are summarized graphically in Figures 56 and 57. Data obtained on supplementary binary alloys are summarized in Table 10.

Recrystallized unalloyed chromium was ductile at 200°F (366°K) and brittle at 150°F (339°K) after 100 hr at 2100°F (1422°K) in helium. After the same exposure to air, chromium sheet was ductile at 1200°F (922°K) and brittle at 1100°F (866°K). These values are used as the baseline of comparison for all other materials.

As shown in Figures 56 and 57, alloying of chromium increased the bend DBTT in the recrystallized condition by varying amounts. The data are plotted as a range, with the open symbol of each pair representing the lowest temperature for a ductile 90° bend and the solid symbol of each pair representing the highest temperature at which brittle fracture or partial ductility was observed on bending. The increase in DBTT that occurs on alloying and the subsequent increase that occurs on air exposure are shown as a function of alloy content in Table 11. Most alloy additions increase the DBTT of chromium in recrystallized condition by 200 to 300°F (111 to 167°C). Elements that produce greater embrittling include W, Mo, Re, Ti, and Cb. The least detrimental effect is produced by rare earth additions, all of which have extremely low solid solubility in chromium.

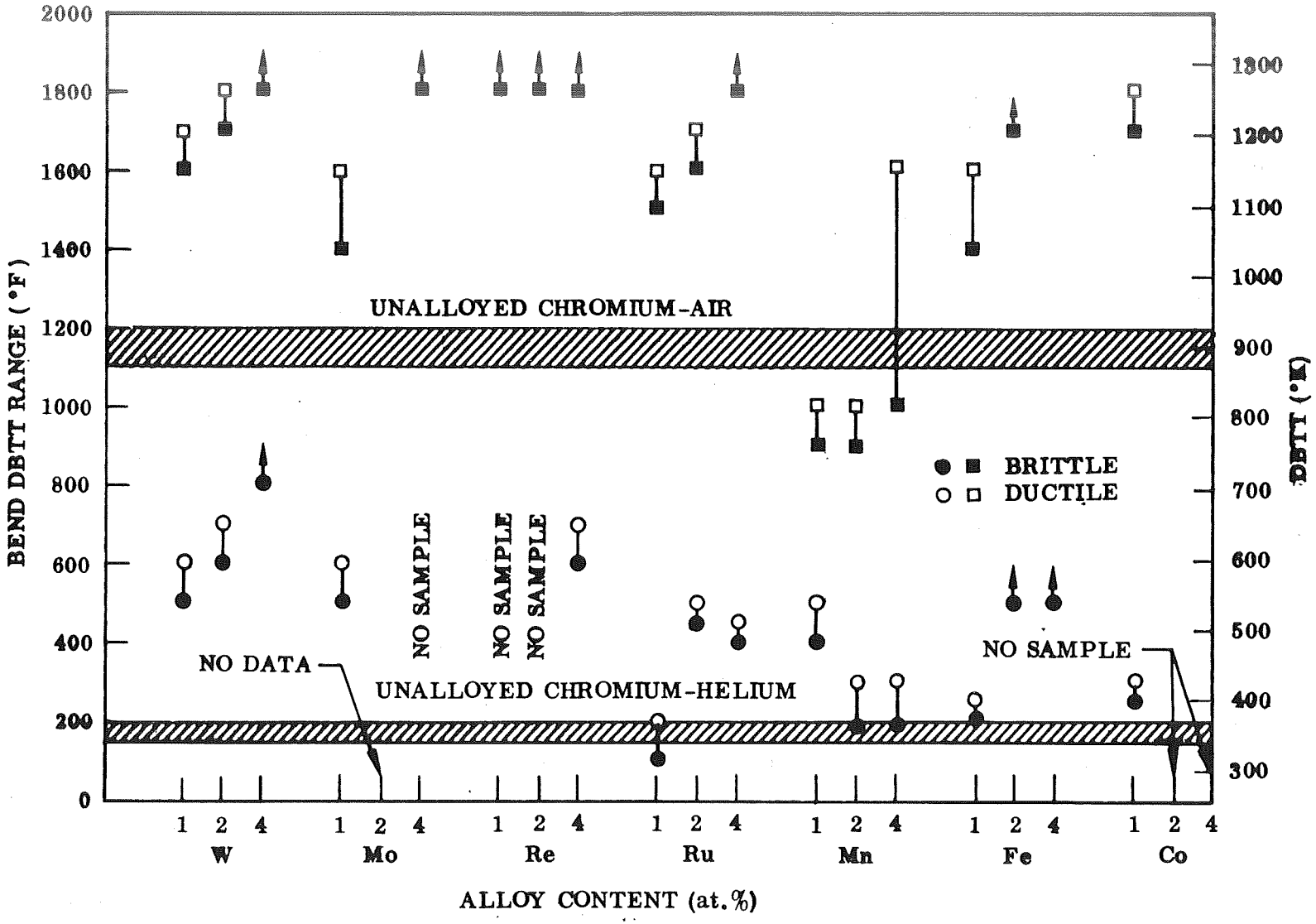

Figure 56 Effect of Solid Solution Strengtheners on Resistance to Nitrogen Embrittlement, Exposed 100 hr-2100°F (1422°K) in Helium (○) and Air (□).

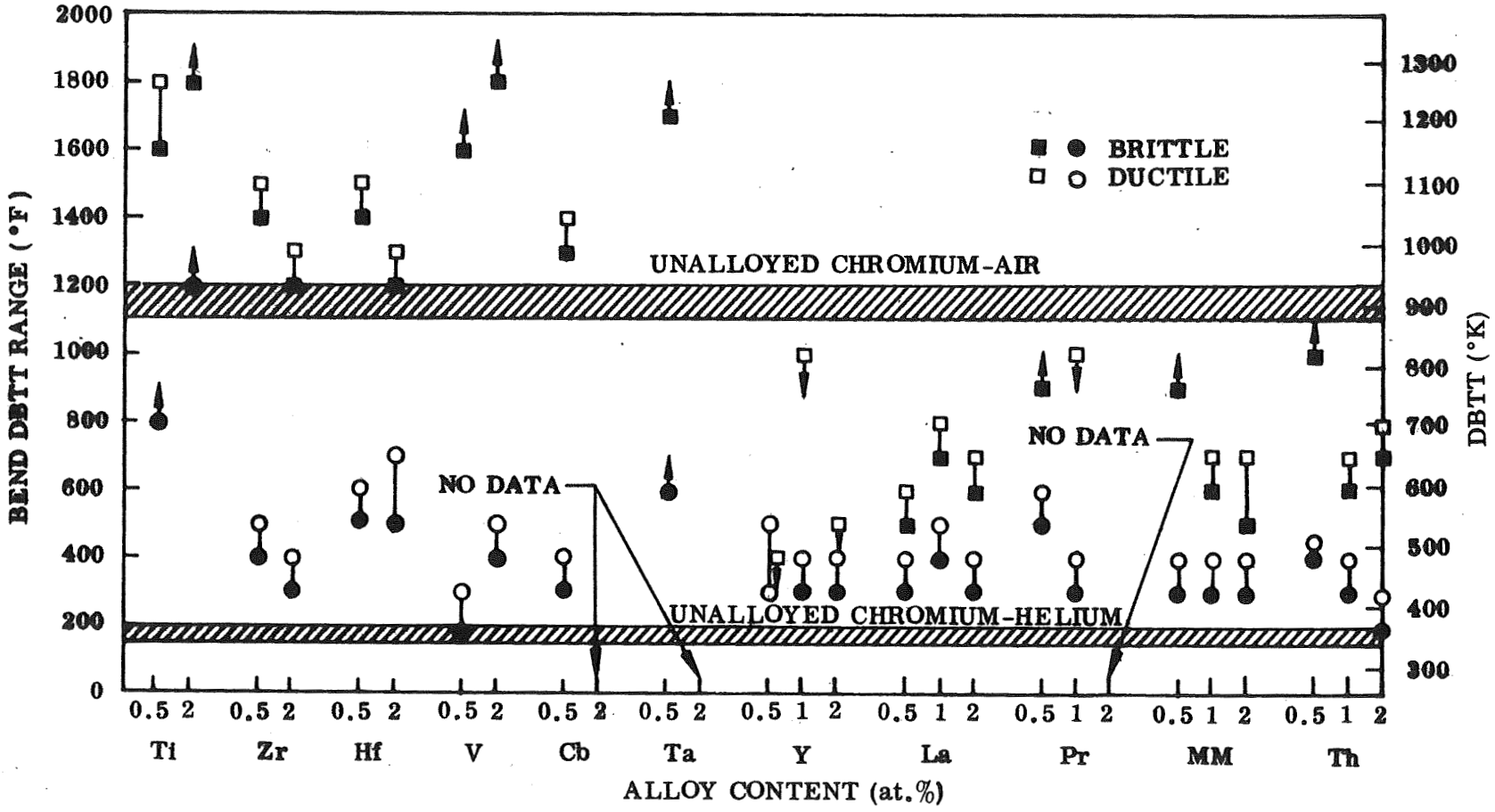

Figure 57 Effect of Nitride Formers and Rare Earths on Resistance to Nitrogen Embrittlement, Exposed 100 hr-2100°F (1422°K) in Helium (○) and Air (□).

Table 10

BEND DBTT OF SUPPLEMENTARY BINARY ALLOYS

Alloy (at.%)	Helium				Air			
	Brittle		Ductile		Brittle		Ductile	
	°F	°K	°F	°K	°F	°K	°F	°K
0.1 Y	200	366	300	422	800	700	>800	>700
0.25Y	300(a)	422	400	478	1000(a)	811	>1000	>811
0.5 Y	300(a)	422	400	478	700	644	>700	>644
0.1 La	300	422	400	478	1000	811	>1000	>811
0.25La	400	478	500	533	800(a)	700	>800	>700
0.25Cb	300(a)	422	400	478	1400	1033	1500	1089
1.0 Cb	600	579	>600	>579	600	579	1600	1144
1.0 Zr	300	422	400	478	1000	811	1200	922
3.0 Zr	200	366	300	422	>1100	>866	1100	866
4.0 Zr								
3.0 Mn	300	422	400	478	1200	922	1400	1033

(a) Partially ductile.

Many of the alloy additions actually increased the shift in DBTT that occurs on air exposure when compared with the behavior of unalloyed chromium. The increase in DBTT for alloys containing W, Mo, Re, Ru, Fe, Co, V, and Cb was 100 to 500°F (56 to 278°K) higher than the 1000°F (560°K) increase found for pure Cr. These additions, in effect, accelerated or intensified nitrogen embrittlement. The alloy additions that either did not increase or actually reduced the shift in DBTT include Mn, Zr, Hf, Y, La, Pr, Mischmetal, and Th. Manganese and the rare earths were the most effective in reducing embrittlement of chromium. In many of the rare earth containing alloys, the DBTT increased from 200 to 300°F (111 to 167°K) on air exposure compared with the 1000°F (560°K) increase for pure Cr. Only two alloys, Cr-05Y and Cr-2.0Y, had virtually no increase in the transition temperature after 100 hr at 2100°F (1422°K) in air.

When the increase in DBTT from alloying is added to the increase from air exposure, the best alloys had a total shift of 400 to 500°F (222 to 278°K) in bend transition temperature compared with 1000°F (566°K) for chromium (Table 11). The net DBTT is about half that found for nitrogen embrittled chromium in the case of average rare earth additions and in all but one case is about double the DBTT of recrystallized unalloyed chromium before air exposure. The rare earth effect was not consistent, however, and many of the alloys were almost as subject to nitrogen embrittlement as unalloyed Cr. One Cr-0.5Y alloy (950) had no increase in DBTT, whereas a second alloy (9125) had more than a 300°F (167°K) increase in the transition temperature under identical conditions of air exposure. In general, the most consistent and greatest effect with respect to reduced nitrogen embrittlement was given by additions of 1 to 2 at.% of Y, La, Mischmetal (Ce-La alloy), and Th. Additions of less than 1% yielded variable results.

Table 11

SHIFT IN DBTT ON ALLOYING AND ON AIR EXPOSURE

Alloy (at.%)	Increase From Alloying		Increase From Air Exposure		Total Increase	
	°F	°K	°F	°K	°F	°K
Cr			1000	560	1000	560
1.0 W	400	222	1100	610	1400	777
2.0 W	500	278	1100	610	1600	888
4.0 W	>600	333	—	—	—	—
1.0 Mo	400	222	1200	666	1600	888
4.0 Re	500	278	>1100	610	>1600	888
1.0 Ru	0	0	1400	777	1400	777
2.0 Ru	300	167	1200	666	1500	833
4.0 Ru	250	139	>1350	750	>1550	860
1.0 Mn	300	167	500	278	800	444
2.0 Mn	100	56	700	388	800	444
3.0 Mn	200	111	1000	560	1200	666
4.0 Mn	100	56	>700	388	>800	444
1.0 Fe	50	28	>1450	805	>1500	833
2.0 Fe	>300	167	—	—	—	—
4.0 Fe	>300	167	—	—	—	—
1.0 Co	100	56	1500	833	1600	888
0.5 Ti	>600	333	—	—	—	—
0.5 Zr	300	167	1000	560	1300	722
1.0 Zr	200	111	1000	560	1200	666
2.0 Zr	200	111	1100	610	1300	722
3.0 Zr	100	56	<1000	560	<1100	610
4.0 Zr	<300	167	>700	388	>1000	560
0.5 Hf	400	222	900	500	1300	722
2.0 Hf	<500	278	>600	333	>1100	610
0.5 V	100	56	>1300	722	>1500	833
2.0 V	300	167	>1300	722	>1600	888
0.25Cb	200	111	1100	610	1300	722
0.5 Cb	200	111	1200	666	1400	777
1.0 Cb	>600	333	—	—	—	—
0.5 Ta	>400	222	—	—	—	—
0.1 Y	100	56	>500	278	>600	333
0.25Y	200	111	>600	333	>800	444
0.5 Y	<300	167	Nil	Nil	<300	167
0.5 Y	200	111	>300	167	>500	278
1.0 Y	200	111	<800	444	<1000	560
2.0 Y	200	111	<100	56	<300	167
0.1 La	200	111	>600	333	>800	444
0.25La	300	167	>300	167	>600	333
0.5 La	200	111	200	111	400	222
1.0 La	300	167	300	167	600	333
2.0 La	200	111	300	167	500	278
0.5 Pr	400	222	>300	167	>700	388
1.0 Pr	200	111	<600	333	<800	444
0.5 MM	200	111	>500	278	>700	388
1.0 MM	200	111	300	167	500	278
2.0 MM	200	111	300	167	500	278
0.5 Th	250	139	>550	305	>800	444
1.0 Th	200	111	300	167	500	278
2.0 Th	100	56	500	278	600	333

5.4 EVALUATION OF TERNARY ALLOYS

Basic Considerations

Analysis of the behavior of binary alloys indicates that Y and the other rare earths (La, Pr, and Mischmetal) and Th are the most effective additions for controlling the nitrogen embrittlement of chromium. As shown in Table 11, these additions have the least tendency to raise the DBTT of chromium by alloying and the greatest ability to restrict pickup of nitrogen and to limit the extent of embrittlement by nitrogen. The "yttrium effect" in chromium has been well documented and appears to be reproducible based on results of many independent investigations (Ref. 19). La, Pr, and Mischmetal additions also have been shown to have a similar effect. These additions appeared to be more effective than Y in controlling the nitridation of a Cr-4Mo solution-strengthened alloy (Ref. 19).

Results of the current study concerning the relative effectiveness of rare earths are in good agreement with those of previous studies. The present work also has shown that thorium is just as effective as the rare earths and can be used as a second high-melting addition to control nitridation. As discussed in section 5.3, yttrium is the only rare earth addition that is solid in the intended service temperature range for chromium. The other rare earths are liquid at 1700°F (1200°K) and promote hot shortness if present in large amounts.

Perhaps the most significant aspect of behavior observed in current studies on binary alloys is the fact that the Y or rare earth effect was not observed or was not consistent at low-level addition. Little improvement was realized with additions of 0.1 to 0.25% Y or La. Excellent resistance was observed with 0.5% La; variable results were achieved with 0.5% Y; and little improvement was found with 0.5% Pr, Mischmetal, or Th. With additions of 1 to 2 at.%, however, excellent resistance to nitrogen embrittlement was realized with all of these additions. These results are not in agreement with those of other investigators who report consistent improvements with rare earth additions in the low-level ranges (Refs. 2,19). The reason for this disagreement may be the low processing temperatures used for many alloys in the current study. Effective control by rare earths was achieved only in alloys processed at temperatures above 2000°F (1366°K).

The use of rare earths per se to control nitridation presents many problems. These additions either promote banded structures with poor properties in the short transverse direction or intergranular segregates of low-melting metals with resultant hot shortness. High levels of alloy additions or high working temperatures are not desirable for these reasons. Complexing of the alloys with a second element designed either to supplement the rare earth addition for control of nitrogen embrittlement or to alter the distribution of the rare earth phase and permit use of higher processing temperatures would be desirable. Based on the evaluation of binary alloy behavior, Zr or Hf is the best candidate for addition for this purpose.

Zirconium and hafnium have low solid solubility in chromium and form a compound phase that is randomly distributed in the structure. This phase (Cr_2Zr or Cr_2Hf) has a marked ability to refine the grain structure and to prevent grain coarsening. Zr and Hf do not form compounds or low-melting eutectics with Y and other rare earths or

thorium and have some mutual solid solubility with these elements. In addition, as discussed in section 5.3, this phase appears to be a sink for interstitials and may reduce the amount of nitrogen taken into solution. Also, Zr and Hf promote the formation of oxide scales that adhere to the metal.

Although these elements do not have a significant effect in reducing the DBTT of chromium on air exposure, they may provide a very useful effect as a supplement to the rare earths. Recent studies by Clark (Ref. 19) indicate that small additions of Zr and Hf enhance the ability of Y to control nitridation in carbide-strengthened alloys. The study of ternary alloys in the Cr-Zr(Hf)-Y(La) and Cr-Zr(Hf)-Th systems appears to be important from several points of view. A study of high-purity ternary systems such as these should aid considerably in developing an improved understanding of alloy behavior with respect to nitridation resistance.

Manganese is the only other alloy addition that appears to have any promise for control of nitrogen embrittlement. Alloys with 1 to 2 at.% manganese are significantly resistant to nitridation and compare favorably with some of the chromium-rare earth alloys. Manganase in this range is in solid solution, and no secondary phases or precipitates of Mn are formed. As shown in section 5.3, the Cr-Mn alloys develop thick Cr_2N cases below the oxide scales but do not form continuous intergranular networks of nitrides, unlike other solid solution additions.

The problem of using manganese for control of nitrogen embrittlement is related to the need for complexing to improve oxidation resistance and further enhance nitridation resistance. Cr-Mn alloys have poor resistance to oxidation and form scales that spall readily on cooling. Complexing with Th or rare earths does not appear to be desirable, since manganese forms intermetallic compounds and very low melting eutectic systems with these metals. This would be expected to further detract from the already undesirable characteristics of rare earth additions with regard to hot shortness in Cr. Manganese also forms compounds and low-melting eutectics with Zr and Hf. These elements might be acceptable modifiers and would appear to be more desirable than the rare earths. Zr and Hf, however, do not markedly improve oxidation resistance and have little effect on nitrogen embrittlement of chromium. Although some useful alloys might be developed in a Cr-Mn-Zr(Hf) system, it was concluded that study of other alloys containing the rare earths would better suit the overall objectives of this program. As a result, no further work with manganese as an addition to chromium was undertaken.

Structure and Properties

Four ternary alloys were selected for the evaluation of alloy complexing behavior:

- Cr-0.5Y-1.0Th
- Cr-2Zr-1.0Th
- Cr-2Zr-0.25La
- Cr-3Zr-0.1Y

These alloys were formulated on the basis of additive and complementary effects for each element. Large amounts of Zr and Th were used to produce a large amount of second phase to control nitrogen by reduced solubility or gettering. The small rare earth additions were selected to produce oxide scales that would greatly restrict nitrogen pickup. The excess of these metals in the structure also would control internal nitridation. Zirconium should further enhance oxidation behavior and limit nitrogen pickup by improving adherence of the oxide. All additions were held to levels at which the secondary phases should not produce quality or hot-shortness problems. The samples were exposed to air for 100 hr at 2100°F (1422°K) and evaluated for structures, hardness, and bend DBTT. The results are summarized in Table 12 and Figures 58 through 63.

Each of the ternary alloys containing zirconium was more resistant to nitrogen embrittlement than either of the respective binaries at the same level of addition. For example, as shown in Table 12, a Cr-2Zr-1Th alloy was ductile at 400°F (478°K) and had no increase in DBTT after 100 hr at 2100°F (1422°K) in air. The Cr-1Th and Cr-2Zr binary alloys had a DBTT of 700°F (644°K) and 1300°F (978°K), respectively. This ternary was the most nitridation-resistant alloy studied in this program. The Cr-0.5Y-1.0Th, on the other hand, was perhaps the least nitridation-resistant composition. It was severely embrittled by air exposure and the samples absorbed so much oxygen and nitrogen that they were severely warped and deformed in both the longitudinal and transverse directions. Only one sample was suitable for bend testing, and it was glass brittle at 500°F (533°K). The Zr-La and Zr-Y alloys with 0.1–0.25% rare earth content had a resistance to embrittlement comparable to that found for binary alloys containing 1–2 at.% Y or La. They were far more resistant to embrittlement than simple binaries with corresponding low levels of the rare earths or zirconium.

Zirconium had the most dramatic effect in complexing alloys with thorium. As shown in Figure 58, a Cr-0.5Y-1Th alloy had long stringers of thorium with some yttrium in solid solution and small islands of yttrium with some thorium in solution. The phase diagram indicates that the second phase should be α-thorium with dissolved yttrium at a 66:33 atom ratio of Th:Y. However, at a 60:40 ratio, a two-phase structure with α-Y containing dissolved Th can exist as a second phase (Ref. 17). By complexing a 1% Th alloy with 2Zr, small islands of thorium appear to be nucleated on particles of the Cr_2Zr phase. The result is a structure with a random distribution of small particles as opposed to the long stringers and laminates normally found in Cr-Th alloys.

The effect of this structural alteration on oxidation/nitridation behavior is shown in Figure 59. On heating in air, the Th and Y phases in the Cr-Th-Y alloy were completely oxidized and there was a notable migration of thorium toward the surface. Massive stringers of oxidized Th-Y were formed in the metal beneath the oxide scale. The severe internal oxidation was responsible for the gross distortion of the samples and the severe embrittlement. Nitrogen also was dissolved in the alloy, as shown by the precipitation of Cr_2N platelets within the grains. No nitride case was formed beneath the oxide scale, however, indicating restricted nitrogen absorption and lack of saturation. In the Cr-Zr-Th alloy, the small islands of Cr_2Zr and Th also appeared to be oxidized or at least were darkened by the air exposure. A Cr_2N case of variable thickness was formed beneath the oxide scale and small islands of Cr_2N were observed at grain intersections. No evidence of Cr_2N platelets precipitating within the grains was found. The hardness of alloy increased by 20 DPH units but the

Table 12

NITRIDATION RESISTANCE OF TERNARY ALLOYS

Alloy (at.%)	Weight Gain in Air (mg/cm^2)	Hardness (DPH)		Bend DBTT (Brittle/Ductile)					
				Helium		Air		Increase	
		Helium	Air	°F	°K	°F	°K	°F	°C
0.5Y – 1.0Th	10.48	154	197	<300/300	<422/422	500/>500	533/>533	>200	>111
2.0Zr – 1.0Th	5.57	174	193	300/400	422/478	300/400	422/478	Nil	Nil
2.0Zr – 0.25La	3.42	173	206	300/500	422/533	650/800	617/700	300	167
3.0Zr – 0.1Y	5.90	196	197	<300/300	<422/422	400/600	478/589	300	167
100 Cr	12.00	149	150	150/200	339/367	<1200/1200	<922/922	1000	556
0.1 Y	2.44	148	167	200/300	367/422	800/>800	700/>700	>500	>278
0.25La	3.20	158	170	400/500	422/533	800/>800	700/>700	>300	>167
0.5 Y	4.46	161	180	300/500	422/533	<400/400	<478/478	Nil	Nil
1.0 Th	3.47	145	211	300/400	422/478	600/700	589/644	300	167
2.0 Zr	7.59	185	219	300/400	422/478	1200/1300	922/977	900	500
3.0 Zr	11.33	152	203	200/300	367/422	<1100/1100	<977/977	800	444

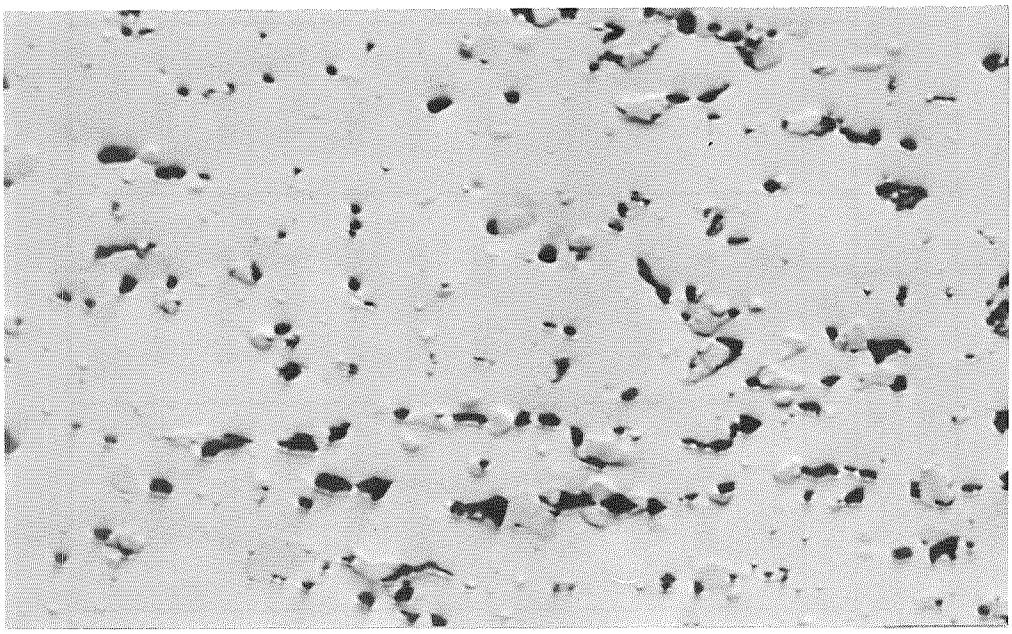

A5684 9142-2 ×1000

Cr-2Zr-1Th

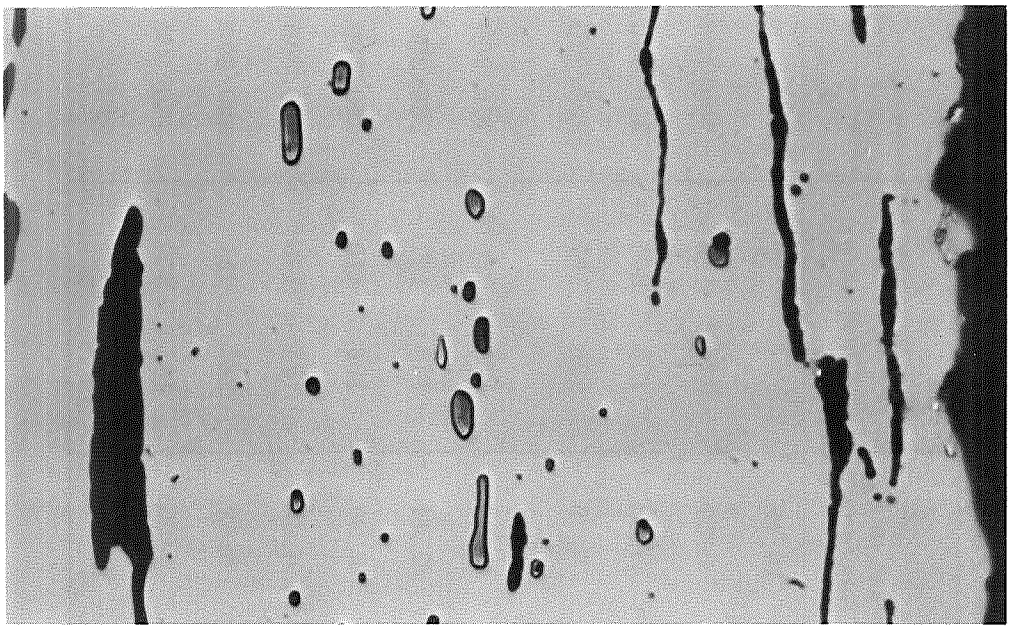

A5691 ×1000 Surface

Cr-0.5Y-1Th

Figure 58 Effect of Zr on the Distribution of Th in Cr-Base Alloys, 100 hr-2100°F (1422°K)-Helium.

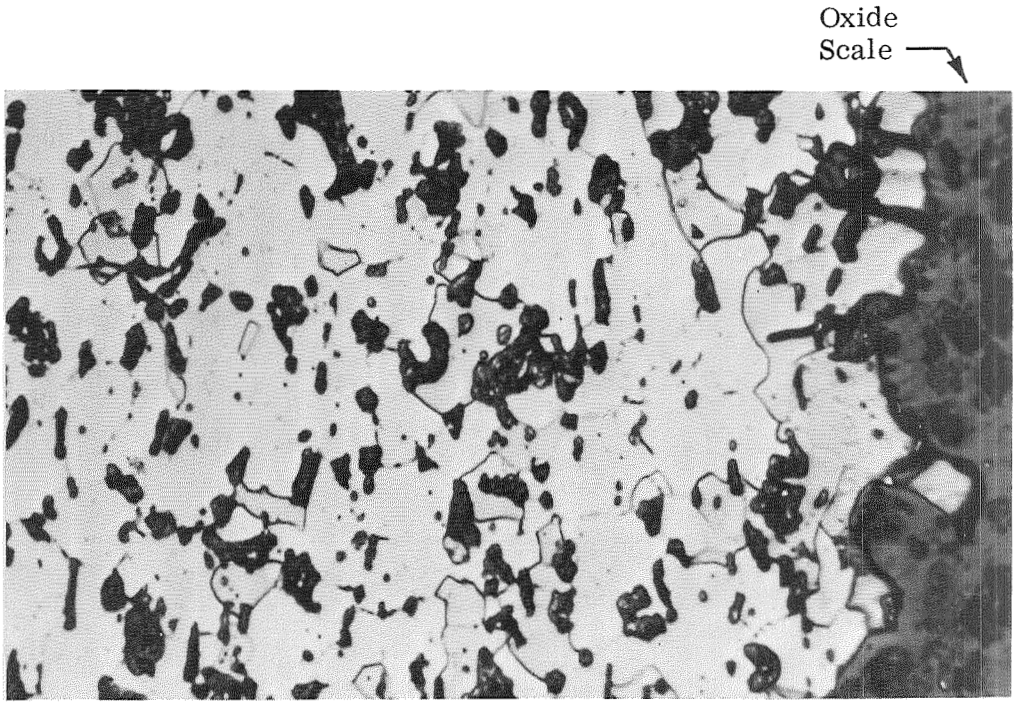

A5881 9142-8 ×1000

Cr-2Zr-1Th
DBTT = > 300 < 400°F (> 122 < 478°K)

A5693 ×1000

Surface

Cr-0.5Y-1.0Th
DBTT = > 500°F (> 533°K)

Figure 59 Effect of Zr on the Structure of Cr-Th Alloys, 100-hr-2100°F (1422°K)-Air.

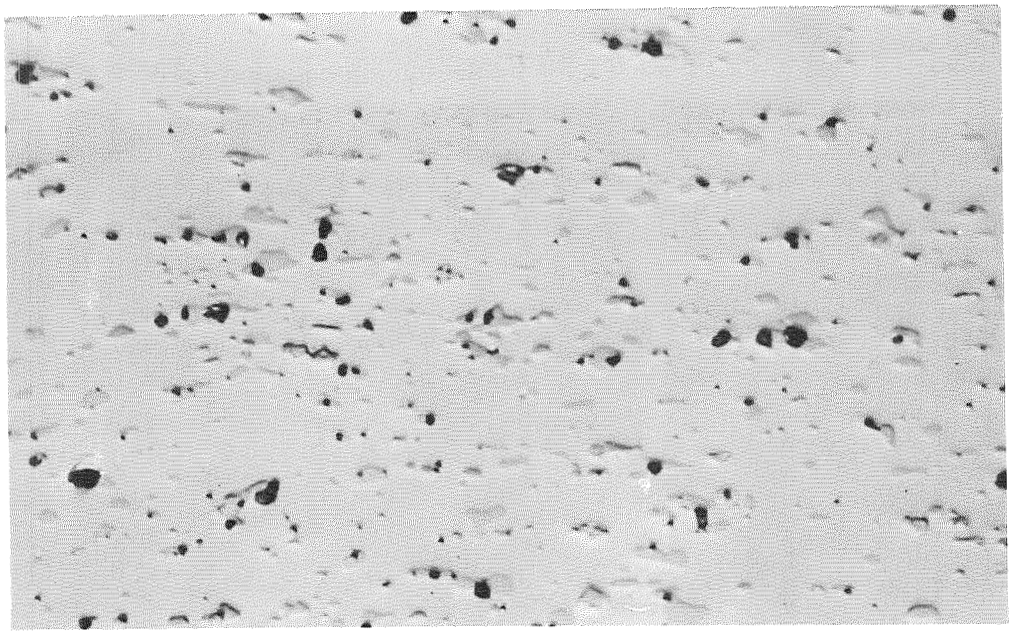

A5692 ×1000

Cr-2Zr-0.25La
100 hr-2100°F (1422°K) He

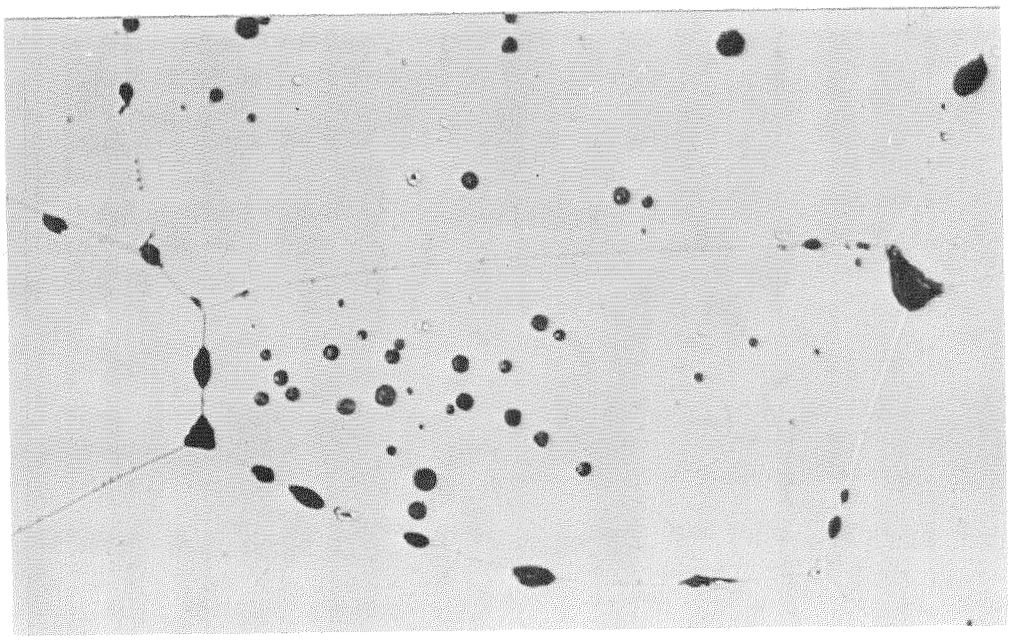

A3583 9127-5 ×1000

Cr-0.25La
50 hr-2100°F (1422°K)-O_2

Figure 60 Effect of Zr on the Distribution of La in Cr Alloys.

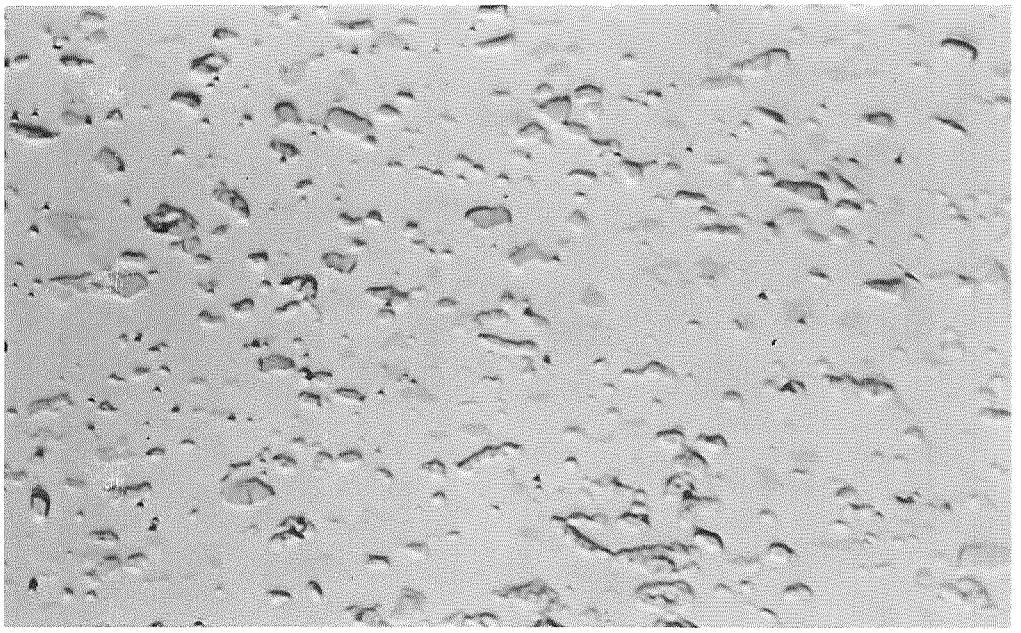

A5699 Cr-3Zr-0.1 Y ×1000

50 hr-2100°F (1422 K)-He

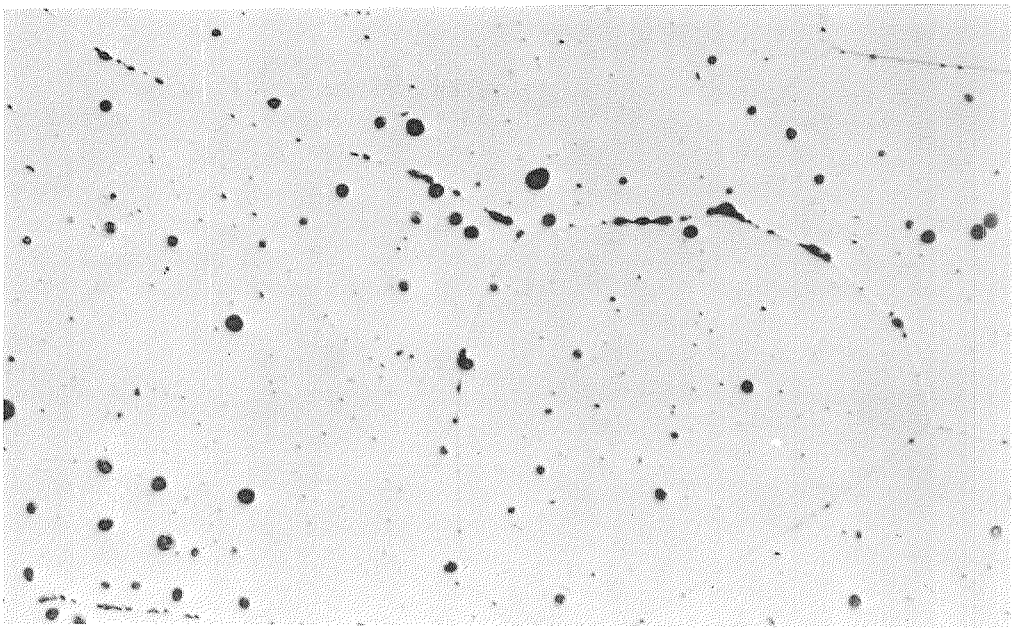

A3572 Cr-0.1 Y ×1000

50 hr-2100°F (1422°K)-O_2

Figure 61 Effect of Zr on the Distribution of Y in Cr Alloys.

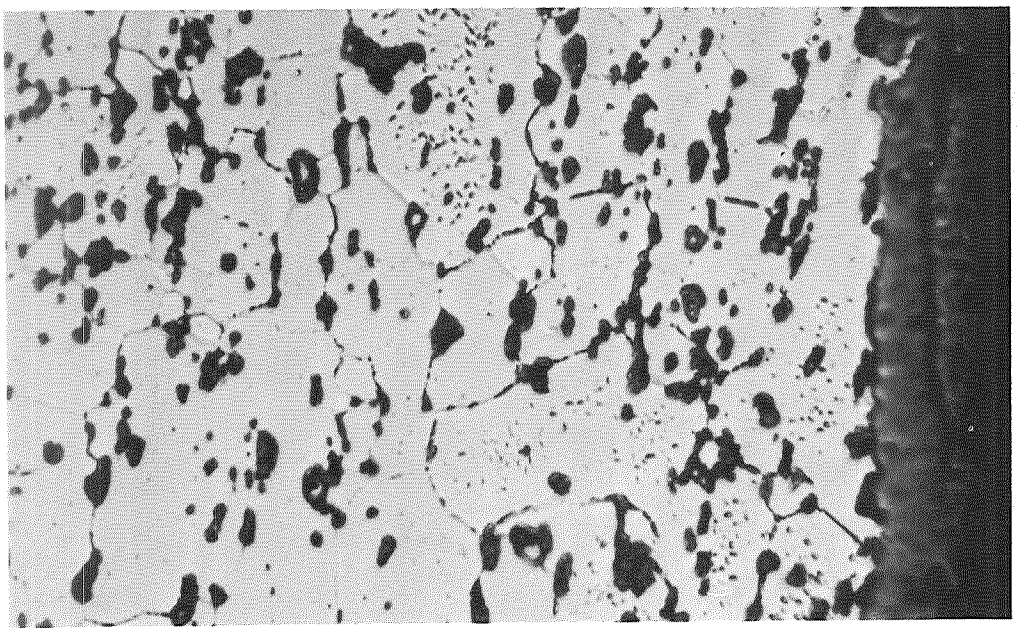

A5884 Cr-2Zr-0.25 La ×1000

DBTT = >650 <800°F
(>616 <700°K)

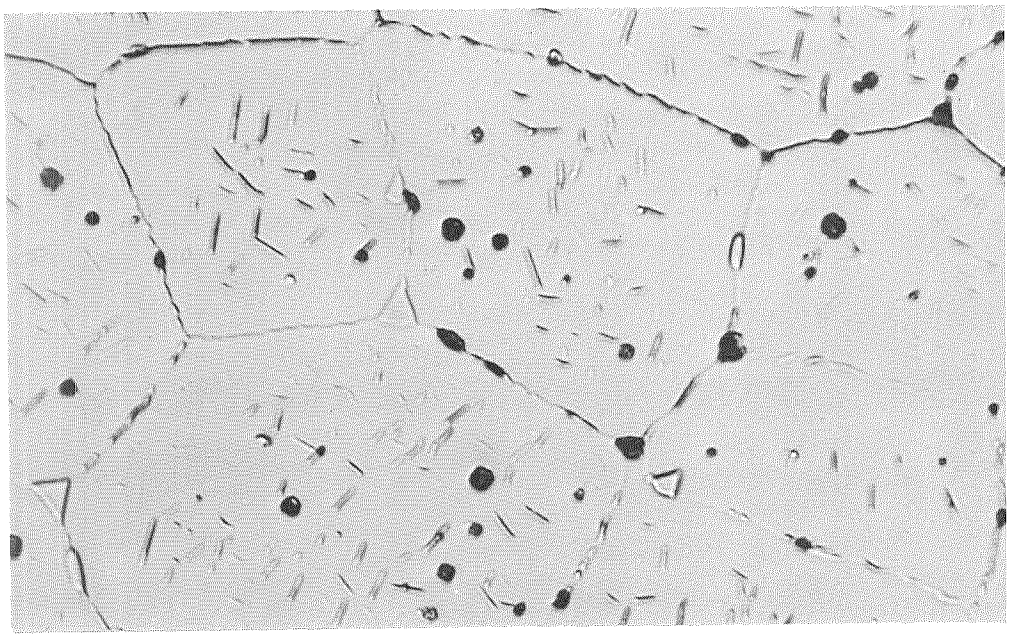

A3563 Cr-0.25 La ×1000

DBTT = >800°F (700°K)

Figure 62 Effect of Zr on the Structure of Cr-La Alloys, 100 hr-2100°F (1422°K)-Air

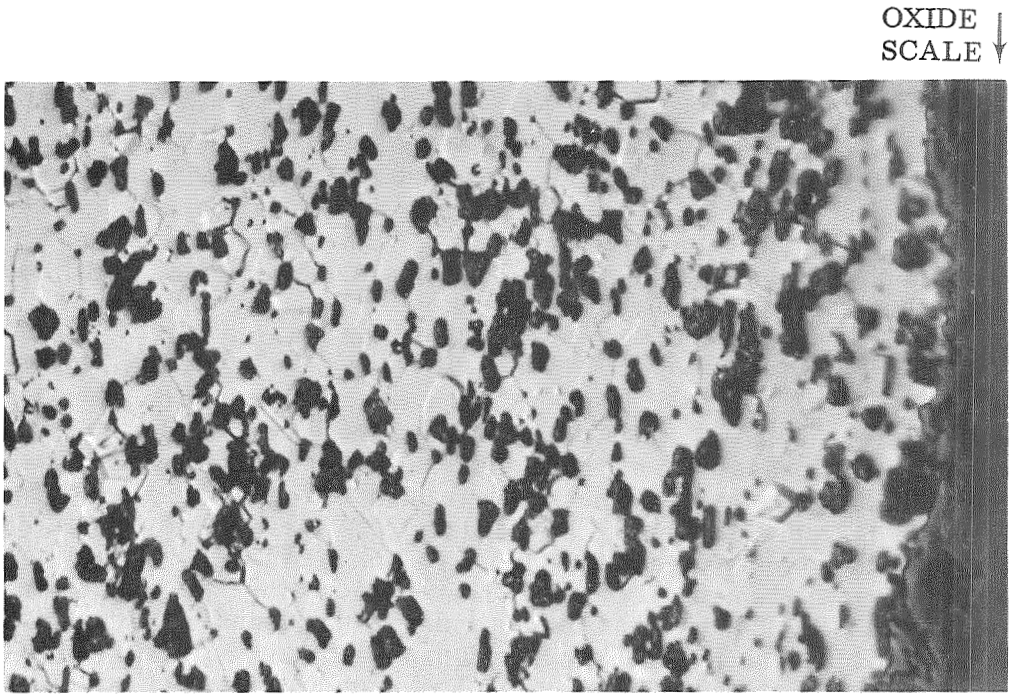

A5882 Cr-3Zr-0.1 Y ×1000

DBTT = 7400 < 600°F
(> 478 < 589°K)

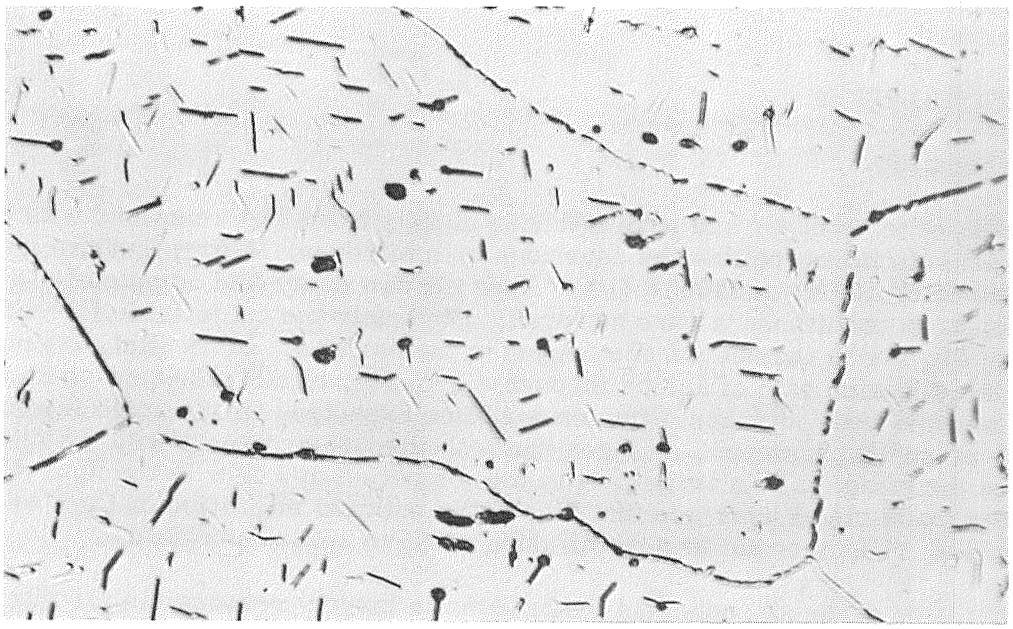

A3566 Cr-0.1Y ×1000

DBTT = >800°F (700°K)

Figure 63 Effect of Zr on the Structure of Cr-Y Alloys, 100 hr-2100°F (1422°K)-Air.

DBTT [400°F (478°K)] was not altered by the air exposure. The alloy retained a very fine-grained structure and was uniform in structure and hardness across the sheet thickness. As shown in Figure 59, the oxide scale was tightly adherent and keyed to the metal with an irregular interface. No voids were found at the oxide/metal interface. The oxide that formed on binary Cr-Zr alloys was similar but much thinner – more like that formed on Cr-Th or Cr-Y(La) alloys. The total weight gain in air was intermediate between that of the two binary systems (Table 12).

The behavior with Cr-Zr-La and Cr-Zr-Y alloys was similar in virtually all respects. As shown in Figures 60 and 61, the Cr_2Zr phase nucleated a fine random dispersion of the excess Y or La phase. On air exposure the structures showed internal oxidation of the Cr_2Zr and rare earth phases and minimum precipitation of a Cr_2N phase within the grains (Figures 62 and 63). The binary rare earth alloys without Zr, on the other hand, had extensive precipitation of Cr_2N platelets within the grains. A few fine Cr_2N platelets were observed in the Cr-2Zr-0.25La alloy and none were found in the Cr-3Zr-0.1La alloy. This behavior is similar to that found for binary alloys of Cr with 2 and 3% Zr (Figure 50). The zirconium addition again had a marked grain refining effect, particularly at the 3% level. The oxide scale formed on both alloys was thin and tightly keyed to the surface. There was no nitride case formed beneath the scale in either alloy, and no large islands of nitride were detected in grains or grain boundaries. As shown in Table 12, the weight gain for the 2Zr-0.25La alloy was the same as that for a 0.25La binary, while that for the 3Zr-0.1Y was intermediate between the weight gains for the 3Zr and 0.1Y binaries. The 2Zr-0.25La alloy hardened by 33 DPH units on air exposure, while hardness of the 3Zr-0.1Y alloy was unchanged.

5.5 PREOXIDATION

Role of Oxidation

The results of tests in air and pure nitrogen clearly show that reactions with oxygen play a vital role in controlling the reactions with nitrogen. Alloys that are not embrittled after 100 hr at 2100°F (1422°K) in air are converted completely to Cr_2N under the same conditions in pure nitrogen. Obviously the oxide scale formed on heating in air blocks the access of nitrogen to the surface. Clark (Ref. 28) points out that the diffusion rate of anions through a growing, tightly adherent scale would be very low and little nitrogen diffusion would be expected. If the scale fractures, blisters, or spalls, however, nitrogen can leak through and react with the alloy. Clark attributes the effect of Y in large part to the formation of a thin Perovskite ($YCrO_3$) film at the oxide metal interface that blocks the outward migration of Cr^{+3} to retard oxidation and, if intact, the inward diffusion of N_2 to retard nitridation.

If the formation of dense, adherent oxide films is largely responsible for nitridation resistance, then selected preoxidation treatment in pure oxygen to form the desired scale should greatly reduce subsequent reactions in air. As shown in section 5.1, preoxidation of a Cr-La alloy to produce an adherent scale did not change the reaction kinetics with pure nitrogen. However, if the scale developed fissures, nitrogen could leak through and no means would be available to repair the damage. The effect of preoxidation could be important in air exposure, where the oxide scale continues to grow and may be able to remain relatively impervious to nitrogen.

It is also significant that all the alloy additions that promote resistance to nitrogen embrittlement (Mn, rare earths, Zr, Hf, Th) are internally oxidized on exposure to pure oxygen or air (sections 5.2 and 5.3). Thus, the solution and inward diffusion of oxygen and possible precipitation of oxides within the alloy also could be a factor that governs reactions with nitrogen. Solid solubility, diffusion rate, or the morphology and distribution of nitride precipitates conceivably could be altered by internal oxidation.

Preoxidation Treatments and Results

Several experiments were conducted to determine the relative influence of surface oxides and internal oxidation on resistance to nitridation and nitrogen embrittlement. Initially, three alloys (Cr-0.25La, Cr-3Mn, and Cr-3Zr) were exposed to pure oxygen for 50 hr at 2100°F (1422°K). The samples were cooled to room temperature, weighed, measured, and reexposed to air for 100 hr at 2100°F (1422°K). Surface oxides formed by preoxidation were left intact. In the second series of tests, pure Cr, Cr-0.5 and 2.0Zr, Cr-1.0 and 2.0Th, Cr-0.5Y-1.0Th, Cr-2Zr-1Th, and Cr-3Zr-0.1Y alloys also were exposed to pure oxygen for 50 hr at 2100°F (1422°K). However, the oxide scale developed on these alloys was removed completely prior to the air exposure of 100 hr at 2100°F (1422°K). The preoxidized samples were hand-polished on 120-grit SiC paper until all traces of oxide were gone and only a clean, bare metal alloy surface remained. Both series of samples were then evaluated for structure, hardness, and bend DBTT. Results are presented in Table 13 and Figures 64 through 67.

A major reduction in the reaction with air and a marked increase in resistance to nitrogen embrittlement was realized when preoxidized alloys with oxide scales intact on the surface were exposed to air. The weight gain in air after 100 hr at 2100°F (1422°K) for a Cr-3Zr dropped from 11–12 mg/cm^2 for untreated to 1.58 mg/cm^2. The preoxidized alloy was ductile at 300°F (422°K) after air exposure and was not embrittled by nitrogen. As shown in Figure 64, no nitride case formed beneath the oxide scale and no nitride particles precipitated in the grains or grain boundaries. The effect with a Cr-0.25La was equally striking. The preoxidized alloy with scale intact gained no measurable weight after 100 hr in air at 2100°F (1422°K). As shown in Figure 65, there was no trace of nitride beneath the oxide scale or in the grains and grain boundaries. An absolute barrier to nitrogen appeared to have been achieved in this case.

The Cr-3Mn alloy behaved quite differently. Most of the oxide scale formed on this alloy spalled on cooling after preoxidation. On subsequent exposure to air, the weight gain was similar to that of normal sheet, since the bare metal was exposed. However, as shown in Table 13, the bend DBTT for the preoxidized sheet after air exposure was 200°F (111°K) below that of sheet that had not been preoxidized. This behavior indicated that internal oxidation has some effect on nitridation and nitridation embrittlement.

Tests with Cr-Zr, Cr-Th, and ternary alloys in which the oxide scale from preoxidation was removed completely before air exposure prove conclusively that internal oxidation has a major influence on embrittlement by nitrogen. In most of the cases, the weight gain in air was similar to that found for samples that were not preoxidized. Reforming the oxide contributes to most of this gain. The two ternary alloys containing Y or La had significantly lower weight gain in the preoxidized state. This may reflect some change in surface condition that alters the nature of the oxide formed on

Table 13

RESULTS OF PREOXIDATION STUDY

Alloy	50 Hr-2100°F (1422°K)-O_2 Weight Gain (mg/cm^2)	100 Hr-2100°F (1422°K)-Air Weight Gain (mg/cm^2)		Bend DBTT (Brittle/Ductile) 100 Hr-2100°F (1422°K)-Air					
	Preoxidized	Normal	Pre-oxidized	Helium		Normal		Preoxidized	
				°F	°K	°F	°K	°F	°K
Cr	7.77	12.00	6.91[a]	–	–	<1200/1200	<922/922	1100/1200[a]	866/922
Cr-0.25La	1.68	2.95, 4.09	Nil[b]	400/500	478/533	800/>800	700/>700	600/700[b]	589/645
Cr-3.0Mn	14.80	20.57, 14.18	17.40[b]	300/400	422/478	1200/1400	922/1033	1000/1200[b]	811/922
Cr-0.5Zr	5.27	4.34	4.63[a]	400/500	478/533	1400/1500	1033/1089	900/1000[a]	755/811
Cr-2.0Zr	5.61	7.59	8.04[a]	300/400	422/478	1200/1300	922/978	600/700[a]	589/645
Cr-3.0Zr	6.54	11.33, 11.99	1.58[b]	200/300	366/422	<1100/1100	<866/866	<300/300[b]	<422/422
Cr-1.0Th	1.78	3.47	3.15[a]	300/400	422/473	600/700	589/645	400/600[a]	473/589
Cr-2.0Th	3.01	3.83	3.22[a]	200/300	366/422	700/800	645/700	600/800[a]	589/700
Cr-0.5Y-1.0Th	8.74	10.48	4.46[a]	–	–	500/>500	533/>533	700/>700[a]	645/>645
Cr-2.0Zr-1.0Th	4.67	5.57	3.01[a]	300/400	422/473	300/400	422/473	400/500[a]	473/533
Cr-3.0Zr-0.1Y	6.70	5.90	2.92[a]	<300/300	<422/422	400/600	473/589	500/600[a]	533/589

(a) Oxide scale from preoxidation removed from surface before air exposure.
(b) Oxide scale from preoxidation left on surface for air exposure.

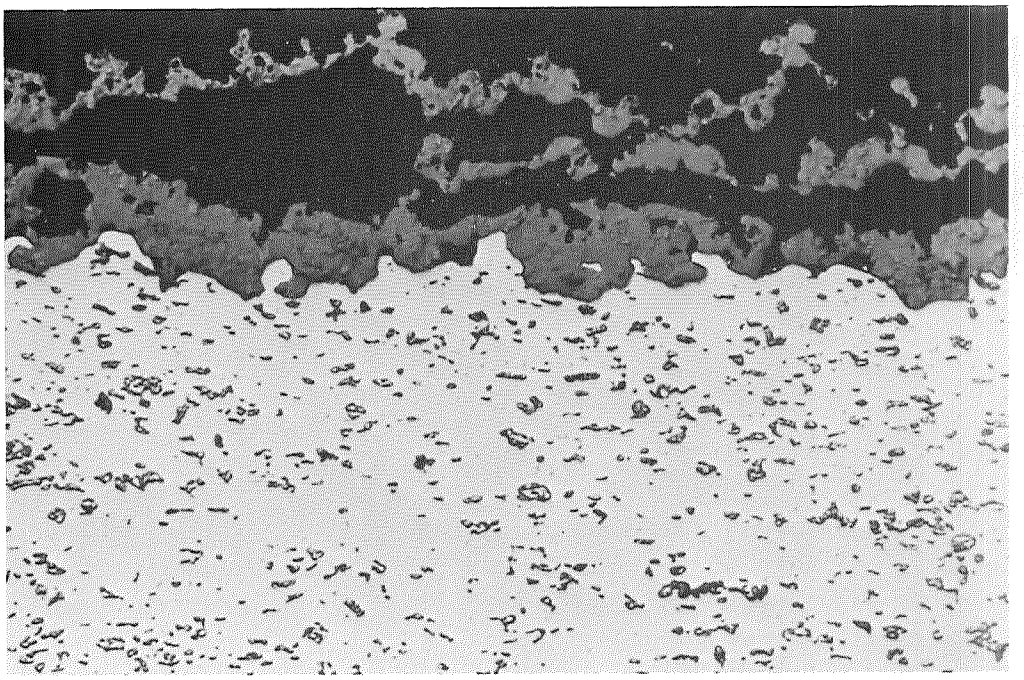

A3585 ×500

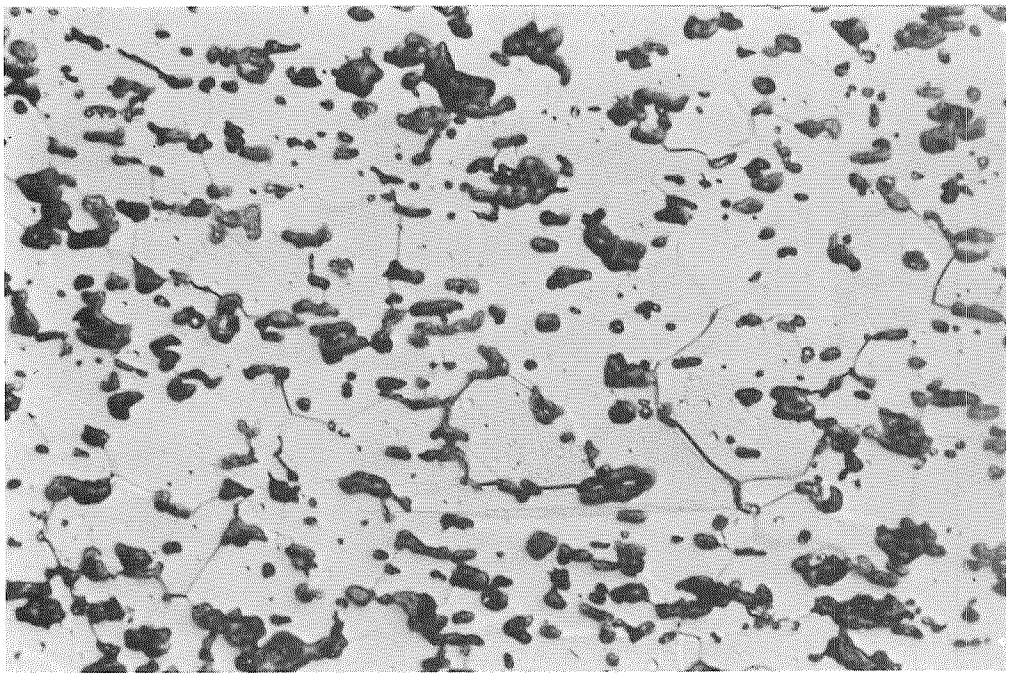

A3586 ×1000

DBTT = <300°F (<422°K)

Figure 64 Structure of Cr-3Zr (9136-12) Preoxidized 50 hr-2100°F (1422°K)-Air and Exposed to Air 100 hr-2100°F (1422°K)-Air, Scale Intact.

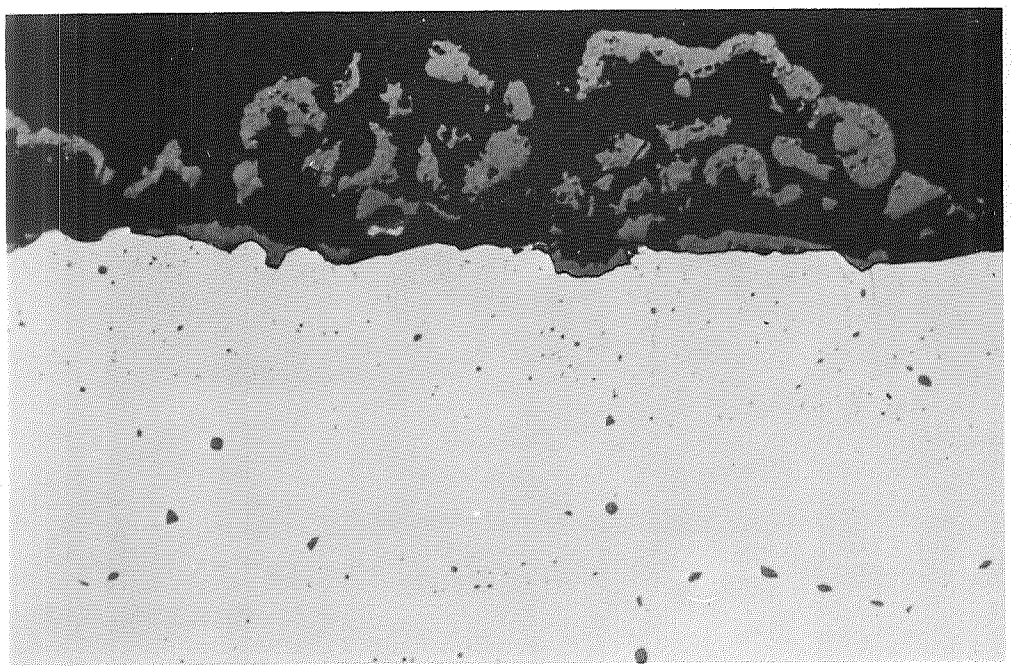

A3587 ×500

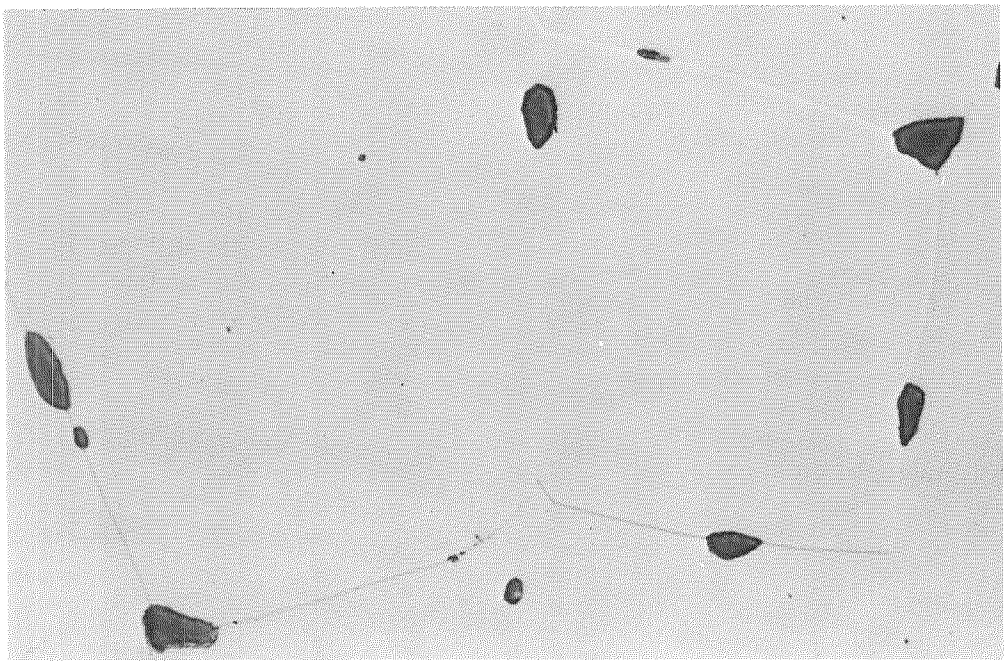

A3588 ×1000

DBTT = 700°F (644°K)

Figure 65 Structure of Cr-0.25La (9127-13) Preoxidized 50 hr-2100°F (1422°K)-Air and Then Exposed 100 hr-2100°F (1422°K)-Air, Scale Intact.

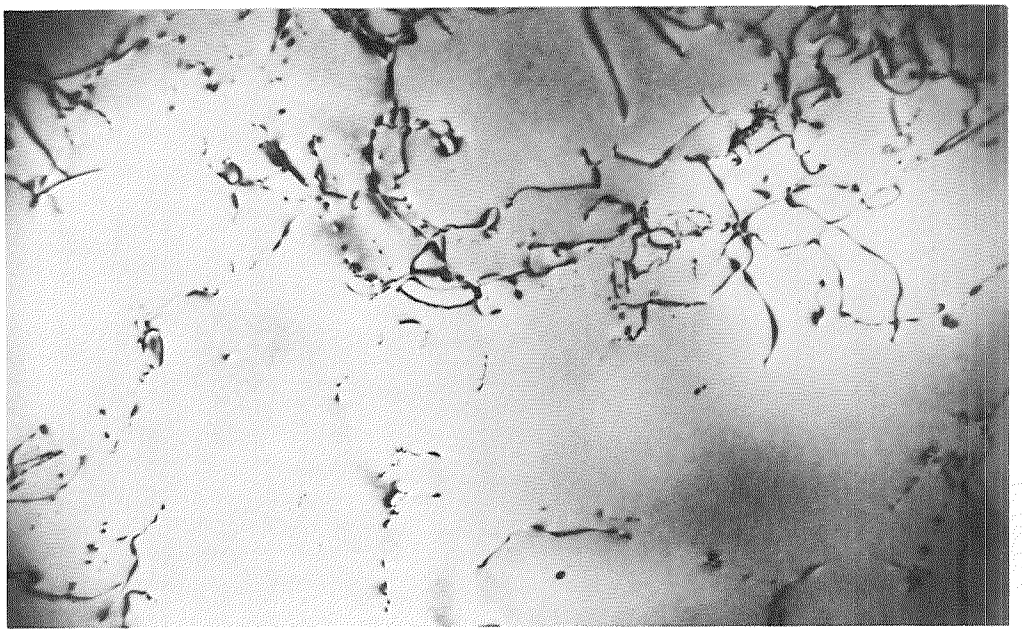

D109 ⟷ 1250 Å 9100-4 ×48,000

100 hr-2100°F (1422°K)-Air

D114 ⟷ 2000 Å 9100-11 ×30,000

50 hr-2100°F (1422°K)-Air + 100 hr-2100°F (1422°K)-Air

Figure 66 Fine Structure of Normal and Preoxidized Cr-2Zr Alloy After Air Exposure (×30,000-48,000).

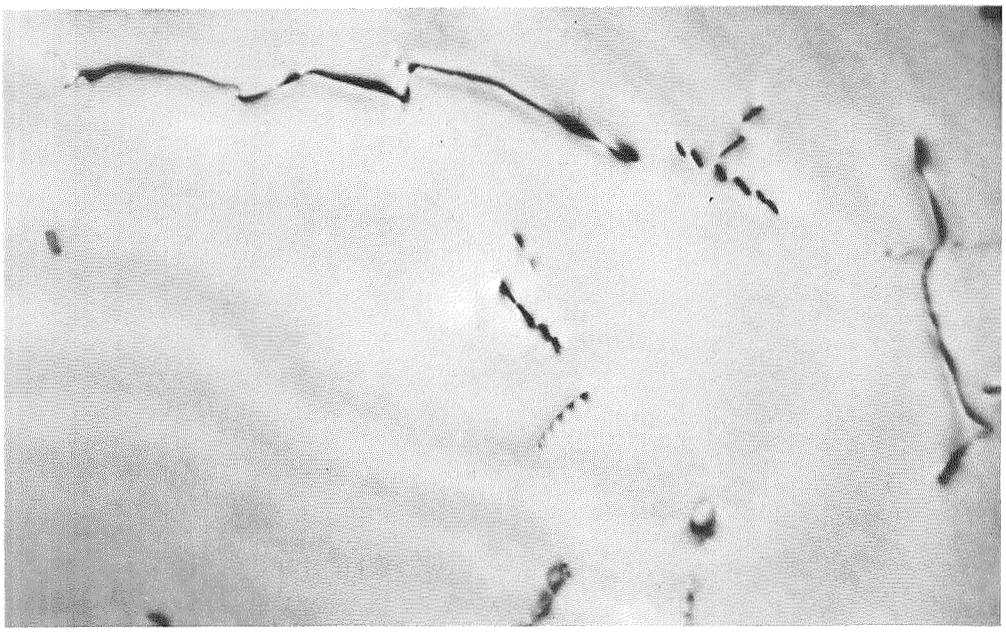

D234 ⟷ 500 Å 9100-4 ×120,000

100 hr-2100°F (1422°K)-Air

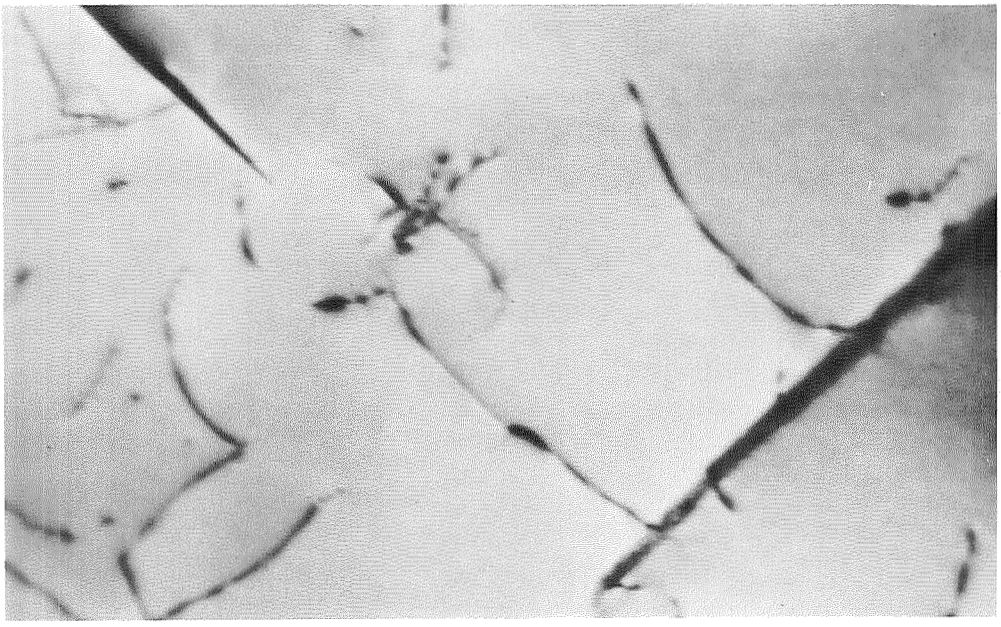

D239 ⟷ 500 Å 9100-11 ×120,000

50 hr-2100°F (1422°K)-Air + 100 hr-2100°F (1422°K)-Air

Figure 67 Fine Structure of Normal and Preoxized Cr-2Zr After Air Exposure (×120,000).

exposure to air or the fact that internal oxidation reduces the subsequent pickup of oxygen and/or nitrogen by the alloy.

The bend DBTT of three of the four binary alloys was reduced significantly by preoxidation prior to air exposure. Even though the oxide scale has been removed and the surface was free to react with air, the alloys either picked up less nitrogen or were more tolerant of nitrogen contamination. The weight gain data and microstructures indicate that the tolerance for nitrogen is increased. As shown in Figure 66 and 67, the preoxidized Cr-2Zr alloy contained many Cr_2N platelets after air exposure and the general structure with respect to nitride precipitates was about the same as that of samples that were not preoxidized. Figure 66 shows a Cr_2N platelet growing out from a large particle of the Cr_2Zr intermetallic with several other platelets aligned at right angles. The fine structure of these alloys as revealed by transmission electron microscopy at magnifications to 120,000 revealed no significant differences.

One notable feature apparent in both preoxidized and normal Cr-2Zr alloys in the formation of fine precipitates along dislocation lines. In all samples, the dislocations appeared to be pinned by many ultrafine precipitates. It could not be determined if these were oxides, nitrides, or the Cr_2Zr intermetallic. There was no evidence of general matrix precipitation (other than Cr_2N platelets) in either material. Also, no tendency to substructure formation was found in any of the samples.

Metallographic study revealed that nitride cases were formed beneath the oxide scale on some of the preoxidized air-exposed samples. Case formation was irregular, however; several samples were completely free of a nitride case, but nitride cases formed on all the air-exposed samples that were not preoxidized. A more striking effect was observed on the internal structure. All the preoxidized samples had a greatly reduced amount of large nitride precipitates and compared to the air-exposed samples were essentially free of gross precipitates in grains and grain boundaries. Only the very fine nitride precipitates were developed in the preoxidized alloys. A similar effect was found for the Cr-0.5Zr alloy.

Tests with Cr-Th alloys and ternary alloys containing Th, Y, or La showed no significant effect of preoxidation on the bend DBTT. With these materials, either the removal of the oxide scale was not offset by a significant amount of internal oxidation or the DBTT after normal air exposure was too low for any further reduction by internal oxidation. Results with the Cr-Zr alloys indicate that the latter case may be governing. All of these materials had a DBTT of 800°F (700°K) or less, which was not lowered by the preoxidation treatment. Preoxidation of the Cr-Zr alloys lowered the DBTT to the range of 700 to 1000°F (644 to 811°K)—about the same level. Lower values of DBTT were realized only when the oxide scale was not removed from the surface before exposure to air.

The behavior of pure chromium suggests that selective internal oxidation of the alloy addition is controlling behavior. The DBTT of pure chromium is not affected by oxidation prior to air exposure (Table 13). As shown in Figure 30 (section 5.2), a few oxide particles form in the grain boundaries, indicating some degree of internal oxidation. The effect, however, was insignificant compared with that observed on

preoxidation of Cr-Zr binary or ternary compositions. It is significant that the total weight gain in air was greatly reduced for unalloyed chromium by heating in oxygen for 50 hr at 2100°F (1422°K) before air exposure. With all the oxide scale removed, the sample still showed less total reaction. There was no significant difference with respect to nitride case and precipitate formation, indicating that reduced reaction with oxygen occurred. Again, this may be due to changes in surface condition or to the fact that the alloy has been saturated with oxygen.

Section 6

ANALYSIS OF RESULTS

6.1 MECHANISM OF NITROGEN EMBRITTLEMENT

A delineation of the mechanisms by which alloying reduces the nitrogen embrittlement of chromium should be based upon an understanding of the mechanisms of brittleness in chromium. Both mechanisms must be compatible, and a knowledge of how nitrogen embrittles chromium and other factors that affect brittle fracture will aid considerably in developing an understanding of the alloying effects. A thorough review of this subject has been made by Maykuth and Gilbert (Ref. 2). Unfortunately, the mechanism of nitrogen brittleness in chromium has not been established conclusively. However, a sufficient understanding has been developed to indicate the most likely mechanisms, and these will provide an adequate basis for the analysis of alloying effects.

Brittle Fracture

The fracture process occurs in two steps: crack initiation and crack propagation. Work to date on recrystallized chromium indicates that cracks initiate at the grain boundaries, and in the brittle range they propagate by cleavage along preferred planes. The cube face (100) is the most commonly observed cleavage plane in chromium. This also is the preferred habit plane for precipitation of chromium nitride (Cr_2N) (Ref. 21). The stress concentration for the initiation of fracture is believed to be due to a slip-induced grain boundary crack (Ref. 2). Grain boundary cracks will develop if slip in one grain cannot nucleate slip in an adjoining grain. Thus, any barrier to slip can promote crack formation.

One of the major unresolved problems in the brittleness of chromium is whether crack initiation or crack propagation governs brittle behavior. The fact that nonpropagating cracks have not been found in chromium tested in tension below the DBTT is cited as the primary evidence that crack initiation controls the DBTT (in tension). The first crack to form propagates immediately to failure. Cracks propagate readily in single-crystal chromium at 32°F (273°K). Maykuth and Gilbert (Ref. 2) conclude that ductile behavior in recrystallized chromium at low temperatures [below 570°F (573°K)] is possible only so long as crack initiation is prevented. Thus, in tension tests the DBTT is controlled by crack initiation and it is through the effect of different variables on the crack initiation process that the DBTT is varied. Once a crack has formed, however, the ease of propagation is the major factor that results in failure. In evaluating the effects of alloying, therefore, both factors still must be taken into consideration.

The variables most likely to alter the crack initiation process include purity, grain size and shape, precipitates (particularly at boundaries), and substructure. All effects attributed to interstitials and their interaction with lattice defects will tend

to impede slip and promote initiation of cleavage. Mechanisms of particular importance include dislocation locking by Cotrell atmospheres and precipitates or dislocation blockage by stable substructures. Any factors that impede dislocation motion and make yielding difficult will promote cracking at the grain boundaries. Since grain boundary area is a function of grain size, coarse-grain materials would be expected to resist crack formation (lower DBTT) purely as a result of a lower probability for slip blockage at a boundary. Fine-grained material would be expected to crack more readily (high DBTT) due to the large number of barriers to slip and potential sites for crack initiation.

The reason why cracks once formed can propagate so readily by cleavage in chromium is not clearly defined. There is some evidence to indicate that this is an intrinsic property of the chromium lattice with respect to the ease of dislocation movement. Materials having a high Peierls' force for dislocation motion or materials in which dislocations are pinned by impurities cannot yield readily near the tip of a fast-moving crack at low temperatures. Such materials can exhibit a temperature-dependent brittleness. Again, Cotrell or precipitate locking by impurities could be a major contributor to cleavage cracking. Precipitates, particularly those whose habit plane is also the cleavage plane, also can act to concentrate stress and promote cleavage.

Surface energy of the new surface produced may be an important factor and also should be considered. A crack will propagate only if the strain energy released by unloading the small volume of material at the tip of the crack is greater than the energy absorbed in creating the new surface (Ref. 22). The effective surface energy for crack propagation in single crystals of 3% Si-Fe decreases tremendously with temperature from 240,000 ergs/cm^2 at 195°K to 1400 ergs/cm^2 at 20°K (Ref. 23). Thus, any effect of alloying, impurities, or atmospheres on surface energy could significantly influence ease of crack propagation as a function of temperature.

Crack propagation also may be dependent on grain size and orientation. Cleavage fractures generally are more difficult to propagate in polycrystalline materials due to orientation changes at grain boundaries, and some observations suggest that crack propagation is more difficult in fine-grained materials (Ref. 24).

Role of Nitrogen

The exact role that nitrogen plays in the processes of crack initiation and propagation has not been defined. Nitrogen appears to embrittle chromium under some conditions at all levels of addition. Room-temperature brittleness has been found in recrystallized chromium with as little as 10 ppm nitrogen (Ref. 2). This may be the result of nitride precipitates rather than retained nitrogen in solid solution. The available solid solubility data for nitrogen in chromium (Refs. 25,26) do not extend below 1000°C (1273°K). The solid solubility determined by Seybolt (Ref. 25) using gas/metal equilibrations is reported to be 0.028 wt% (0.10 at.%) at 1000°C, the lowest temperature of measurement. A Vant Hoff plot of Seybolt's data has been extrapolated to lower temperatures in an effort to estimate probable solubility limits (Figure 68). Klein and Claurer (Ref. 26) determined nitrogen solubility between 400 and 900°C using internal friction techniques. Their data also are plotted in Figure 68. Both solubility curves indicate an exceeding low solid solubility at low temperatures. Gilbert and Klein suggest 10^{-9} ppm at room temperature. Seybolt results extrapolate to give solubilities of 1 ppm by weight (0.0001 wt%) at 960°F (789°K) and 0.0053 ppm by weight at

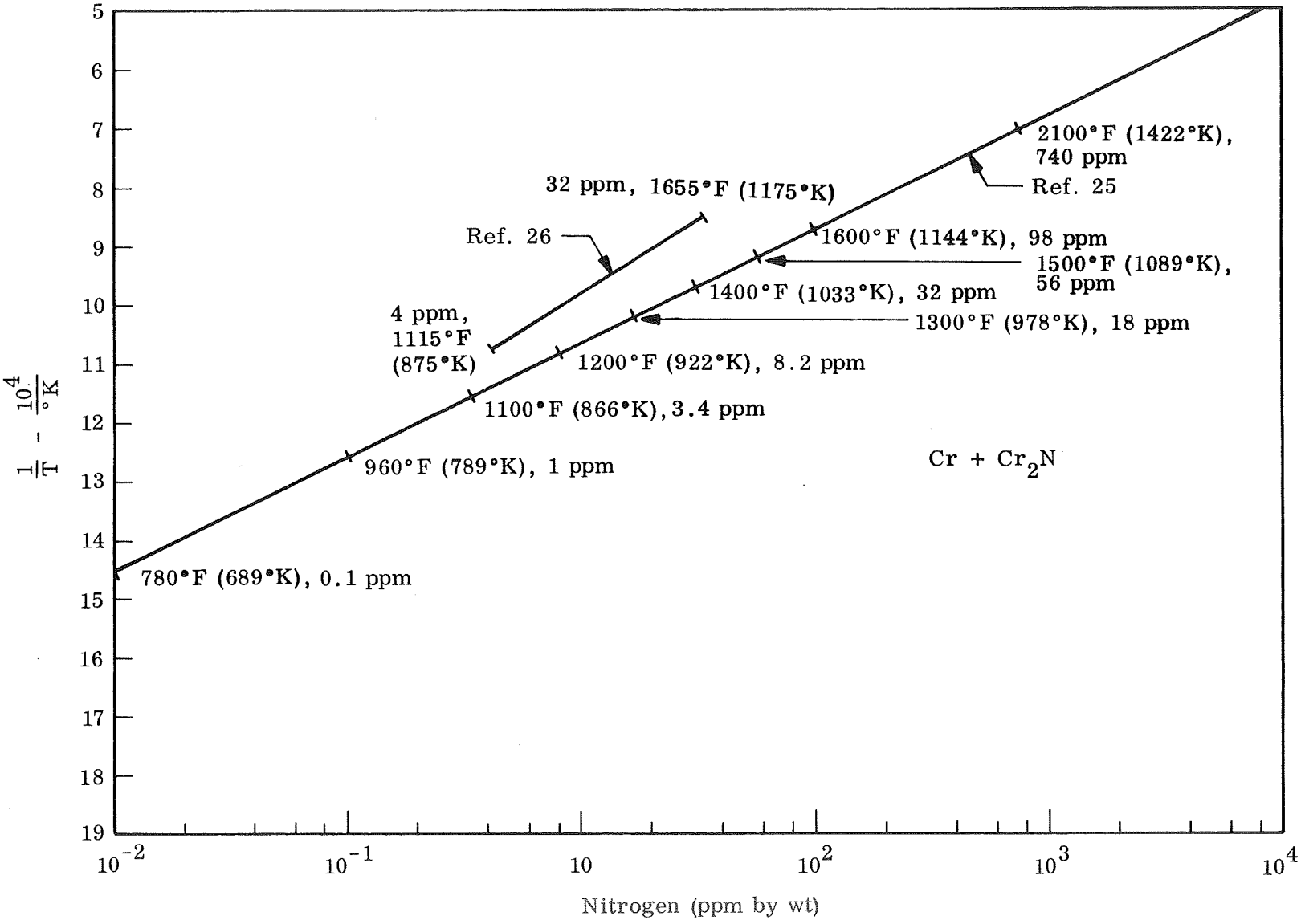

Figure 68 Solid Solubility of Nitrogen in Chromium

600°F (589°K). If the alloy approaches equilibrium at or below this temperature, the solid solubility will be negligible.

The actual amount retained in solid solution at low temperature, however, would depend on the kinetics of precipitation and the rate of cooling. Klein and Claurer (Ref. 26) established that nitrogen can be quenched into solid solution in chromium by rapid cooling. The internal friction peak for nitrogen increased from $0.3\ Q^{-1} \times 10^3$ to $2.0\ Q^{-1} \times 10^3$ when a wire (air cooled) was reheated to 1000°C and quenched in water. A 47-mil-diameter wire with 170 ppm nitrogen could be quenched (in water) to a supersaturated solid solution at room temperature. The nitrogen precipitated as a nitride on heating at 153−200°C and the internal friction peak height for N_2 dropped from $2.2\ Q^{-1} \times 10^3$ to zero in 2 hr. On air cooling, virtually all the nitrogen precipitates and little, if any, is retained in solid solution. Diffusion of nitrogen is very rapid in chromium and Klein and Claurer (Ref. 26) stated the diffusivity as

$$D = 0.35 \times 10^{-5} e^{-\frac{20,500}{RT}}$$

They concluded that precipitation kinetics were so rapid that it was unlikely for nitrogen to remain in solution above a few hundred degrees Centigrade. As will be discussed in section 6.2, large amounts of nitrogen are in solution in all the Cr alloys exposed to air at high temperature but the nitrogen precipitates as Cr_2N on air cooling. Precipitation could not be suppressed by water quenching in these samples (30 mils thick).

Based on the information available, it appears that nitride precipitates, rather than the nitrogen retained in solid solution (Cotrell atmospheres), may be the more likely cause of dislocation pinning which could contribute to ease of crack initiation or propagation at low temperature. Gilbert and Klein (Ref. 27) found that chromium wire with 10-15 ppm N_2 had a lower DBTT [by 133 to 176°F (74 to 98°K)] when it was water quenched from high temperature than after it was fully aged to precipitate all the nitrogen as Cr_2N. They concluded that nitrogen in solution was less detrimental than nitrogen precipitated as nitrides. These authors point out that other investigators who report an increase in DBTT after rapid cooling have not cooled with sufficient speed, or have had too high a supersaturation to quench in the solid solution, and the DBTT increased as a result of formation of ultrafine precipitates (Ref. 27).

Surface Effects

One other factor of importance in analyzing the results of tests and evaluations conducted in the current program is that all DBTT tests were made in bending with three-point loading. Under such conditions, stress and strain are not uniform. The highest tensile stress and strain occur in the outer fibers of the surface opposite that in contact with the punch. The punch contact surface is in compression. Stress will vary in magnitude and direction through the sheet thickness and will be zero at the neutral axis. The foregoing discussion on mechanisms of brittle fracture assumes a homogeneous material with a uniform stress distribution. Cracks can nucleate throughout the cross section. In bending, however, crack initiation will be restricted to the

outer fibers and crack initiation will be sensitive to surface conditions. In specimens exposed to oxygen or air, cracks may initiate in an oxide or nitride case or at the interface of the oxide or nitride with the metal. The contribution of surface alteration to crack initiation must be carefully considered.

6.2 CONTROL OF EMBRITTLEMENT BY ALLOYING

There are at least six potential mechanisms by which alloying could control nitrogen embrittlement, all of which are compatible with the accepted mechanisms of embrittlement in chromium. The first and most obvious is the formation of a surface barrier such as an oxide film that prevents access of nitrogen to the metal. The second mechanism, and the one most commonly cited in the literature, is the scavenging effect in which the alloy addition reacts preferentially to form a harmless nitride or nitrogen-rich phase. Other possibilities include reduced diffusivity of nitrogen, reduced solubility for nitrogen, alteration of the morphology and distribution of nitride precipitates, and changes in the basic structure of the matrix (including such factors as grain size, shape, and orientation; substructure; dislocation density; and general defect structure). Each of these possible mechanisms will be analyzed separately to determine if the results of this investigation indicate a significant role for a particular factor.

Nitrogen Barriers

This study has proved conclusively that a growing oxide film on chromium is an effective but incomplete barrier to nitrogen. In the absence of an oxide or in the absence of oxygen if an oxide film already exists, the metal is rapidly converted to Cr_2N. A 30-mil-thick sheet is converted completely to nitride in 40 to 50 hr at 2100°F (1422°K). With a pure Cr_2O_3 scale on unalloyed chromium, the metal is saturated with nitrogen but only the outer 4 to 5 mils on each side is converted to the nitride (case) in 100 hr at 2100°F (1422°K).

Alloying of chromium with Cb, Zr, Hf, Th, Y, La, Pr, and Mischmetal will further reduce the total reaction with nitrogen. Columbium forms a very protective subscale, and no nitride case will form in a 100-hr exposure to air. The rare earths will restrict Cr_2N case formation to a depth of less than 1 mil on each side exposed to air. None of these additions, however, prevents the alloy from dissolving nitrogen, and in most cases the alloy is saturated with nitrogen after exposure. In general, there is no correlation between the DBTT and the ability of the oxide scale to limit access of nitrogen to the metal. Alloys such as Cr-0.5Y and Cr-2Zr-1Th that did not have any increase in DBTT after 100 hr at 2100°F (1422°K) in air contained nitride precipitates, massive internal nitrides, and a finite nitride case beneath the oxide scale. The alloys must be saturated with nitrogen in order to form a case of Cr_2N on the surface. Alloys such as Cr-0.5Cb, on the other hand, did not form a nitride case and hence were not fully saturated as a result of the very protective oxide, but they embrittled even more than unalloyed chromium by exposure to air.

Clark (Ref. 20) suggests that thin layers of Cr_2N on the surface of chromium have a marked embrittling effect. A Cr_2N case 1 to 5 $\times 10^{-4}$ in. (2.54 to 12.7 $\times 10^{-4}$ cm) thick on chromium was reported to increase the DBTT by 400°F (222°K). A

5×10^{-4} in. (1.27×10^{-3} cm) case on a Cr-Zr-Ti-C alloy increased the DBTT by 1000°F (555°K). In the present study, alloys with 0.5% Y and 2Zr-1Th developed nitride cases 5×10^{-4} to 10^{-3} in. (1.27 to 2.54×10^{-3} cm) thick with no increase in bend DBTT after 100 hr at 2100°F (1422°K) in air. All alloys containing 1 to 2 at.% rare earths had nitride cases in this thickness range with a maximum increase in DBTT of 300°F (167°K). No evidence has been found to indicate that a nitride case on the surface per se creates a major increase in DBTT.

As indicated in section 6.1, however, the role of a nitride case on the surface when samples are tested in bending must be considered carefully. Samples converted completely to Cr_2N were found to be brittle in bending at 1800°F (1255°K). Thus, cracks will initiate in the nitride case on bending at all temperatures and may propagate through the substrate. One example of this is shown in Figure 69. The upper surface in both pictures is the tension side of the bend sample some distance away from the maximum stress (bend) region. In one alloy (Cr-2Mn) the test was at 1200°F (922°K) where a ductile 90° bend was made and cracks in the nitride case terminated just below the interface. There was insufficient energy to propagate through the substrate. In the second example (Cr-1W), the bend was made in the brittle range at 1600°F (1144°K) and fractures from the case penetrated deep into the metal by a cleavage mode.

The nitride case not only is a source for initiating cracks at all bend temperatures but also is a source for precracking alloys before any loads are applied. This effect is shown in Figure 70. The Cr_2N case does not match the thermal expansion of the alloy and will develop craze cracks on cooling from the exposure temperatures. These cracks often penetrate into the alloy and produce a very sharp surface crack before any bends are made. The depth of penetration into the alloy appears to depend on whether the cracks develop at a temperature above or below the DBTT for the alloy under the particular conditions imposed (thermal stress). The least penetration was found for the alloys having the lowest DBTT (Cr-Y).

The significance of this behavior is that under such conditions crack initiation may no longer be the factor governing the DBTT. As discussed in section 6.1, crack initiation rather than propagation is believed to control the DBTT. With a nitride case, just the reverse may be true. All alloys will develop cracks with ease at all temperatures and the DBTT measured in bending should reflect changes in crack propagation behavior. Thus, to analyze the effects of alloying, major consideration should be given to factors that could influence the propagation of cracks.

The results of oxidation studies conducted on this program are in agreement with those of Clark (Ref. 20) concerning the role of an oxide scale in reducing the overall reaction with nitrogen. The indicated mechanism by which rare earths produce an effective scale, however, is not in agreement with the model proposed by Clark. He concludes that Y (or other rare earths) forms a Perovskite oxide ($RECrO_3$) layer at the interface between the normal Cr_2O_3 scale and the metal. The enhanced oxidation resistance conferred by the rare earths results from the fact that this phase reduces the concentration gradient and hence the flux of Cr^{+3} ions which diffuse outward and govern the rate of oxidation. In addition, this phase or other changes in the Cr_2O_3 oxide, such as reduced thickness, keying by rare earth oxides, changes in strength or plasticity by dissolved rare earth oxides, and rare earth oxide vacancy sinks, act singly or

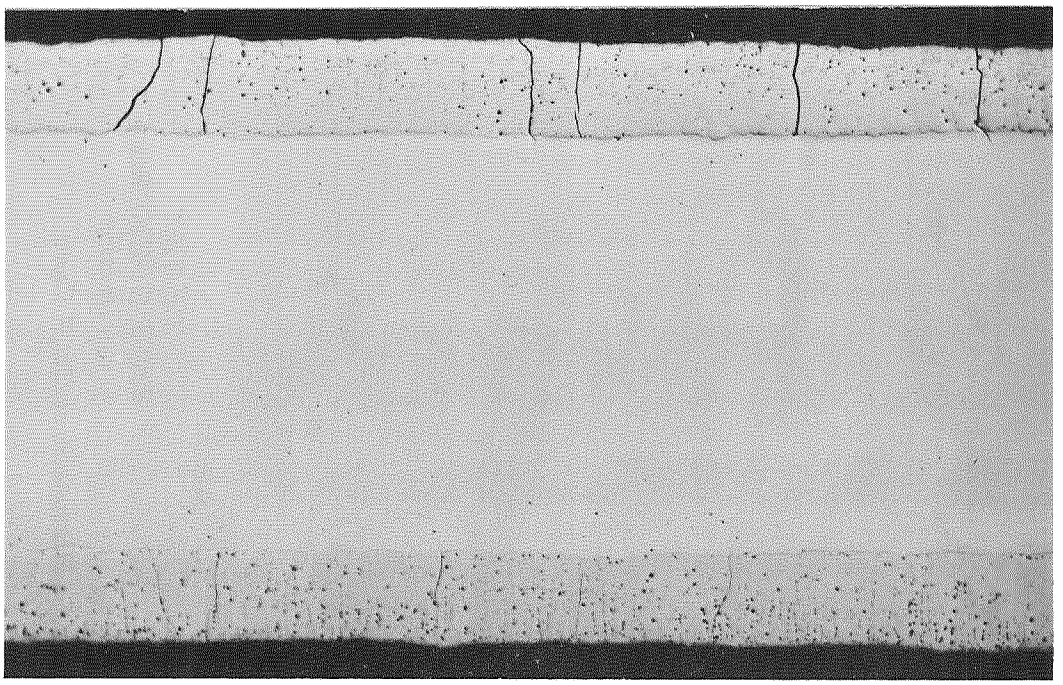

A1697 ×100

Cr-2Mn (948-4)
1200° F (922° K) Bend, Ductile

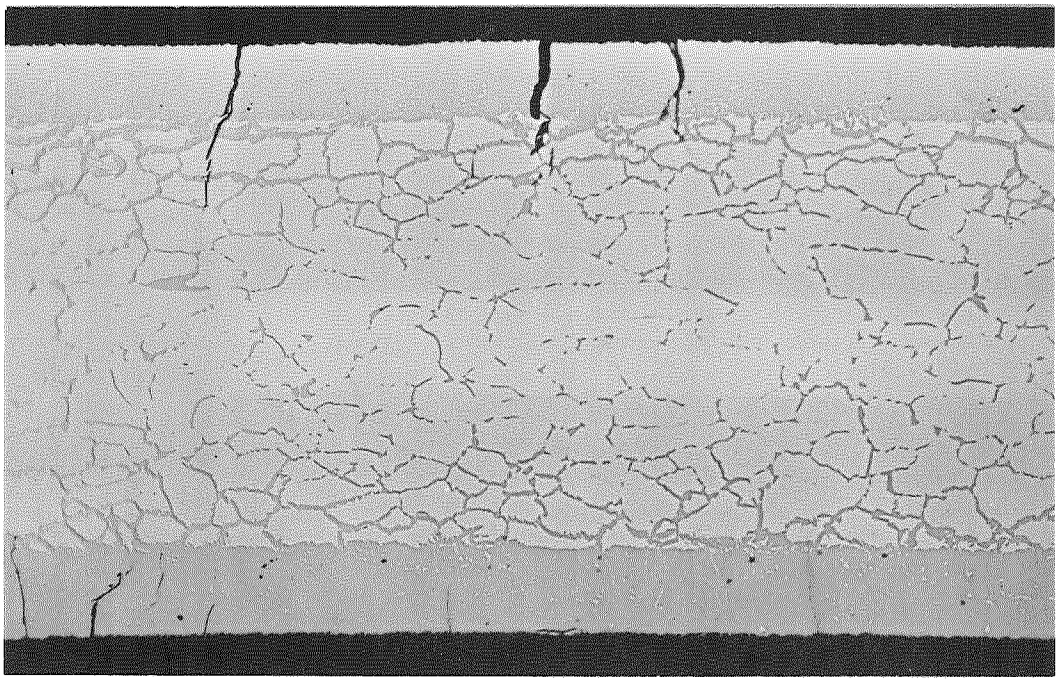

A1695 ×100

Cr-1W (957-6)
1600° F (1144° K) Bend, Partially Ductile

Figure 69 Propagation of Cracks Originating in Cr_2N Case.

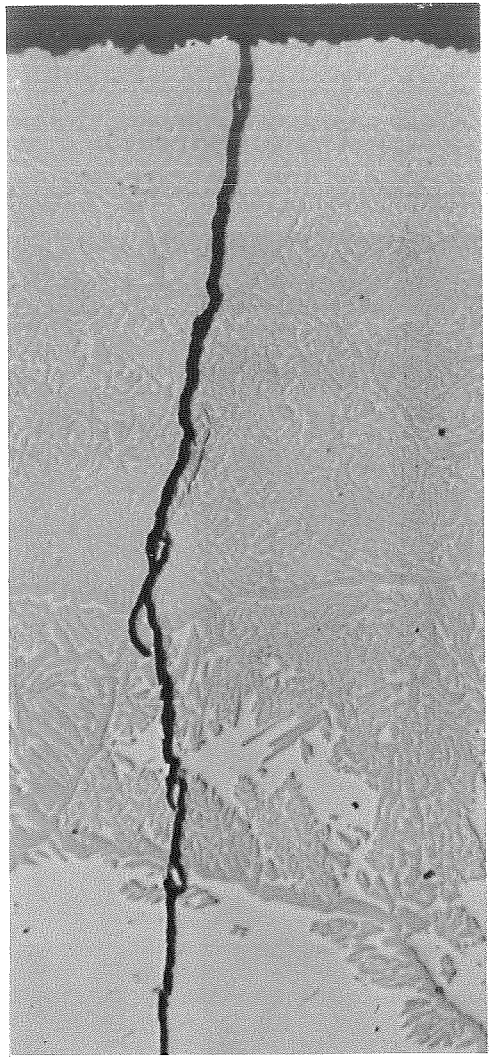

A1690 ×500

Cr-2Re
1600° F (1144° K) Bend
Brittle

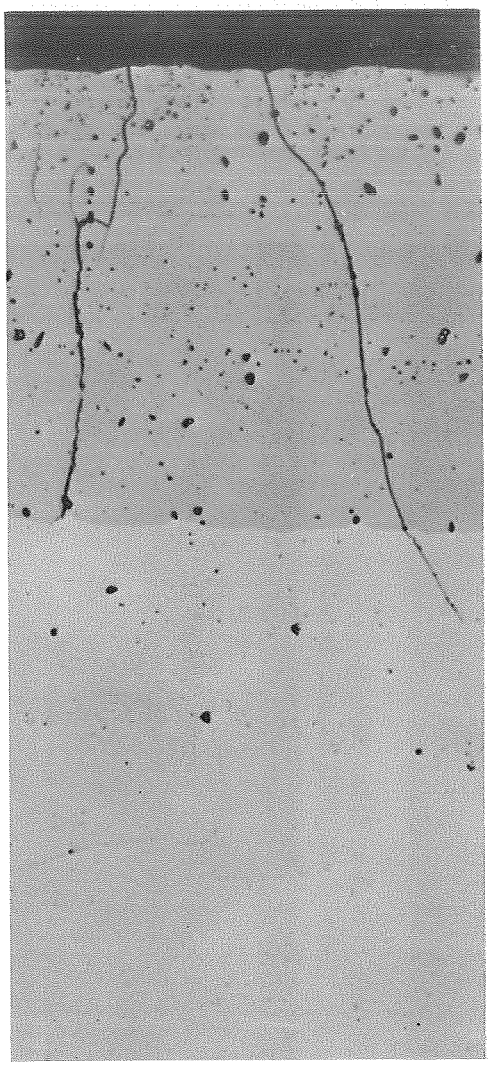

A1698 ×500

Cr-2Mn
1200° F (922° K) Bend
Ductile

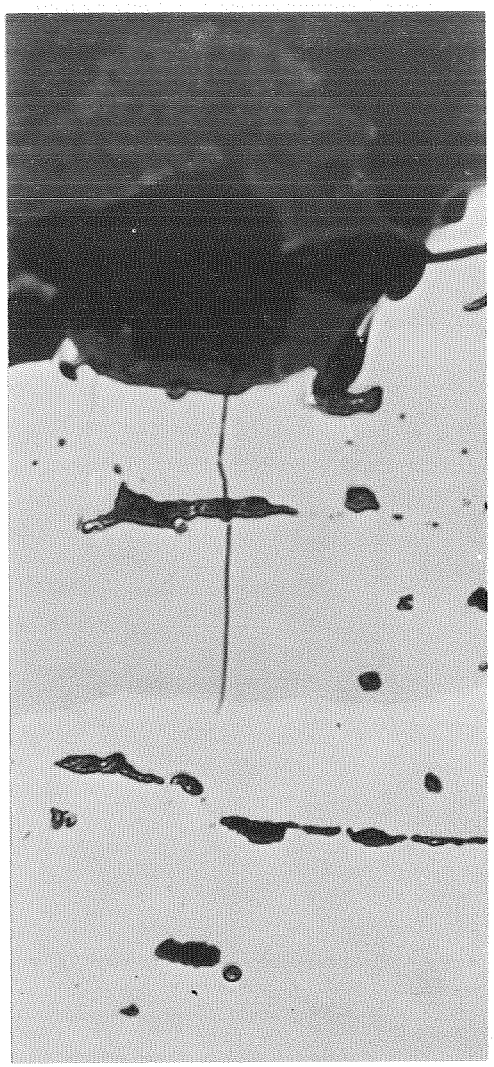

A3556 ×2000

Cr-0.5Y
800° F (700° K) Bend
Ductile

Figure 70 Precracking of Cr Alloys by Thermal Expansion Mismatch of Cr_2N Case.

together to block the inward transport of nitrogen. All factors that can prevent cracking, buckling, or lamination (which are considered necessary for nitrogen to pass through the scale) will retard nitridation.

As shown in sections 5.2 and 5.3, the oxide scales on rare earth containing alloys develop by a pseudologarithmic rate process. Very similar behavior has been reported for a Cr-5 vol% Y_2O_3 composite by Seybolt (Ref. 28). He attributed the departure from parabolic behavior to dissolution of Y_2O_3 into the Cr_2O_3 scale and alteration of the interface with the metal, perhaps by $YCrO_3$. In the present program, electron probe scans were made across the oxide scale, nitride case, and metal interface on Cr-0.25 and 0.5Y alloys exposed to oxygen and air for 100 hr at 2100°F (1422°K). As shown in Figures 71 and 72, there is no significant increase of Y in either the oxide scale or the nitride case (where formed) and no discernible concentration of Y at the oxide/metal, oxide/nitride, or nitride/metal interfaces. The Y spikes observed in the probe scan are for the random islands or stringers of Y (or Y_2O_3, YN) that exist in the alloy and in the nitride case. The nitride case is detected readily beneath the oxide scale in the nitrogen scans, and the oxide case is clearly identified in the oxygen scans. None of the patterns indicate either a concentration of Y in the oxide or nitride, or a concentration of O in the Y phase. The scans of alloys 9125 and 950 in Figure 71 suggest a high concentration of nitrogen in the Y stringers, but the results at this magnification are not conclusive. As will be shown later, high-magnification studies confirmed high nitrogen concentrations in Y stringers.

The results of this study indicate that cavity formation at the interface and subsequent reduction in scale/metal contact area are the primary cause of the observed pseudologarithmic behavior. As discussed in section 5.2, the oxidation process probably continues to be parabolic but appears to be of higher order due to continually decreasing contact points for diffusion. Outward diffusion of Cr^{+3} or vaporization may create initial voids. The improved oxidation resistance is believed to result from a beneficial effect of small amounts of dissolved rare earth oxides on the strength and plasticity of the scale. Prevention of cracking and lamination effectively limits fresh access of oxygen for new scale formation and nitrogen for case formation.

Most of the solid solution alloy additions (W, Mo, Re, Fe, Mn, Co, V, etc.) form oxides with chromium that are not good barriers to nitrogen. On exposure to air, large amounts of nitrogen either diffuse or leak through the oxide scale and dissolve in the alloy. The alloy saturates rapidly and the excess nitrogen reacts to form a thick case of Cr_2N on the surface and in many cases around each grain. All the alloys except manganese promote formation of thick continuous networks of nitride in the grain boundaries. These alloys are severely embrittled intergranularly and have high DBTT. As discussed in section 5.3, the formation of massive intergranular networks is the direct consequence of a ternary solid solution alloy system (Cr-metal-nitrogen) in which an extra degree of freedom exists (by the phase rule) and composition can be a variable in a two-phase field. Thus, once the alloy is saturated, it will continue to absorb nitrogen and form massive internal nitrides at the exposure temperatures.

Manganese is the only solid solution addition for which this behavior was not observed. Cr-Mn alloys had poor oxide scales, saturated rapidly, and formed thick nitride cases. There was little intergranular nitridation, however, and no tendency to form embrittling intergranular networks existed. The reason for this behavior is not clear but

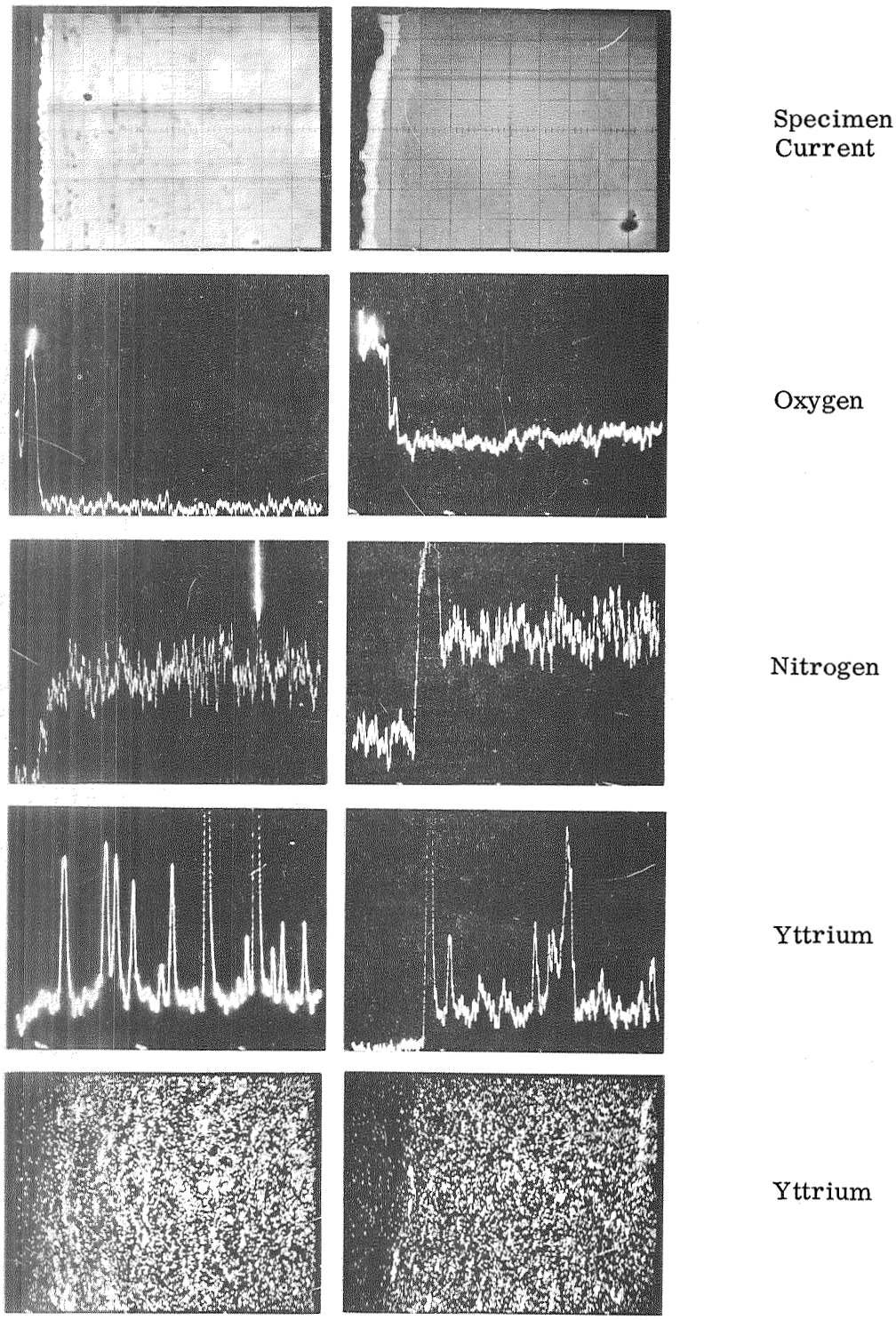

Figure 71 Distribution of O, N, and Y in a Cr-0.25Y Alloy After Exposure to Oxygen and Air (×250 reduced to 50% of original size).

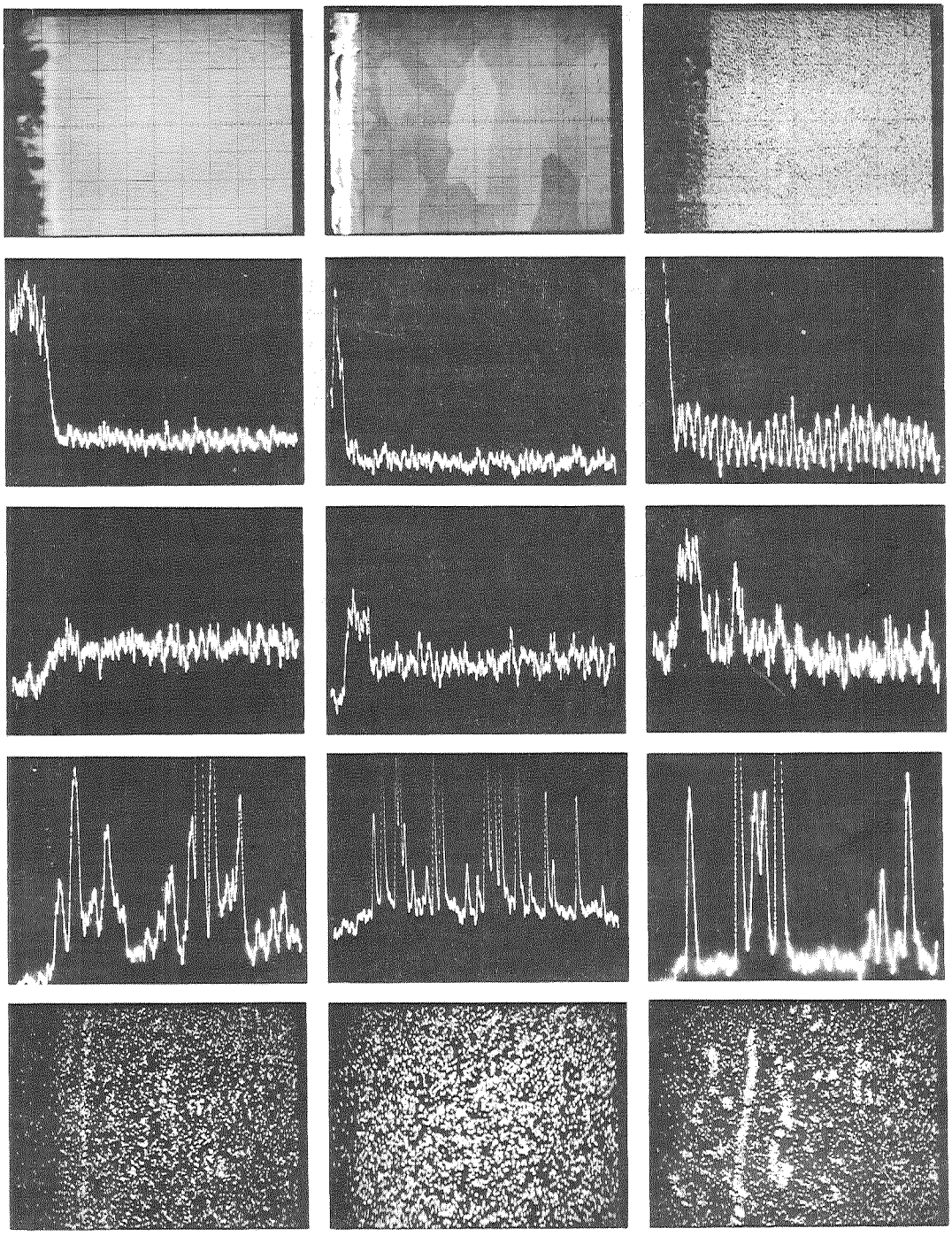

Figure 72 Distribution of O, N, and Y in Cr-0.5Y Alloys Exposed to Oxygen and Air (×250 reduced to 47% of original size).

may be related to the tendency for manganese to promote internal oxidation. Further work is needed to understand this effect. Of all the elements studied, manganese is the best solid solution addition with respect to enhancing resistance to nitrogen embrittlement.

Nitrogen Scavengers

Many investigators have described the role of rare earths in chromium as that of scavengers, elements that preferentially absorb and combine with nitrogen. As shown in Figure 73, there was some indication that stringers of Y in Cr-Y alloys were high in nitrogen. Electron probe scans were made across selected yttrium stringers at high magnification to determine whether this phase acted as a nitrogen sink. The scan of a Cr-0.25Y at a magnification of 4000 revealed a possible increase of oxygen and nitrogen in yttrium stringers of alloys exposed both to pure oxygen (no nitrogen) and to air. This could be the result of a higher background count for these elements over the higher atomic number material or could signify that the yttrium phase scavenged oxygen and nitrogen during melting and processing of the alloy.

The same effect was found for a Cr-0.5Y exposed both to pure oxygen and to air (Figure 74). Again, a very significant increase in nitrogen was indicated for the yttrium stringers of samples exposed only to pure oxygen. This must represent scavenging during processing or perhaps contamination by metallographic polishing. A higher peak for nitrogen was found in yttrium stringers of the sample exposed to air. This would appear to indicate a definite scavenging effect for nitrogen during the air exposure. The small peak observed for oxygen is believed to be an increase in background count over yttrium and does not necessarily indicate oxygen scavenging. Probe sensitivity was set so that an oxygen content corresponding to that in Cr_2O_3 would peak at the top of the screen (photograph).

A second Cr-0.5Y alloy (No. 950) exposed to air was scanned for oxygen and nitrogen with the results shown in Figure 75. Peaks for these elements in Cr_2O_3 and Cr_2N again were set to be at the top of the screen (photograph). The backscattered electron image shows the lower atomic number Cr_2N case on the surface as a dark band on the left. The high atomic number yttrium stringer appears as a light band in the alloy just below the nitride case. The nitrogen scan across the case and stringer indicates a high nitrogen content corresponding to the nitride in both. In addition, the scan across a Cr_2N island formed at one grain intersection also revealed the nitrogen level for the nitride. The corresponding oxygen scan across the nitride case and yttrium stringer indicated only a slight oxygen rise in the stringer. Again, this is believed to be primarily an increase in background count.

These studies indicate that yttrium does scavenge nitrogen in chromium, both during melting and processing and during subsequent air exposure. However, there is no apparent relationship between this action and the DBTT in bending. As seen from the various optical and electron micrographs, the Cr-Y (and other rare earth) alloys become saturated with nitrogen and precipitate a Cr_2N phase on cooling. Cr_2N islands also form at grain intersections or grain boundaries. Some of the Cr_2N platelets precipitate adjacent to the yttrium islands or stringers. In no case were precipitates or particles found that could be identified as YN, and the only scavenging effect was observed for existing yttrium islands and stringers. It is possible that,

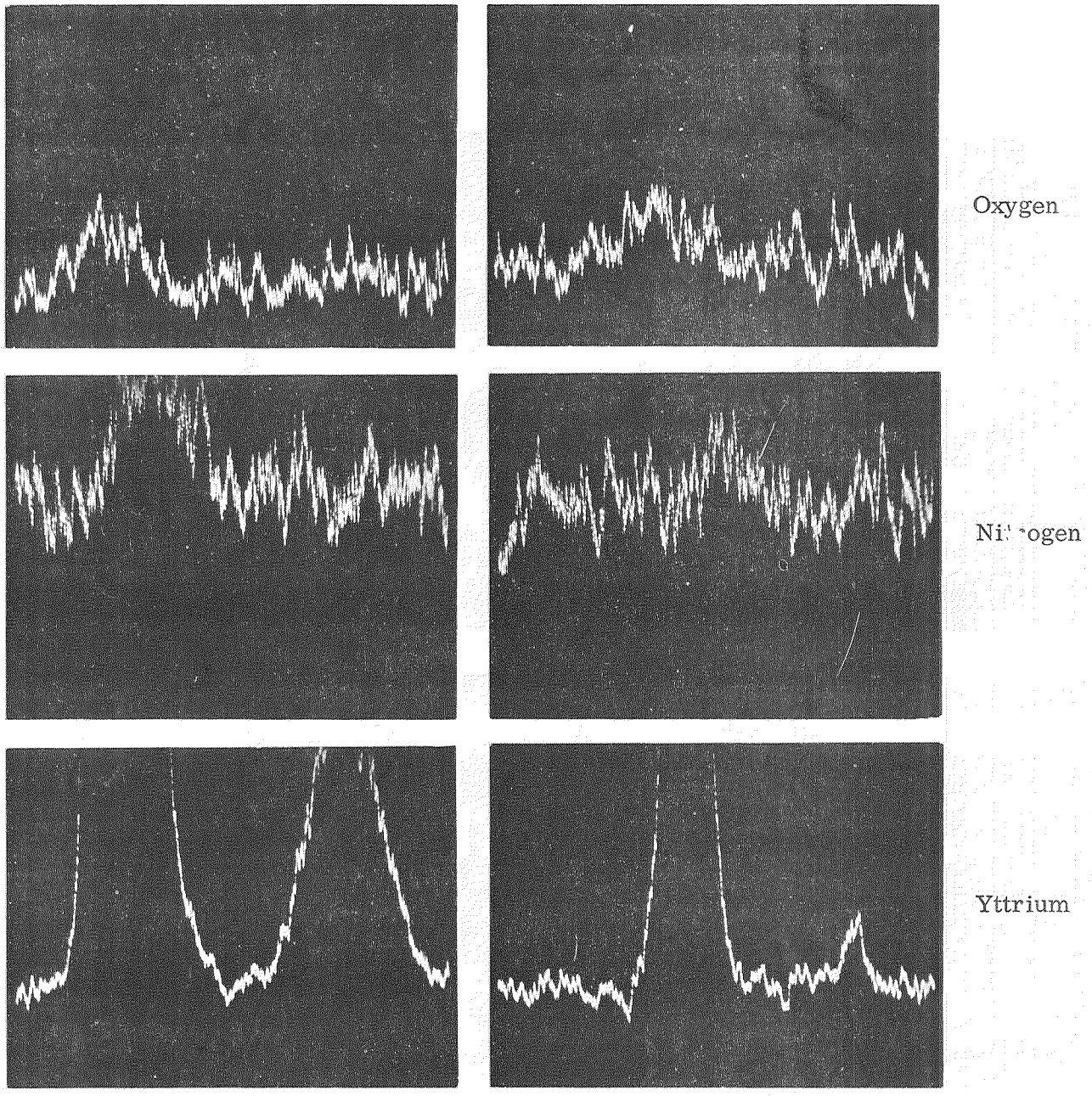

Figure 73 Electron Probe Scan of Yttrium Stringers for Oxygen and Nitrogen in a Cr-0.25Y Alloy (×4000 reduced to 74% of original size).

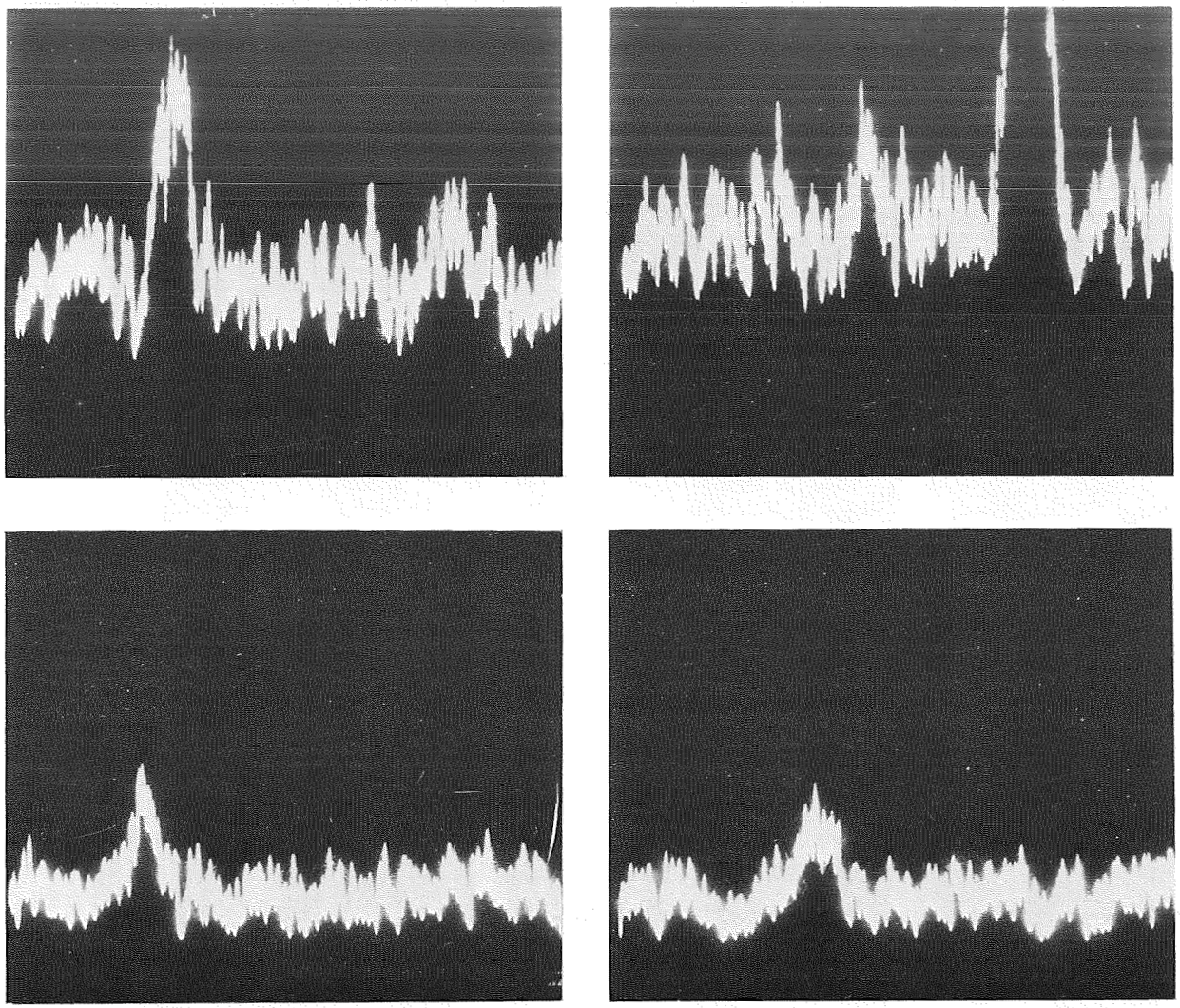

100 hr-2100° F-O_2 | 100 hr-2100° F (1422° K) Air

Figure 74 Distribution of O and N Across Y Inclusion in Cr-0.5 Alloy After Exposure to Air and Oxygen (× 1000 reduced to 95% of original size).

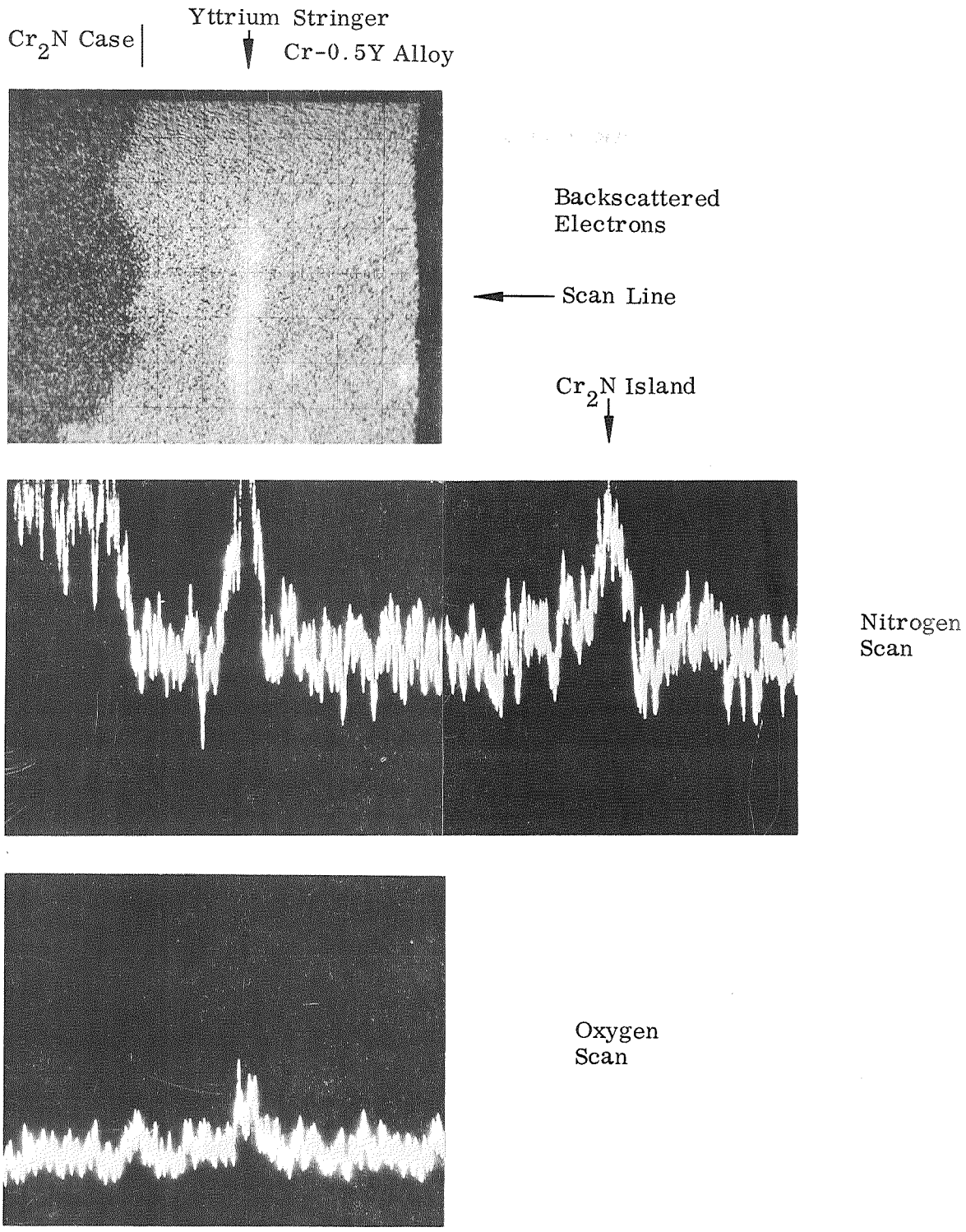

Figure 75 Distribution of O and N in Cr-0.5Y Alloy After 100 hr-2100° F (1422° K)-Air (× 1000 reduced to 82% of original size).

by dissolving excess nitrogen, this phase minimizes or prevents formation of intergranular nitrides which would occur if nitrogen continued to be absorbed after the alloy (Cr solid solution) was saturated. In this respect, the scavenging action would be helpful in preventing severe intergranular embrittlement. However, since the Cr solid solution is saturated with nitrogen and precipitates Cr_2N platelets on cooling without embrittling the alloy, it certainly cannot be concluded that nitrogen scavenging by the yttrium phase is responsible for the improved resistance to embrittlement.

A similar study was conducted to determine if the Cr_2Zr intermetallic phase in Cr-Zr alloys scavenged oxygen or nitrogen during processing and air exposure. Optical micrographs consistently revealed a darkening of the Cr_2Zr intermetallic phase on exposure of the alloys to either oxygen or air. This indicates some type of scavenging action, perhaps different from that characteristic of the rare earth addition. Whereas the rare earths appear to react preferentially with nitrogen, the Cr_2Zr phases appear to react preferentially with oxygen. However, electron probe scans across particles of this phase in a Cr-Zr alloy exposed to both pure oxygen and air indicated no significant increase of either oxygen or nitrogen in the particles (Figure 76). If any scavenging action existed, the levels of interstitials absorbed were beyond the limits of detection by the analytic techniques used.

Probe scans at low magnification revealed that the zirconium content was higher in the banded region where the Cr_2Zr phase was darkened on air or oxygen exposure than it was in the unaffected center of the alloy. Figure 77 reveals a marked enrichment of the contaminated layer with zirconium. No indication of enrichment in oxygen or nitrogen is indicated, however. This behavior, coupled with the discovery of ultrafine precipitates in Cr-Zr alloys exposed to air (Figure 52), suggests that selective internal oxidation of zirconium in solid solution to form ZrO_2 precipitates is occurring. As the matrix loses zirconium by this process, a concentration gradient is established and zirconium diffuses toward the surface. The net result is an enrichment of the outer contaminated layers in zirconium and a depletion of the core.

This effect was observed for all zirconium alloys exposed to oxygen or air and may explain the beneficial effect of preoxidation on the resistance of Cr-Zr alloys to nitrogen embrittlement. As discussed in section 5.5, internal oxidation of Cr-Zr alloys prior to air exposure resulted in an alloy with a much lower DBTT after air exposure. Preoxidation would establish an initial fine dispersion of oxide precipitates, enrich the outer layers of the alloy in zirconium, and perhaps saturate the matrix with oxygen. The effect of preoxidation treatments on the distribution of elements in Cr-Zr alloys is shown in Figure 78. Preoxidation greatly enriched the outer zone in zirconium for chromium alloys with 2 to 3% Zr. The preoxidized Cr-2Zr which was ductile at 700°F (544°K) after air exposure had a much higher concentration of zirconium near the surface than the same alloy without preoxidation. The DBTT of the latter was 1200°F (922°K). No concentration of nitrogen or oxygen was detected in this region in either material, however. A thin nitride case was found beneath the oxide scale of the preoxidized alloy. The oxide scale developed during preoxidation had been removed before the alloy was exposed to air.

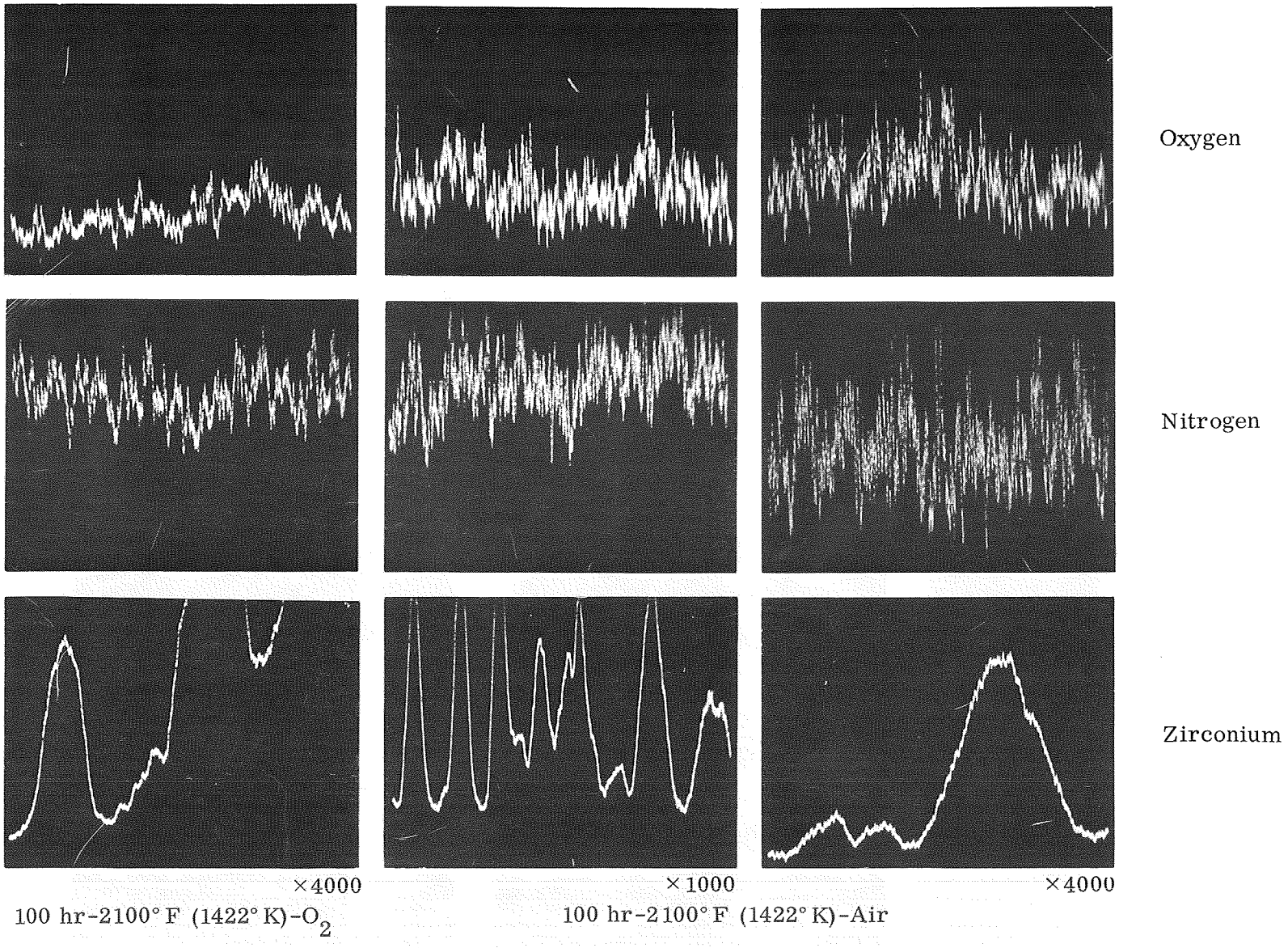

Figure 76 Electron Probe Scan of Cr_2Zr Phase for Oxygen and Nitrogen in a Cr-3Zr Alloy (magnifications reduced 61% of original size).

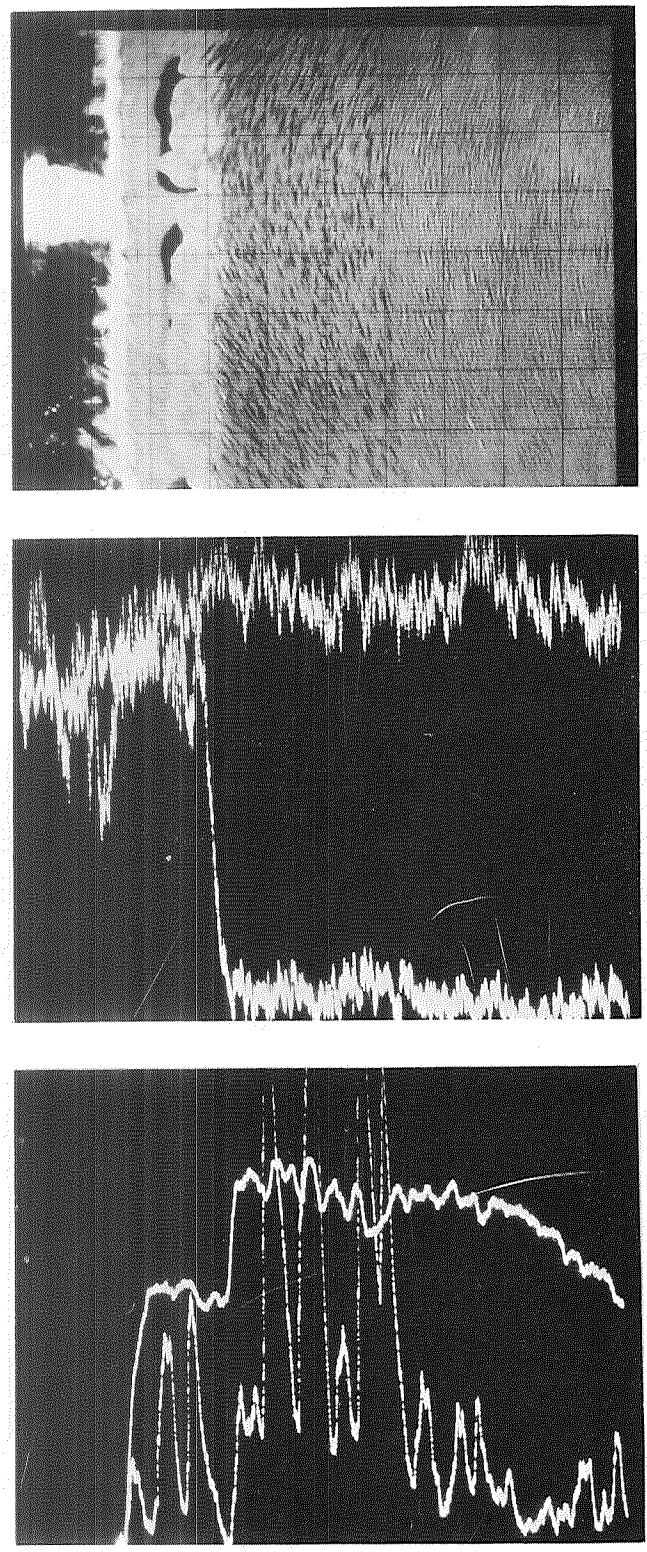

Figure 77 Distribution of Elements in Cr-3Zr Alloy Exposed 100 hr-2100° F (1422° K)-Air (×250 reduced to 88% of original size).

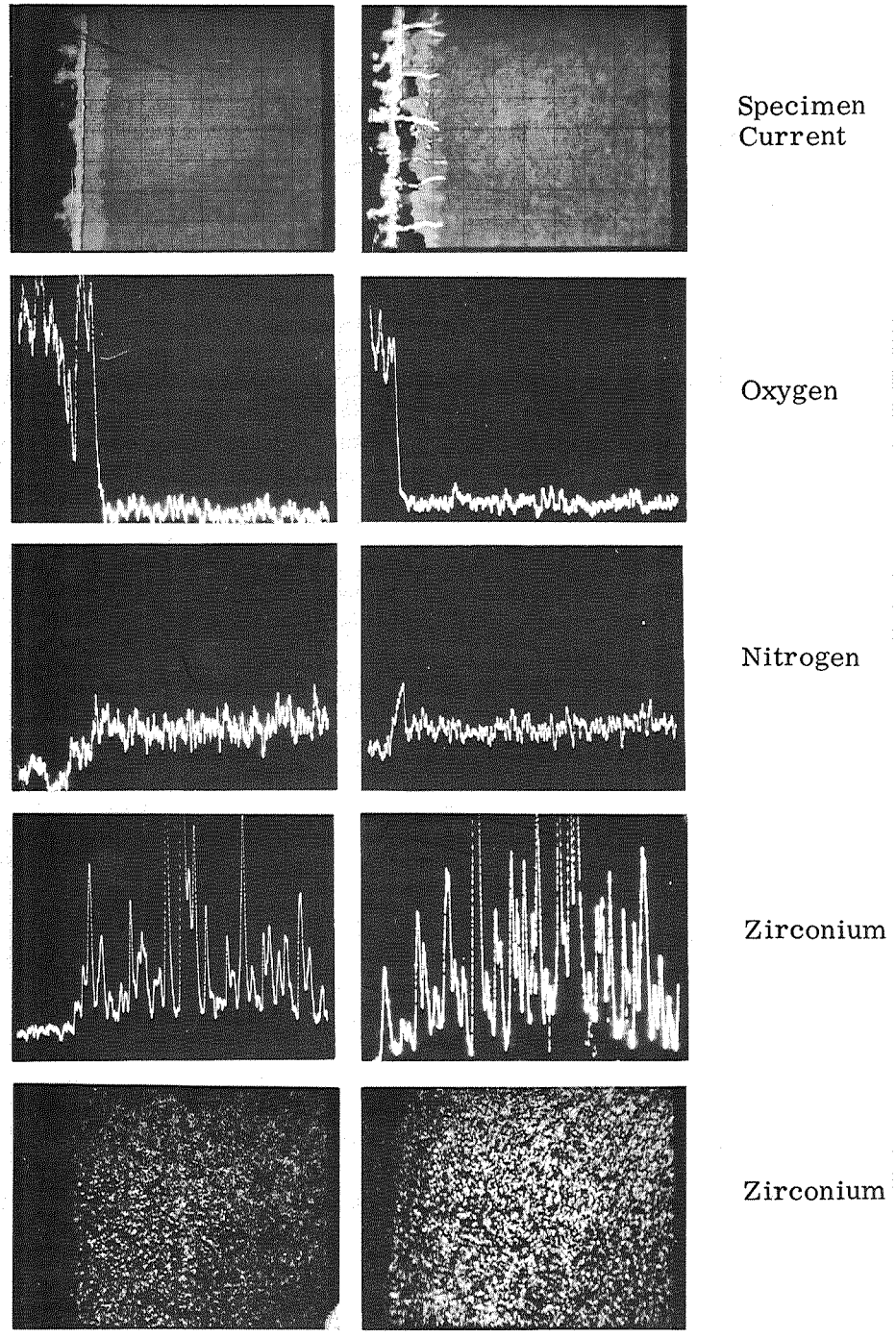

Figure 78 Effect of Preoxidation on Distribution of O, N, and Zr in Cr-2Zr Alloy After Air Exposure (×250 reduced to 47% of original size).

Nitrogen Diffusivity

There is no direct evidence to indicate that the alloy additions that inhibit nitrogen embrittlement have any major effect on the diffusivity of nitrogen in chromium. These elements do not have a significant effect on reaction rates with nitrogen, a process that is diffusion controlled. The controlling step, however, is probably diffusion through a nitride case. All the alloys resistant to embrittlement form nitride cases and have uniform distributions of nitrogen through the sheet thickness. Hardness is uniform through the section. This behavior indicates rapid diffusion of nitrogen and is similar to that observed for alloys that are not resistant to embrittlement.

Chromium nitride platelets having about the same size, shape, and distribution as those found in chromium are found in chromium alloyed with all the rare earths, zirconium, and hafnium. These precipitate on cooling by the diffusion of nitrogen to preferred sites (habit planes). As shown in Figure 69, the solid solubility of nitrogen at the exposure temperature [2100°F (1422°K)] is estimated to be 740 ppm by weight from the data of Seybolt (Ref. 25). At 780°F (689°K) the solubility is about 0.1 ppm by weight from extrapolations of all available data. Klein and Claurer (Ref. 26) have shown that all the nitrogen precipitates on cooling unless very thin sections with low nitrogen content are rapidly cooled in water. A series of cooling rate experiments was conducted to determine if unalloyed chromium and alloys with resistance to embrittlement exhibited any differences in behavior. The results are shown in Figures 79 through 82.

The effect of cooling rate is identical in Cr, Cr-Y, and Cr-La alloys. On air cooling, large platelets of Cr_2N precipitate within the grains or preferred habit planes. A depleted zone is formed along the boundaries and fine spherical particles precipitate in a discontinuous fashion in the grain boundaries. On water quenching, the nitrogen has less time to diffuse and precipitates in a much more uniform distribution within the grains as extremely fine platelets of Cr_2N. It is likely that the precipitation occurs at lower temperatures with a high degree of supersaturation. The nitrogen could not be retained completely in solid solution by water quenching of thin sections [0.030 in. (0.076 cm)]. This behavior was predicted by Klein and Claurer (Ref. 26). The nitride formed on water quenching still forms as platelets of Cr_2N on preferred habit planes, as shown in Figure 82. The precipitates, however, are much smaller than those formed on air cooling. On furnace cooling, where more time for diffusion exists, the nitrogen precipitates almost exclusively in the grain boundaries. The samples were furnace cooled to 900°F(755°K) and air cooled to room temperature. Virtually all the nitrogen has been precipitated from solid solution at 900°F and something less than 1 ppm should be left to precipitate below this temperature. The precipitates form at the most favorable (lowest energy) sites. A few small idiomorphic crystals precipitated in the grains. As shown in Figures 79, 80, and 81, the behavior is similar for chromium and Cr-rare earth alloys. No significant changes in diffusivity are indicated.

Since cooling rate has such a profound effect on structure, it is likely to alter hardness, strength, and ductility. The effect of variations in cooling rate on the hardness of air-exposed samples is summarized in Table 14. Water quenching increases the hardness by an average of about 40 DPH units for unalloyed chromium and a variety of alloys. There is little tendency for hardening on air cooling, and the hardness is about the same as that of furnace-cooled samples. Most of the samples show little hardening

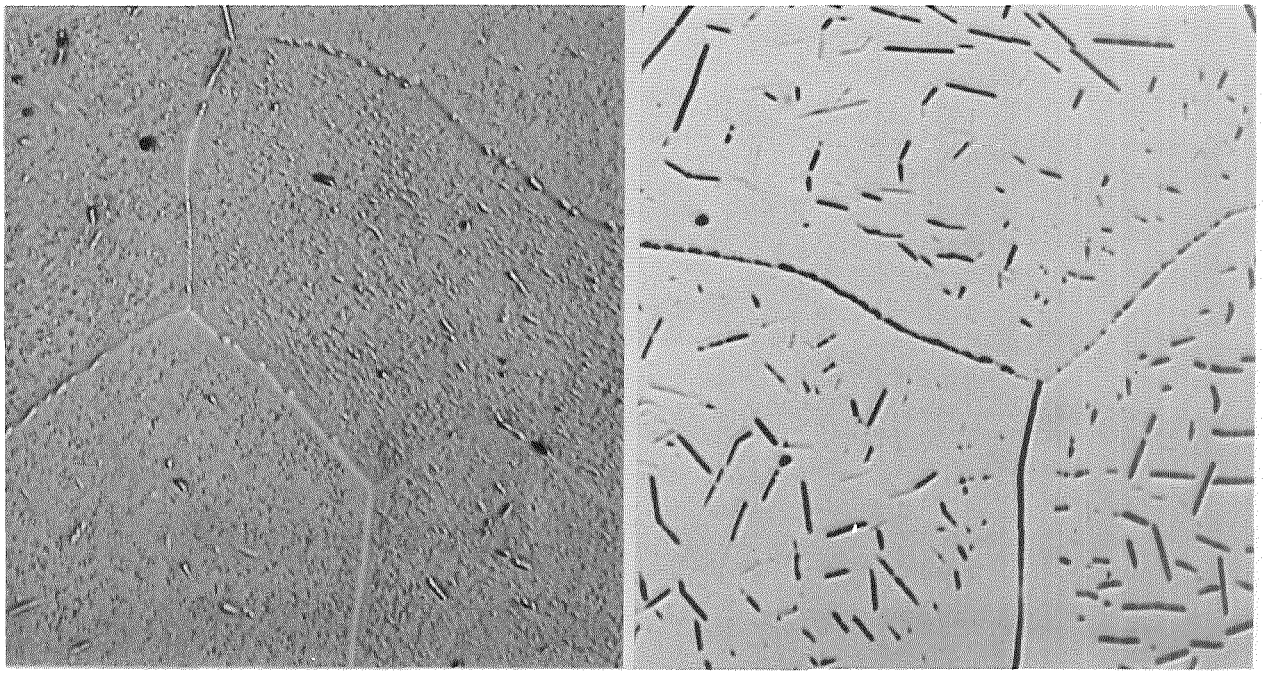

A5698 ×1000 A5685 ×1000

Water Quench Air Cool

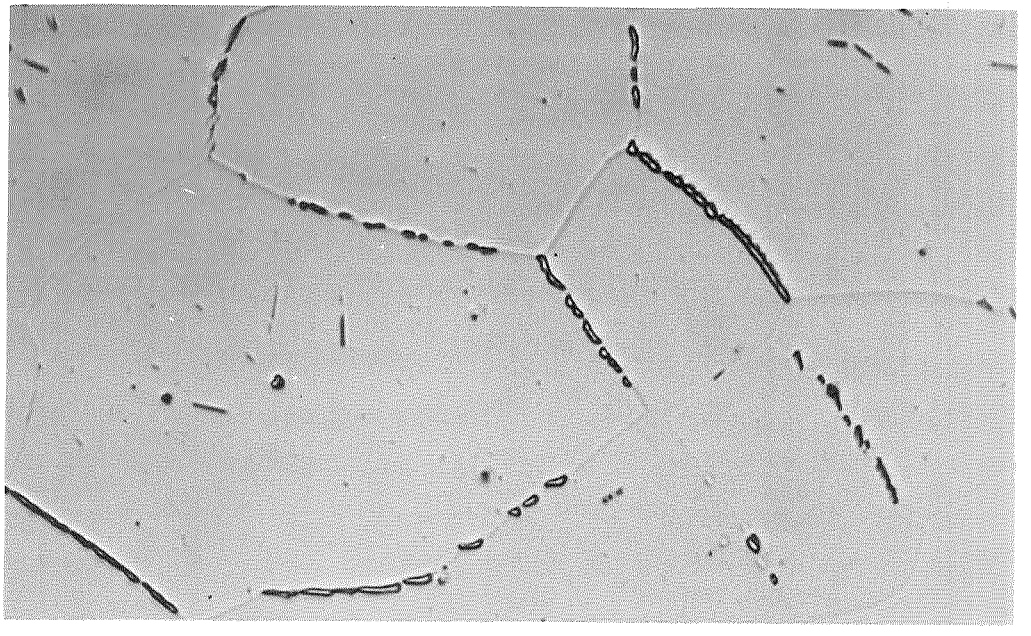

A5690 ×1000

Furnace Cool to
900° F (755° K)

Figure 79 Effect of Cooling Rate on Nitride Phase in Unalloyed Cr (Cr-5), 100 hr-2100° F

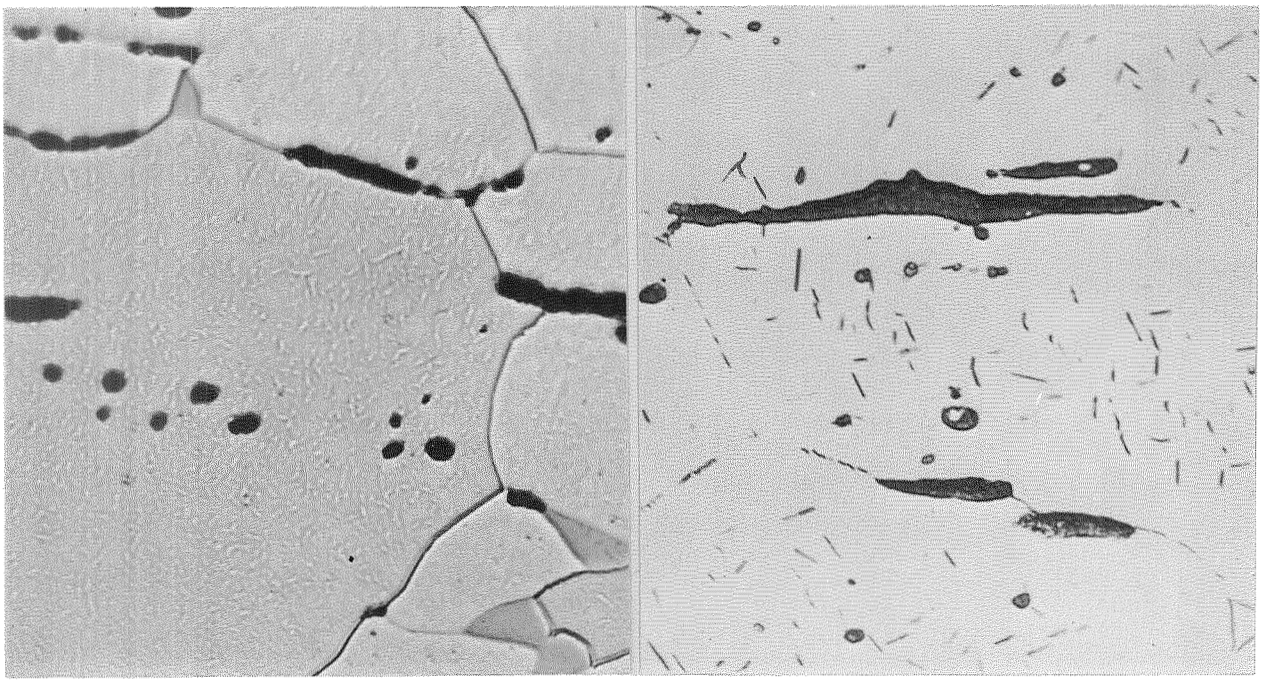

A5696 ×1000 A3575 ×1000

Water Quench Air Cool

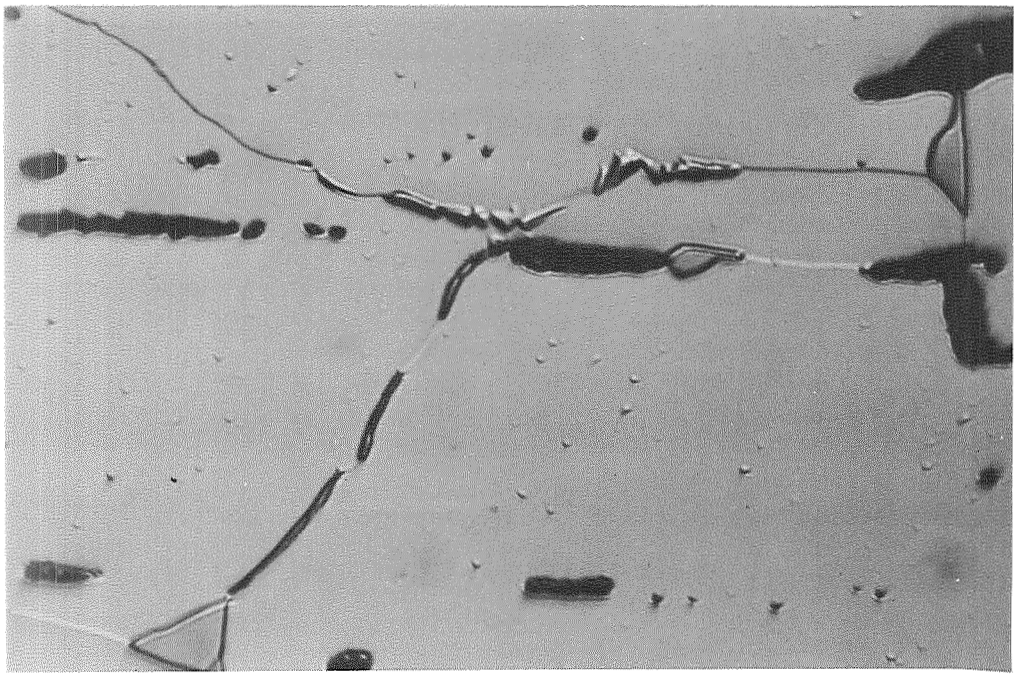

A5683 ×1000

Furnace Cool to
900° F (755° K)

Figure 80 Effect of Cooling Rate on Nitride Phase in Cr-0.5Y (950-8), 100 hr-2100° F (1422° K)-Air

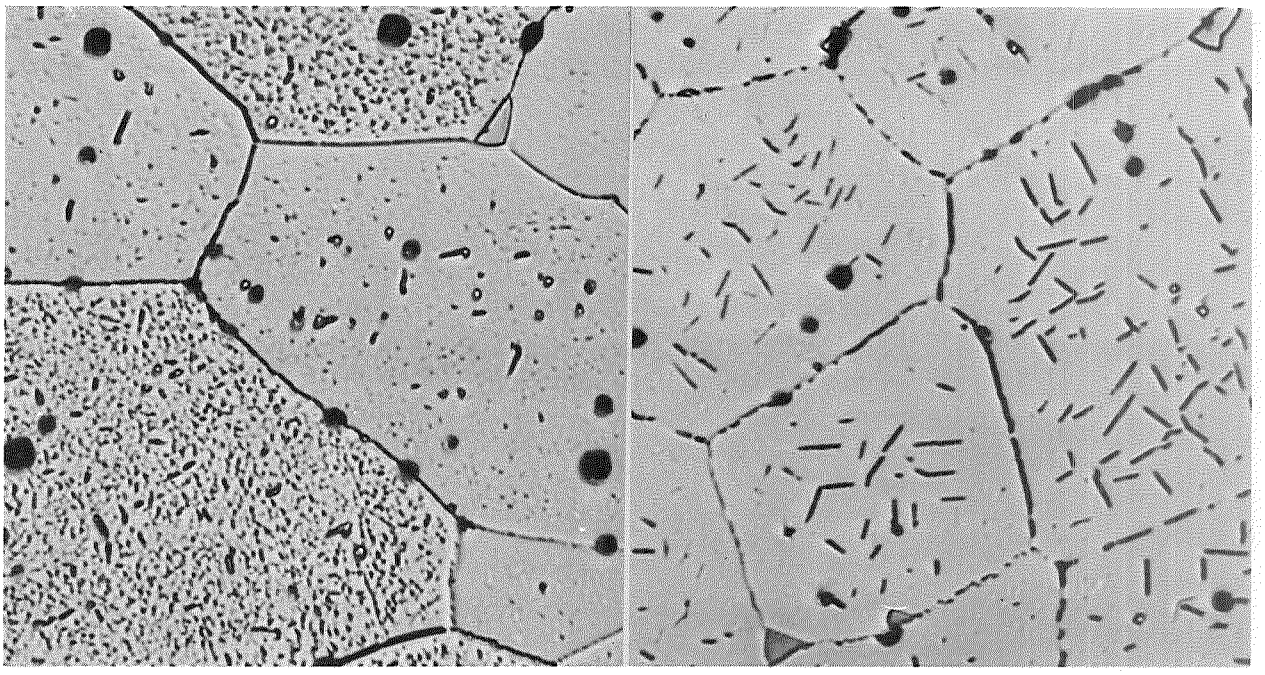

A5697 ×1000 A5694 ×1000

Water Quench Air Cool

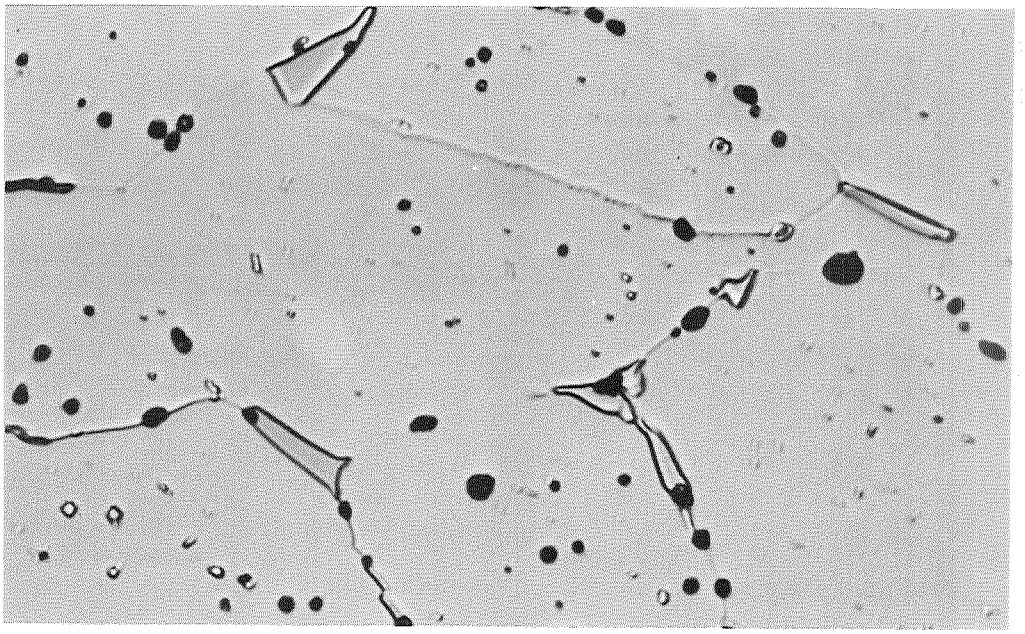

A5695 ×1000

Furnace Cool to
900° F (755° K)

Figure 81 Effect of Cooling Rate on Nitride Phase in Cr-0.25La, 100 hr-2100° F (1422° K)-Air

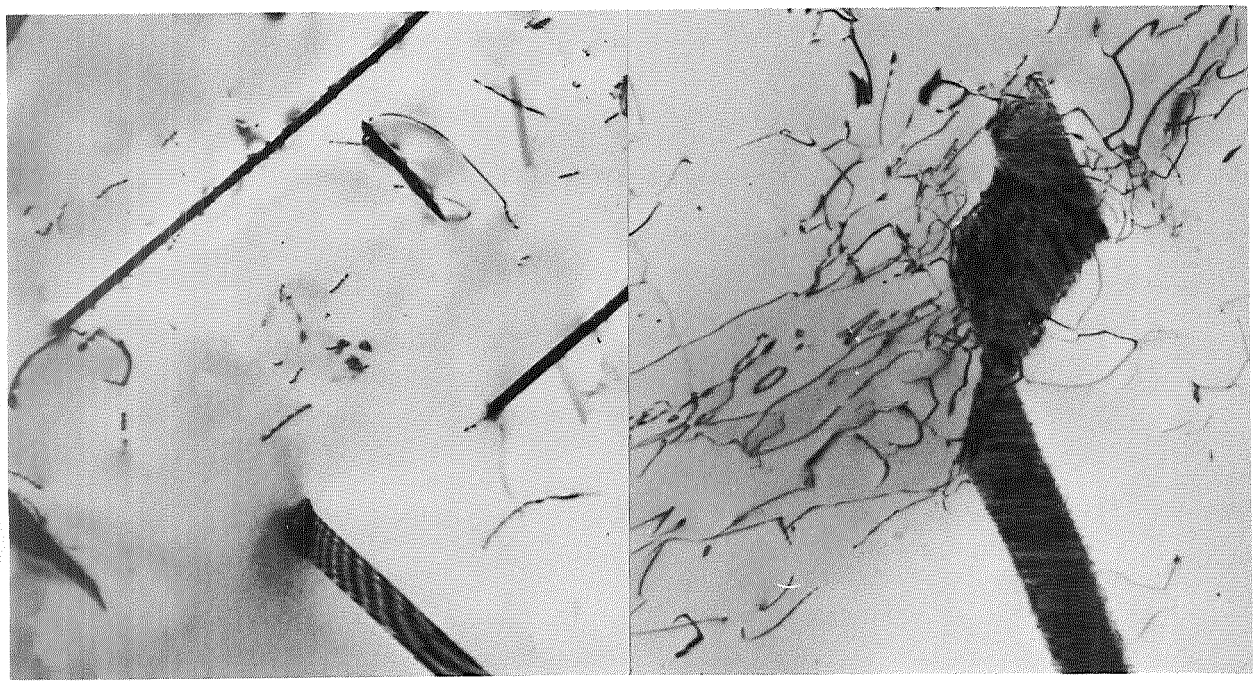

D215 ×30,000 D219 ×30,000

Water Quench ⟷ Air Cool

2000 Å

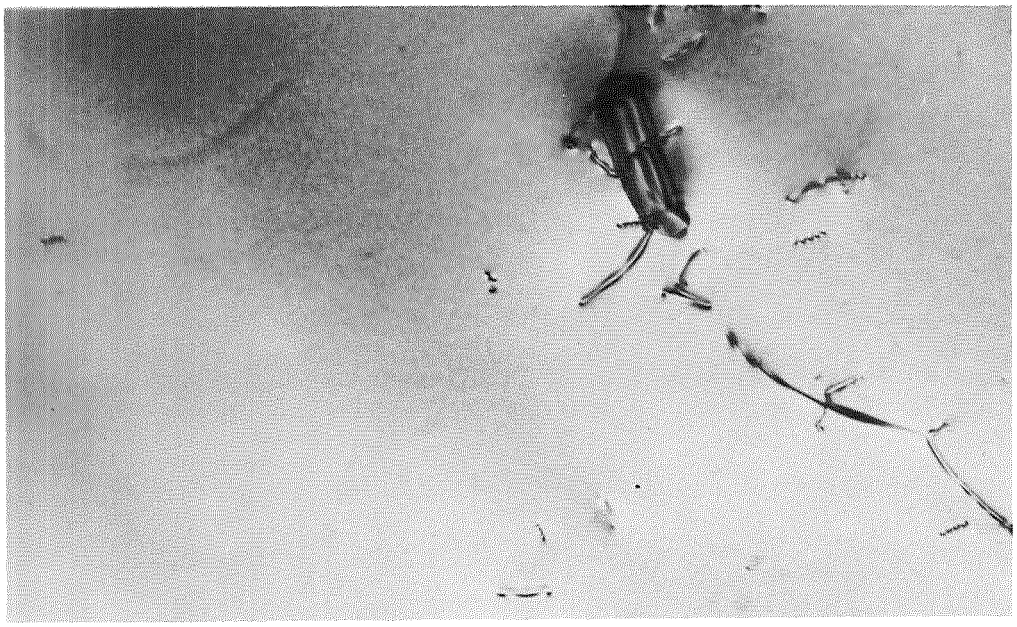

D223 ×30000

Furnace Cool to
900° F (755° K)

Figure 82 Effect of Cooling Rate on Fine Structure of Unalloyed Cr(Cr-4), 100 hr-2100° F (1422° K)-Air

Table 14

EFFECT OF ATMOSPHERE AND COOLING RATE ON HARDNESS
(All values in DPH)

Atmosphere →	Helium	Oxygen	Air			Air, Pre-oxidized	Hardness Change		
Cooling Medium →	Air	Air	Air	Water	Furnace	Air	AC to WQ	AC to FC	FC to WQ
Material ↓									
Unalloyed Cr	149	143	150	195	155	159	+45	+5	+40
Cr-0.25La	158	151	165	197	159	150	+32	-6	+38
Cr-0.5Y (950)	161	—	180	196	160	—	+16	-20	+36
Cr-0.5Y (9125)	158	138	159	—	—	—	—	—	—
Cr-3Zr-0.1Y	196	—	197	256	201	193	+59	+4	+55
Cr-3Zr	152	180	200	—	—	183	—	—	—
Cr-4Fe	279		267	311	246		+46	-19	+65

as a result of air exposure when slow cooled (by air or furnace) from the exposure temperature. This behavior indicates that quench hardening is due either to retention of some nitrogen in solid solution on quenching or to hardening by extremely fine precipitates that form at low temperatures from supersaturated solid solutions. Fine precipitates decorate the dislocation, particularly in the water-quenched sample, as shown in Figure 82. The Cr-3Zr and Cr-0.5Y alloys are hardened slightly by the air exposure, even in the slow-cooled condition. This is believed to be the result of internal oxidation and precipitation of small oxide particles.

Nitrogen Solubility

Rare earths and other elements that improve resistance to nitrogen embrittlement might possibly alter the solid solubility of nitrogen in chromium to either reduce the limit at high temperature or decrease the limit at low temperature. In the first case, the degree of supersaturation would be reduced and the total amount, morphology, and distribution of the nitride precipitates would be altered. In the second case, small amounts of nitrogen would be retained in solution at low temperatures and less ultrafine precipitates (particularly on dislocation lines) would be formed.

There is considerable evidence from metallographic studies to indicate that rare earths, zirconium, hafnium, and thorium do lower to some extent the solid solubility of nitrogen at the exposure temperature [2100°F(1422°K)]. Analytical proof was not possible, however, since after exposure for 100 hr the alloys contain massive nitride islands developed isothermally and contain a total nitrogen content far in excess of any solubility limit. In addition, the rare earth phase has absorbed nitrogen and would contribute to an erroneous result. This effect is shown in Figure 83. Large particles of Cr_2N are found in the boundaries and at grain intersections. In order to determine the precise effect of these alloys on solid solubility, the samples would have to be saturated with nitrogen and the reaction stopped at that point so that no excess nitrogen was absorbed. They could then be analyzed for nitrogen content. However, if the rare earth phases absorbed any nitrogen, the result would be high and in error. Quantitative metallography coupled with cooling rate, aging, and internal friction studies would provide the best indication of changes in nitrogen solubility in the matrix as a function of alloying. In lieu of such measurements, qualitative metallography provides a reasonable indication of behavior.

As shown in Figures 48 and 50, the amount of nitride precipitated in chromium appears to decrease with increasing yttrium and zirconium content. The effect is far more pronounced with zirconium and with the ternary Cr-Zr-Th, Y, La alloys than with the Cr-rare earth binaries (Figures 59 and 63). The ternary alloys show very little nitride in air-cooled structures. A cooling rate study was conducted with an air-exposed Cr-3Zr-0.1Y alloy to determine if this was the result of a true reduction in nitrogen solid solubility or merely a change in kinetics of precipitation. The results (Figure 84) show that very little difference exists in the structure of water-, air-, or furnace-cooled specimens. No visible platelets of Cr_2N are developed on water quenching or air cooling. On furnace cooling, a few intergranular islands of Cr_2N are formed. This alloy still hardens on water quenching, however (Table 14), indicating that a significant level of solid solubility exists.

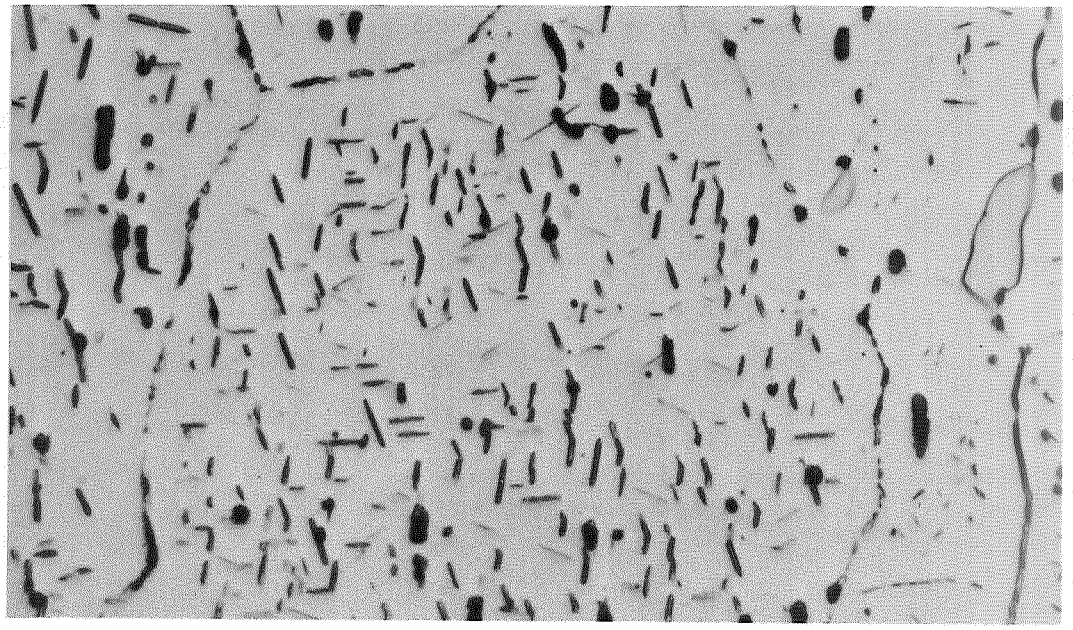

A5880 ×1000

Cr-0.5Y (9125-5)
DBTT = >700° F (644° K)

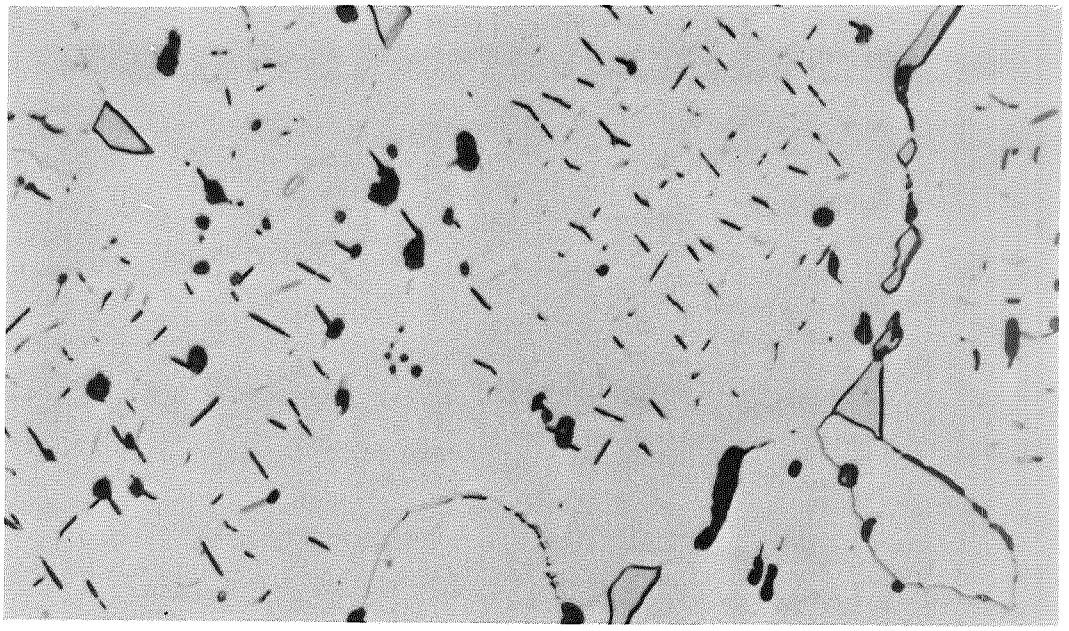

A5883 ×1000

Cr-0.5Y (950-9)
DBTT = <400° F (478° K)

Figure 83 Structure of Cr-0.5Y Alloys With High and Low DBTT After 100 hr-2100° F (1422° K)-Air

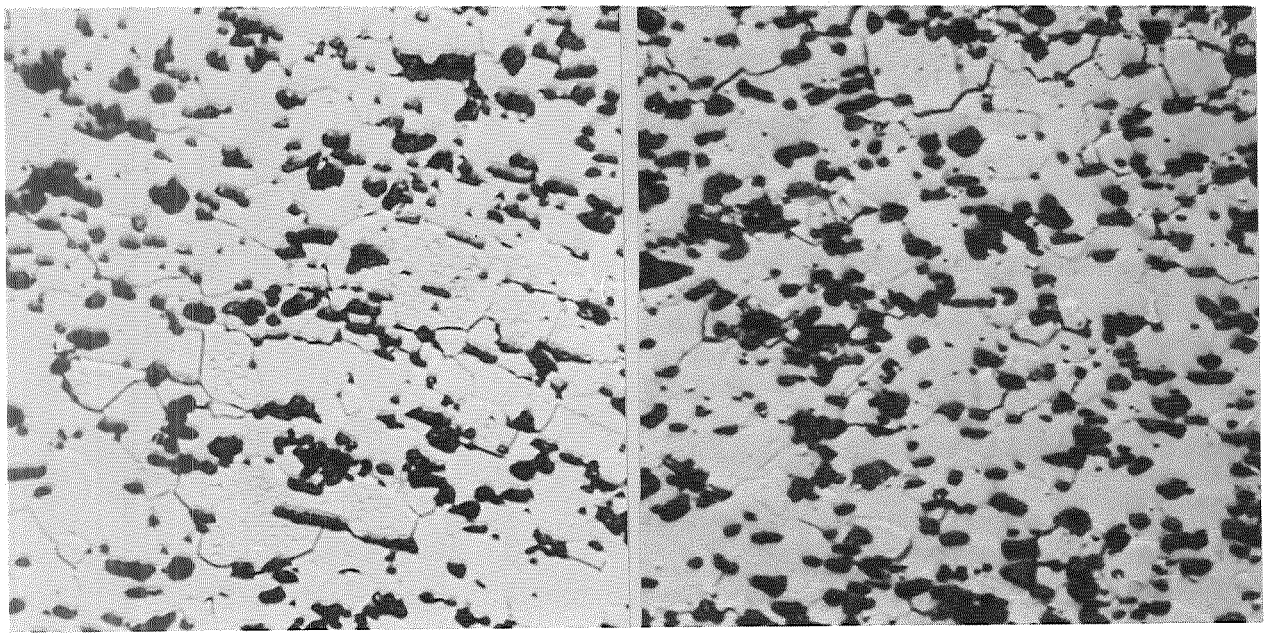

A5685 ×1000 A5882 ×1000

Water Quench Air Cool

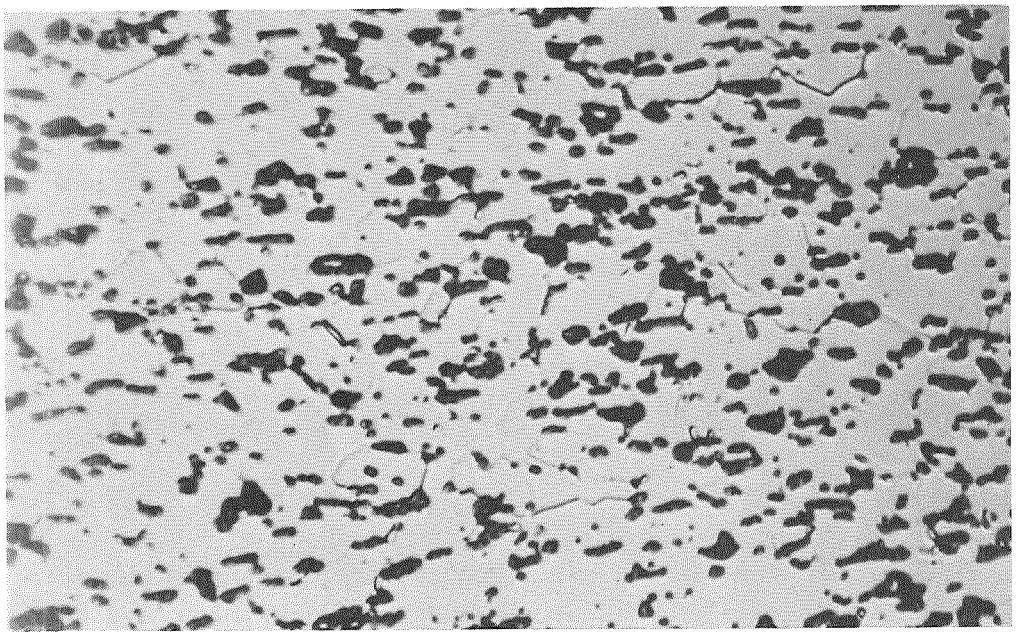

A5688 ×1000

Furnace Cool

Figure 84 Effect of Cooling Rate on Nitride Phases in Cr-3Zr-0.1Y, 100 hr-2100° F (1422° K)-Air

Although these additions do appear to lower solid solubility, no direct correlation between DBTT and nitrogen solubility exists. Simple Cr-Zr binaries with the lowest apparent solubility for nitrogen still have a high DBTT. Cr-rare earth alloys with greater solid solubility have a much lower DBTT.

Nitride Precipitates

Unalloyed chromium and all the alloys studied contain precipitates of Cr_2N in the grains and grain boundaries. Most of the nitride precipitates are in the form of platelets on preferred crystallographic planes. All precipitates have the same appearance, whether in unalloyed chromium or in the various binary or ternary alloys. They are not found when these materials are exposed to helium or oxygen and are present only in air-exposed samples [100 hr-2100°F(1422°K)]. As shown in the preceding section, the size and distribution of the Cr_2N platelets varies with cooling rate. The platelets range in length from a maximum of 0.25 mil (0.000635 cm) to a minimum of perhaps 500 to 1000Å. Alloying with elements that increase resistance to nitrogen embrittlement did not alter these precipitates in any detectable manner and did not result in the formation of any nitride precipitates that were different from those found in unalloyed chromium after air exposure. Alloying with these elements did introduce a variety of oxide/nitride particles in the grains and grain boundaries; however, the large nitrides or oxides did not appear to go into solution at 2100°F (1422°K) and did not appear to be precipitated on cooling. For the most part, they were formed in preparation of the alloy or by internal oxidation/nitridation of secondary phases or alloy solutes at the exposure temperature.

Several investigators have cited the existence of nitride (Cr_2N) platelets on the major cleavage plane (100) in chromium as a probable cause of brittle behavior (Ref. 2). Such particles could act as stress raisers and promote cleavage. It is significant to note in the current study that chromium alloys that are not embrittled at all by exposure to air at 2100°F (1422°K) contain a very large amount of Cr_2N platelets precipitated on preferred planes. As shown in Figure 83, a Cr-0.5Y with a DBTT of <400°F (<478°K) has a very large concentration of these precipitates in the grains. The same alloy which had a higher DBTT due to a processing variation has a larger concentration of such platelets and most likely a higher nitrogen content. The difference in precipitates, however, cannot be the reason for the embrittlement in one case and not in the other. Also, it should be noted that Cr-3Zr alloys contain few, if any, platelets of Cr_2N, yet have a DBTT as high or higher than that of unalloyed Cr. There is no consistent pattern of behavior to link the Cr_2N platelet precipitates with variations in DBTT.

In the search for a common pattern of behavior, it was observed from transmission studies that unalloyed Cr and alloys of Cr with Y, La, and Zr all had very fine precipitates decorating the dislocations in air-exposed samples. Examples of this can be seen in these illustrations presented in preceding sections of this report: Figures 51, 52, 66, and 67. Very fine precipitates, 10 to 100 Å in diameter, are formed in the Cr-Y and Zr alloys. Many of these appear to form in rows on preferred planes (Figure 52). Close examination of the dislocations in these samples reveals many of these fine particles precipitated on dislocation lines. Initially, it was believed that some of the fine precipitates, especially in Cr-Zr alloys, were oxides formed by

internal oxidation. However, transmission studies of Cr-3Zr alloys exposed to oxygen did not reveal many fine precipitates of the type observed in air-exposed samples. As seen in Figure 85, most of the dislocations in an oxygen-exposed sample are not decorated by precipitates and do not appear to be pinned. A fairly large number of dislocations also are evident. Dislocations that are free of precipitates also are seen in the Cr-3Zr exposed to helium (Figure 86). When the same alloy is exposed to air, however, fine precipitates decorate many of the dislocations (Figure 87). It is concluded from this observation that the precipitate is a nitride and not an oxide or intermetallic phase.

A similar precipitate is formed on dislocations in unalloyed Cr, Cr-Y, and Cr-Zr alloys exposed to air at 2100°F (1422°K). Examples are shown in Figures 88, 89, and 90. Close inspection reveals many dislocations decorated with small precipitates that are closely spaced in a line. The effect appears to be one of closely spaced particles with small segments of a dislocation bowed between the particles. It is believed that these dislocations existed or were formed during cooling to room temperature and that the low-temperature precipitation of Cr_2N occurred on these energetically favorable sites. It has been well established that interstitials tend to segregate to point defects, dislocations, and grain boundaries and that these are natural sites for subsequent precipitation.

The existence of fine precipitates on many dislocations is one factor that is common to all chromium alloys after exposure to air at high temperature. Cooling rate studies reveal that most of the nitrogen has been precipitated from solid solution as Cr_2N platelets at temperatures above 900°F (755°K). No platelets are seen in chromium that has been slow cooled to this temperature and then cooled rapidly (by air) from there to room temperature. Fine precipitates on dislocations are seen in this material, however, suggesting formation at temperatures below 900°F (755°K). The same fine precipitates are seen in chromium that has been water quenched or air cooled directly from 2100°F (1422°K). These samples also contain the Cr_2N platelets that are not present in the sample that was furnace cooled to 900°F (755°K).

Defect Structure

It is concluded from the foregoing analysis that the defect structure controls the ductile/brittle behavior of chromium contaminated with nitrogen. It is postulated that all the nitrogen precipitates from solid solution on cooling to room temperature and that the material which precipitates in the low-temperature range comes out preferentially as very fine particles on existing dislocations. The dislocations will be tightly locked by these precipitates, and the metal cannot yield and deform plastically unless the dislocations are freed or new dislocations are generated. If neither can occur in sufficient amount at the temperature of stressing, conditions are set for both the initiation and the propagation of brittle cleavage fracture.

Ductility can be restored in two ways, both requiring a specific increase in temperature: (1) the precipitates may redissolve to free the pinned dislocations or (2) thermally activated dislocation sources may become operative. This is believed to give rise to the DBTT which now is viewed as the temperature at which dislocations will be unpinned or new sources activated in sufficient quantity for plastic deformation to occur in response to loads applied. The role of alloying additions in lowering the

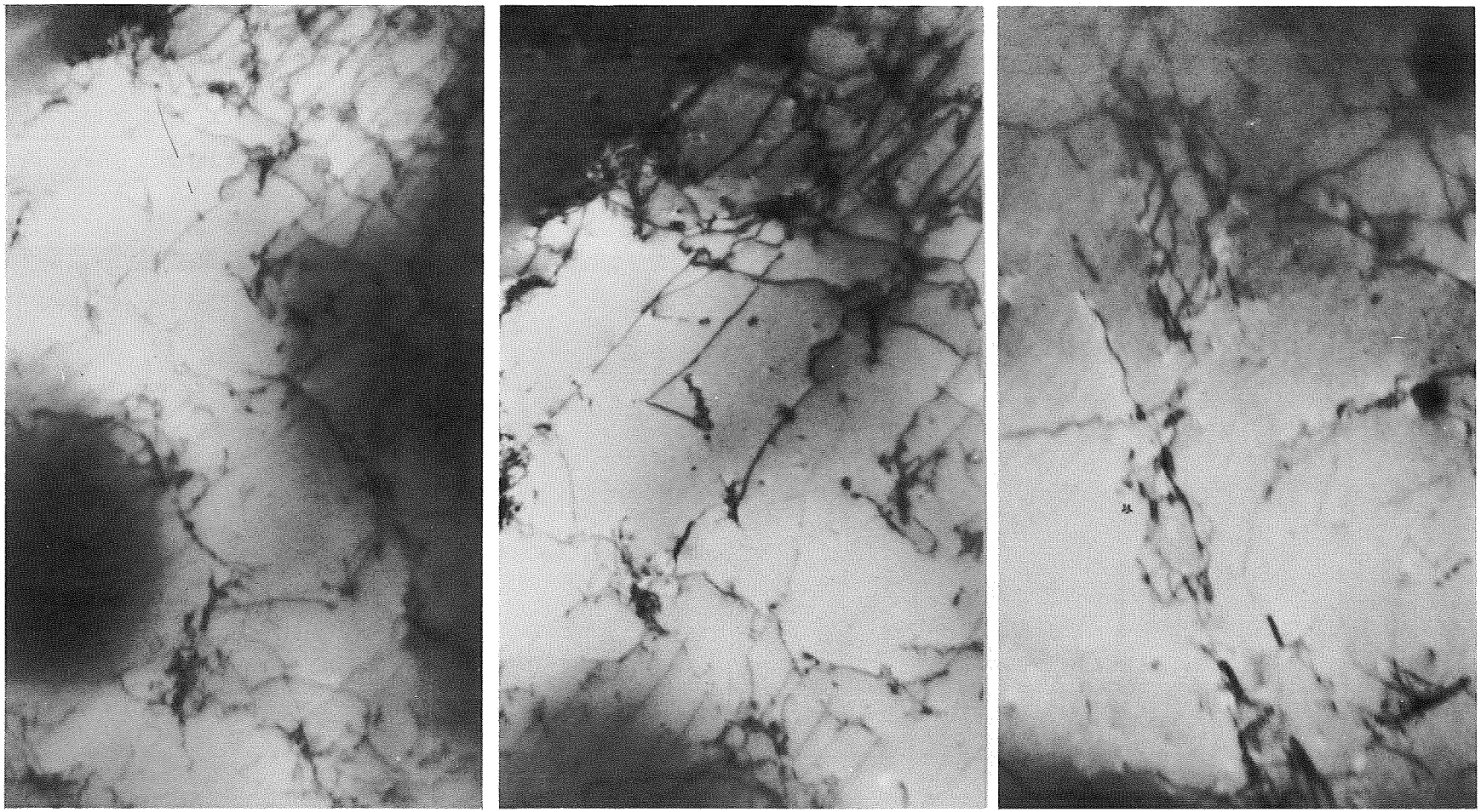

D5 ×30000 Dark Field

D6 ×48000 Bright Field

D10 ×48000 Dark Field

Cr 3Zr (9136-9)
50 Hr-2100° F (1422° K)-O_2

Figure 85 Dislocations in Cr-3Zr Alloy Exposed to Oxygen at 2100° F

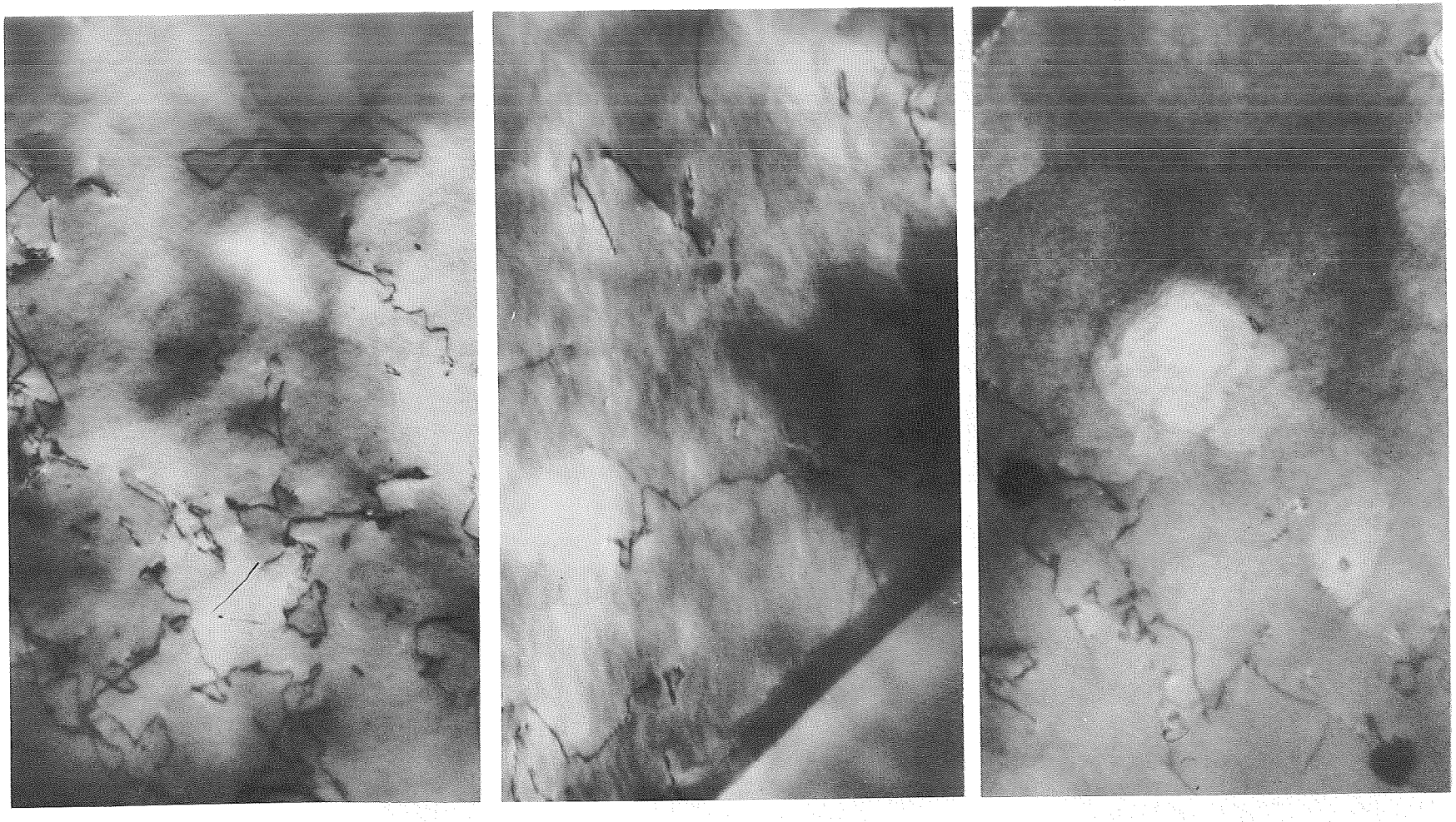

C630 ×48000 C636 ×48000 C633 ×48000

Dark Field Bright Field Dark Field

Cr-3Zr (9136-9)
100 Hr-2100° F-He

Figure 86 Dislocations in a Cr-3Zr Alloy Exposed to Helium at 2100° F (1422° K).

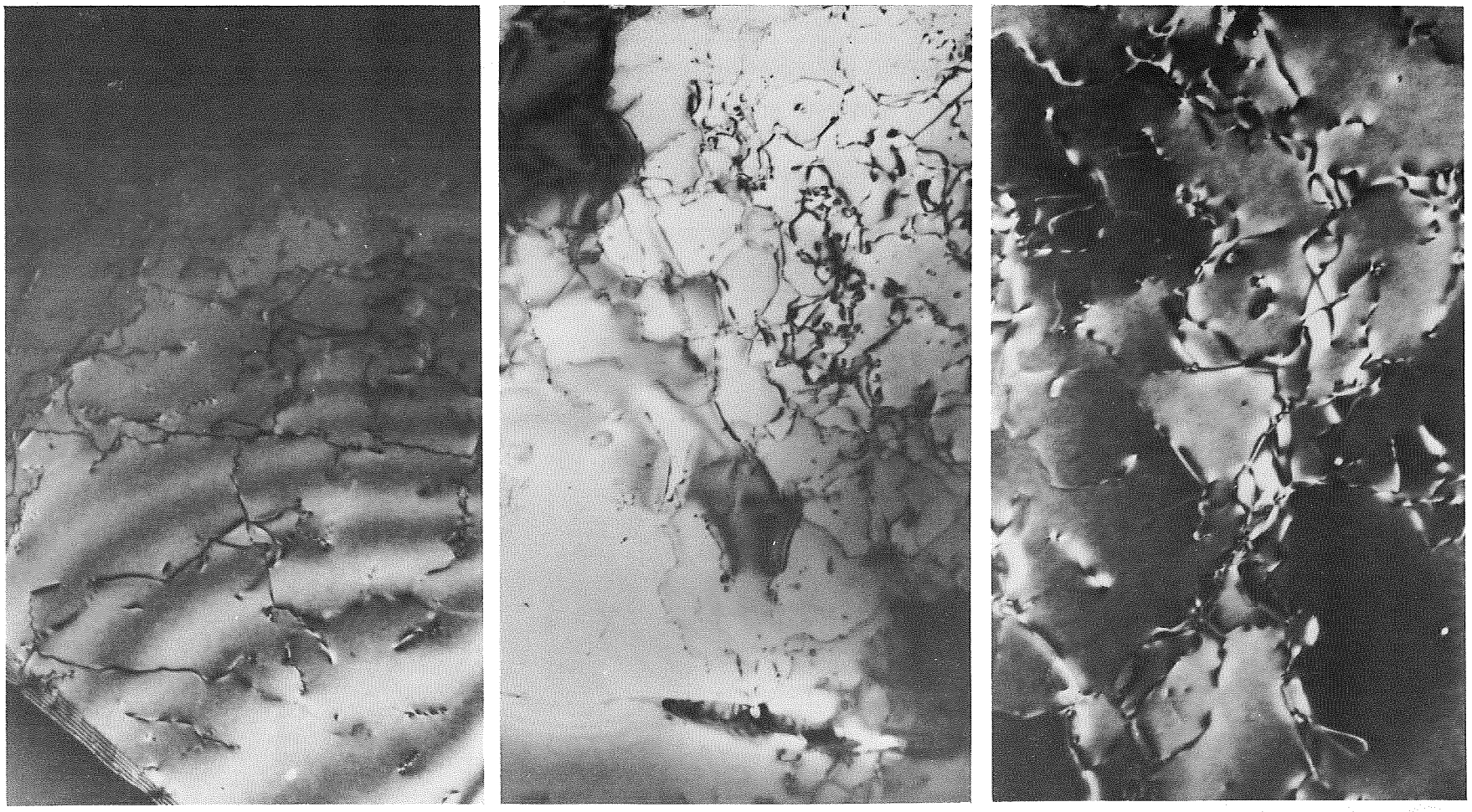

C653 ×48000 D1 ×48000 D4 ×80000

Dark Field Bright Field Dark Field

Cr-3Zr (9136-6)
100 Hr-2100° F-Air

Figure 87 Precipitation on Dislocations in a Cr-3Zr Alloy Exposed to Air.

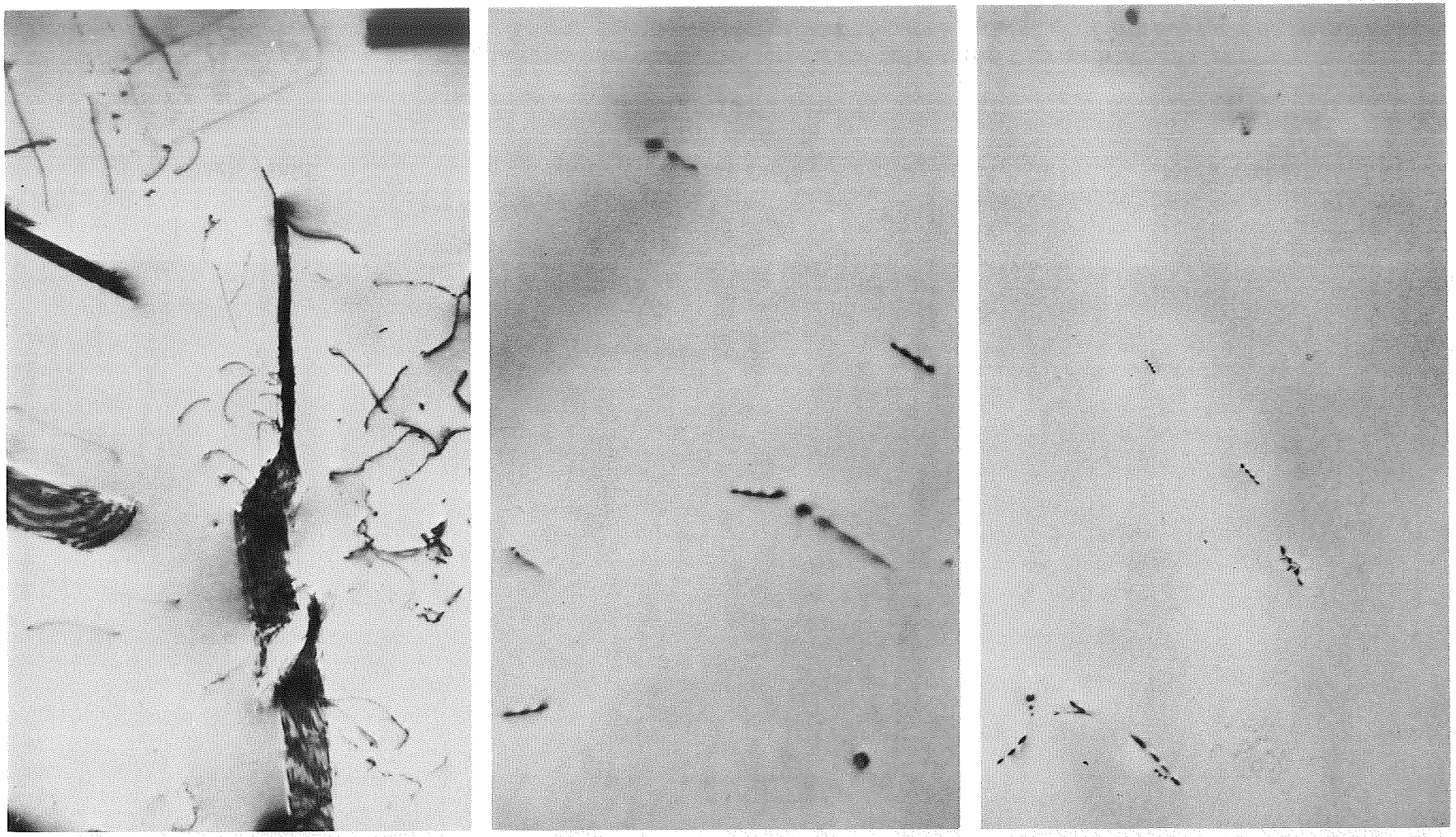

D216 Water Quench ×30000 D222 Air Cool × 120000 D224 Furnace Cool ×30000

Cr (NASA)

50 Hr-2100° F (1422° K)-O_2 + 100 Hr-2100° F (1400° K)-Air

Figure 88 Dislocations and Precipitates in Preoxidized Unalloyed Chromium

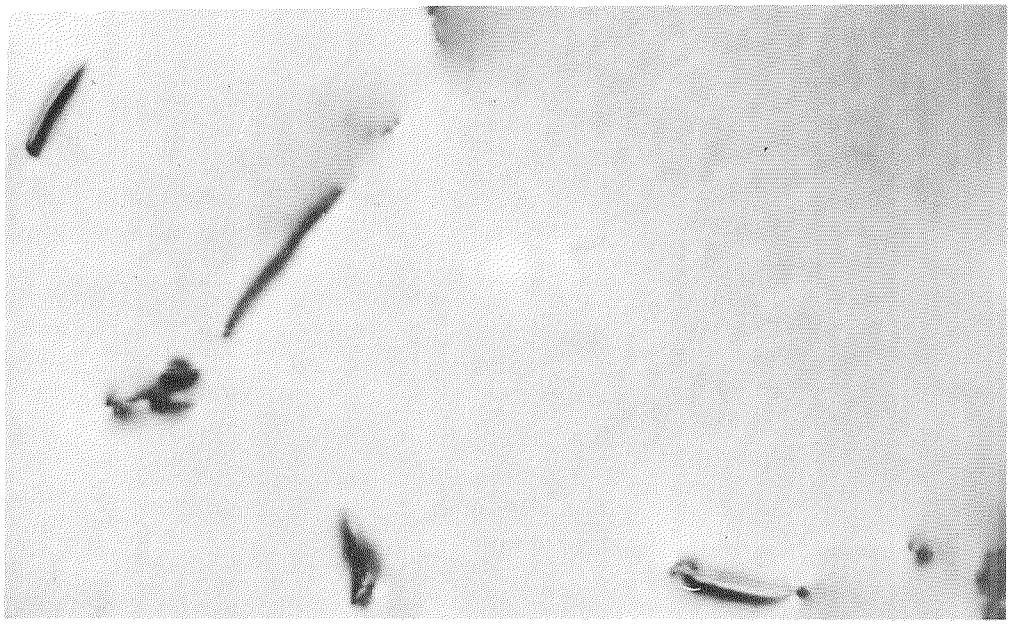

D229 ×120,000

500 Å

9125-5

DBTT = >700° F (644° K)

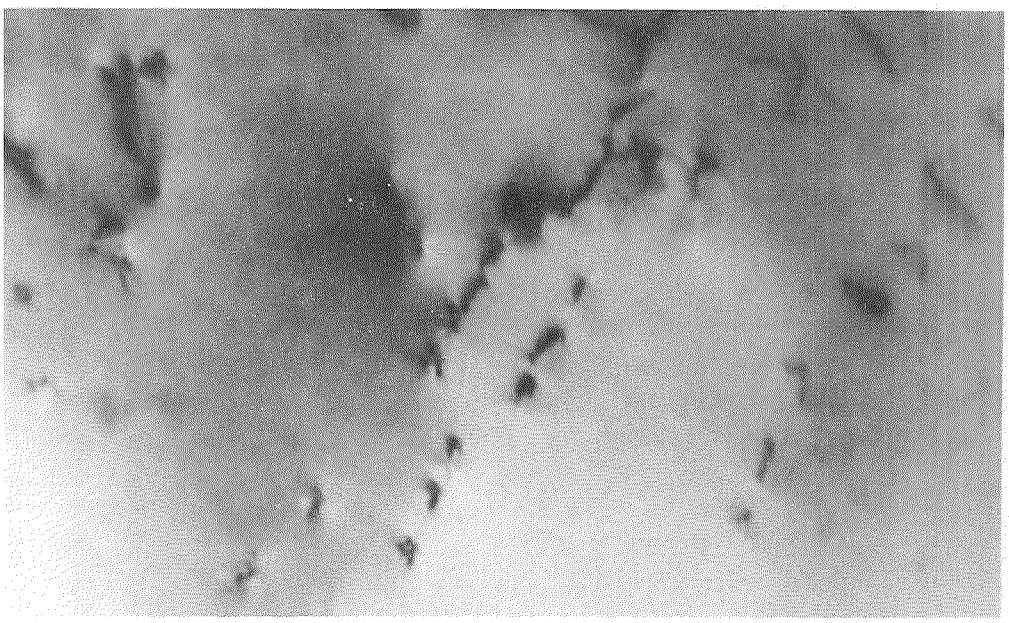

D232 ×120,000

500 Å

950-14

DBT = <400° K (478° K)

Figure 89 Fine Structure of Cr-0.5Y Alloys With High and Low DBTT After 100 hr-2100° F (1422° K)-Air Exposure

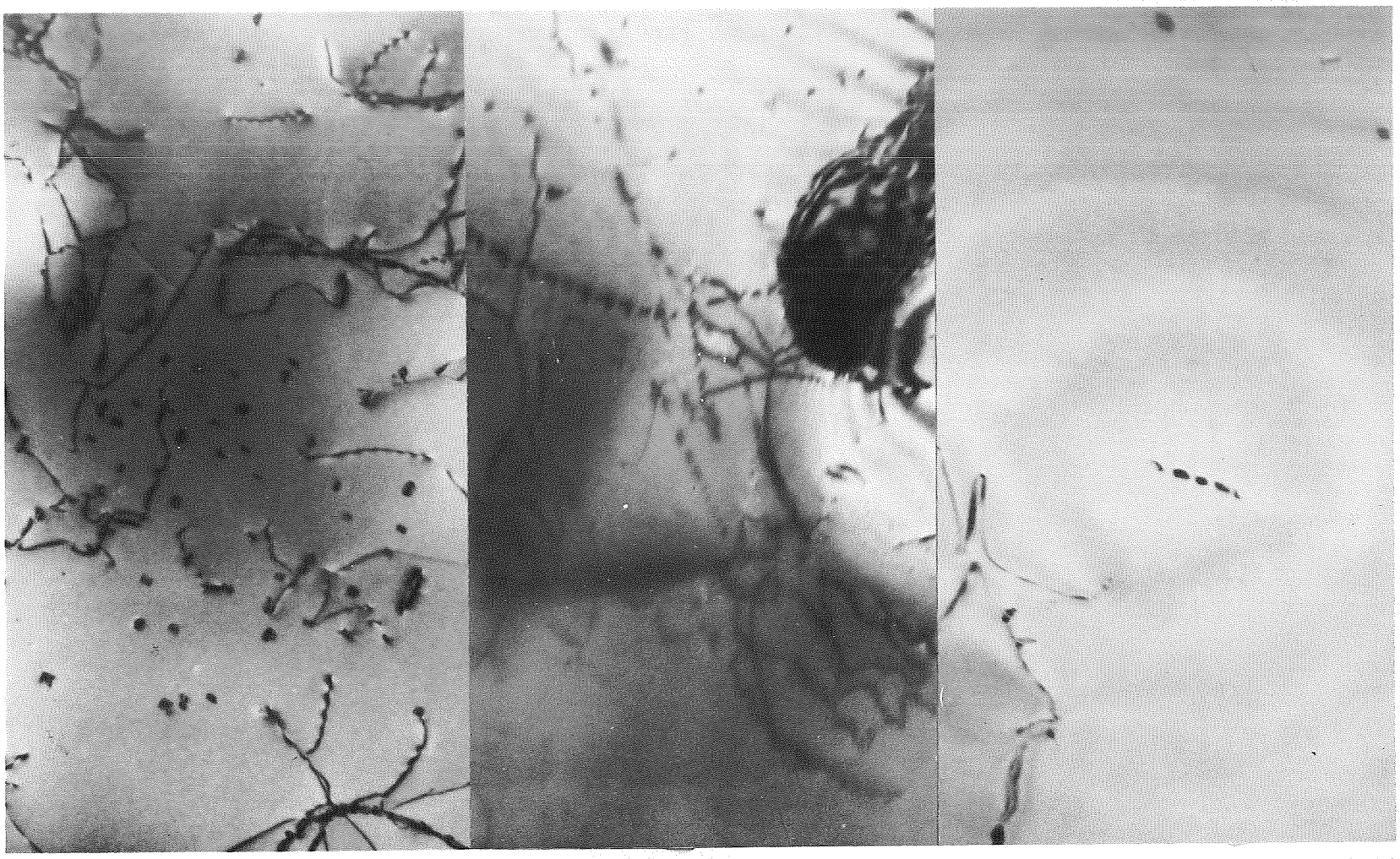

D102 ×30000 D112 ×80000 D223 ×120000

Cr-2Zr (9100-4)
100 Hr-2100° F (1422° K)-Air

Figure 90 Dislocations and Precipitates in Cr-2Zr

DBTT becomes apparent when the nature of additions that will reduce the DBTT is considered. The only elements found to be effective are those that form insoluble dispersions of a second phase and/or will be internally oxidized to form dispersions of oxides along grain boundaries or in grains. The role of these additions is considered to be one of providing dispersed phases that will activate dislocation sources and provide a sufficient quantity of unpinned dislocations to accommodate slip and result in ductile behavior.

A considerable amount of information supports the conclusion that dispersed particles enhance the ductility of metals by activation of dislocation sources. Ratliff et al. (Ref. 28) found that the DBTT of tungsten was reduced continuously with increasing additions of ThO_2 or ZrO_2 particles up to 8 vol%. It was concluded that fine particles of these oxides acted in conjunction with fine-grained structures to impede crack propagation and brought about dislocation multiplication, thereby lowering the DBTT. It has long been known that additions of MgO and Y_2O_3 lower the DBTT of chromium (Ref. 2). Although some investigators attribute this to a scavenging effect, it appears more likely that the primary role of these oxides is one of dislocation source activation. Kayano and Koda (Ref. 29) found that the yield drop in iron was associated with dislocation nucleation around precipitates when aging or straining. Under applied stress, dislocation multiplication occurs from loops or helicies nucleated by precipitated particles. The stress concentration around such particles will nucleate dislocations during straining. Ashby (Ref. 30) reports that the difference in coefficient expansion between particle and matrix produces strain in the interface on cooling which is relieved by nucleation of dislocations. Other investigators have confirmed Ashby's observations and found that localized forests of secondary dislocations are built up in the neighborhood of dispersed particles. The local stresses around the particles will operate favorably placed Frank-Reed sources within tangles around the particles. Thus, particles and associated tangles can be both obstacles and sources of slip.

Direct observation of such effects have been found in Cr-Zr and Cr-Y alloys exposed to air. In Figure 91, a small particle of the Cr_2Zr phase in the center photograph is clearly indicated to be activating dislocation sources at the interface or surrounding strain field. These dislocations are not pinned like others in the surrounding area and probably were formed after the nitrogen precipitated from solution. They are mobile dislocations and act to accommodate slip. The long Cr_2N platelet in the right-hand photograph does not appear to be activating dislocation sources. The interfacial energy of such precipitates is not favorable for occurrence of this process.

Tangles of dislocations are seen around four particles of the Cr_2Zr phase in Figure 92. Again, most of these are unpinned and many appear to have cross slipped. Pinned dislocations that were formed or existed while cooling through the nitrogen precipitation range are clearly seen. A similar effect for the yttrium phase in a Cr-0.5Y alloy is shown in Figure 93. Many tangles of unpinned dislocations are observed around particles of the yttrium phase.

Dislocation loops will be nucleated around precipitate particles by plastic deformation if the stress and interface conditions are favorable (Ref. 29). The stress concentration around irregularly shaped particles will favor nucleation of dislocations by deformation. However, if the interface is regular, insufficient stress concentration may restrict dislocation nucleation (Ref. 29). Thus, particle size, shape, interfacial energy, residual stress, and applied load will govern the ability of dispersed phases to

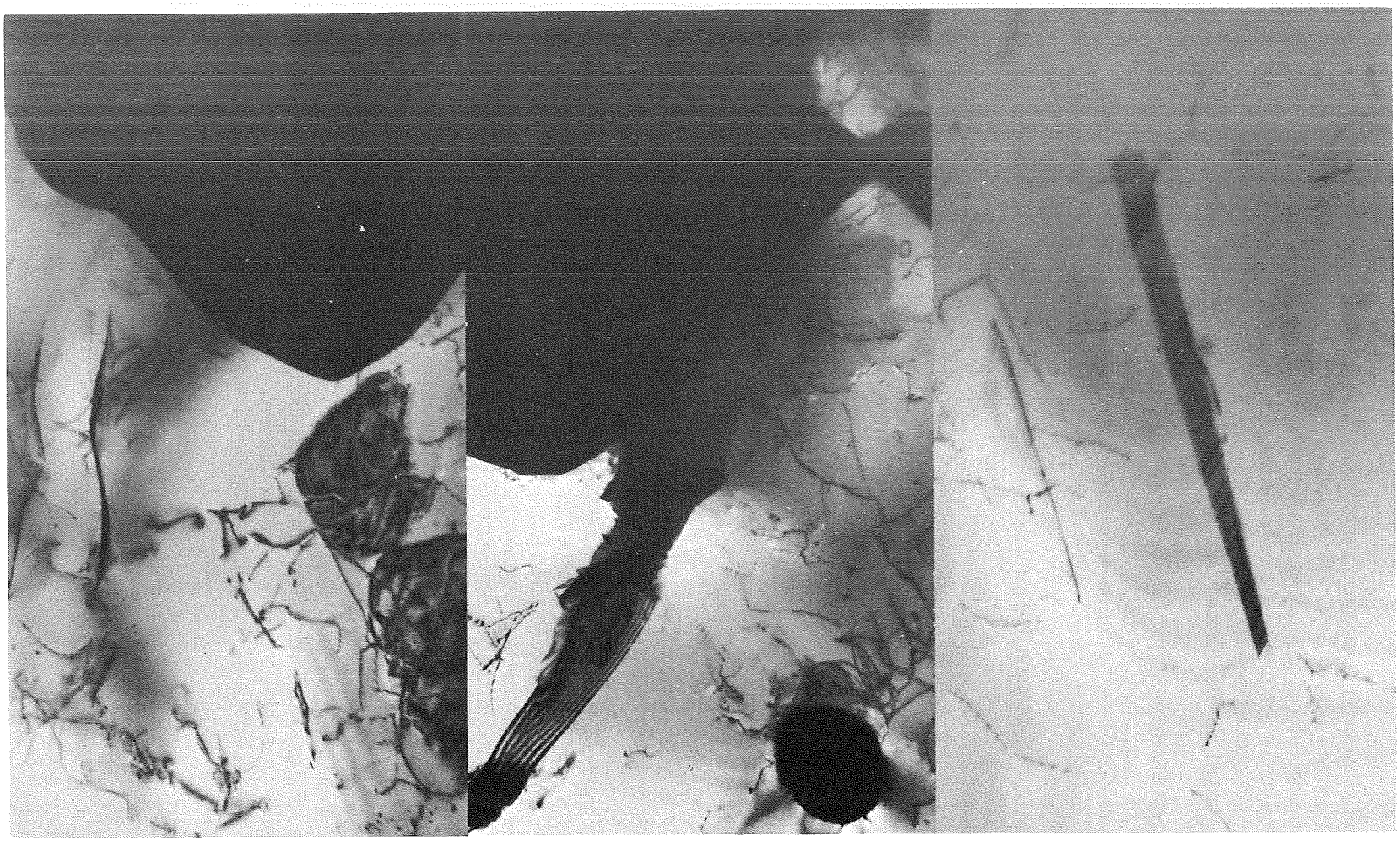

D120 ×30000 D118 ×30000 D237 ×60000

Cr-2Zr (9100-11)
50 Hr-2100° F (1422° K)-O_2 + 100 Hr-2100° F (1422° K)-Air

Figure 91 Dislocations and Precipitates in Preoxidized Cr-2Zr.

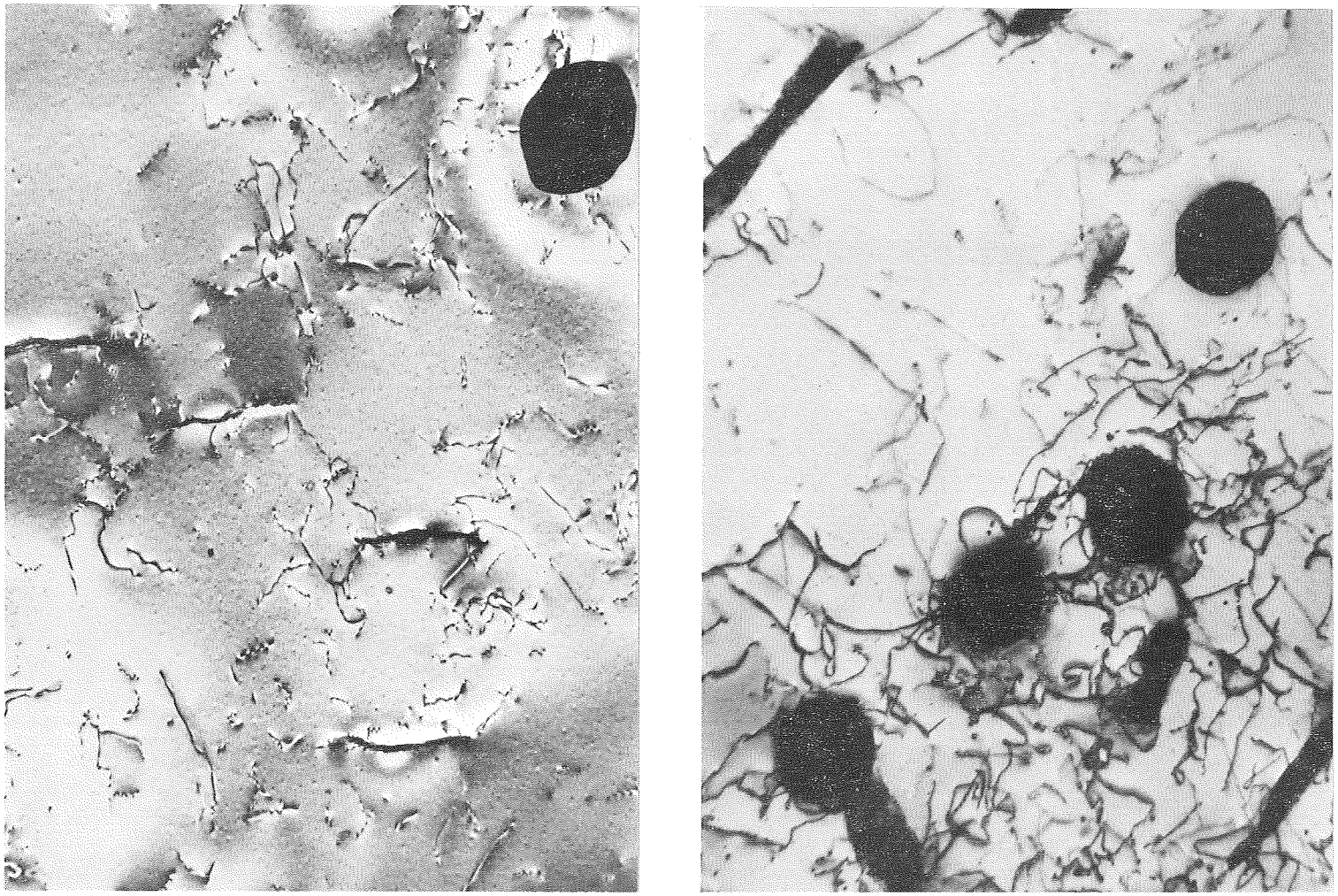

D90 ×30,000 D92 ×30,000

Cr-0.5 Zr
100 Hr-2100° F (1422° K)-Air

Figure 92 Dislocations and Precipitates in Cr-0.5Zr Alloy.

D81 ×30,000

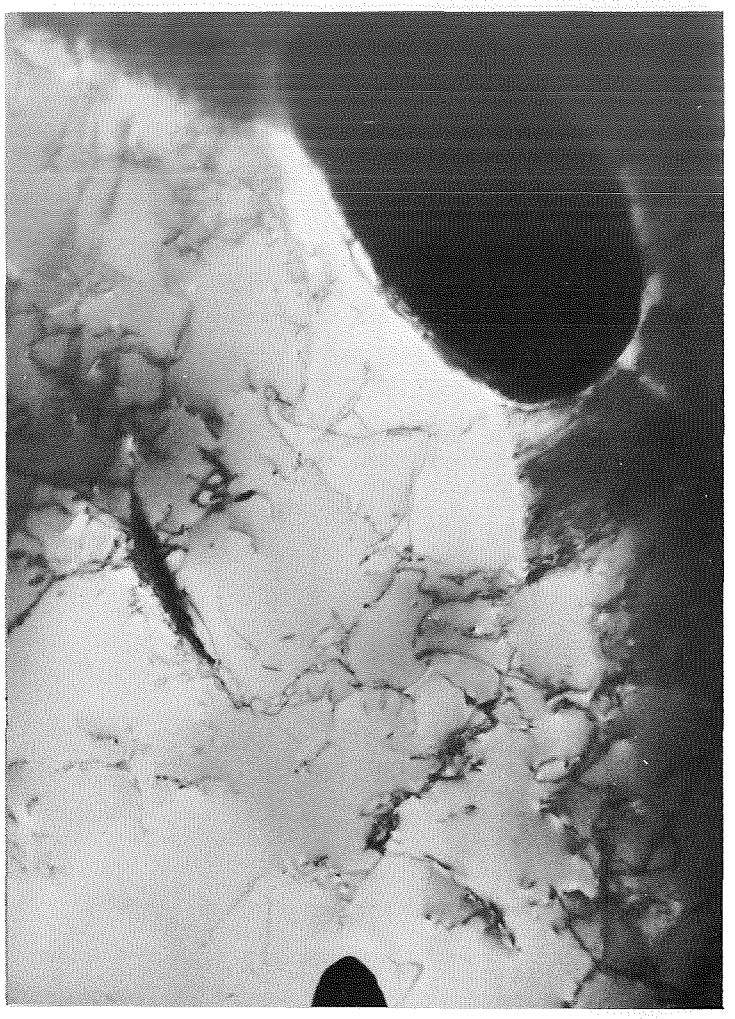

D82 ×30,000

Cr-0.5Y (9125-5)
100 Hr-2100° F (1422° K)-Air

Figure 93 Dislocations and Precipitates in Cr-0.5Y.

activate dislocations. This would explain why Cr_2N platelets are not effective whereas dispersion of oxides, intermetallics, or rare earths which do not precipitate from solid solution with regular or semicoherent interfaces are effective. Differences in thermal expansion also may be a very important factor. Chromium nitride is more closely matched to chromium in thermal expansion than Cr_2O_3. The higher mismatch between oxide particles and the matrix would generate higher stress around particles on cooling and could activate many more dislocation sources to accommodate slip. The beneficial effect of internal oxidation on Cr-Zr alloys is most likely the result of creating oxide dispersions that are more effective sources of dislocations.

It has been known for many years that small amounts of prestrain above the DBTT will generate sufficient mobile dislocations to promote ductile behavior at lower temperature. It is postulated that particles of rare earths, rare earth oxides or nitrides, and intermetallics introduced by alloying chromium with elements known to lower DBTT in the presence of nitrogen accomplish the same effect in localized regions around the particles. This model is consistent with all observed aspects of behavior and represents a reasonable assessment of the mechanism by which alloying controls the nitrogen embrittlement of chromium.

Section 7
CONCLUSIONS

(1) The most effective alloy additions for controlling the nitrogen embrittlement of chromium are the rare earths (yttrium, lanthanum, Mischmetal, and praseodymium) and thorium. Binary alloys containing 1 to 2 at.% of these elements have bend ductile-to-brittle transition temperatures of 300 to 400°F (422 to 478°K) before and 400 to 700°F (478 to 644°K) after exposure to air for 100 hr at 2100°F (1422°K). Yttrium is the most effective of these elements and limits the increase in bend DBTT to less than 100°F (56° C or K).

(2) The addition of 2 to 3 at.% zirconium (and probably hafnium) to chromium – rare earth or thorium alloys greatly increases the effectiveness of these elements in retarding nitrogen embrittlement. A Cr-2Zr-1Th alloy is ductile in bending at 400°F (478°K) (as-recrystallized), and the DBTT is not increased by exposure to air for 100 hr at 2100°F. The nitridation resistance of alloys having less than 1 at.% of the rare earths is improved significantly by the addition of zirconium.

(3) The nitridation resistance of chromium alloys having a low content of rare earths (0.1 to 0.5 at.%) also is improved by selective internal oxidation prior to air exposure. In addition, binary alloys of chromium with zirconium (hafnium) become more resistant to embrittlement in air when heated in pure oxygen for 50 to 100 hr at 2100°F prior to exposure. The effect is the result of an in-depth selective oxidation of rare earths or zirconium and does not depend on the formation of surface oxide scales.

(4) The distribution of rare earth and thorium phases in chromium alloys is modified and greatly improved by the addition of 2 to 3 at.% zirconium (hafnium). A random distribution of small particles with minimum banding and segregation is produced. The Cr_2Zr intermetallic phase nucleates a fine, uniform dispersion of the rare earths and thorium.

(5) Most of the elements that have significant solid solubility in chromium either have no influence or decrease the resistance of chromium to nitrogen embrittlement. Solid solution alloys tend to form thick surface cases and continuous intergranular networks of chromium nitride on air exposure.

(6) Manganese is the only solid solution addition that improves nitridation resistance and is second to the rare earths and thorium in ability to retard embrittlement. Binary alloys having 1 to 2 at.% manganese have a DBTT of 900 to 1000°F (755 to 811°K) after 100 hr at 2100°F in air. The effectiveness of manganese also can be improved by prior internal oxidation treatments.

(7) Solutes with a strong tendency to form oxides or nitrides (Cb, V, Ta, Ti) have a deleterious effect at levels above 0.5 at.%. These elements are selectively oxidized on air exposure and form large amounts of oxides in the grains or grain boundaries which embrittle the alloys.

(8) The effect of alloying on nitrogen embrittlement does not appear to be related to changes in the nitride case or nitride precipitates in the alloy. Alloying tends to reduce nitrogen pickup by formation of improved oxide scales and may decrease nitrogen solubility to some degree. However, even alloys that are not embrittled on air exposure have a thin nitride case on the surface and large amounts of nitride precipitate in the grains. Chromium nitride is precipitated in all cases, and structures are similar to those of unalloyed chromium.

(9) The mechanism by which alloy additions control embrittlement appears to be related to the ability of secondary phases or oxide particles to nucleate dislocation sources. It is postulated that brittleness results from dislocation pinning by small chromium nitride particles that precipitate on cooling. The secondary alloy phases or oxide particles in the matrix serve to nucleate and multiply the free dislocations which are needed for ductile behavior. The alloy additions that most effectively reduce nitrogen embrittlement are very sparingly soluble in solid chromium and introduce a large amount of dispersed secondary phases or oxide particles.

Section 8
RECOMMENDATIONS

The results of this program can readily be factored into current and future alloy development programs. Most of the promising chromium alloys designed within the past few years rely on carbide phase strengthening and use small additions of rare earths with zirconium and hafnium for enhanced resistance to oxidation and nitrogen embrittlement. The guidelines developed by this program indicate that these alloys can be optimized for strength and nitridation resistance by minor adjustments in composition and processing. Specifically, it is recommended that every effort be made to minimize the amount of residual solutes in chromium (after carbide precipitation) and to balance composition and processing for optimum amount, morphology, and distribution of secondary (nonstrengthening) phases. While carbide precipitates are needed to strengthen the alloy, oxide or intermetallic dispersions will be needed to provide ductility at low temperature. Further work is required, however, to establish the exact nature of the structures that must be produced and to delineate the optimum compositions and processes. Specific problems that should be addressed in order to provide this understanding are delineated in the following paragraphs.

- The exact nature of dispersions required to generate dislocations for low temperature ductility in the presence of nitrogen must be determined. Specifically, the ability of secondary phases to activate dislocation sources should be correlated with size, shape, composition, distribution, and concentration. Also to be determined are (1) whether oxides, nitrides, intermetallic compounds, and excess rare earth metals are equally effective and (2) if grain boundary particles are more effective than particles within the grain.

- Controlled processes for producing suitable dispersions in chromium need to be developed. Studies involving rare earths indicate that variations in annealing and deformation temperatures affect the ability of the rare earth particles to promote ductility. Once the parameters for an effective dislocation source in chromium are identified, methods by which the dispersions can be attained in a reproducible manner should be evaluated. Consideration should be given to internal odixation or nitridation of reactive elements, redistribution of insoluble phases by controlled thermal-mechanical processing, and addition of metal oxides by powder metallurgy techniques.

- Further studies from a fracture mechanics point of view should be made of brittle fracture in chromium alloys. It is necessary to clarify the relative contributions of crack initiation and crack propagation to the DBTT in bending and in tension. Since cracks are introduced by simple thermal cycling in the presence of a thin nitride case, it is important to define the conditions under which existing cracks will

propagate or will be stopped by plastic deformation. Behavior should be studied in the presence of secondary particles that have been added to control low-temperature ductility.

- Additional work on the pinning of dislocations by nitride precipitates on cooling is needed to assess the overall potential for maintaining ductile behavior at low temperature by means of secondary phases. The behavior on cyclic exposure in the presence of dispersions and stable substructures is of particular importance. The effectiveness of these to generate dislocations on repeated cycling and to continue to promote ductile behavior must be established. The tendency to form stable pinned substructures that could embrittle the alloy by a combination of creep straining and repeated thermal cycling should be investigated. Further work on the mechanisms by which nitride precipitates can embrittle chromium and secondary particles can promote ductility is needed.

Section 9
REFERENCES

1. T. E. Tietz and J. W. Wilson, Behavior and Properties of Refractory Metals, Stanford University Press, Stanford, Calif., 1965, pp. 40–101.

2. D. J. Maykuth and A. Gilbert, Chromium and Chromium Alloys, DMIC Report 234, 1 Oct 1966.

3. J. W. Clark and C. S. Wukusick, Development of High Temperature Chromium Alloys, NASA CR-5-4486, Semi-Annual Report No. 1, Oct 1965.

4. K. E. Solie and O. N. Carlson, "The Effect of Nitrogen on the Ductile-to-Brittle Transition of Chromium," Trans. AIME, Vol. 230, Apr 1964, pp. 480–485.

5. N. E. Ryan, "An Appraisal of Possible Scavenger Elements for Chromium and Chromium Alloys," J. Less Common Met., Vol. 6, 1964, pp. 21–35.

6. F. Hendersen, S. T. M. Johnstone, and H. L. Wain, "The Effect of Nitride Formers on the Ductile-Brittle Transition in Chromium," J. Inst. Met., Vol. 92, 1963–1964, pp. 111–117.

7. R. A. Perkins and J. L. Lytton, Effect of Processing Variables on the Structure and Properties of Refractory Metals, AFML-TR-65-234, Part I, Jul 1965.

8. R. A. Perkins, Effect of Processing Variables on the Structure and Properties of Refractory Metals, AFML-TR-65-234, Part II, May 1967.

9. R. M. Bonesteel, D. J. Rowcliffe, and T. E. Tietz, "Mechanical Properties and Structure of Internally Oxidized Nb-1Zr Alloy," Proceedings of the Conference on Strengthening of Metal and Alloys, Supplement to Trans. Japan Inst. Met., Vol. 9, 1968, pp. 597–602.

10. E. P. Abrahamson and N. J. Grant, "Brittle to Ductile Transition Temperatures of Binary Chromium-Base Alloys," ASM Trans., Vol. 50, 1958, pp. 705–721.

11. A. H. Sully, Metallurgy of the Rarer Metals. 1. Chromium, Academic Press, London, 1954.

12. J. L. Lytton and T. E. Tietz, "The Effect of Lüders Straining on the Tensile Flow Behavior of Arc Cast Mo Sheet," Trans. AIME, Vol. 230, 1964, p. 241.

13. R. W. Fountain and J. Chipman, "Solubility and Precipitation of Vanadium Nitride in Alpha and Gamma Iron," Trans. AIME, Vol. 212, 1958, pp. 737–748.

14. W. C. Coons, "Sample Preparation for Ceramic Microstructural Analysis," Ceramic Microstructures, eds., Fulrath and Pask, John Wiley and Sons, New York, 1968, Ch. 6.

15. U. R. Evans, An Introduction to Metallic Corrosion, E. Arnold Co., London, 1947.

16. M. Hansen, Construction of Binary Alloys, McGraw-Hill Book Co., New York, 1958.

17. R. P. Elliott, Constitution of Binary Alloys, First Supplement, McGraw-Hill Book Co., New York, 1965.

18. F. A. Shunk, Constitution of Binary Alloys, Second Supplement, McGraw-Hill Book Co., New York, 1969.

19. J. W. Clark, Development of High-Temperature Chromium Alloys, NASA CR-72731, Nov 1970.

20. J. W. Clark, Development of Cr-Li-Y_2O_3 Coatings for Chromium-Base Alloys, NASA-CR-72763, Feb 1971.

21. S. Yoshidu, Y. Ohbu, and N. Nagata, "Effect of Prestraining on the Ductility of Pure Chromium," Trans. Japan Inst. Met., Vol. 1, 1960, p. 49.

22. A. A. Griffith, Phil. Trans. Roy. Soc. London, Vol. A221, 1920.

23. J. J. Gillman, J. Appl. Phys., Vol. 31, 1960.

24. J. R. Low, Jr., "The Fracture of Metals," Prog. Mat. Sci., Vol. 12, No. 1, 1963.

25. A. U. Seybolt and R. A. Oriani, Trans. AIME, Vol. 206, 1956, pp. 556–562.

26. M. J. Klein and A. H. Claurer, "Nitrogen Induced Internal Friction in Chromium," Trans. AIME, Vol. 223, 1965, pp. 1771–1776.

27. A. Gilbert and M. Klein, "The Effect of Cooling Rate on the Ductile to Brittle Bend Transition of Chromium Wire," Letters to the Editor, Acta Met., Vol. 14, 1966, p. 541.

28. J. L. Ratliff, D. J. Maykuth, H. R. Ogden, and R. I. Jaffee, "Tungsten Sheet Alloys With Improved Low Temperature Ductility," Trans. AIME, Vol. 230, 1964, p. 490

29. K. Kayano and S. Koda, "The Role of Dislocation Nucleaction Around Precipitates in the Mechanical Properties of a Fe-C Alloy," Proc. Internat. Conf. on Strength of Metals and Alloys, Tokyo, 1967.

30. M. F. Ashby, "Deformation of Internally Oxidized Copper Base Alloys," eds., Thomas and Washburn, Electron Microscopy and Strength of Crystals, Interscience Publishers, New York, 1963.

Appendix A

EXTRUSION AND ROLLING DATA

Alloy Addition	Nominal Composition		Sample No.	Program Task	Extrusion Data											Rolling Data							
	At. %	Wt. %			Canning Material[a]	Preheat Temp. °F	Preheat Temp. °K	Container Temp. °F	Container Temp. °K	Maximum Load Tons	Maximum Load Kg	Cooling Medium	Sheet Bar Condition	Annealing Temp. °F	Annealing Temp. °K	Canning Material	Preheat Temp. °F	Preheat Temp. °K	Roll Temp. °F	Roll Temp. °K	Sheet Condition	Annealing Temp. °F	Annealing Temp. °K
Unalloyed	100 Cr	100 Cr	98-1	I	Fe	2200	1478	570	572	150	136,200	Air	Rough Surface	2400	1589	Bare	1800	1255	800	700	Small cracks	2400	1589
W	1.0	3.4	957		Fe+Mo					105	95,400	Al_2O_3	Rough Surface				2000	1366			Edge cracks, end splits	2300	1533
	2.0	6.7	958							115	104,400	Kaowool	Good Quality								Good quality	2400	1589
	4.0	12.8	959							146	132,700	Al_2O_3					2000	1366			Good quality	2400	1589
Mo	1.0	1.8	960							108	98,200						2050	1394			Edge cracks, end splits	2300	1533
	2.0	3.6	961							118	107,200						2100	1422			Badly cracked, no samples		
	4.0	7.0	962							140	127,100					Fe	2400	1589			Good quality	2300	1533
Re	1.0	3.5	963							108	98,200					Bare	2200	1478			Few surface cracks	2300	1533
	2.0	6.8	964							112	101,700						2200	1478			Edge cracks, end splits	2300	1533
	4.0	13.0	965		Fe+Mo	2200	1478	570	572	122	111,700	Al_2O_3	Good Quality			Fe	2000	1366			Good quality	2400	1589
Ru	1.0	1.9	944		Mo	2400	1589	570	572	250	22,700	Air	Cracked – Mo can										
	1.0	1.9	9101		Fe+Mo	2200	1478	570	572	88	79,800	Al_2O_3	Good Quality			Fe					Good quality		
	2.0	3.8	945					75	296	145	131,700					Bare					Edge cracks		
	4.0	7.5	946					570	572	125	113,500	Al_2O_3									Good quality		
Mn	1.0	1.05	947							100	90,700	Kaowool										2400	1589
	2.0	2.1	948	I						95	86,300	Al_2O_3							800	700		2300	1533
	3.0	3.1	9128	II						85	77,200	Kaowool				Fe			75	296	Good quality	2000	1367
	4.0	4.2	949	I	Fe+Mo					89	80,800	Al_2O_3	Good Quality			Bare			800	700	Edge cracks, end split	2300	1533
Fe	1.0	1.07	914		Fe					130	118,000	Kaowool	Rough Surface								Rough surface	2400	1589
	2.0	2.14	915							134	122,600												
	4.0	4.3	916		Fe					128	116,200	Kaowool	Rough Surface				2000	1366			Rough surface		
Co	1.0	1.24	919		Fe+Mo					130	118,000	Al_2O_3	Good Quality				2150	1450			Edge cracks		
	2.0	2.26	920		Fe+Mo					122	110,900	Al_2O_3	Good Quality				2100	1432			Badly cracked, no samples		
	4.0	4.5	921		Mo	2200	1478			250	227,000	Kaowool	Cracked – Mo can										
	4.0	4.5	9102		Fe+Mo	2400	1589			110	100,000	Al_2O_3	Good Quality			Fe	2000	1366	75	297	Good quality		
Ti	0.5	0.46	925		Fe+Mo	2200	1478			123	111,700		Good Quality			Bare			800	700			
	2.0	1.84	937		Mo-Fe	2200	1478			131	119,000		Cracked – Mo can										
	2.0	1.84	992		Fe+Mo	2400	1589			123	111,700		Good Quality			Fe							
Zr	0.5	0.9	940		Mo	2400	1589			141	128,000		Cracked – Mo can										
	0.5	0.9	999	I	Fe+Mo	2200	1478			84	76,200		Good Quality										
	1.0	1.7	9129	II	Fe+Mo	2200	1478			95	86,300		Good Quality										
	2.0	3.5	939	I	Mo	2400	1589			200	181,400		Cracked – Mo can										
	2.0	3.5	9100	I	Fe+Mo	2200	1478			95	86,300		Good Quality										
	3.0	5.1	9134	II	Fe+Mo					96	87,200		Good Quality						75	296			
	4.0	6.8	9148	III	Fe+Mo					97	88,100	Al_2O_3	Good Quality						800	700			
Hf	0.5	1.7	917	I	Fe					124	112,700	Kaowool	Rough Surface			Bare							
	2.0	6.55	918		Fe+Mo			570	572	172	156,200	Al_2O_3	Good Quality			Bare							
V	0.5	0.5	938		Fe-Mo			75	296	110	100,000	Kaowool	Cracked – Thick Mo Liner										
	0.5	0.5	996		Fe+Mo			570	572	77	69,900	Al_2O_3	Good Quality								Edge cracks, end splits		
	2.0	2.0	941		Fe-Mo			75	296	149	135,300		Cracked – Thick Mo Liner				2000	1366				2400	1589
	2.0	2.0	997	I	Fe+Mo	2200	1478	570	572	85	77,200	Al_2O_3	Good Quality	2400	1589	Bare	2100	1422	800	700	Edge and surface cracks	2300	1533

Appendix A (Cont.)

Alloy Addition	Nominal Composition		Sample No.	Program Task	Extrusion Data											Rolling Data							
	At. %	Wt. %			Canning Material[a]	Preheat Temp. °F	Preheat Temp. °K	Container Temp. °F	Container Temp. °K	Maximum Load Tons	Maximum Load Kg	Cooling Medium	Sheet Bar Condition	Annealing Temp. °F	Annealing Temp. °K	Canning Material	Preheat Temp. °F	Preheat Temp. °K	Roll Temp. °F	Roll Temp. °K	Sheet Condition	Annealing Temp. °F	Annealing Temp. °K
Cb	0.25	0.44	9131	II	Fe+Mo	2200	1478	570	572	97	88,100	Al_2O_3	Good Quality	2400	1589	Fe	2000	1366	75	296	Good quality	2400	1589
	0.5	0.89	912	I	Fe	↓	↓	↓	↓	132	120,000	Kaowool	Rough Surface	↓	↓	Bare	↓	↓	800	700	Edge cracks	↓	↓
	1.0	1.8	9130	II	Fe+Mo	↓	↓	↓	↓	124	112,600	Al_2O_3	Good Quality	↓	↓	Fe	↓	↓	75	296	Good quality	↓	↓
	2.0	3.5	913	I	Fe	2200	1478	75	296	250	227,000	Air	Cracked – Rapid Cool	↓	↓	↓	↓	↓	↓	↓	↓	↓	↓
	2.0	3.5	993	↓	Fe+Mo	2400	1589	570	572	159	144,400	Al_2O_3	Cracked – Slow Ram Speed	↓	↓	↓	↓	↓	↓	↓	↓	↓	↓
Ta	0.5	1.7	942	↓	Fe-Mo	2200	1478	75	296	142	129,000	↓	Cracked – Mo Liner	↓	↓	↓	↓	↓	↓	↓	↓	↓	↓
	0.5	1.7	994	↓	Fe+Mo	2200	1478	570	572	105	95,400	↓	Good Quality	↓	↓	↓	↓	↓	800	700	↓	↓	↓
	2.0	6.6	943	↓	Not Extruded, Ingot Contaminated With Cu																		
	2.0	6.6	995	I	Fe+Mo	2200	1478	570	572	157	142,500	↓	Cracked – Brittle Alloy	2400	1589	Fe	2000	1366	↓	↓	↓	2400	1589
Y	0.1	0.2	9123	II	↓	2000	1367	↓	↓	70	63,600	Al_2O_3	Good Quality	1800	1255	Bare	1900	1311	↓	↓	↓	1800	1255
	0.25	0.42	9124	↓	↓	2000	1367	↓	↓	90	81,700	Kaowool	↓	1800	1255	↓	1900	1311	↓	↓	↓	1800	1255
	0.5	0.85	9125	II	↓	2000	1367	↓	↓	87	79,000	Kaowool	↓	1800	1255	↓	1900	1311	↓	↓	↓	1800	1255
	0.5	0.85	950	I	↓	2200	1478	↓	↓	75	68,100	Kaowool	↓	2400	1589	↓	2000	1366	↓	↓	↓	2100	1422
	1.0	1.7	951	I	↓	2200	1478	↓	↓	100	90,700	Al_2O_3	↓	2400	1589	↓	2000	1366	↓	↓	↓	2100	1422
	2.0	3.4	952	I	↓	2200	1478	↓	↓	95	86,200	↓	↓	2400	1589	↓	2000	1366	800	700	↓	2100	1422
La	0.1	0.3	9126	II	↓	2000	1367	↓	↓	95	86,200	↓	↓	1800	1255	↓	1900	1311	75	296	↓	1800	1255
	0.25	0.7	9127	II	↓	↓	↓	↓	↓	95	86,200	↓	↓	1800	1255	↓	1900	1311	75	296	↓	2000	1367
	0.5	1.3	967	I	↓	↓	↓	570	572	88	79,800	↓	↓	2000	1366	↓	2000	1366	75	296	↓	2000	1367
	1.0	2.6	968	↓	↓	↓	↓	75	296	190	172,400	↓	↓	2000	1366	↓	↓	↓	800	700	Good quality	2000	1367
	2.0	5.2	969	↓	↓	2000	1367	570	572	97	88,100	↓	Small Tears	2000	1366	↓	↓	↓	75	296	Edge cracks	2000	1367
Pr	0.5	1.3	953	↓	↓	2200	1478	↓	↓	95	86,200	↓	Good Quality	2400	1589	↓	↓	↓	800	700	Good quality	2400	1589
	1.0	2.7	954	↓	↓	2200	1478	↓	↓	80	72,600	Al_2O_3	↓	2400	1589	↓	↓	↓	↓	↓	Edge cracks	2400	1589
	2.0	5.2	955	↓	↓	2200	1478	↓	↓	88	79,800	Kaowool	↓	2400	1589	↓	↓	↓	↓	↓	Badly cracked, no samples		
MM[b]	0.5	1.3	970	↓	↓	2000	1367	↓	↓	109	99,000	Al_2O_3	↓	2000	1285	↓	↓	↓	↓	↓	Good quality	2000	1367
	1.0	2.7	971	↓	↓	↓	↓	570	572	100	90,700	↓	↓	↓	↓	↓	↓	↓	↓	↓	↓	2000	1367
	2.0	5.2	972	↓	↓	↓	↓	75	296	135	122,500	↓	↓	↓	↓	↓	↓	↓	↓	↓	↓	2000	1367
Th	0.5	2.2	980	↓	↓	↓	↓	570	572	90	81,700	↓	↓	↓	↓	↓	↓	↓	↓	↓	↓	1800	1255
	1.0	4.3	981	↓	↓	↓	↓	↓	↓	81	73,500	↓	↓	↓	↓	↓	↓	↓	↓	↓	↓	1800	1255
	2.0	8.3	982	I	↓	2000	1367	↓	↓	78	70,800	↓	↓	2000	1285	Bare	↓	↓	800	700	↓	1800	1255
Zr/Y	3.0/0.1	5.1/0.2	9141	III	↓	2200	1478	↓	↓	97	88,100	↓	↓	2400	1589	Fe	↓	↓	75	296	Good quality	2400	1589
Zr/La	2.0/0.25	3.4/0.65	9145	↓	↓	↓	↓	↓	↓	95	86,200	↓	↓	↓	↓	↓	↓	↓	↓	↓	Surface cracks	2400	1589
Zr/Th	2.0/1.0	3.3/4.2	9142	↓	↓	↓	↓	↓	↓	95	86,200	↓	↓	↓	↓	↓	↓	↓	↓	↓	Good quality	1800	1255
Y/Th	0.5/1.0	0.8/4.3	9143	III	Fe+Mo	2200	1478	570	572	75	68,200	Al_2O_3	Good Quality	2400	1589	Fe	2000	1366	75	296	Good quality	1800	1255

(a) Fe-Mo – Fe can, 0.060–0.075-in. (0.152–0.190 cm) Mo liner.
Mo-Fe – Mo can, 0.060–0.075-in. (0.152–0.190 cm) Fe liner.
Fe+Mo – Fe can, 0.005-in. (0.013 cm) Mo liner.
Fe – Fe can, no liner.
Mo – Mo can, no liner.

(b) Misch metal.

Appendix B

NITROGEN REACTION RATE DATA (2100°F-1422°K)
(1 cc N_2 = 1.125 mg N_2)

Cr (98)

Hours	cc N_2 (1)
0.62	6
1.75	26
2.13	54
3.07	71
5.12	91
6.13	9
7.28	107
10.10	131
13.40	158
22.95	233
20.35	266
37.40	293
4.680	317
54.80	322
70.75	345
100.00	348

12.42 cm^2 (2)
3.2189 gm (3)

Cr-1W (951)

Hours	cc N_2
4.65	74
16.36	131
20.68	192
28.80	209
35.40	237
45.60	265
53.20	275
71.75	324
97.75	329

12.36 cm^2
3.1467 gm

Cr-20W

Hours	cc N_2
2.60	66
7.50	109
11.13	131
14.48	151
22.78	196
31.80	218
37.55	240
46.83	276
55.57	288
48.82	336

12.61 cm^2
3.3952 gm

Cr-4W

Hours	cc N_2
2.52	58
7.45	101
11.03	123
14.40	141
22.70	186
31.70	210
37.47	228
46.73	261
55.48	278
98.72	336

13.13 cm^2
3.7397 gm

Cr-1.0Mo

Hours	cc N_2
0.28	26
4.78	104
11.53	163
20.85	225
29.18	242
35.50	270
45.80	302
53.40	312
72.30	354
97.75	378

13.13 cm^2
3.8341 gm

Cr-4Mo

Hours	cc N_2
2.65	64
7.55	110
11.20	136
14.53	155
22.83	202
31.87	228
37.58	250
46.90	289
55.62	301
98.87	339

12.72 cm^2
3.3742 gm

Cr-1.0Re

Hours	cc N_2
1.83	30
4.08	48
8.42	74
17.43	111
26.87	117
27.93	133
31.77	145
41.02	169
44.77	176
48.15	179
99.35	223

7.77 cm^2
2.0317 gm

Cr-2Re

Hours	cc N_2
1.78	49
4.23	71
8.40	107
16.80	153
20.20	169
27.88	193
31.20	211
40.20	245
44.70	253
48.10	261
99.33	331

12.26 cm^2
3.2515 gm

Cr-4.0Re

Hours	cc N_2
0.98	28
1.38	36
4.00	67
10.80	115
20.98	167
29.02	194
35.17	215
45.88	248
56.17	267
72.87	306
100.00	317

12.77 cm^2
3.5050 gm

Cr-1.0Ru

Hours	cc N_2
1.25	47
2.0	70
6.3	104
9.6	136
18.4	193
21.9	211
27.2	226
40.5	277
49.4	292
100.00	328

12.69 cm^2
3.2133 gm

Cr-2.0Ru

Hours	cc N_2
0.38	30
3.43	78
9.73	130
15.0	169
23.45	222
27.75	234
34.1	248
38.2	269
47.4	303
57.9	308
80.3	320

13.01 cm^2
3.6318 gm

Cr-4.0Ru

Hours	cc N_2
0.33	30
3.7	93
9.73	140
14.98	185
23.42	248
27.65	265
34.05	278
43.30	336
57.90	333
80.30	339

13.01 cm^2
3.8103 gm

Cr-1.0Mn

Hours	cc N_2
0.23	14
4.77	92
11.50	152
20.80	214
29.10	231
35.50	262
45.80	293
53.40	301
72.20	356
97.80	360

13.23 cm^2
3.3917 gm

Cr-2.0Mn

Hours	cc N_2
0.22	7
4.70	75
11.43	129
20.75	188
29.00	199
35.40	227
45.70	258
53.30	270
72.00	313
97.60	317

12.32 cm^2
3.0608 gm

Cr-4.0Mn

Hours	cc N_2
1.68	56
4.08	83
8.32	127
16.72	185
20.67	204
27.73	232
31.65	249
40.83	284
44.53	297
48.00	307
99.22	365

12.96 cm^2
3.2975 gm

Cr-1.0Fe

Hours	cc N_2
0.67	40
1.32	69
1.77	78
3.08	90
5.06	111
6.03	119
7.17	128
10.00	153
13.27	181
22.80	244
37.20	294
46.60	326
54.6	336
70.6	373
100.00	373

12.48 cm^2

Cr-2.0Fe

Hours	cc N_2
1.07	73
1.83	91
3.15	112
5.15	138
7.26	156
13.33	214
22.90	276
30.30	309
46.80	361
54.80	356
70.70	365
100.00	352

12.30 cm^2

Cr-4.0Fe

Hours	cc N_2
0.75	28
1.32	61
3.4	111
6.1	153
7.2	169
10.0	207
13.2	244
22.8	311
30.2	326
46.3	340
54.4	328
70.3	335
100.00	317

12.50 cm^2

Cr-1Co

Hours	cc N_2
0.52	23
3.42	77
9.78	136
15.0	176
23.55	233
27.82	247
34.20	262
38.25	281
47.50	333
58.00	338
80.50	344

12.44 cm^2
3.073 gm

Cr-0.5Ti

Hours	cc N_2
0.72	50
1.12	60
3.65	109
6.91	147
9.84	171
14.25	204
23.2	257
30.9	290
37.7	317
47.2	399
62.1	363
71.75	377
81.90	382
96.50	397

12.47 cm^2
3.3490 gm

Cr-2.0Ti

Hours	cc N_2
0.5	40
1.2	54
2.6	88
6.3	128
7.9	142
10.4	160
14.8	192
23.9	260
32.0	274
37.4	290
56.6	328
96.5	348

1.80 cm^2
2.660 gm

Cr-0.5Zr

Hours	cc N_2
1.25	54
2.0	76
6.3	106
9.6	136
18.4	188
21.9	203
27.2	218
40.5	266
49.4	284
100.00	340

12.67 cm^2
3.1375 gm

Cr-2.0Zr

Hours	cc N_2
1.0	42
3.1	70
5.0	87
8.0	109
11.8	141
20.5	199
32.6	210
49.0	263
56.3	284
68.9	335
95.3	353

11.97 cm^2
3.0136 gm

Cr-0.5Hf

Hours	cc N_2
0.58	32
3.72	63
7.00	82
10.10	96
14.25	103
23.33	137
37.90	175
47.25	183
62.25	204
71.80	222
82.10	234
96.60	243

8.25 cm^2
2.1461 gm

Cr-2.0Hf

Hours	cc N_2
0.53	32
3.69	106
6.92	146
10.0	168
14.25	199
23.25	250
37.75	309
47.75	332
62.20	355
71.80	366
81.90	373
96.50	389

12.63 cm^2
3.935 gm

Cr-0.5V

Hours	cc N_2
2.47	62
7.38	110
10.97	130
14.35	152
22.65	198
31.63	223
37.40	250
44.67	283
55.43	302
98.65	355

12.58 cm^2
3.2544 gm

Cr-2.0V

Hours	cc N_2
1.73	45
4.15	69
8.35	109
16.75	161
20.73	175
28.80	201
31.68	219
40.90	253
44.62	267
48.07	274
99.27	334

12.18 cm^2
3.0983 gm

Cr-0.5Cb

Hours	cc N_2
0.36	9
3.83	61
7.14	79
10.02	93
14.39	113
23.45	145
31.05	165
47.40	195
62.40	216
70.30	226
82.25	232
96.18	248

8.18 cm^2
2.0845 gm

Cb-0.5Ta

Hours	cc N_2
1.02	38
4.07	82
10.80	139
21.03	202
29.13	236
35.20	257
46.0	292
56.25	313
72.95	354
100.00	353

12.49 cm^2
3.1478 gm

Cr-0.5Y

Hours	cc N_2
0.7	24
2.18	59
4.63	91
7.18	114
11.80	145
14.50	168
23.80	213
31.90	223
37.25	243
49.50	279
71.70	325
95.10	333

12.24 cm^2
3.0528 gm

Cr-1.0Y

Hours	cc N_2
0.65	19
2.13	53
4.60	85
7.10	110
11.72	140
14.42	159
23.75	206
31.80	229
37.20	250
49.40	295
71.70	343
95.0	356

13.08 cm^2
3.2966 gm

Cr-2.0Y

Hours	cc N_2
1.18	29
1.90	53
4.53	83
7.07	107
11.65	133
14.39	146
23.75	184
31.75	206
37.20	222
49.40	256
71.60	298
95.00	328

12.75 cm^2
3.1712 gm

Cr-0.5La

Hours	cc N_2
1.0	10
3.1	67
5.0	84
8.0	106
11.8	137
20.5	195
27.6	204
32.6	216
34.5	223
49.0	267
56.3	276
60.4	293
68.9	327
95.3	344

12.51 cm^2
3.1215 gm

Cr-1.0La

Hours	cc N_2
1.0	36
4.02	80
10.82	128
20.98	184
29.05	212
35.18	238
45.92	271
56.17	290
72.87	330
100.00	343

12.39 cm^2
3.0728 gm

Cr-1.0La(a)

Hours	cc N_2
5.2	80
19.2	174
23.0	192
27.7	210
49.6	275
72.6	323

12.47 cm^2
3.1413 gm

Cr-2.0La

Hours	cc N_2
1.0	42
3.1	66
5.0	79
8.0	102
11.8	132
20.5	189
32.6	199
34.5	209
49.0	249
60.4	279
68.9	313
95.3	346

12.55 cm^2
3.1750 gm

Cr-0.5Pr

Hours	cc N_2
0.45	26
3.4	72
9.75	120
14.98	158
23.50	206
27.80	216
34.18	228
38.22	247
47.4	280
57.9	287
80.3	318

11.87 cm^2
2.9736 gm

Cr-1.0Pr

Hours	cc N_2
1.23	40
1.92	59
4.53	98
7.11	126
10.7	158
14.41	174
23.75	222
31.75	247
37.2	265
49.5	297
71.6	313
95.0	319

12.43 cm^2
3.0796 gm

Cr-0.5Mn

Hours	cc N_2
1.25	49
2.0	73
6.3	117
9.6	138
18.4	193
21.9	206
27.2	218
40.5	266
49.4	270
100.00	320

12.54 cm^2
3.1360 gm

Cr-1.0Mn

Hours	cc N_2
1.25	36
2.0	62
6.3	96
9.6	125
18.4	180
21.9	194
27.2	208
40.5	232
49.4	248
100.00	307

12.83 cm^2
3.2482 gm

Cr-2Mn

Hours	cc N_2
1.0	26
4.05	70
10.85	122
21.02	182
29.10	213
35.20	236
45.97	271
56.22	291
72.92	331
100.00	333

12.49 cm^2
3.1298 gm

Cr-0.5Th

Hours	cc N_2
1.0	42
3.1	66
5.0	82
8.0	104
11.8	136
20.5	192
27.6	192
32.6	202
34.5	213
49.0	254
56.3	263
60.4	291
69.9	317
95.3	341

12.08 cm^2
3.0287 gm

Cr-1.0Th

Hours	cc N_2
0.5	60
1.0	66
2.6	92
6.3	127
7.9	139
10.4	153
14.8	181
23.9	231
32.0	252
37.4	270
56.6	322
96.5	388

12.47 cm^2
3.2677 gm

Cr-2Th

Hours	cc N_2
0.5	8
1.0	25
2.6	53
6.3	89
7.9	103
10.4	118
14.8	144
23.9	196
32.0	216
37.4	232
56.6	282
96.5	354

12.49 cm^2
3.2922 gm

(1) Total nitrogen consumed in cc measured at ambient temperature and pressure.
(2) Original total surface area, sum of 2-3 samples.
(3) Original total sample weight, sum of 2-3 samples.
(a) Preoxidized in O_2 at 2100°F(1422°K) for 50 hr.

Appendix C

OXYGEN REACTION RATE DATA (2100°F-1422°K)

Cr-(98)		Cr-0.25Y		Cr-0.1La		Cr-0.25Cb		Cr-1.0Zr		Cr-3.0Mn	
Hours	cc O_2[a]	Hours	cc O_2	Hours	cc O_2	Hours	cc O_2	Hours	cc O_2	Hours	cc O_2
2.2	15	0.4	6	0.4	5	2.2	8	2.7	8	2.7	26
6.4	21	4.0	12	4.0	6	6.4	15	7.3	12	7.3	47
11.8	23	9.7	15	9.7	8	11.8	21	14.8	18	14.8	70
21.9	36	19.9	16	19.9	10	21.9	37	24	22	24	86
29.3	40	28.3	13	28.3	10	29.3	38	33.2	14	33.2	92
46.4	57	44.0	16	44.0	10	46.4	60	38.5	21	38.5	104
60.2	64	47.8	10	47.8	12	60.2	76	50.5	22	50.5	116
69.9	72	67.9	16	67.9	12	69.6	85	61.4	24	61.4	130
81.3	73	82.6	19	82.6	11	81.3	84	74.5	25	74.5	139
93.9	82	98.3	17	98.3	13	93.9	93	85.9	27	85.9	148
101.4	84					101.4	90	100.2	27	100.2	157
12.36 cm^2[b]		11.58 cm^2		11.68 cm^2		12.18 cm^2		12.53 cm^2		12.59 cm^2	

Cr-0.1Y		Cr-0.5Y		Cr-0.25La		Cr-1.0Cb		Cr-3.0Zr	
Hours	cc O_2	Hours	cc O_2	Hours	cc O_2	Hours	cc O_2	Hours	cc O_2
0.4	8	0.4	14	2.7	12	2.7	13	2.2	19
4.0	12	4.0	12	7.3	14	7.3	16	6.4	33
9.7	16	9.7	16	14.8	16	14.8	41	11.8	43
19.9	19	19.9	19	24	18	24	56	21.9	64
28.3	17	28.3	14	33.2	10	33.2	71	29.3	72
47.8	18	44.0	17	38.5	17	38.5	88	46.4	97
67.9	24	47.8	14	50.5	17	50.5	121	60.2	109
82.6	22	67.9	17	61.4	17	61.4	147	69.9	122
98.3	21	82.6	14	74.5	21	74.5	181	81.3	124
		98.3	14	85.9	20	85.9	212	93.9	136
				100.2	20	100.2	250	101.4	141
11.98 cm^2		12.09 cm^2		12.63 cm^2		12.78 cm^2		12.36 cm^2	

(a) Cumulative volume consumed at ambient temperature and pressure. 1 cc = 1.31 mg.

(b) Initial total surface area; sum of three samples.

Appendix D

AIR REACTION RATE DATA

Cr-0.1Y				Cr-0.25Y				Cr-0.5Y			
2100°F (1422°K)		2400°F (1589°K)		2100°F (1422°K)		2400°F (1589°K)		2100°F (1422°K)		2400°F (1589°K)	
Hours	Mg	Hours	Mg(a)	Hours	Mg	Hours	Mg	Hours	Mg	Hours	Mg
No Data		0.5	33	0.5	3.5	0.5	49.5	0.5	1.0	0.5	11.5
		1	41	1	7.0	1	63.5	1	1.5	1	17.5
		2	50	2	11.5	2	82.5	2	2.0	2	25
		4	60.5	4	15.5	4	106.5	4	3.0	4	33.5
		5	63	5	18.5	5	114.5	5	3.5	5	36.5
		6	64	6	20.0	6	121.5	6	4.0	6	38.5
		7	65	7	21.0	7	127.5	7	4.5	7	40.5
		8	66	8	22.0	8	133.5	8	5.0	8	42
		9	67.5	9	22.5	9	138.5	9	5.0	9	43.5
		10	68.5	10	23	10	142.5	10	5.5	10	108.5
		11	74	15	24.5	15	161	15	6.0	15	125
		11.5	92	20	25	20	175	20	6.0	20	131.5
		12	106	25	28	21	177.5	25	6.5	25	137.5
		13	107.5	30	29.5	21.5	178	30	7.5		
		14	107	35	31	22	255	50	8.0		
		15	107	40	32.5	23	285	55	8.5		
		20	106.5	45	33.5	24	298.5	60	Pen Failed To Record		
		25	106.5	50	36	25	303.5	↓			
				55	337			95			
				60	38.5			100	9.0		
				65	39.5						
				70	43						
				75	44.5						
				80	46.5						
				85	47.5						
				90	47.5						
				95	48.5						
				100	49.5						
		11.73 cm^2 (b)		13.96 cm^2		13.45 cm^2		13.96 cm^2		15.30 cm^2	

(a) Cumulative weight gain.
(b) Initial total surface area.

Appendix D (Cont.)

Cr-0.1La				Cr-0.25La				Cr-0.25Cb			
2100°F (1422°K)		2400°F (1589°K)		2100°F (1422°K)		2400°F (1589°K)		2100°F (1422°K)		2400°F (1589°K)	
Hours	Mg	Hours	Mg	Hours	Mg	Hours	Mg	Hours	Mg	Hours	Mg
0.5	1.0	0.5	40	2	0.5	0.5	19.5	0.5	3	0.5	169
1	2.0	1	77	3	1.0	1	28.0	1	5	1	234
2	3.0	2	107.5	5	1.5	2	40.5	2	8.5	2	316
3	4.0	3	113	7	2.0	3	48.5	3	11	3	376
4	5.0	4	116.5	20	2.25	4	54.0	4	13	4	425
5	6.5	5	121.5	30	2.75	5	59.0	5	15	5	466
10	10.0	6	151.5	40	3.0	6	63.0	6	17	6	500
15	13.5	7	204.5	60	3.25	7	67.0	7	18.5	7	527
20	15.0	8	212	80	3.50	8	70.0	8	20	8	546
25	19.0	9	213.5	100	3.50	9	72.5	9	21	9	560
30	22.0	10	215			10	74.5	10	21.5	10	571
35	23.0	15	220			15	83.5	15	27	15	609
40	25.0	20	217			20	90.5	20	30.5	20	633
45	26.5	25	213.5			25	94.5	25	35	21.6	633
50	28.5							30	37.5		
55	31.0							35	40.5		
60	32.5							40	43		
65	34.5							45	45		
70	36.5							50	47		
75	38.5							55	49		
80	42.0							60	51		
85	43.0							65	52.5		
90	45.0							70	54		
95	48.0							75	55		
100	48.5							80	57.5		
								85	59		
								90	60		
								95	61		
								100	62		
14.25 cm^2		14.77 cm^2				10.96 cm^2		10.50 cm^2		12.38 cm^2	

Appendix D (Cont.)

Cr-10Cb				Cr-1.0Zr				Cr-3Zr			
2100°F (1422°K)		2400°F (1589°K)		2100°F (1422°K)		2400°K (1589°K)		2100°F (1422°K)		2400°F (1589°K)	
Hours	Mg	Hours	Mg	Hours	Mg	Hours	Mg	Hours	Mg	Hours	Mg
0.5	2	0.5	72.5	0.5	0.5	0.5	48	0.5	13	0.5	74
1	3.5	1	85	1	1	1	74	1	17.5	1	84.5
2	5	2	100.5	2	2	2	106	2	24	2	94.5
3	6	3	111.5	3	3	3	132	3	27.5	3	100.5
4	7	4	120.5	4	4	4	154	4	30.5	4	105.5
5	8	5	129	5	5	5	174	5	33.5	5	108.5
6	9	6	137.5	6	5.5	6	193	6	35.5	6	111.5
7	10	7	146.5	7	6.0	7	211	7	37.5	7	114
8	11	8	154.5	8	6	8	229	8	39.5	8	116.5
9	12	9	163.5	9	6.5	9	246	9	41	9	118
10	12.5	10	172	10	7	10	260	10	43	10	120
15	16.5	15	219	15	8	15	315	15	49.5	15	126.5
20	45	20	263.5	20	8.5	20	332	20	55	20	135.5
25	67.5	25	308	25	9.5	25	340	25	60	25	142.5
30	72			30	10			30	64.5		
35	75.5			60	10.5			31	77.5		
40	79.5			100	10.5			32	102		
45	82.5							33	105		
50	90.5							35	109		
55	93							40	115.5		
60	95							45	119.5		
65	96.5							50	122.5		
70	97.5							55	124.5		
75	98.5							60	127		
80	99.5							65	129		
85	100.5							70	131		
90	101.5							75	133		
95	102.5							80	134.5		
100	104							85	136.5		
								90	137.5		
								95	139		
								100	140.5		
11.76 cm^2		11.47 cm^2		8.33 cm^2		8.71 cm^2		11.21 cm^2		13.40 cm^2	

Appendix D (Cont.)

Cr-3.0Mn			
2100°F (1422°K)		2400°F (1589°K)	
Hours	Mg	Hours	Mg
0.5	23	0.5	49
1	30.5	1	70.5
2	40	2	101
3	50	3	123.5
4	56	4	142.5
5	60.5	5	159
10	77	6	172
15	81	7	186
20	102	8	198
25	111	9	208
30	119.5	10	219
35	127	15	268
40	133	20	296
45	139.5	25	318
50	144		
55	148.5		
60	153		
65	157.5		
70	161.5		
75	166		
80	169.5		
85	172.5		
90	176		
95	180		
100	183		
11.97 cm^2		12.19 cm^2	

Appendix E

MICROHARDNESS DATA

[Conditions: 100 hr-2100°F(1422°K). All readings in excess of 500 KHN are in nitride case. Definitions: A: Air. D: DPH instead of KHN.]

Mils	KHN
Cr(He)	
Random	156
	143
	141
	158
	158
	134
	149
Cr(A)^{D}	
5	155
10	141
15	155
Cr(O)^{D}	
5	152
10	144
13.5	139
15	139
Cr(O + A)^{D}	
5	167
10	160
15	149
Cr-1W(A)	
2	1138
5.4	249
8.0	219
9.5	235
11.6	223
14.0	201
16.6	182
1.7	1693
5.7	208
7.5	219
9.8	185
12.0	235

Mils	KHN
Cr-1W(A)	
13.8	219
16.2	185
2.0	1470
4.5	223
6.5	249
9.0	253
12.8	223
15.0	179
17.5	219
Cr-1W(He)	
Random	208
	208
	235
	208
	235
Cr-2W(A)	
1.0	2078
3.5	1971
6.2	284
8.5	322
13.5	322
17.2	284
0.7	2078
3.5	2196
7.0	284
10.5	284
15.0	309
18.5	284
0.7	2461
3.0	1470
6.5	284
10.5	274
14.0	322

Mils	KHN
Cr-2W(A)	
17.0	253
Cr-2W(He)	
Random	258
	231
	235
	284
	223
Cr-4W(A)	
3.2	1815
8.8	390
11.0	331
14.4	381
17.2	319
3.1	1971
7.8	379
11.3	375
16.0	341
3.1	1871
9.2	268
12.5	309
17.6	309
Cr-4W(He)	
Random	219
	279
	274
	268
	302
Cr-1Mo	
3.0	1871
6.4	215
9.7	208
10.8	219
11.4	204

Mils	KHN
Cr-1Mo(A)	
13.6	208
16.2	204
3.7	1497
5.8	235
9.0	231
10.5	219
12.1	191
15.1	208
17.8	219
2.4	1613
6.1	240
9.1	258
11.7	194
14.2	198
17.6	204
Cr-1Mo(He)	
Random	166
	159
	188
	179
	188
Cr-4Mo(A)	
1.0	2078
4.0	328
5.8	374
8.0	322
10.0	322
12.3	322
14.1	284
16.0	304
0.7	1444
5.0	284
7.7	336

Mils	KHN
Cr-4Mo(A)	
9.5	353
12.0	309
14.0	284
16.0	284
0.9	178
5.8	342
9.0	274
12.0	330
15.0	284
Cr-4Mo(He)	
Random	290
	268
	284
	263
	284
Cr-1Re(A)	
1.7	1235
7.4	211
10.5	201
15.0	198
20.0	244
24.5	263
2.4	976
6.4	191
9.5	235
12.3	191
17.0	185
20.5	154
1.2	1345
7.2	244
9.1	215
11.3	219
13.8	219

Mils	KHN
Cr-1Re(A)	
17.5	191
Cr-1Re(He)	
Random	166
	191
	208
	168
	179
Cr-2Re(A)	
1.0	1345
4.1	1138
7.3	1138
10.0	328
14.0	235
16.5	219
20.0	235
2.0	1235
7.3	235
10.0	244
14.0	219
19.0	204
2.3	1539
9.0	204
11.5	188
14.5	215
17.0	208
26.0	219
Cr-2Re(He)	
Random	194
	174
	179
	194
	182

Mils	KHN
Cr-4Re(A)	
3.0	1235
7.5	263
11.5	296
13.0	296
16.5	263
1.0	1235
8.0	274
11.5	253
14.0	274
17.0	244
2.5	976
10.0	274
13.0	253
15.5	235
18.5	227
Cr-4Re(He)	
Random	258
	227
	249
	208
	227
Cr-1Ru(A)	
1.0	1693
4.0	219
6.5	223
9.5	194
12.0	191
15.0	198
17.5	208
1.0	1470
3.0	240
6.0	219
8.0	253

Appendix E (Cont.)

Mils	KHN
Cr-1Ru(A)	
11.0	204
14.0	236
17.5	227
1.0	1971
3.5	208
6.0	227
9.5	253
13.0	249
15.5	227
Cr-1Ru(He)	
Random	179
	179
	185
	179
	179
Cr-2Ru(A)	
1.2	1138
3.0	249
9.0	244
12.0	235
14.2	284
15.2	244
0.8	1093
2.5	284
4.5	268
7.0	240
9.8	268
12.7	253
15.5	240
18.6	284
1.0	1871
3.5	244
6.0	244
8.8	253
12.5	284
15.0	284
	12.0

Mils	KHN
Cr-2Ru(He)	
Random	258
	263
	275
	258
	268
Cr-4Ru(A)	
1.2	564
4.7	322
6.0	274
9.4	274
14.3	263
20.5	296
1.3	598
3.4	318
10.1	290
19.3	284
1.3	348
3.5	302
8.8	300
16.4	307
Cr-4Ru(He)	
Random	284
	268
	258
	274
Cr-1Mn(A)	
3.5	2196
5.6	159
11.0	188
15.2	171
18.4	198
2.5	1613
4.8	194
7.7	168
9.8	168
168	

Mils	KHN
Cr-1Mn(A)	
15.0	204
2.5	208
5.3	174
8.0	182
10.0	168
13.6	174
17.7	161
Cr-1Mn(He)	
Random	132
	145
	147
	156
	137
Cr-2Mn(A)	
4.0	1910
6.5	198
11.0	198
13.0	161
15.7	179
4.7	1568
8.0	194
10.2	188
13.0	191
16.0	179
4.8	1727
6.8	208
10.2	161
12.3	166
14.5	166
18.0	179
Cr-2Mn(He)	
Random	159
	174
	171
	159
	145

Mils	KHN
Cr-3Mn(A)^{D}	
Random	163
	171
	154
Cr-3Mn(O)^{D}	
Random	153
	147
	136
Cr-3Mn(He)	
Random	157
	155
	151
Cr-4Mn(A)	
5.0	1922
8.4	191
12.3	198
16.3	194
4.2	1871
7.5	194
10.4	182
16.0	194
4.3	1871
8.1	201
12.4	191
17.0	231
Cr-4Mn(He)	
Random	163
	161
	163
	159
	163
Cr-1Fe(A)	
1.5	1483
2.8	1497
4.8	174
7.2	174
9.6	198

Mils	KHN
Cr-1Fe(A)	
12.0	204
14.5	249
1.9	1950
2.4	1971
4.3	188
10.7	197
19.8	188
0.5	2245
1.0	1871
4.8	215
7.9	198
9.7	211
11.0	219
13.0	188
14.2	201
16.4	194
Cr-1Fe(He)	
Random	179
	174
	168
Cr-2Fe(A)	
0.8	686
1.8	215
9.9	204
12.6	249
16.7	235
1.0	1613
3.0	208
9.1	211
17.3	208
1.0	1138
3.2	223
11.5	244
20.3	240
Cr-2Fe(He)	
Random	249
	231

Mils	KHN
Cr-4Fe(A)	
2.0	284
3.5	244
4.3	240
5.0	263
11.6	263
16.0	274
1.3	249
2.8	263
5.2	244
6.6	336
7.6	339
12.0	274
13.2	274
15.2	284
1.7	253
3.0	263
5.2	258
7.0	284
9.4	297
11.0	284
13.0	268
Cr-4Fe(He)	
Random	284
	309
Cr-1Co(A)	
3.0	1744
4.2	244
7.9	235
10.0	168
14.7	284
19.0	249
1.2	1613
4.1	240
9.7	240
17.1	235
1.0	1693

Mils	KHN
Cr-1Co(A)	
2.5	227
9.0	235
17.0	227
Cr-1Co(He)	
Random	219
	219
	231
	211
Cr-0.5Ti(A)	
1.5	1568
4.6	1470
7.5	1539
9.5	263
11.7	253
14.8	268
15.5	284
17.0	284
19.0	284
1.2	1971
3.2	1761
7.3	1971
9.2	263
10.7	284
12.6	284
14.3	263
16.4	258
19.2	263
1.4	1761
4.0	1744
6.5	1744
9.3	274
11.2	274
13.8	263
15.3	263
17.7	295
19.0	274

Mils	KHN
Cr-0.5Ti(He)	
Random	179
	171
	166
	179
Cr-2.0Ti(A)	
1.2	244
4.0	240
6.2	235
11.0	198
14.5	296
1.0	263
5.0	309
8.5	520
12.5	506
16.5	534
0.7	284
2.3	274
4.5	351
8.5	468
12.5	549
0.5	302
3.0	249
6.0	322
8.5	336
12.0	403
15.0	309
0.5	296
4.0	219
7.0	263
11.0	240
15.0	284
0.3	309
3.0	235
7.0	263
10.0	231
14.0	219

Mils	KHN
Cr-2Ti(He)	
Random	215
	249
	231
	258
	208
Cr-0.5Zr(A)	
1.0	1871
4.0	284
6.0	223
8.5	215
11.0	201
14.0	204
1.0	1288
3.5	249
6.5	219
9.0	208
13.0	201
16.5	211
5.0	1345
3.0	235
5.5	211
9.0	258
13.5	359
16.5	315
Cr-0.5Zr(He)	
Random	179
	156
	154
	156
	179
Cr-2Zr(A)	
1.2	219
4.0	211
8.0	198
10.5	253
13.5	244

Mils	KHN
Cr-2Zr(A)	
17.3	204
1.0	235
4.5	253
8.2	208
12.0	211
15.7	211
1.5	235
5.0	223
8.5	211
12.0	223
16.0	215
Cr-2Zr(He)	
Random	188
	181
	188
	182
	179
Cr-1Zr(A)^{D}	
Random	173
	176
	177
Cr-1Zr(O)^{D}	
Random	140
	152
	130
Cr-1Zr(He)^{D}	
Random	186
	185
	202
Cr-3Zr(A)^{D}	
Random	209
	206
	188
	206
	195
	194

Mils	KHN
Cr-3Zr(O)^{D}	
Random	185
	168
	192
	185
	177
	198
	196
Cr-3Zr(O+A)^{D}	
Random	193
	183
	174
Cr-3Zr(He)^{D}	
Random	140
	155
	160
Cr-4Zr(A)^{D}	
Random	201
	212
	199
Cr-4Zr(He)^{D}	
Random	152
	147
	150
Cr-0.5Hf(A)	
1.0	268
3.8	244
6.1	227
9.0	208
12.0	215
18.0	208
1.2	296
5.8	194
8.9	240
12.0	198
16.2	279
1.5	274

Mils	KHN
Cr-0.5Hf(A)	
5.1	253
8.5	253
13.0	249
15.3	244
18.6	253
Cr-0.5Hf(He)	
Random	185
	204
	198
	204
Cr-2Hf(A)	
1.2	198
8.8	191
16.0	204
1.2	204
5.0	215
9.5	198
13.5	194
18.7	168
1.8	244
3.5	191
5.0	185
7.0	191
9.5	191
12.5	204
16.4	188
Cr-2Hf(He)	
Random	188
	211
	182
	191
	198
Cr-0.5V(A)	
1.7	1645
4.3	322
6.6	284

Mils	KHN
Cr-0.5V(A)	
9.5	263
11.8	231
15.7	240
2.2	1779
5.0	325
8.3	258
12.2	215
15.2	219
4.2	594
8.0	253
10.0	211
13.0	244
17.2	249
Cr-1/2V(He)	
Random	179
	182
	182
	166
	174
Cr-2V(A)	
0.9	284
3.3	284
6.5	284
10.0	328
14.0	296
17.5	336
20.5	336
1.5	368
5.6	284
8.3	322
11.3	336
17.0	322
2.5	1539
5.0	302
8.5	308
11.8	329

Mils	KHN
Cr-2V(A)	
16.0	302
19.0	309
Cr-2V(He)	
Random	174
	191
	163
	174
	198
Cr-0.25Cb(A)^{D}	
Random	189
	195
	199
Cr-0.25Cb(O)^{D}	
Random	144
	132
	134
Cr-0.25Cb(He)^{D}	
Random	158
	155
	160
Cr-0.5Cb(A)	
0.9	235
1.8	227
7.9	231
19.5	227
1.0	244
8.0	249
17.0	223
0.8	253
6.3	244
13.0	235
Cr-0.5Cb(He)	
Random	219
	208
	215
	215

Appendix E (Cont.)

Mils	KHN
Cr-1Cb(A)^{D}	
Random	205
↓	194
↓	186
Cr-1Cb(O)^{D}	
Random	194
↓	207
↓	207
Cr-1Cb(He)^{D}	
Random	197
↓	205
↓	209
Cr-0,5Ta(A)	
1.0	1470
5.5	1693
10.5	263
13.0	235
15.5	211
1.2	1971
5.5	1470
9.5	215
11.5	223
13.5	244
16.5	227
1.5	1971
5.0	2078
9.5	235
12.5	268
16.0	215
Cr-0,5Ta(He)	
Random	198
↓	161
↓	191
↓	179
↓	171

Mils	KHN
Cr-0,5Y(A)	
1.2	179
2.9	194
4.9	182
7.8	185
10.7	208
13.8	201
1.2	1613
3.4	179
5.1	166
7.8	191
10.4	191
13.6	198
16.8	166
2.0	166
3.6	152
4.9	188
8.0	179
10.2	154
14.8	179
Cr-0,5Y(He)	
Random	161
↓	159
↓	161
Cr-0,5Y(He)^{D}	
Random	159
↓	158
↓	159
Cr-0,5Y(A)^{D}	
Random	165
↓	146
↓	171
↓	154
Cr-0,5Y(O)^{D}	
Random	131
↓	141
↓	146
↓	134
↓	133
↓	142
↓	139

Mils	KHN
Cr-01Y(A)^{D}	
Random	173
↓	169
↓	159
Cr-0,1Y(O)^{D}	
Random	148
↓	142
↓	142
Cr-0,1Y(He)^{D}	
Random	168
↓	135
↓	142
Cr-0,25Y(A)^{D}	
Random	173
↓	177
↓	176
Cr-0,25Y(O)^{D}	
Random	147
↓	150
↓	150
Cr-0,25Y(He)^{D}	
Random	151
↓	146
↓	150
Cr-1,0Y(A)	
2.0	179
4.5	166
10.0	194
15.4	171
2.0	156
6.2	168
8.0	174
13.4	179
18.0	156
2.0	215
5.4	188
8.0	185

Mils	KHN
Cr-1Y(A)	
13.0	179
17.9	219
18.2	219
Cr-1Y(He)	
Random	191
↓	179
↓	171
↓	182
Cr-2Y(A)	
1.5	171
3.5	182
5.3	182
8.0	204
14.0	211
15.7	223
1.9	191
4.0	201
7.6	231
11.0	215
14.0	249
17.7	194
1.8	204
5.6	179
9.5	191
19.0	194
Cr-2Y(He)	
Random	179
↓	168
↓	179
↓	191
Cr-0,1La(A)^{D}	
Random	177
↓	173
↓	174

Mils	KHN
Cr-0,1La(O)^{D}	
Random	151
↓	142
↓	152
Cr-0,1La(He)^{D}	
Random	159
↓	153
↓	138
Cr-0,25La(A)^{D}	
Random	167
↓	170
↓	176
↓	167
↓	165
↓	162
Cr-0,25La(O)^{D}	
Random	143
↓	144
↓	155
↓	146
↓	153
↓	154
Cr-0,25La(He)^{D}	
Random	158
↓	160
↓	155
Cr-0,25La (O + A)^{D}	
Random	155
↓	150
↓	142
Cr-0,5La(A)	
1.0	1345
2.0	194
5.0	179
10.0	194
15.0	185
20.0	185
1.0	1470
2.5	215
6.0	215
10.5	179
15.0	194
17.5	191
1.0	1871

Mils	KHN
Cr-0,5La(A)	
2.0	204
7.0	211
12.0	201
18.0	215
Cr-0,5La(He)	
Random	132
↓	135
↓	147
↓	143
↓	132
Cr-1La(A)	
4.0	166
7.0	191
10.0	219
12.0	198
16.0	219
5.5	204
8.5	215
11.5	201
15.0	201
1.0	1345
3.0	171
6.0	179
9.0	201
12.0	156
15.0	191
1.0	1779
2.5	166
5.5	179
8.5	194
11.5	182
14.5	201
Cr-1La(He)	
Random	156
↓	171
↓	161
↓	152
↓	166

Mils	KHN
Cr-2La(He)	
0.5	1613
1.0	179
3.5	185
7.0	163
11.0	215
15.0	179
0.5	1288
1.5	219
5.5	179
12.0	198
14.5	171
1.0	1971
2.0	191
5.5	204
8.5	185
12.0	185
15.0	244
Cr-2La(He)	
Random	143
↓	135
↓	145
↓	135
↓	145
Cr-0,5Pa(A)	
1.0	2078
2.5	182
4.3	194
8.5	215
11.2	211
14.1	231
19.7	240

Mils	KHN
Cr-1/2Pr(A)	
0.9	2078
3.7	240
7.0	191
9.6	215
12.5	215
18.7	188
0.9	1971
3.0	215
9.0	204
17.6	215
Cr-1/2Pr(He)	
Random	211
↓	198
↓	194
↓	204
Cr-1Pr(A)	
2.5	174
4.4	179
7.1	161
10.5	159
14.0	159
18.1	154
1.7	159
5.0	179
9.0	154
12.6	145
15.8	174
19.2	185
1.2	179
2.1	188
4.7	182
6.6	168
9.0	204
14.0	

Mils	KHN
Cr-1Pr(He)	
Random	166
↓	179
↓	191
↓	163
↓	204
↓	188
Cr-0,4Mn(A)	
0.5	1470
2.0	211
6.0	227
10.5	185
14.0	198
17.5	194
00.7	235
1.5	191
5.0	182
10.0	188
14.0	182
18.5	185
0.6	1613
2.0	188
7.0	215
12.0	198
16.5	219
Cr-0,5Mn(He)	
Random	179
↓	179
↓	152
↓	179
↓	158
Cr-1Mn(A)	
0.5	1971
2.0	204
4.5	211
8.0	211
12.0	215

Mils	KHN
Cr-1Mn(A)	
16.5	168
0.5	1345
5.0	227
8.0	198
11.0	198
16.0	198
20.0	201
1.0	1539
3.0	198
6.5	204
10.0	182
13.5	179
17.0	194
19.5	194
Cr-1Mn(He)	
Random	194
↓	161
↓	185
↓	179
↓	163
Cr-2Mn(A)	
3.5	231
6.0	208
9.0	168
12.5	215
16.0	194
19.0	208
0.5	1693
1.5	194
5.0	198
7.5	171
12.0	191
15.5	219
1.0	2078
3.5	219
7.5	194

Mils	KHN
Cr-2Mn(A)	
10.0	198
16.0	194
18.0	227
Cr-2Mn(He)	
Random	159
↓	179
↓	168
↓	179
↓	161
Cr-0,5Th(A)	
2.0	1779
4.0	201
6.5	201
10.0	179
13.0	182
2.0	2078
4.5	208
7.5	171
10.5	174
14.0	168
1.5	1693
3.5	211
6.5	191
12.5	179
16.0	198
Cr-0,5Th(He)	
Random	194
↓	161
↓	194
↓	179
↓	161
Cr-1Th(A)	
0.5	1288
1.5	235
4.2	211
8.2	219

Mils	KHN
Cr-1Tb(A)	
13.8	198
1.3	1470
3.5	219
7.0	198
11.5	219
15.0	211
0.4	1693
1.5	211
4.2	211
7.2	201
10.5	198
13.7	211
16.5	179
Cr-1Tb(He)	
Random	143
↓	159
↓	139
↓	130
↓	159
Cr-2Th(A)	
4.5	284
8.5	235
11.0	211
14.0	191
16.0	182
2.5	253
5.0	253
9.0	244
10.5	198
12.0	208
13.5	219
1.5	231
10.0	201
13.0	215
15.5	215
17.0	208

Mils	KHN
Cr-2Th(He)	
Random	156
↓	161
↓	152
↓	166
↓	168
Cr-0,5Y-1Th(A)^{D}	
5	195
15	195
25	202
Cr-0,5Y-1Th(He)^{D}	
Random	160
↓	152
↓	149
Cr-0,5Y-1Th(O+A)^{D}	
5	170
15	180
25	177
Cr-2Zr-1Th(A)^{D}	
5	209
15	194
25	215
Cr-2Zr-1Th(He)^{D}	
Random	161
↓	186
↓	176
Cr-2Zr-1Th(O+A)^{D}	
5	228
15	213
25	193
Cr-2Zr-0,25La(A)^{D}	
5	209
15	194
25	215
Cr-2Zr-0,25La(He)^{D}	
Random	168
↓	172
↓	186

Mils	KHN
Cr-3Zr-0,1Y(A)^{D}	
5	192
15	207
25	210
Cr-3Zr-0,1Y(He)^{D}	
Random	186
↓	193
↓	201
Cr-3Zr-0,1Y(O+A)^{D}	
5	190
15	193
25	189
15	193
15	215

Appendix F

BEND DATA

Alloy	Sample Number	Condition	Test Temperature		Bend Angle (deg)	Maximum Load		Comments
			°F	°K		Lb	Kg	
Cr	98-13	R	200	366	Nil	15.57	7.05	Brittle
	98-1	R	250	394	90	20.3	9.13	Ductile
	98-6	R	300	422	90	23.5	10.7	Ductile
	98-7	H	150	339	Nil	20.5	9.32	Brittle
	98-4	H	200	366	90	25.5	11.6	Ductile
	98-15	H	250	394	135	25.0	11.38	Ductile
	Cr-1	PA	1000	811	80	20.3	9.23	Partially ductile
	Cr-2	PA	1100	866	90	9.57	4.35	Partially ductile (cracks)
	Cr-4	PA	1200	922	90	20.7	9.41	Ductile
	Cr-3	A	1400	1033	90	20.7	9.41	Ductile
	Cr-5	A	1200	922	90	24.2	11.0	Ductile
Cr-1W	957-1	H	400	478	Nil	11.6	5.27	Brittle
	957-2	H	600	589	90	45.4	20.6	Ductile
	957-3	H	500	533	Nil	16.4	7.45	Brittle
	957-4	A	1700	1200	90	26	11.8	Ductile
	957-5	A	1800	1255	90	23	10.45	Ductile
	957-6	A	1600	1144		19.2	8.72	Partially ductile
Cr-2W	958-1	H	400	478	Nil	6.0	2.73	Brittle
	958-2	H	600	589	85	54.2	24.6	Partially ductile, cracked
	958-4	H	700	644	90	55.5	25.2	Ductile
	958-8	A	1600	1144	Nil	15.8	7.18	Brittle
	958-9	A	1700	1200	Nil	19.0	8.63	Brittle
	958-10	A	1800	1255	90	28.4	12.9	Ductile
Cr-4W	959-1	H	400	478	Nil	10.5	4.78	Brittle
	959-2	H	600	589	Nil	12.0	5.46	Brittle
	959-7	A	—		—	—		—
	959-8	A	1800	1255	Nil	11.0	5.0	Brittle
	959-9	A	1600	1144	Nil	11.3	5.13	Brittle

R : Recrystallized 1 hr, 2400°F, helium.
H : 100 hr, 2100°F (1422°K), helium.
A : 100 hr, 2100°F (1422°K), air.
O : 100 hr, 2100°F (1422°K), oxygen.
PA: 50 hr, 2100°F (1422°K), oxygen + 100 hr, 2100°F (1422°K), air.

Appendix F (Cont.)

Alloy	Sample Number	Condition	Test Temperature °F	Test Temperature °K	Bend Angle (deg)	Maximum Load Lb	Maximum Load Kg	Comments
Cr-1Mo	950-1	H	400	478		33.8	15.38	Partially ductile
	950-2	H	600	589	90	47.2	21.4	Ductile
	950-3	H	500	533		32.6	14.81	Partially ductile
	950-4	A	1200	922	Nil	7.5	3.41	Brittle
	950-5	A	1400	1033	Nil	7.3	3.32	Brittle
	950-6	A	1600	1144	90	23.5	10.68	Ductile
Cr-4Mo	962-4	H	Sample broken					
	962-5	A	1600	1144	Nil	3.2	1.45	Brittle
	962-6	A	1800	1255	Nil	2.0	0.91	Brittle
Cr-1Re	963-1	H	Sample broken					
	963-2	A	1800	1255		22.8	10.38	Partially ductile
	963-3	A	1600	1144	Nil	15.2	6.91	Brittle
	963-4	A	1800	1255	Nil	17.0	7.72	Brittle
Cr-2Re	964-1	H	Sample broken					
	964-2	A	1600	1144	Nil	2.5	1.14	Brittle
	964-3	A	1800	1255	Nil	1.0	0.45	Brittle
	964-4							
Cr-4Re	965-1	H	400	478		31.0	14.1	Partially ductile
	965-2	H	600	589		24.2	11.0	Partially ductile
	965-3	H	700	644	90	44.4	20.2	Ductile
	965-7	A	1700	1200	Nil	5.10	2.32	Brittle
	965-8	A	1800	1255		21.2	9.63	Brittle
	965-12	A	Sample broken					
Cr-1Ru	9101-1	He	400	478	90	34.1	15.5	Ductile
	9101-2	He	100	311	Nil	2.5	1.1	Brittle
	9101-3	He	200	366	90	37.2	16.8	Ductile
	9101-4	A	1600	1144	90	26.0	11.8	Ductile
	9101-5	A	1500	1089	Nil	24.5	11.13	Brittle
			1400	1033	Nil	25.0	11.37	Brittle
Cr-2Ru		R	150	339		48.3	21.95	Partially ductile
	945-1	H	300	422	Nil	17.3	7.86	Brittle
	945-2	H	450	505	Nil	22.0	10.0	Brittle
	945-3	H	500	533		42.7	19.4	Ductile
	945-4	A	1200	922	Nil	25.7	11.7	Brittle
	945-5	A	1600	1144	90	36.0	16.38	Partially ductile, edge cracked
	945-6	A	1700	1200	90	33.0	15.0	Ductile

Appendix F (Cont.)

Alloy	Sample Number	Condition	Test Temperature °F	Test Temperature °K	Bend Angle (deg)	Maximum Load Lb	Maximum Load Kg	Comments
Cr-4Ru	946-11	R	300	422	90	56.6	25.45	Ductile
	946-10	R	200	366	90	62.8	28.55	Ductile
	946-12	R	100	311		78.0	35.42	Partially ductile
	946-13	R	150	339	90	79.0	35.9	Ductile
	946-1	H	500	533		43.2	19.65	Ductile, incomplete bend
	946-3	H	400	478	Nil	34.1	15.5	Brittle
	946-2	H	450	505	90	49.8	22.62	Ductile
	946-4	A	1400	1033	Nil	22.6	10.28	Brittle
	946-5	A	1600	1144	Nil	29.0	13.18	Brittle
	946-6	A	1800	1255		27.3	12.4	Partially ductile, cracked
Cr-1Mn	947-1	H	400	478	90	31.6	14.37	Partially ductile
	947-2	H	600	589	90	33.2	15.1	Ductile
	947-3	H	500	533	90	33.2	15.1	Ductile
	947-4	A	1000	811	90	33.5	15.22	Ductile, one edge cracked
	947-5	A	900	755		26.7	12.14	Partially ductile
	947-6	A	1600	114	90	16.0	7.27	Failed at crack
Cr-2Mn	948-1	H	400	478	90	31.0	14.1	Ductile
	948-2	H	200	422	Nil	16.8	7.63	Brittle
	948-3	H	300	366	90	28.0	12.72	Ductile
	948-4	A	1200	922	90	34.8	15.82	Ductile, slight edge crack
	948-5	A	1000	811	90	27.5	12.5	Ductile
	948-6	A	800	700	Nil	20.0	9.08	Brittle
Cr-4Mn	949-1	H	400	478	90	40	18.19	Ductile
	949-2	H	200	366	Nil	18.5	8.41	Brittle
	949-3	H	300	422	90	45.8	20.8	Ductile
	949-4	A	1600	1144	90	29.0	13.18	Ductile
	949-5	A	900	755		28.0	12.72	Partially ductile
	949-6	A	1000	811		33.3	15.13	Partially ductile
Cr-1Fe	914-11	R	250	394	54	31.2	14.18	Partially ductile
	914-13	R	300	422	90	33.3	15.22	Ductile
	914-1	H	200	366	Nil	12.5	5.68	Brittle
	914-4	H	250	394	90	46.5	21.15	Ductile
	914-2	H	300	422	90	34.5	15.68	Ductile
	914-8	A	1400	1033	Nil	4.3	1.95	Brittle
	914-5	A	1600	1144	90	31.0	14.1	Ductile

Appendix F (Cont.)

Alloy	Sample Number	Condition	Test Temperature		Bend Angle (deg)	Maximum Load		Comments
			°F	°K		Lb	Kg	
Cr-2Fe	915-6	R	200	366	90	36.0	16.38	Ductile
	915-12	R	250	394	90	35.8	16.28	Ductile
	915-11	R	300	422	90	36.5	16.1	Ductile
	915-2	H[a]	300	422	63	47.5	21.6	Partially ductile
	915-3	H[a]	400	478	Nil	19.0	8.63	Brittle
	915-1	H[a]	500	533	Nil	15.0	6.82	Brittle
	915-7	A	1600	1144	Nil	5.0	2.27	Brittle
	915-8	A	1700	1200	Nil	4.5	2.04	Brittle
Cr-4Fe	916-7	R	300	422	90	45.0	20.45	Ductile
	916-3	H[a]	300	422	Nil	22.0	10.0	Brittle
	916-1	H[a]	400	478	Nil	31.5	14.32	Brittle
	916-2	H[a]	500	533	Nil	25.0	11.37	Brittle
	916-11	A	1600	1144	Nil	3.0	1.36	Brittle
	916-12	A	1700	1200	Nil	0.7	0.32	Brittle
	916-13	A	1800	1255		17.0	7.72	Partially ductile
	916-14	A	1000	811	Nil	12.5	5.68	Brittle
	916-15	A	1200	922	Nil	11.8	5.36	Brittle
	916-16	A	1400	1033	Nil	16.0	7.27	Brittle
Cr-1Co	919-1	H	300	422	90	98.0	44.6	Ductile
	919-2	H	200	366		36.6	16.58	Partially ductile
	919-3	H	250	394		31.0	14.1	Partially ductile
	919-4	A	1700	1200		16.0	7.27	Partially ductile
	919-5	A	1600	1144		16.5	7.5	Partially ductile, cracked
	919-6	A	1800	1255	90	17.6	8.0	Ductile
Cr-1/2Ti	925-7	R	500	533	Nil	1.2	0.55	Brittle
	925-1	H[b]	700	644	90	45.0	20.45	Cracked, partially ductile
	925-3	H[b]	600	589	Nil	16.8	7.63	Brittle
	925-2	H[b]	800	700	Nil	17.2	7.82	Partially ductile
	925-4	A	1400	1033	Nil	18.0	8.18	Brittle
	925-5	A	1600	1144	Nil	17.0	7.72	Brittle
	925-8	A	1800	1255	90	33.0	15.0	Ductile
Cr-2Ti	992-1	H	800	700	Nil	10.0	4.54	Brittle
	992-2	H	1000	811	Nil	12.4	5.64	Brittle
	992-3	H	1200	922	Nil	4.4	2.0	Brittle
	992-4	A	1600	1144	Nil	Nil	–	Brittle
	992-5	A	1700	1200	Nil	2.8	1.27	Brittle
	992-6	A	1800	1255	Nil	1.4	0.64	Brittle

(a) Contaminated.
(b) SiO_2 fused to surface and reacted.

Appendix F (Cont.)

Alloy	Sample Number	Condition	Test Temperature		Bend Angle	Maximum Load		Comments
			°F	°K	(deg)	Lb	Kg	
Cr-1/2Zr	999-1	He	600	589	90	29.8	13.55	Ductile
	999-2	He	400	478		18.6	8.45	Partially ductile
	999-3	He	500	533	90	29.3	13.31	Ductile
	999-4	A	1400	1033	Nil	27.2	12.37	Brittle
	999-5	A	1500	1089	90	44.0	20.0	Ductile, one edge cracked
	999-6	A	1600	1144	90	40.0	18.18	Ductile
Cr-2Fe	9100-1	He	400	478	90	39.7	18.05	Ductile
	9100-2	He	200	366	Nil	27.5	12.5	Brittle
	9100-3	He	300	422		33.0	15.0	Partially ductile
	9100-4	A	1200	922	90	56.2	25.55	Ductile
	9100-5	A	1000	811	Nil	35.0	15.9	Brittle
	9100-6	A	1100	866		41.5	18.87	Partially ductile
Cr-1/2Hf	917-1	H	500	533		35.0	15.9	Partially ductile
	917-2	H	700	644	90	37.5	17.05	Ductile
	917-3	H	600	589	90	38.0	17.28	Ductile
	917-5	A	1400	1033	Nil	29.0	13.18	Brittle
	917-6	A	1600	1144	90	41.8	19.0	Ductile
	917-7	A	1500	1089	90	47.0	21.37	Ductile
Cr-2Hf	918-1	H	700	644	90	66.0	30.0	Ductile
	918-2	H	500	533	Nil	24.4	11.1	Brittle
	918-3	H	Broke in handling					
	918-7	A	1400	1033	90	51.5	23.4	Ductile
	918-8	A	1200	922	Nil	32.5	14.78	Ductile
	918-9	A	1300	978	90	46.0	20.9	Ductile
Cr-1/2V	996-1	H	400	478	90	29.4	13.37	Ductile
	996-2	H	200	366	Nil	16.1	7.32	Brittle
	996-3	H	300	422	90	36.0	16.37	Ductile
	996-7	A	1600	1144	Nil	22.2	10.1	Brittle
	996-8	A	1700	1200	90	35.7	16.22	Ductile
	996-9	A	1800	1255	90	31.0	14.1	Ductile
Cr-2V	941-1	H	400	478		30.6	13.91	Partially ductile
	941-2	H	600	589	90	43.8	19.9	Ductile
	941-3	H	500	533	90	33.8	15.37	Ductile
	941-4	A	1600	1144	Nil	2.7	1.23	Brittle
	941-5	A	1800	1255	Nil	2.5	1.14	Brittle
	941-6	A						

Appendix F (Cont.)

Alloy	Sample Number	Condition	Test Temperature °F	Test Temperature °K	Bend Angle (deg)	Maximum Load Lb	Maximum Load Kg	Comments
Cr-1/2Cb	912-2	H	300	422	Nil	3.1	1.41	Brittle
	912-4	H	700	644	90	46.7	21.22	Ductile
	912-3	H	500	533	90	53.5	24.32	Ductile
	912-6	A	1400	1033	90	46.2	21.0	Ductile
	912-7	A	1200	922	Nil	27.0	12.28	Brittle
	912-8	A	1300	978	Nil	27.5	12.5	Brittle
Cr-1/2Ta	994-1	H	400	478	Nil	17.6	8.0	Brittle
	994-2	H	600	589	90	41.0	18.62	Partially ductile, cracked
	994-3	H						Sample broken
	994-4	A	1700	1200	90	31.8	14.45	Partially ductile, cracked
	994-5	A	1600	1144	90	33.1	15.05	Partially ductile, cracked
	994-6	A	1400	1033	Nil	21.2	9.63	Brittle
Cr-1/2Y	950-15	R	80	300		30.5	13.87	Partially ductile
	950-12	R	80	300		31.0	14.1	Partially ductile
	950-10	R	95	308		27.5	12.5	Partially ductile
	950-11	R	130	328	90	27.7	1.26	Ductile
	950-1	H	200	366	Nil	17.0	7.72	Brittle
	950-2	H	300	422	Nil	17.8	8.09	Brittle
	950-3	H	500	533	90	21.0	9.55	Ductile
	950-7	A	1200	922	90	43.5	19.78	Ductile
	950-8	A	1000	811	90	47.8	21.75	Ductile
	950-9	A	800	700	90	42.2	19.2	Ductile, edge cracked
	950-13	A	600	589	90	19.0	8.63	Ductile
	950-14	A	400	478	90	26.2	11.9	Ductile
Cr-1Y	951-1	H	500	589	90	28.5	12.95	Ductile
	951-2	H	300	422	Nil	21.0	9.55	Brittle
	951-3	H	400	478	90	27.5	12.5	Ductile
	951-7	A	1200	922	90	46.5	21.13	Ductile, edge tears
	951-8	A	1300	978	90	40.5	18.4	Ductile
	951-9	A	1000	811	90	50.0	22.73	Ductile, edge tears
Cr-2Y	952-10	R	128	330	Nil	4.3	1.95	Brittle
	952-2	H	500	533	90	28.5	12.95	Ductile
	952-2	H	300	422		31.0	14.09	Partially ductile
	952-1	H	400	478	90	30.8	14.0	Ductile
	952-7	A	1200	922	90	44.0	20.0	Ductile
	952-8	A	1000	811	90	52.2	23.72	Ductile
	952-19	A	500	589	90	49.0	22.05	Ductile

Appendix F (Cont.)

Alloy	Sample Number	Condition	Test Temperature °F	Test Temperature °K	Bend Angle (deg)	Maximum Load Lb	Maximum Load Kg	Comments
Cr-1/2La	967-1	He	400	478	90	23.7	10.78	Ductile
	967-2	He	200	366	Nil	9.04	4.08	Brittle
	967-3	He	300	422		22.3	10.13	Partially ductile
	967-4	A	600	589	90	41.2	18.75	Ductile
	967-5	A	400	478	Nil	10.3	4.68	Brittle
	967-6	A	500	533	Nil			Brittle
Cr-1La	968-1	H	400	478		21.5	9.78	Partially ductile
	968-2	H	600	589	90	32.0	14.54	Ductile
	968-3	H	500	533	90	28.7	13.04	Ductile
		A	700	644		26.5	12.5	Partially ductile
		A	800	700	90	39.4	17.9	Ductile
Cr-2La	969-1	He	400	478	90	23.3	10.59	Ductile
	969-2	He	200	366	Nil	10.6	4.8	Brittle
	969-3	He	300	422	Nil	15.6	7.1	Brittle
	969-4	A	800	700	90	37.4	17.0	Ductile
	969-5	A	600	589	Nil	23.6	10.72	Brittle
	969-6	A	700	644	90	33.7	15.32	Ductile
Cr-1/2Pr	953-1	H	400	478	90	24.7	11.22	Cracked in center
	953-2	H	500	533	90	27.5	12.50	Cracked in center
	953-3	H	600	589	90	25.4	11.53	Ductile, no cracks
	953-4	A	500	533	Nil	19.7	8.85	Brittle
	953-5	A	700	644	Nil	~25	11.35	Brittle
	953-6	A	900	755		44	20.0	Partially ductile, cracked
Cr-1Pr	954-10	R	134	330	Nil	13.3	6.04	Brittle
	954-1	H	500	533	90	25.8	11.72	Ductile
	954-2	H	300	422		27.7	12.60	Partially ductile
	954-3	H	400	478	90	24.3	11.06	Ductile
	954-7	A	1200	922	90	41.5	18.88	Ductile, edge cracked
	954-8	A	1300	978	90	38.0	17.28	Ductile
	954-9	A	1000	811	90	46.5	21.13	Ductile
Cr-1/2MM	970-1	He	400	478	90	21.5	9.78	Ductile
	970-2	He	300	422	Nil	8.3	3.78	Brittle
	970-3	He	200	366	Nil	8.5	3.86	Brittle
	970-4	A	600	589	Nil	16.8	7.63	Brittle
	970-5	A	800	700		28.2	12.82	Partially ductile
	970-6	A	900	755		27.2	12.36	Partially ductile

Appendix F (Cont.)

Alloy	Sample Number	Condition	Test Temperature °F	Test Temperature °K	Bend Angle (deg)	Maximum Load Lb	Maximum Load Kg	Comments
Cr-1MM	991-1	He	400	478	90	21.5	9.78	Ductile
	991-2	He	300	422		18.2	8.27	Partially ductile
	991-3	He	200	366	Nil	9.2	4.18	Brittle
	991-4	A	600	589		28.2	12.82	Partially ductile
	991-5	A	Sample broken					
	991-6	A	700	644	90	39.8	18.08	Ductile
Cr-2MM	972-1	H	400	478	90	25.5	11.58	Ductile
	972-2	H	200	366	Nil	9.2	4.18	Brittle
	972-3	H	300	422		11.7	5.32	Partially ductile
	972-4	A	500	533		26.2	11.9	Partially ductile
	972-5	A	600	589	Nil	0.5	0.23	Brittle, pre-cracked
	972-6	A	700	644	90	36.2	16.45	Ductile
Cr-1/2Th	980-1	H	500	533	90	19.8	9.0	Ductile
	980-2	H	450	505	90	19.7	8.95	Ductile
	980-3	H	400	478		20.8	9.45	Partially ductile
	980-4	A	600	589	Nil	21.7	9.85	Brittle
	980-5	A	800	700	Nil	29.5	13.4	Brittle
	980-6	A	1000	811	Nil	23.5	10.68	Brittle
Cr-1Th	981-1	H	400	478	90	26.5	12.03	Ductile
	981-2	H	200	366	Nil	15.7	7.14	Brittle
	981-3	H	300	422		21.2	9.63	Partially ductile
	981-4	A	800	700	90	53.2	24.20	Ductile
	981-5	A	600	589	Nil	11.0	5.0	Brittle
	981-6	A	700	644	90	49.5	22.5	Ductile
Cr-2Th	982-1	H	400	478	90	33.8	15.37	Ductile
	982-2	H	200	366	Nil	10.0	4.54	Brittle
	982-3	H	300	422	80	35.0	15.9	Ductile
	982-4	A	600	589	Nil	10.0	4.54	Brittle
	982-5	A	700	644	Nil	18.5	8.41	Brittle
	982-6	A	800	700	90	50.0	22.74	Ductile
Cr-1Y	9123-2	H	400	478	90	19.5	8.86	Ductile
	9123-4	H	300	422	90	24.5	11.13	Ductile
	9123-3	H	200	366	Nil	11.6	5.27	Brittle
	9123-7	A	400	478	Nil	16.1	7.32	Brittle
	9123-5	A	500	533	Nil	18.2	8.27	Brittle
	9123-6	A	800	700	Nil	27.3	12.4	Brittle
	9123-8	O	400	478	90	23.2	10.54	Ductile
	9123-9	O	300	422	90	22.6	10.28	Ductile
	9123-1	O	200	366	Nil	11.8	5.36	Brittle

Appendix F (Cont.)

Alloy	Sample Number	Condition	Test Temperature		Bend Angle	Maximum Load		Comments
			°F	°K	(deg)	Lb	Kg	
Cr-0.25Y	9124-4	H	400	478	90	17.5	8.95	Ductile
	9124-3	H	300	422	60	17.6	8.0	Partially ductile
		H						
	9124-5	A	400	478	Nil	21.5	9.77	Brittle
	9124-7	A	600	589	Nil	19.3	8.77	Brittle
	9124-6	A	1000	811	90	37.2	16.9	Partially ductile
	9124-10	O	400	478	90	24.3	11.05	Ductile
	9124-9	O	300	422	90	22.0	10.0	Ductile
	9124-8	O	200	366	90	30.0	13.63	Ductile
Cr-0.5Y	9125-4	H	400	478	90	21.0	9.54	Ductile
	9125-3	H	300	422	20	15.2	6.82	Partially ductile
	9125-2	H	200	366	Nil	14.7	6.68	Brittle
	9125-7	A	400	478	Nil	15.3	6.96	Brittle
	9125-6	A	600	589	85	38.4	17.45	Partially ductile
	9125-5	A	700	644	Nil	21.7	9.86	Brittle
	9125-9	O	400	478	90	26.0	11.82	Ductile
	9125-10	O	300	422	90	26.2	11.9	Ductile
	9125-8	O	200	366	45	22.3	10.13	Partially ductile
Cr-1La	9126-3	H	400	478	90	20	9.09	Ductile
	9126-3	H	300	422	Nil	10.2	4.64	Brittle
		H						
	9126-7	A	400	478	Nil	20.8	9.46	Brittle
	9126-6	A	700	644	45	22.5	10.22	Partially ductile
	9126-5	A	1000	811	75	34.6	15.72	Partially ductile
	9126-8	O	400	478	90	24.4	11.08	Ductile
	9126-10	O	300	422	Nil	10.3	4.62	Brittle
Cr-0.25La	9127-2	H	400	478	Nil	3.9	1.77	Brittle
	9127-3	H	500	533	90	20.1	9.13	Ductile
		H						
	9127-10	A	400	478	Nil	7.3	3.32	Brittle
	9127-9	A	700	644	45	27.8	12.62	Partially ductile
	9127-8	A	800	700	75	28.5	12.95	Partially ductile
	9127-7	O	400	478	Nil	9.7	4.41	Brittle
	9127-6	O	500	533	90	20.3	9.23	Ductile
	9127-12	PA	400	478	Nil	8.0	3.64	Brittle
	9127-13	PA	600	589	45	18.6	8.45	Partially ductile
	9127-14	PA	700	644	90	22.7	10.32	Ductile

Appendix F (Cont.)

Alloy	Sample Number	Condition	Test Temperature		Bend Angle	Maximum Load		Comments
			°F	°K	(deg)	Lb	Kg	
Cr-0.25Cb	9131-4	H	400	478	90	26.5	12.04	Ductile
	9131-3	H	300	422	30	22.2	10.08	Partially ductile
		H						
	9131-7	A	1400	1033	Nil	2.0	0.91	Brittle
	9131-6	A	1600	1144	90	39.7	18.03	Ductile
	9131-5	A	1500	1089	90	33.6	15.28	Ductile
	9131-10	O	400	478	Nil	5.7	2.59	Brittle
	9131-9	O	500	533	70	26	11.81	Partially ductile
	9131-8	O	800	700	90	32.1	14.6	Ductile
Cr-1Cb	9130-4	H	400	478	Nil	20.7	9.41	Brittle
	9130-3	H	500	533	Nil	17.0	7.72	Brittle
	9130-2	H	600	589	90	19.7	8.95	Ductile
		A						
		A						
	9130-6	O	800	700	90	18.3	8.32	Ductile
	9130-7	O	700	644	Nil	8.3	3.77	Brittle
Cr-1Zr	9129-4	H	400	478	90	25.7	11.68	Ductile
	9129-3	H	300	422	Nil	19.5	8.86	Brittle
		H						
	9129-10	A	1400	1033	90	34.8	15.82	Ductile
	9129-9	A	1200	922	90	38.5	17.5	Ductile
	9129-8	A	1000	811	45	29.8	13.55	Partially ductile
	9129-7	O	400	478	90	29.7	13.50	Ductile
	9129-6	O	500	533	90	29.0	13.18	Ductile
	9129-5	O	300	422	90	29.0	13.18	Ductile
Cr-3Zr	9136-4	H	400	478	90	34.5	15.68	Ductile
	9136-3	H	300	422	90	35.9	16.31	Ductile
	9136-2	H	200	366	Nil	27.7	12.58	Brittle
	8136-7	A	1400	1033	90	43.9	19.95	Ductile
	9136-6	A	1200	922	90	50.0	22.73	Ductile
	9136-5	A	1100	866	90	45.5	20.68	Ductile
	9136-10	O	400	478	75	37.2	16.9	Partially ductile
	9136-9	O	500	533	90	>50	22.73	Ductile
	9136-8	O	300	422	Nil	24.6	11.18	Brittle
	9136-12	PA	800	700	90	23	10.45	Ductile
	9136-14	PA	400	478	90	27.7	12.59	Ductile
	9136-13	PA	300	422	90			Ductile
Cr-2Zr	9100-10	PA	600	589	30	34.5	15.68	Partially ductile
	9100-11	PA	800	700	90	54.8	24.95	Ductile
	9100-12	PA	900	755		45.4	20.62	Ductile

Appendix F (Cont.)

Alloy	Sample Number	Condition	Test Temperature		Bend Angle (deg)	Maximum Load		Comments
			°F	°K		Lb	Kg	
Cr-3Mn	9128-4	H	400	478	90	23.1	10.5	Ductile
	9128-3	H	300	422	75	22.5	10.23	Partially ductile
	9128-2	H	200	366	Nil	12.70	5.77	Brittle
	9128-9	A	1000	811	Nil	12.8	5.82	Brittle
	9128-10	A	1200	922	Nil	13.7	6.23	Brittle
	9128-8	A	1400	1033	90	18.5	8.41	Ductile
	9128-7	O	400	478	90	22.0	10.0	Ductile
	9128-9	O	300	422	90	19.6	8.91	Ductile
	9128-5	O	200	366	90	24.1	10,91	Ductile
Cr-3Mn	9128-12	PA	800	700	Nil	7.3	3.32	Brittle
	9128-13	PA	1200	922	90	15.4	7.0	Ductile
	9128-14	PA	1000	811	Nil	7.8	3.54	Brittle
Cr-2Th	982-10	PA	400	478	Nil	14.7	6.68	Brittle
	982-11	PA	800	700	90	47.0	21.37	Ductile
	982-12	PA	600	589	Nil	11.0	5.0	Brittle
Cr-1Th	981-10	PA	800	700	90	42.8	19.48	Ductile
	981-11	PA	600	589	90	24.0	10.91	Ductile
	981-12	PA	400	478	Nil	19.0	8.63	Brittle
Cr-0.5Zr	999-10	PA	1000	811	90	21.0	9.55	Ductile
	999-11	PA	900	755	20	34.3	15.59	Partially ductile
	999-12	PA	800	700	30	38.4	17.45	Partially ductile
Cr-3Zr-0.1Y	9141-1	H	300	422	90	43.2	19.62	Ductile
	9141-2	H	400	478	90	42.0	19.1	Ductile
	9141-3	PA	500	533	Nil	23.5	10.68	Brittle
	9141-4	PA	600	589	90	41.0	18.63	Ductile
	9141-6	PA	500	533	Nil	19.7	8.95	Brittle
	9141-7	A	200	366	Nil	10	4.54	Brittle
	9141-8	A	400	478	Nil	5	2.27	Brittle
	9141-9	A	600	589	80	51.6	23.45	Partially ductile
Cr-2Zr-1Th	9142-1	H	400	478	90	24.5	11.13	Ductile
	9142-2	H	300	422	30	33.0	15.0	Partially ductile
	9142-4	PA	300	422	Nil	24.3	11.05	Brittle
	9142-5	PA	400	478	20	17.1	7.77	Partially ductile
	9142-6	PA	500	533	90	23.0	10.45	Ductile
	9142-3	A	400	478	90	52	23.62	Ductile
	9142-8	A	300	422	Nil	11	5.0	Brittle

Appendix F (Cont.)

Alloy	Sample Number	Condition	Test Temperature		Bend Angle	Maximum Load		Comments
			°F	°K	(deg)	Lb	Kg	
Cr-0.5Y-1Tb	9143-1	He	400	478	90	9.6	4.36	Ductile
	9143-2	H3	300	422	90	16.2	7.36	Ductile
	9143-4	PA	700	644	Nil	23.6	10.72	Brittle
	9143-5	PA	600	589	20	22.8	10.47	Partially ductile
	9143-3	A	400	478	30	27.5	12.5	Partially ductile
	9143-7	A	300	422	Nil	3.2	1.45	Brittle
	9143-8	A	500	533	Nil	18.0	8.18	Brittle
Cr-2Zr-0.25La	9145-1	He	500	533	90	39.5	17.95	Ductile
	9145-2	He	300	422	Nil	8.0	3.64	Brittle, pre-cracked
	9145-3	A	500	533	Nil	22.5	10.22	Brittle
	9145-4	A	800	700	90	55.2	25.1	Ductile
	9145-5	A	650	616	Nil	15.7	7.13	Brittle, pre-cracked
Cr-4Zr	9148-1	He	500	533	90	40.5	18.4	Ductile
	9148-2	He	300	422	30	43.3	19.7	Partially ductile
	9148-3	A	500	533	Nil	4.5	2.04	Brittle
	9148-4	A	800	700	Nil	3.5	1.59	Brittle
	9148-5	A	1200	922	Nil	43.3	19.7	Brittle

Appendix G
NEW TECHNOLOGY

The new technology developed under this program is described below. The page numbers in the text where the new technology is discussed in detail are referenced for each item.

ITEM 1 – Extrusion Canning for Chromium (pp. 14–17)

The surface condition of chromium extrusions is improved markedly by using a 5-mil (0.0127-cm) unalloyed molybdenum sheet liner to separate the surface from the steel can. The use of thin molybdenum liner permits extrusions to be made in inexpensive steel cans and eliminates the need for canning in solid molybdenum. The liner is sufficiently thin to preclude cracking of the billet on cooling and is sufficiently thick to give an improved sidewall condition.

ITEM 2 – Volumetric Reaction Rate Measurement (pp. 20–22, 28–34, 38–50)

It has been demonstrated that accurate measurements of gas-metal reaction rates in one-component gas systems where the reaction rate is high can be made by simple volumetric (gas consumption) techniques. The ability to use volumetric techniques significantly reduces the cost of testing and greatly increases the number of samples that can be tested at one time.

ITEM 3 – Internal Oxidation of Chromium and Its Alloys for Control of Embrittlement (pp. 58–64, 112–121)

Chromium and its alloys are not embrittled on heating in pure oxygen, even though significant amounts of internal oxidation occur. Alloys containing rare earths, thorium, zirconium, and hafnium can be oxidized internally to produce oxide dispersions that will, in certain cases, lower the DBTT and increase the resistance to nitrogen embrittlement. Preoxidation treatment of alloys is a simple and effective means of increasing the resistance to nitrogen embrittlement on subsequent exposure to air.

ITEM 4 – Control of Rare Earth Dispersions in Chromium Alloys (pp. 103–112)

The addition of 1 to 3 at.% zirconium (and probably hafnium) breaks up the large stringers and segregates rare earth or thorium secondary phases in chromium. The $ZrCr_2$ phase formed by this addition nucleates a random dispersion of small particles of rare earths or thorium in the structure. This should improve transverse properties and eliminates one of the objectionable features of using rare earths to control nitrogen embrittlement.

ITEM 5 – Nitridation-Resistant Chromium Alloys (pp. 103–112)

Chromium alloys having improved resistance to nitridation and nitrogen embrittlement are produced by alloying 2 to 3 at.% zirconium (and probably hafnium) with 0.1 to 0.5 at.% yttrium or lanthanum or 1 at.% thorium. The zirconium addition increases the effectiveness of rare earths and thorium at low concentrations of these elements. This should improve the producibility of rare-earth-containing alloys and result in more consistent behavior with respect to resistance to nitridation.

ITEM 6 – Control of Nitrogen Embrittlement in Chromium by Dispersed Phases (pp. 149–164)

The mechanism by which additions of alloys controls the nitrogen embrittlement of chromium is related to the ability of secondary phases or oxide particles to nucleate dislocation sources. This study has demonstrated that the key to improved alloy behavior lies in control of the morphology and distribution of these phases. The discovery can readily be factored into current alloy development programs. The best approach to alloying for resistance to nitrogen embrittlement is to restrict solid solution additions, strengthen with carbide dispersions, alloy with rare earths or thorium in combination with zirconium or hafnium to produce secondary phases (intermetallics, elements, or oxides) to act as dislocation sources, and process with controlled thermal-mechanical treatments to produce a uniform, fine, random dispersion of the ductility-controlling particles.

DISTRIBUTION LIST
(The number in parentheses is the number of copies sent to the addressee.)

Air Force Office of Scientific Research
Propulsion Research Division
USAF Washington, D.C. 20525

Attn: Library

Army Materials Research Agency
Watertown Arsenal
Watertown, Massachusetts 02172

Attn: Director

Battelle Memorial Institute
505 King Avenue
Columbus, Ohio 43201

Attn: Defense Metals Information Center
Attn: Dr. R. I. Jaffee
Attn: Mr. E. Bartlett

Bureau of Naval Weapons
Department of the Navy
Washington, D.C. 20525

Attn: RRMA-2/T. F. Kearns, Chief
Attn: Mr. I. Machlin

Defense Documentation Center
Cameron Station
5010 Duke Street
Alexandria, Virginia 22315

Department of the Navy
ONR
Code 429
Washington, D.C. 20525

Headquarters
Wright-Patterson AFB, Ohio 45433

Attn: Mr. N. Geyser, MAMP
Attn: MATB
Attn: MAAM/Technical Library
Attn: AFSC-FTDS
Attn: AFML:MAM
Attn: MAG/Directorate of Materials

Jet Propulsion Laboratory
4800 Oak Grove Drive
Pasadena, California 91102

Attn: Library

NASA-Ames Research Center
Moffett Field, California 94035

Attn: Library

NASA-Flight Research Center
P. O. Box 273
Edwards, California 93523

Attn: Library

NASA-Goddard Space Flight Center
Greenbelt, Maryland 20771

Attn: Library

NASA Headquarters
600 Independence Avenue
Washington, D.C. 20546

Attn: RAP/N. F. Rekos
Attn: RRM/G. C. Deutch
Attn: RRM/R. H. Raring

NASA-Langley Field
Virginia 23365

Attn: 214/Irvin Miller

NASA-Langley Research Center
Langley Field, Virginia 23365

Attn: Library

NASA-Lewis Research Center
21000 Brookpark Road
Cleveland, Ohio 44135

Attn: 3-13/G. M. Ault
Attn: 3-19/Technology Utilization Office
Attn: 49-1/S. Grisaffe
Attn: 105-1/N. T. Saunders
Attn: Library (60-3) (3)
Attn: 5-5/Report Control Office
Attn: 105-1/J. R. Stephens (12)
Attn: 49-1/J. P. Merutka
Attn: 77-3/L. W. Schopen
Attn: 105-1/W. D. Klopp (2)
Attn: 105-1/R. W. Hall
Attn: 49-1/J. C. Freche
Attn: 49-1/H. B. Probst

NASA-Manned Space Flight Center
Houston, Texas 77058

Attn: Library

NASA-Marshall Space Flight Center
Huntsville, Alabama 35812

Attn: Library

NASA Scientific & Technical Information Facility
P. O. Box 33
College Park, Maryland 20740 (6)

Oak Ridge National Laboratory
Oak Ridge, Tennessee 37830

Attn: Technical Reports Library

United States Air Force
San Antonio Air Material Area
Kelley AFB, Texas 78241

Attn: SANEPJ/A. E. Wright, Chief Jet Engine Section

U.S. Army Aviation Materials Laboratory
Port Eustis, Virginia 23604

Attn: SMOFE-APG/John White, Chief

U.S. Atomic Energy Commission
Washington, D.C. 20545

Attn: Technical Reports Library

Advanced Metals Research Corp.
149 Middlesex Turnpike
Burlington, Massachusetts 01804

Attn: J. T. Norton

Aerospace Corporation
Reports Acquisition
P. O. Box 95085
Los Angeles, California 90045

Allegheny Ludlum Steel Corp.
Research Center
Alabama and Pacific Avenues
Prackenridge, Pennsylvania 15014

Attn: Library

American Society for Metals
Metals Park
Novelty, Ohio 44073

Attn: Library

Alloy Surfaces, Inc.
100 South Justison Street
Wilmington, Delaware 19899

Attn: Mr. George H. Cook

Avco Space Systems Division
Lowell Industrial Park
Lowell, Massachusetts 01851

Attn: Library

The Bendix Corporation
Research Laboratories Division
Southfield, Michigan 48075

Attn: Library

Boeing Company
P. O. Box 733
Renton, Washington 98055

Attn: SST Unit Chief, W. E. Binz

Case Institute of Technology
University Circle
Cleveland, Ohio 44106

Attn: Library

Chromalloy Corporation
169 Western Highway
West Nyack, New York 10994

Attn: Mr. L. Maisel

City College of New York
Dept. of Chemical Engineering
New York, New York 10031

Attn: Mr. R. A. Graff

Denver Research Institute
University Park
Denver, Colorado 80210

Attn: Library

Douglas Aircraft Company
3000 Ocean Park Boulevard
Santa Monica, California 90406

Attn: Library

E. I. du Pont de Nemours and Co., Inc.
1007 Market Street
Wilmington, Delaware 19898

Attn: Dr. Warren I. Pollack

E. I. du Pont de Nemours and Co., Inc.
Pigments Dept., Metal Products
Wilmington, Delaware 19898

Attn: Library

Fansteel Metallurgical Corporation
Number One Tantalum Place
North Chicago, Illinois 60064

Attn: Library

Firth Sterling, Inc.
Powder Metals Research
P. O. Box 71
Pittsburgh, Pennsylvania 15230

Attn: Library

Ford Motor Company
Materials Development Dept.
20000 Rotunda Drive
P. O. Box 2053
Dearborn, Michigan 48123

Attn: Mr. Y. P. Telang

General Electric Company
Advanced Technology Laboratory
Schenectady, New York 12305

Attn: Library

General Electric Company
Materials Development Lab. Oper.
Advance Engine and Tech. Dept.
Cincinnati, Ohio 45215

Attn: Mr. L. P. Jahnke
Attn: Mr. M. Levinstein
Attn: Mr. W. Hagel

General Electric Company
Nuclear Systems Programs
Space Systems
Cincinnati, Ohio 45215

Attn: R. G. Frank

General Motors Corporation
Allison Division
Indianapolis, Indiana 46206

Attn: Mr. D. K. Hanink,
Materials Lab.

General Technologies Corporation
708 North West Street
Alexandria, Virginia 22314

Attn: Library

Howmet Corporation
Misco Division
One Misco Drive
Whitehall, Michigan 49461

Attn: Mr. S. Wolosin

IIT Research Institute
Technology Center
Chicago, Illinois 60616

Attn: Mr. V. Hill
Attn: Library

Ilikon Corporation
Natick Industrial Center
Natick, Massachusetts

Attn: Library

International Nickel Company
P. D. Merica Research Laboratory
Sterling Forest
Suffern, New York 10901

Attn: Library

Arthur D. Little, Inc.
20 Acorn Park
Cambridge, Massachusetts

Attn: Library
Attn: Dr. Joan Berkowitz

Lockheed Palo Alto Research Laboratory
Materials and Sciences, Org. 52-30
3251 Hanover Street
Palo Alto, California 94304

Attn: Dr. E. C. Burke

Massachusetts Institute of Technology
Metallurgy Dept., RM-8-305
Cambridge, Massachusetts 02139

Attn: Library

Narmco Research & Development Div.
Whittaker Corporation
3540 Aero Court
San Diego, California 92123

Attn: Library

Nuclear Materials Company
West Concord, Massachusetts 01781

Attn: Library

Ohio State University
Columbus, Ohio 43210

Attn: Library

Pratt & Whitney
Div. of United Aircraft Corp.
Manufacture Engineering
Aircraft Road
Middletown, Connecticut 06457

Attn: Mr. Frank Talboom

Rensselaer Polytechnic Institute
Troy, New York 12180

Attn: Library

Sherritt Gordon Mines, Ltd.
Research and Development Div.
Fort Saskatchewan, Alberta, Canada

Attn: Library

Spartan Aviation, Inc.
Aviation Services Division
P. O. Box 51239
Dawson Station
Tulsa, Oklahoma 07052

Attn: Mr. M. Ortner

Stanford Research Institute
Menlo Park, California

Attn: Library (Technical)

Stanford University
Palo Alto, California 94305

Attn: Library

Sylvania Electric Products
Sylcor Division
Cantiague Road
Hicksville, L. I., N. Y. 11802

Attn: Mr. L. Sama

Texas Instruments, Inc.
Materials and Controls Div.
P. O. Box 5474
Dallas, Texas 75222

Attn: Mr. Gene Wakefield

TRW Inc.
23555 Euclid Avenue
Cleveland, Ohio 44117

Attn: H. A. Fisch

Union Carbide Corporation
Stellite Division
Technology Department
Kokomo, Indiana 46901

Attn: Library (Technical)

United Aircraft Corporation
400 Main Street
East Hartford, Connecticut 06108

Attn: Research Library
Attn: E. F. Bradley, Chief,
Materials Engineering

United Aircraft Corporation
Pratt and Whitney Division
West Palm Beach, Florida 33402

Attn: Library

Universal-Cyclops Steel Corporation
Bridgeville, Pennsylvania 15017

Attn: Library

University of Dayton
Research Institute
300 College Park Avenue
Dayton, Ohio 45409

Attn: Library

University of Illinois
Dept. of Ceramic Engineering
Urbana, Illinois 61801

Attn: Mr. J. Wurst

University of Pittsburgh
Center for Study of Thermodynamic
Properties of Materials
409 Engineering Hall
Pittsburgh, Pennsylvania 15213

Attn: Dr. G. R. Fitterer

University of Washington
Ceramics Department
Seattle, Washington 98101

Attn: Dr. J. Mueller

Wah Chang Corporation
Albany, Oregon 97321

Attn: Library

Westinghouse Electric Corporation
Research Laboratories
Beulah Road, Churchill Buro.
Pittsburgh, Pennsylvania 15235

Attn: Mr. R. Grekila

Westinghouse Electric Corporation
Westinghouse Astronulcear Lab.
P. O. Box 10864
Pittsburgh, Pennsylvania 15236

Attn: Mr. W. Buckman

Whitfield Laboratories
P. O. Box 287
Bethel, Connecticut 06801